Photovoltaic Soiling Characterisation and Performance Mapping in Nigeria

Submitted by

Yusuf Nadabo Chanchangi

to the

University of Exeter as a thesis for the
Degree of Doctor of Philosophy
by
Research in Renewable Energy

April 2021

I certify that all material in this thesis which is not my own work, has been identified and that any material that has previously been submitted and approved for the award of a degree by this or any other University has been acknowledged.

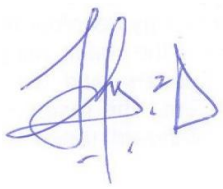

……

Abstract

In Nigeria, the rapid population increase and the overreliance on fossil fuel have created significant environmental, health, political and economic consequences leading to severe socio-economic drawbacks. These factors have developed a wide gap between energy demand and supply due to insufficient local production, necessitating the need for a clean energy supply for all. The photovoltaic device's economic and environmental merits have made it the most suitable clean energy alternative to help developing countries such as Nigeria achieve the SDG-7. However, apart from the device's low efficiency, which is undergoing intensive study across the globe, another omnipresent factor is surface soiling, which is grossly underestimated and has a deleterious impact on a solar cell's performance. The accumulation of dust on photovoltaic (PV) devices adversely impacts their performance and is grossly underestimated. It is location-dependent and influenced by a number of factors, which raises concern for the potential investor, policymakers, engineers, and local populace in regions where the soiling rate and potential threats remain relatively unexplored. Energy losses from PV due to dust is an issue that cannot be ignored and can be an obstacle to achieving renewable energy targets in Nigeria. In this context, this thesis presents several mitigation techniques available to maintain a certain level of performance.

This research begins with a systematic review of related literature on the country's energy crisis and renewable energy potential, leading to an overview of solar energy potential and penetration in the country, resulting in a comprehensive literature review on the effect of dust on PV performance. Several studies investigating factors influencing dust accumulation were conducted: First, indoor research investigated soiling on photovoltaic modules, focusing on dust properties and PV surface materials as influencing factors. Solar simulators, the spectrometer and SEM/EDX, were used to characterise the effect of accumulation of 13 different samples (ash, bird droppings, carpet dust, cement, charcoal, clay, coarse sand, laterite, loam soil, salt, sandy soil, stone dust and wood dust) on PV performance. Besides, the same experiment examines the performance of two leading PV covering materials (low iron glass and acrylic plastic). Outdoor studies investigated the influence of angular dependencies and

optical losses in Abuja and across the country's six geopolitical zones by employing a low-cost coupon holder to expose low iron glass (50 mm x 50 mm) considering time stamp (annual, seasonal, and monthly variation). Soiled coupons were subjected to optical characterisation using a spectrometer and imaging analysis by employing SEM/EDX. Four PV modules (Monocrystalline Silicon, Polycrystalline Silicon, Cadmium Telluride and amorphous Silicon) were exposed in the Northern region to investigate PV yield reduction and correlate with yield measured under standard conditions. Low iron coupons were also exposed at the same period to determine the optical losses using a spectrometer and minerals morphology employing SEM/EDX. Finally, a correlation *in-situ* study to examine five cost-effective PV soiling mitigation techniques was conducted to determine the most effective and suitable approach by employing two types of PV surface covering materials (low iron glass and acrylic plastic) considering seasonal variation.

The findings confirm that the country is blessed with enormous solar energy potential. However, its penetration is low, and the majority of the population is suffering from energy starvation. Findings from the review highlight dust accumulation on PV as one of the main obstacles preventing solar energy penetration. The indoor study findings reveal alarming losses showing that charcoal has the worst degradation effect on PV performance with approximately 98% reduction in short circuit current, while salt seems to have the most negligible impact with about 7%. It shows that acrylic plastic accumulates more dust than low iron glass and wet deposition promotes more adhesion on coupons than dry deposition.

The outdoor studies' results revealed that the highest reduction in transmittance was recorded on a horizontally positioned coupon with a significant decrease of about 88% and lowest on a vertically positioned coupon with a reduction in the region of 1%. Similarly, the most significant mass of 12.56 g/m^2 was recorded on a horizontally exposed coupon. It is observed that higher losses were recorded on a coupon positioned in the horizontal plane. Optical losses findings were used to develop soiling, which was correlated with another map revealing a significant variation. The PV performance experiment results reveal a significant decrease

of I_{SC} on all the modules with 73% on a-Si and the lowest of about 65% Si. It shows a yield loss of 78.3% for a-Si, 77% for CdTe, 70% for pc-Si, and 68.6% for the mc-Si module. Efficiencies decline of 78% for a-Si, 77% for CdTe, 71% for pc-Si and 71% for mc-Si. The optical loss results validated the output performance losses with a similar trend.

The cleaning technique experimental findings show that the self-cleaning approach provides high preventive and restorative performance during the wet season, with about 99% on a low iron glass. Both manual cleanings with squeegee/water and self-cleaning demonstrated a 95% performance during the dry season on a low iron glass coupon. The least effective performance was recorded on the natural cleaning during the dry season with about 28% reduction in a month.

The ramifications caused by soiling cannot be overlooked or overemphasised; thus, it is recommended to deploy PV modules in outdoor conditions and further examine each soiling mitigation technique's effectiveness and cost analysis over a longer duration in different regions.

Table of Contents

Acknowledgement

In the name of ALLAH, the beneficent, and the merciful. All praises and gratitude are due to Allah, and peace and blessings go to His Messenger (Muhammad, peace be upon him).

Oh, Almighty ALLAH! All praises and gratitude be to YOU, Praise upon Praise! And thanks to YOU! Thanks upon Thanks! The cherisher and lord of the worlds, for giving me the foresight, strength and endurance to embark and finish this research work.

Secondly, I wish to express my sincere gratitude to my parents, Alhaji Y. Nadabo Chanchangi and Hajiya Ba'aba Nadabo. My step-mothers, Hajiya Amina & Hajiya Halima. My lovely wife: Na'ima, It is from these people that I derive my greatest inspiration, and I thank them all for their relentless support and encouragement,

This work would not have been possible without the Nigerian Government's financial support through a PhD grant from the PTDF (Petroleum Technology Development Fund), with additional financial support from the JUICE (Joint UK Indian Renewable Energy Centre). Therefore, I gratefully acknowledge your support and thank you.

This acknowledgement will be incomplete without a worthy mention and salutation to my mentor, tutor, and supervisor: Prof. Tapas K. Mallick, who has ensured that this project has become a reality, not a fantasy. I also wish to register my profound appreciation and gratitude to Dr Aritra Ghosh, Dr Senthilarasu Sundaram, Dr Asif Tahir, Dr Hasan Baig, and Dr Anurag Roy, and William Cameron for the support I received from you all and the entire staff (particularly Joe Pickles, Gavyn Rollinson, Uren Sharon, Mark Plummer, Daniela Farina, and Amrita Sharma), research technician (especially Brian Stratton, James Yule, and Phil Nesbitt) of the renewable energy department, college of engineering, mathematics and physical sciences, University of Exeter, Penryn campus. I gratefully acknowledge the support, guidance, and assistance of Richard Little throughout my PhD research, Richard you have been very supportive! Thank you!

The study was undertaken along with the Nigerian Civil Aviation Authority (Jamilu Tanko) Solar Energy Research Centre Usman Dan Fodio University, Sokoto (Yusuf Ganda, Yayaha, and Nura), National Centre for Energy Research and Development, University of Nigeria Nsukka (Sudum Esaenwi), and Dornier Aviation Nigeria (Rosemary, Mustapha, Solomon Attah, Abel Aratus, Moses, Daniel Malu, Waje, Emmanuel Nkut, Joshua and Mr Edo), Bayero University, Kano (Engr. Haruna Dayyabu, Dr Muhammad Buhari, and Abdulhameed Maina), Amina (Mamma), Ayaji Sale, and Nafiu Yusuf. I gratefully acknowledge the assistance and expertise of all the people involved in this research.

I wish to thank my children (Yusuf, Amina, Aisha, Ahmad and Muhammad), family members, friends (MO 1, Walter, Lisa Hagan and her husband, Samuel Barton, Hannah Meinertzhagen, and Sarah Walsh), and colleagues (Marvin, Eze, Suleiman, Mussad, Abdulmuhsin, Shubranshu, and Asma) for supporting, inspiring and motivating me during my study at the University of Exeter.

Finally, many thanks go to the administrative (Vicky Colton and Claire) and examining team (Dr Markus Muller, Prof Abusara, and Prof Yupeng Wu) for accepting and putting a significant amount of their time into reviewing and conduction viva, which is a significant milestone in my life.

Thank you, all.

Dedication

This thesis is dedicated to my late uncle Alhaji Ahmadu Chanchangi. May ALLAH forgive his shortcomings, and may his perfect soul continue to rest in peace, "*Amin*".

List of figures

List of tables

List of publications

Journal Articles Published

1. Chanchangi, Y. N., Ghosh, A., Sundaram, S., and Mallick, T. K. (2020). Dust and PV Performance in Nigeria: A review. *Renewable and Sustainable Energy Reviews* ***121*** (2020): 1.

2. Chanchangi, Y. N., Ghosh, A., Sundaram, S., and Mallick, T. K. (2020). An analytical indoor experimental study on the effect of soiling on PV, focusing on dust properties and PV surface material. *Solar Energy* ***203*** (2020): 46–68.

3. Chanchangi, Y. N., Ghosh, A., Sundaram, S., and Mallick, T. K. (2021). Angular Dependencies of Soiling Loss on Photovoltaic Performance in Nigeria. *Solar Energy.*

4. Chanchangi, Y. N., Roy, A., Ghosh, A., Sundaram, S., and Mallick, T. K. (2021) *In-Situ* assessment of low-cost mitigation techniques in Northern Nigeria. *Energy Conversion and Management, 244*, 114442. doi:https://doi.org/10.1016/j.enconman.2021.114442

Journal Articles Submitted or in Process

5. Chanchangi, Y. N., Roy, A., Ghosh, A., Sundaram, S., and Mallick, T. K. (2021) Solar energy potential and penetration in Nigeria.

6. Chanchangi, Y. N., Ghosh, A., Sundaram, S., and Mallick, T. K. (2021) Soiling mapping through optical losses for Nigeria.

7. Chanchangi, Y. N., Baig, A., Ghosh, A., Sundaram, S., and Mallick, T. K. (2021) Soiling on PV performance influenced by weather parameters in Northern Nigeria.

8. Chanchangi, Y. N., Baig, H., Ghosh, A., Sundaram, S., and Mallick, T. K. (2021) PV performance with dust and temperature.

Conference Articles

9. Chanchangi, Y. N., Ghosh, A., Sundaram, S., and Mallick, T. K. (2019) Effect of dust formation on the PV module's performance in Nigeria: A preliminary study. *PVSAT-15 Conference C101 of the SOLAR ENERGY Society,* Scarman Centre, University of Warwick, Coventry, UK. The Solar Energy Society**:** 97-100.

10. Chanchangi, Y. N., Ghosh, A., Sundaram, S., and Mallick, T. K. (2021) Impact of Dust on PV Performance in Nigeria. 38th European Photovoltaic Solar Energy Conference and Exhibition, September 6 - 10, 2021, in Lisbon, Portugal.

Award Received:

Best Student Poster Prize by the Institute of Physics at the Photovoltaic Science Application and Technology Conference – PVSAT 15.

Funding Received:

Petroleum Technology Development Fund (PTDF)

PTDF Nigeria provided tuition fees, maintenance fees, and bench fees for the PhD research.

Joint UK-India Clean Energy Centre (JUICE)

JUICE funding provided financial support to carry out field research works in Nigeria and to acquire equipment.

SuperSolar International Conference Fund Award

SuperSolar provided conference award to attend European Photovoltaic Solar Energy Conference and Exhibition, 38th EU PVSEC.

Nomenclature

Item	Description	Unit
A	Hamaker constant	mole/m^2/second
ε	Dielectric constant	e2·GeV−1·fm−1
εo	The permittivity of free space	F/m
g	Gravitational acceleration	m/s^2
θ	Theta – contact angle or Zenith	°
p	Density	g/m^3
R	radius	m
TiO_2	Titanium dioxide	ml
γ	The surface tension of water	$mN·m^{-1}$
ζ	Distance b/w flat surface and particle	m
S(λ)	Relative spectral distribution of solar radiation	$W·m^{-2}$
T (λ)	Spectral transmission	%
Δλ	Change in wavelength	nm
φ	PV electrical output parameters	W, A, and V
SLPV	PV soiling	%
I_{SC}	Short circuit current	A
V_{OC}	Open circuit voltage	V
FF	Fill factor	FF
I_{max}	Load current which maximises the output power	A
V_{max}	Voltage that maximises the power output	V
P_{max}	Maximum power output of a module	W
$P_{max,clean}$	Maximum power output of a clean module	W
$P_{max,dusty}$	Maximum power output of a dusty module	W
surf	Particle surface	m

A	The cross-sectional area of a dust particle	μm^2
Lproj	The longest length of a dust particle	µm
P	The perimeter of the dust particle.	µm
I	iota- Separation distance	μm^2
β	Tilt angle	°
PV_{OUT_total}	Total photovoltaic output at global tilted irradiation	W
τ_x	Transmittance data of a coupon positioned at an angle relative to a horizontal surface	%
τ_{clean}	Transmittance data of a clean coupon	%
$\tau_{\beta(optimum)}$	The light transmittance of a coupon at the optimum angle of Abuja (13°)	%
$\tau_{\beta(90)}$	The transmittance of a coupon that was vertically positioned (90° to the horizontal plane)	%
$\tau_{\beta(45)}$	The transmittance of a coupon that was positioned in 45°	%
PV_{Out}	PV output	W
$PV\_out\ (\beta_{(90)})$	PV output with soiled coupon at vertical position (90°)	W
$PV\_out\ (\beta_{(45)})$	PV output with soiled coupon at tilt position (45°)	W
$PV\_out\ (\beta_{(optimum)})$	PV output with soiled coupon at optimum position (13°)	W
$PV\_out\ (\beta_{(0)})$	PV output with soiled coupon at horizontal position (0°)	W
$W_{(soiled\ coupon)}$	Weight of a soiled coupon,	g/m^2
$W_{(clean\ coupon)}$	Weight of coupon after cleaning	g/m^2
P_{out}	Power output	W
$\Delta\tau_x$	Transmittance change of an exposed coupon at an unknown angle	%

µm	micrometre	µm
P_{mpp}	Power at the maximum power point	W
I_{mpp}	Current, at the maximum power point	A
V_{mpp}	Voltage at the maximum power point	V
µg/m^3	micro gram/meter cube	µg/m^3
A	The active area of the PV module	m^2
G	Incident solar irradiance	W/m^2
η	Efficiency	%
$\Delta\eta$	Change in efficiency	%
PR	Performance ratio	*PR*
E	Actual incident radiance	W/m^2
P_{rated}	Power output under STC	Wp
$\mathrm{Mass}_{(A\ D)}$	accumulated dust mass on Coupon	g/m^2
$\mathrm{Mass}_{(clean\ coupon)}$	Mass of a clean coupon	g/m^2
$\mathrm{Mass}_{(soiled\ coupon)}$	Mass of soiled coupon	g/m^2
CO	Carbon Monoxide	g/m^3
O_3	Ozone	g/m^3
NO_2	Nitrogen oxide	g/m^3
SO_2	Sulphuric oxide	g/m^3
PM_{10}	Particulate Matter 10 micrometres and smaller	µm
$PM_{2.5}$	Particulate Matter 2.5 micrometres and smaller	µm
P_{out}	Power output	W
$\Delta_{\tau_{(Optimum)}}$	Calculated change of transmittance of a coupon at an optimum angle	%
$\beta_{(x)}$	The optimum tilt angle of a particular station	°
$\beta_{(0)}$	Horizontal plane	°
$\beta_{(45)}$	The tilt angle of 45°	°
$\Delta_{\tau_{(0)}}$	Soiling losses recorded on a coupon positioned on a horizontal plane	%

$\Delta_{\tau_{(45)}}$	Soiling losses recorded on a coupon positioned at 45˚	%
Z_K^*	The smooth estimate produced by Kriging interpolation	N/A
λ_i	Weight for Zi	N/A
$Zi,$	Variable	N/A
Z_V	Actual value	N/A
$\bar{C}(V,\ V)$	Covariance between the variables of the samples	N/A
μ	Lagrange parameter	mole/m^2/second
$\bar{C}(v_i, V)$	Covariance b/w the estimations and samples variables	N/A
δ	Declination angle	°
π	Pie	PI
n	n^{th} day	d
ω	Solar hour angle	°
ω_{sr}	Sunrise angle	°
ω_{ss}	Sunset angle	°
θ	Zenith	°
γ	Azimuth angle	°
α	Solar altitude angle	°
H_B	Direct (beam) radiation	W/m^2
H_D	Diffuse radiation	W/m^2
H_d	Diffuse radiation on a horizontal	W/m^2
R_d	Tilt factor	°
H_o	Extra-terrestrial daily incident solar radiation on the earth's horizontal surface	W/m^2
(H_R)	Reflected radiation	W/m^2
H_g	Global solar radiation incident on a horizontal surface	W/m^2
R_r	Tilt factor for reflected solar radiation	W/m^2

ρ	Surface albedo	*P*
VX	Visibility	m
SiO_2	Silicon oxide-titanium dioxide	g
HDMS	Hexamethyldisilazane	ml
TBOT	tetrabutyl orthotitanate	ml
TEOS	Tetraethyl-orthosilicate	ml
TTiP	Titanium (IV) isopropoxide	ml
Dry	Dry season	months
Wet	Wet season	months
ANN	Annual	months
$S_{(H\&S)}$	Safety (health and safety)	%
$R_{(I)}$	Reliability	%
$M_{(O+M)}$	Maintenance (operation and maintenance cost)	%
$E_{(D+Q)}$	Engineering design (Design and quality)	%
$O_{(O+P)}$	Operation (operational and success probability)	%
CDC	Solution C, Solution D, and Solution C	N/A
γ^{lv}	Liquid surface free energy	mN/m or mN m^{-1}
γ^{sv}	Coupon surface free energy	mN/m or mN m-1
γ^{sl}	The interfacial free energy	mN/m or mN m-1
θ	Contact angle	°
OH●	Hydroxide	mg
O_2^-	Oxygen	mg/L
DI	deionised water	ml
ZnO	Zinc oxide	ml
ITO	Indium Tin Oxide	ml
M-ZnO	The microspheres Zinc oxide	ml
C_i	Initial cost	€ or ₦
C_m	The estimated monthly cost of maintenance.	€ or ₦

$\sum p_{(PPE)}$	The total price of all the PPEs required,	€ or ₦
$p_{(tool)}$	The price of the tool.	€ or ₦
$\sum p_{(mat)}$	The summation price of coating materials,	€ or ₦
W^{flex}	Wages for re-coating	€ or ₦
$\sum p(comp^1)$	The summation price of all components used in fabricating the mechanised platform.	€ or ₦
$\sum p(com)$	The summation of all the components (example: wiper lade and battery) must be changed after one year of operation.	N/A
w	The wages for coating the hydrophobic layer on the coupons.	€ or ₦
cyc	The number of cycles required in a month,	n/yrs
L	The labour	hrs
Q_{H_2O}	The quantity of required water.	ml
l	Number of workers,	N/A
$p_{(PPE)}$	The price of *PPE*	€ or ₦
t_2	the time coating is expected to degrade and requires re-coating (48 months)	hrs
$p_{(tool)}$	The price of a tool	€ or ₦
$o_{(tool)}$	The number of tools	N/A
t_1	Time considering 12 months maintenance cycle.	months
p	Price	€ or ₦

Abbreviations

Item	Description
3D	3 Dimension
ABV	Abuja
ABS	Acrylonitrile Butadiene Styrene
AOT	Aerosol optical thickness
BAPV	Building attached PV
BIPV	Building Integrated PV
CREN	Council for Renewable Energy
$^{\circ}C$	Degree centigrade
DC	Direct Current
DNI	Direct normal irradiation
E	East Direction
EDS	Electrodynamic Screens
ELEV	Terrain elevation
ENU	Enugu
EU	European Union
GHG	Green House Gasses
GHI	Global horizontal irradiation
GHI_{opta}	Global tilted irradiation at an optimum angle
IRENE	International Renewable Energy Agency
ITD	Inter-Tropical Displacement
ITCZ	Inter-Tropical Convergence Zone
KAD	Kaduna
LDH	Light Dust haze
LOS	Lagos
MENA	The Middle East & North Africa
MIU	Maiduguri
MSHA	Mine Safety and Health Administration
NIR	Near Infra-Red
NNPC	Nigerian National Petroleum Corporation
NOM	Nominal

N	North Direction
NREEEP	Nigerian Renewal Energy and Energy Efficiency Policy
OPTA	The optimum tilt angle of the PV module
PM	Particulate Matter
PHC	Port Harcourt
PPE	Personal protective equipment
PTDF	Petroleum Technology Development Fund
PV	Photovoltaic
PVOUT _total	Total photovoltaic output and global tilted irradiation
SALSA	Search, Appraisal, Synthesis, and Analysis
SHIP	Super Hydrophilic Plane
SHOP	Super Hydrophobic Plane
SOK	Sokoto
S	South Direction
STC	Standard test condition
TDH	Thick Dust haze
TEMP	Temperature
TSP	Total Suspended Particles
UAE	United Arab Emirates
UK	United Kingdom
USA	United States of America
UTC	Coordinated universal time
UV	Ultraviolet
VIPV	Vehicle integrated PV
VIS	Visual
WAT	West African Time
WEC	World Energy Council
W	West Direction

Units

Item	Description
A	Amphere (unit of current)
cm	centimetre
°	Degree
€	Euro (European currency)
eV	electron-volt
g	Gram
g/m^2	Gram per metre square
GW	Giga Watt
GWth	Giga Watt thermal
hrs	Hours
km/h	kilometre per hour
kWh/m^2	kilowatt-hour per metre square
kWp	kilowatt power
m	metre
µm	micrometre
mm	millimetre
mJ/m^{-2}	milli Joule per square metre
MJ/m^2	Mega Joule per square metre
mN/m or mN m^{-1}	millinewton/metre
m/s	metre/second
MW	MegaWatt
MWp	MegaWatt power
MWh/m^2	Megawatt hour per metre square
₦	Naira (Nigerian Currency)
nm	nanometre
V	Volts (unit of voltage)
W/m^2	Watt per metre square

1 Chapter One - Introduction

1.1 Introduction

1.1.1 Background of Nigeria's energy system

The rapid increase of the world population and present-day industrial development and lifestyle has created a massive gap between the demand and energy supply. This gap demands a rapid increase of substantial clean, stable and reliable energy supply. The over-dependency on depleting fossil fuels in generating energy for our daily requirements is increasingly affecting our environment and deteriorating human health. Access to stable and reliable power is still a dream for most developing countries. This is ominous for developing countries, as energy access is vital to economic growth, socio-economic activities, agricultural activities, and living standards. In this research, energy is referred to as electricity. According to Akinyele et al. (2015); Sanusi and Owoyele (2016); Baurzhan and Jenkins (2016); and Monyei et al. (2017), about 1.2 billion individuals are still living without access to modern (stable) energy, with about 50% of them residing in Sub-Saharan Africa. Nigeria, the country with the highest population in the region, has about 100 million citizens living without clean and stable energy (Yakubu and Ifeanyi-Nwaoha, 2017; Akinyele et al., 2017). The country is suffering from acute energy poverty.

Nigeria is a country blessed with abundant conventional energy resources (Non-Renewable) and renewable energy resources (Biomass, Hydro, Solar and Wind) that are sufficient to satisfy the demand of its populace and export the excess to neighbouring countries as a tradable commodity to generate funds. Thus far, the in-house supply is still inadequate and unable to meet the country's demand, and this is continuously increasing due to a sustained increase in population, requiring an immediate response before it reaches an unrecoverable situation. This inadequacy of supply has several consequences. The Nigerian government has disbursed billions of dollars over the last two decades to improve and boost energy supply using conventional energy resources, yet the country is still plagued with severe energy shortages (Usman et al., 2015). This energy supply poses challenges to both the rural and urban populations. However, the problem

is most severe in the rural areas, where the majority of the population lives without access to the national grid, and besides, even the majority of urban dwellers suffer from an unstable and insufficient power supply. The frequent power outages have compelled many Nigerians to adopt self-energy generation using various fossil fuel-powered generators to generate electricity for domestic, commercial and industrial consumption. The by-products of this have adverse effects on both humans and the environment.

Energy deficit leads to poverty, economic decline, a low standard of living, social hardship, and many more negative impacts. Conversely, a constant and stable energy supply is fundamental to the development of a nation. According to Ikem et al. (2016), energy supply is the pivot that supports the wheel of development of a country. Ayodele and Ogunjuyigbe (2015); Oseni (2012); Oyedepo (2012a); Rafindadi (2016); Anumaka (2012) and Akuru et al. (2017) established that stable and reliable energy (electricity) supply is particularly significant, and it is an essential ingredient and a necessary tool that plays a vital role in the economic development, poverty reduction, industrial, agriculture, manufacturing, commerce, infrastructural development, employment, and security. It also plays a vital role in ensuring that basic needs and services (food and water, housing, health services and education) are provided. Development can only be achieved and sustained when all the nation's population has stable and reliable energy access. Anumaka (2012) emphasised that the contemporary world depends on abundant energy for developmental growth.

Moreover, Nigeria's energy poverty is alarming; thus, unceasing research on the energy situation to provide possible solutions to mitigate the problem is imperative. Bugaje (1999) also stated that many of the population live without access to the grid, making the situation even more concerning. Several types of research have been conducted to explore the potentials of clean and reliable energy in Nigeria. Sambo (2009) stated that clean energy is the solution for Nigeria's acute energy crisis, predominantly in rural areas. Ajayi and Ajayi (2013) indicated that fossil fuel by-products are very harmful to humans and deleterious to the environment as such renewable energies as clean energy should be considered viable options available in Nigeria for sustainable electricity

production. Aliyu et al. (2015) also believe that there is a need to rigorously pursue renewable energy technology to conquer Nigeria's continuing energy deficit to underpin economic development.

Several prior studies have established that a sufficient and stable energy supply is vital to any country's development. Adaramola et al. (2014) confirmed that renewable energy sources are inexhaustible, clean, and environmentally friendly. Low access to electricity in Nigeria also has a negative impact on industrial activities. According to Aliyu et al. (2015), a nation's industrial growth is directly proportional to available energy resources. Steer et al. (2000) stated that energy is an essential key element for a nation's economic growth, and it is the powerhouse that drives the economy. Without the minimum required access to energy for many of its population, a nation cannot develop and sustain itself beyond a subsistence economy.

Prior studies show that renewable energy can resolve the persisting energy crisis in the country that has lasted for over two decades. Shaaban and Petinrin (2014) concluded that the country is suffering from an acute electricity deficit and advocate that the use of renewable energy can solve the persisting energy crisis in the country by bridging the demand and supply gap as well as improving the living standards of the people residing in the rural areas. Ohunakin (2010) conducted a study on the current and future perspectives on renewable energy application in Nigeria. The research concluded that energy demand is very high and continuously increasing because of the continuous increase in the population. The researcher further recommended a need to exploit the renewable energies available and diversify the energy supply. Anumaka (2012) concluded that the Nigerian government alone could not provide adequate funding to supply electricity. They recommended that private and foreign investors are required to promote the integration of renewable energy to minimise the low access to electricity in rural areas. Mohammed et al. (2013) concluded that renewable energy could serve as a solution to the energy poverty in the rural areas and further recommended that in order to keep up with the pace of rapid population growth in the country, there is a need to exploit renewable energy to compensate for the energy deficit.

Aliyu et al. (2015) reviewed Nigeria's primary renewable energies and potentials. They recommended the integration of renewable energy in the supply mix. Ikem et al. (2016) presented an overview of the Nigerian national electricity grid, identified an inadequate flow of information regarding renewable energy, and recommended that the Nigerian government pursue the renewable energy policy that is not yet implemented. Oseni (2011) presented an analytical review of the overall performance of the electricity sector and stated Nigeria is a country blessed with abundant renewable energy resources and recommended that use of the resources can increase the electricity supply and reduce adverse consequences caused by fossil fuel on both the environment and its inhabitants. The research further stated that renewable energy resources could also increase access to a reliable and stable supply, sustaining its growth. Samba (2009) presented the role of renewables in bridging the energy demand and supply gap. This prominent researcher in Nigeria concluded that renewable energy is a viable option that can solve the country's persisting energy crisis. Akuru et al. (2017) highlighted the potential of renewable energy in Nigeria and concluded that a 100% supply of renewable energy is possible in Nigeria because it has already been achieved elsewhere; however, it is costly.

Ajayi et al. (2016) assessed solar and wind resources' potentials in Northern Nigeria and concluded that solar photovoltaic technology is a viable option to facilitate sustainable development goals. This shows that renewable energy from PV is an appropriate solution to this global energy crisis to reduce GHG emissions from clean energy generation with a naturally replenishable source.

However, due to PV system exposure to outside conditions, dust formation affects the technology's performance. This causes detrimental optical disturbance to the solar irradiance transmittance to the solar PV cell by reflecting, absorbing and scattering the rays, leading to overall performance degradation. Dust accumulation is considered the third most significant factor influencing a solar PV module's performance after solar radiation and temperature (John et al., 2016). It is challenging to generalise the loss level caused by soiling on a PV module because the severity of soiling impact varies with geographical location

and seasonal climatic conditions (John et al., 2016; Kazmerski et al., 2016). This presents a serious concern requiring rigorous research.

1.2 Nigeria's energy scenario

Nigeria is facing severe challenges in electricity generation and supply. The country's electricity supply has sunk into a quagmire for over two decades. The supply is grossly insufficient and inadequate to meet the population's demand, which is continuously increasing.

The national grid supply is mainly characterised by continuous fluctuations, frequent power outages and system instability (Onohaebi and Eseosa, 2014). According to Oseni (2016), a typical Nigerian house has access to an average of five hours of electricity supply daily from the national grid. Ajayi and Ajayi (2013) stated that the national grid's Nigerian electricity production has not been sufficient to meet the country's demand, promoting self-generation using traditional biomass and fossil fuel. As stated earlier, Nigeria has an approximate population of over 200 million with an average estimated demand of 31.2 GW, and the country has an installed capacity of 14.38 GW with an average supply capacity of 6 GW (Akuru et al. 2017). This implies that the electricity generation system can only produce about 40% of its installed capacity. If the thumb of rule, which says every 1,000,000 people require a minimum of 1000 MW, is applied to Nigeria, it will require about 200 000 MW (200 GW). Electricity production from renewable sources, excluding hydroelectric, is still 0% (World Bank, 2017b).

The government is making various attempts to resolve the energy crisis, but the progress is painfully slow. A considerable amount of money has been invested in the sector over the last two decades, but a slight improvement was recorded. Almost $20 billion was used to revive the Nigerian electricity sector, but with minimal effect. No one can appropriately account for the money. The power supply that is inadequate and unreliable continues to drive people to self-energy generation using traditional firewood's fossil fuel. A significant number of lives have been lost due to the emission of these fossil fuel generators. These have serious negative repercussions on our health and the environment.

According to WEC (2020), indicators such as energy access, renewable energies, corruption, trade barriers, and liquefied natural gas are the critical uncertainty that Nigeria's leaders are struggling with; energy poverty, electricity prices, energy subsidy, and energy efficiency are significant uncertainties requiring government attention in 2020. Figure 1.1 shows the uncertainty factors, their priority level and their impacts and signalling factors (WEC, 2020).

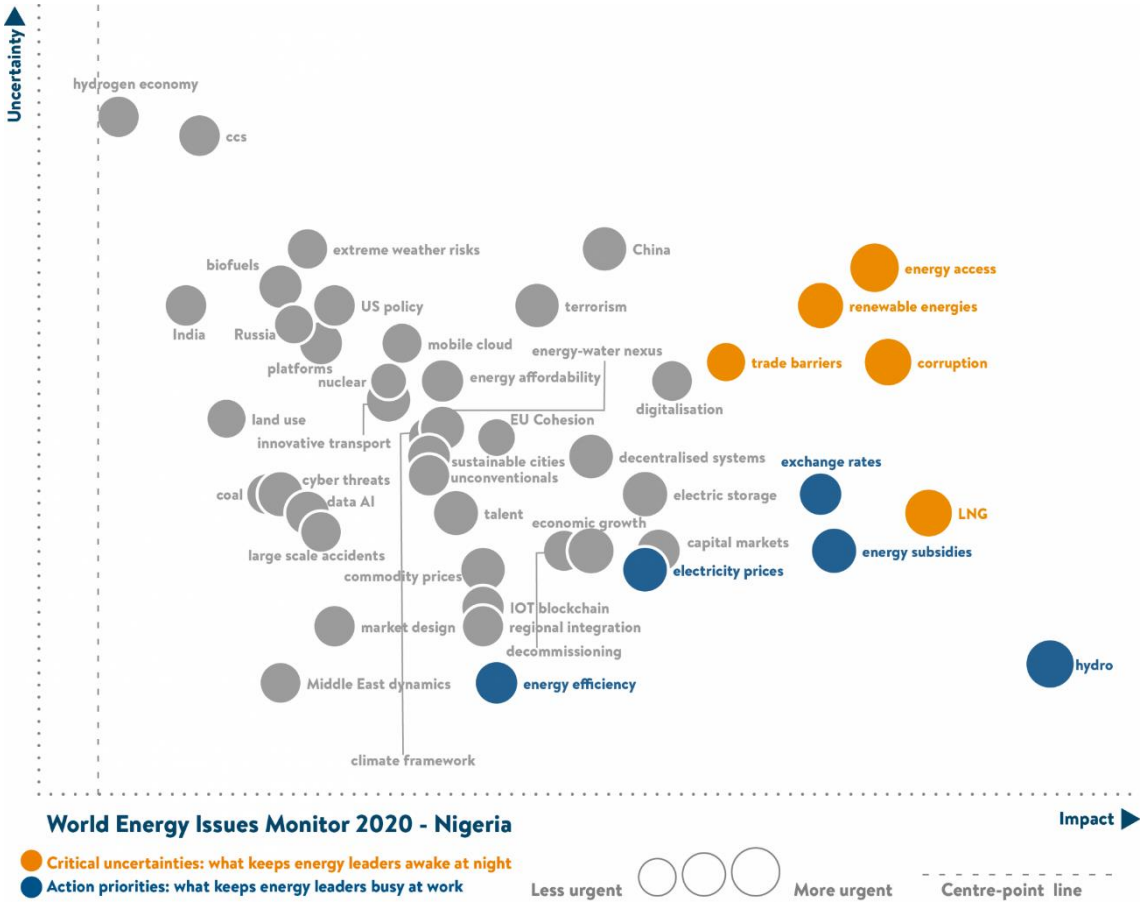

Figure 1.1: Energy Uncertainty Indicator (WEC, 2020).

The insufficient supply of electricity and drop in the oil and gas prices in the international oil market has dragged Nigeria's economy into a recession. However, it has been projected that the country's economy will recover before 2021 (AfDB, 2017). This ravaging economic recession is among the factors compelling large numbers of Nigerians to use technologies that are not environmentally friendly. The country's inadequate electricity supply is caused

by corruption, government negligence, outdated infrastructures, illegal electricity connection and consumption, and many other factors.

1.2.1 Nigeria's energy crisis

An accessible, affordable, stable, and environmentally friendly energy supply plays a vital role in economic growth by improving productivity and reducing poverty. Nigeria has been engulfed in an energy crisis for over two decades, paralysing a wide range of industrial and commercial activities, leading many of the population to live below the poverty line. The country is endowed with substantial conventional energy resources (fossil fuel) and renewable energy resources (such as solar, biomass, wind power and hydropower). Renewable energy, mostly under-exploited, is estimated to be greater than the amount of fossil fuel available. Solar energy has been identified as the renewable energy with the highest potential in the country (Bugaje, 1999), yet its penetration into the supply mix is still minimal. Oyedepo (2012) also believes that solar energy has endless potential and is the most promising renewable energy resource.

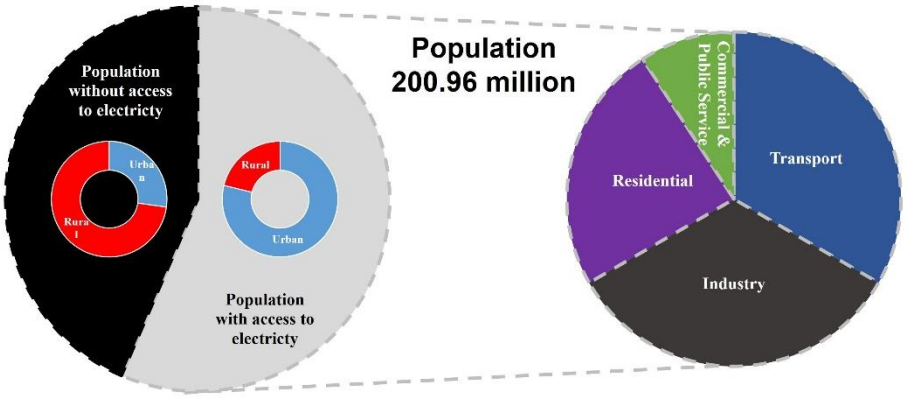

Figure 1.2: Energy consumption overview in Nigeria (World Bank, 2021).

The continuous rapid population increase and over-reliance on fossil fuels as sources of energy and also the primary sources of revenue are causing several economic drawbacks in Nigeria. The country's electricity supply is inadequate, unstable and does not meet the demand. The country's rapid population growth is one of the problems that has necessitated a swift increase in its energy demand. The growth requires an inevitable increase in energy supply to support

livelihoods, industrialisation, increased food demand, and improved living standards.

Nigeria has an estimated population of over 200 million, 56.5% connected to the national grid, receiving erratic and irregular electricity supply (World Bank, 2020). Therefore, about just under 50% of the country does not have access to the national electricity grid and about 80% of the population that lack access to the national grid lives in rural communities (World Bank, 2020). The variations are further illustrated in Figure 1.2, showing consumption according to the sector. According to Emetere et al. (2016), the few Nigerians connected to the national grid barely have 5 (Five) hours of constant and steady electricity supply daily. According to Oyedepo (2012), 87,639 was reported as the minimum system average interruption duration index (SAIDI) in Nigeria, which is high. In 2016, Nigerian electricity consumption per capita was about 0.14 MWh/Capita, and in 2018, it was still 0.2 MWh/Capita, which is very low compared to other developing countries (IEA, 2020).

According to NERC (2020), the peak generation was attained on 31st January 2019, where about 9 MW (201.340 GWh) was generated and supplied, which was a one-day event. It was not repeated as the generation fluctuates between 3MW and 5MW (NERC, 2020). This supply was achieved from various power generation companies, which included Power Holding Company of Nigeria (PHCN), Niger Delta Power Holding Company (NDPHC), Nigerian integrated power projects (NIPP) and other independent power plants (IPP). Other ongoing natural gas and hydropower projects are taking place around the country to increase the supply mix, but not all of these would be adequate to satisfy the local demand. The primary source of electricity in the country is thermal (powered by fossil fuel) and hydro. In 2018, Nigeria produced 36.277 TWh of electricity distributed in the following manner: 6.458 TWh of hydroelectricity, 2.8 TWh solar, and 29.791 Gas TWh, as illustrated in Appendix A - Figure 0.2, which also highlights the previous trend (IEA, 2020). Electricity production from renewable sources, excluding hydroelectric, has started increasing, but the country is far from reaching its solar energy target, which is 500 MW by 2025, to provide 80% of its population with clean energy (IEA, 2020).

In Nigeria, about 70% of its population depends on firewood to generate energy, and about 80% rely on combustible biomass (Emodi et al., 2017; Mohammed et al., 2013). In 2013 more than 95% of rural and about 49% of the urban population use solid fuels for energy production (WHO, 2017). This heavy reliance on firewood causes two significant negative impacts: the emission of harmful gases that causes air pollution and continuous deforestation. These have profound implications for both our ecosystem and its inhabitants. In 2008, about 33,685.062 kt CO_2 was emitted from liquid fuel consumption, about 84.341 kt CO_2 was emitted from solid fuel consumption, and about 20,670.879 kt CO_2 was emitted from gaseous fuel consumption (World Bank, 2017c). These emissions are mainly from the industrial and residential application of fossil-fuelled generators to complement the energy supply, posing a severe negative consequence to humans and the environment. Nigerians are buying the generators regardless of the negative repercussions they might cause.

Akinyele et al. (2017) stated that the continuous release and emission of anthropogenic pollution from fossil-fuelled generators contributes to climate change. It promotes GHG emissions (Green House Gases), and it is detrimental to human health. Usman et al. (2014) documented a report where a family of seven people was found dead due to the fumes (by-products) of fossil-fuelled generators in Lagos. Similarly, Ayodele and Ogunjuyigbe (2015) reported that a family of 4 people was found dead in September 2014 because of by-products (carbon monoxide) of diesel generators. They also reported that by-products of fossil-fuelled generator killed 4 (four) children and their 80 (eighty) year old grandmother. According to WHO (2017), about 95,300 deaths per year were recorded due to Nigeria's indoor air pollution. Emodi et al. (2017) also stated that about 79,000 Nigerians died due to indoor smoke inhalation caused by dependence on firewood. The bye product emissions from these generators are harmful gases and are very dangerous.

Electricity consumption by the industrial sector has been declining, but domestic use has increased. According to Oseni (2011), industrial energy consumption decreased from 62.9% to 9.7% in 35 years, with a reduction of 20% being

recorded in 2011 alone. The researcher further stated that domestic electricity consumption increased from 37.1% to 63.8%. This shows that the population is rising, and industries are shutting down and/or using alternative sources to generate their electricity. The continuous multiple power outages and unpredictable supply have an extremely negative impact on Nigeria's economy. It has paralysed the country's industrial sector by compelling them to adopt self-energy generation using fossil fuel generators, increasing production costs.

Adaramola et al. (2014) noted that a recent survey shows that the self-generation of electricity in producing an item in Nigeria is about 30% to 40% of the production cost, while in countries like China, it is just 5% to 10%. According to AfDB (2017), Nigeria's manufacturing sector recorded a general decline in 2016. It has been estimated that about 272 firms have shut down, which causes industrial capacity utilisation of electricity to automatically drop to 35.4% in 2016 from 51.4% in 2015. Similarly, Aliyu et al. (2015) pointed out that to produce an item in Nigeria will cost 9 (nine) times more than to make it in China because self-energy generation constitutes about 40% of the total production cost. They further stated that MAN (Manufacturers Association of Nigeria) reported that about $11,340 million is spent on fuelling and maintaining fossil-fuelled generators weekly. The high cost of production will increase the retail price of an item, and if an alternative is available, the consumer might want to obtain the cheaper option. This data indicates that the lack of a stable electricity supply seriously affects the country's industrial and manufacturing sectors. The self-energy generation is not an alternative to enterprises such as communication companies in Nigeria because it is almost their primary source of electricity. These companies require a steady and uninterrupted electricity supply to power the network and support communication technologies).

Consumption of electricity has significantly reduced in the industrial sector but increases in residences. According to Oseni (2011), energy consumption decreased from 62.9% to 9.7% from 1970 to 2005 and reduced by 20% in 2011. Similarly, the researcher further stated that electricity consumption increased from 37.1% to 63.8% in residences in the same period.

Apart from the adverse effects of fossil fuel generators, their cost of maintenance is very high. The Nigerian government is losing huge sums due to power outages. Trillions of Naira (Nigerian Currency) is spent on running and maintaining fossil-fueled generators. The Nigeria Council for Renewable Energy (CREN) estimates that power outages lead to a loss of N126 billion (US$ 984.38 million) annually (CREN 2009, cited by Nnaji et al. 2010). In Nigeria, most commercial businesses, either large or small, rely on generators as their source of electricity. According to Oyedepo (2012a), the South African telecommunication giant and the largest mobile company in Nigeria (MTN) is estimated to have 6,000 generators installed in their various base stations in the country and are operating for about 19 hrs/day, which requires diesel that totals about $5.5 million monthly. Similarly, this applies to their counterparts, such as Airtel, GLO, and Etisalat. Yusuf (2014); Akuru et al. (2017) reported that about ₦350 billion is spent on an annual basis by industries on fuel to power generators to produce electricity, and this is part of the estimated total of N796.4 billion spent in the country annually on fuel generator sets for electricity generation. Similarly, Ayodele and Ogunjuyigbe (2015) also reported that it had been estimated that N3.5 Trillion had been spent on running and maintaining fossil-fuelled generators in Nigeria. This has placed Nigeria as the highest user of generators globally, with more than 60 million households having their generators, making the country the highest importer of generators in the world (Ayodele and Ogunjuyigbe, 2015). Considering the high costs of fossil fuel alone used in running power generators in Nigeria, it is evident that renewable energy such as solar energy systems is becoming a cheaper alternative (Mohammed et al., 2017).

According to Oyedepo (2012a), despite the abundant natural resources reserves (fossil fuel and others) in Nigeria, with the present rate of exploitation and extraction, it has been estimated that reserves (of non-renewable energy) will be low to the point where it would be uneconomical to continue the exploration after the next 40 years. It will, therefore, become necessary to start exploring and triggering the adoption of other alternative sources such as renewable energy systems and implement them as soon as possible. The renewable energy potential in the country is enormous, and according to Sambo (2009), renewable energy in Nigeria is a viable solution to the current energy crisis in the country.

The country's potential is more than 1.5 times that of fossil fuel resources in energy terms (Shaaban and Petinrin, 2014). Harnessing renewable energy resources such as solar energy can solve all the persisting problems affecting the country's electricity supply, thereby promoting sustainable urban and rural socio-economic development. Aliyu (2017); Shaaban and Petinrin (2014) point out that solar energy is the backbone and driving force of the other renewable energies such as hydro, biomass and wind. Ozoegwu et al. (2017) also believe that solar energy should be considered the highest priority as a source of energy both in Nigeria and worldwide.

1.3 Problem statement

Given the above energy crisis and the extremely strong evidence to support employing renewable energy, particularly solar energy, as a possible solution, the study has identified that PV penetration is facing technical barriers such as environmental factors (dust accumulation) that prevent it from generating optimal yield a couple of days after installation. Dust accumulation or soiling presents a significant challenge to PV's performance in arid and semi-arid regions by preventing the light from reaching the solar cells that could get excited to generate electricity. The dust deposition rate is location dependent, highly related to human activities, and influenced by several factors. Nigeria requires immediate integration of renewable energy to resolve its energy deficit and achieve sustainable development goal seven (SDG-7), ensuring access to clean, reliable, sustainable and affordable energy for all. Moreover, solar photovoltaic is the most suitable option for the region as recommended. However, the Saharan dust activity could significantly impact the PV in the Northern region, while soot from oil exploration could adversely impact the technology performance in the South.

1.4 Aims and objectives

This study aims to address an energy deficiency by investigating the primary factors influencing the occurrence of a barrier that reduces the PV penetration through its performance reduction or failure in a region with massive solar energy potential. It also aims to provide a solution that would sustain the technology's performance to encourage acceptability and ensure clean energy delivery to all.

The objectives of this study are outlined as follows:

- To review the Nigerian energy crisis, renewable energy, and focusing solar energy potential and penetration in the country.
- To review the impact of soiling on PV performance in a global and local context.
- To investigate the influence of dust particle samples on soiling considering two deposition approaches (wet and dry) on two different covering materials (acrylic plastic and low iron glass).
- To design and develop a low cost and durable soiling station that could provide accurate optical loss data and investigate angular dependencies of soiling rate.
- To investigate the influence of weather parameters (wind, rain, and humidity) on PV soiling and correlate the PV yield performance in both standard test and extreme outdoor conditions.
- To investigate the correlation between optical losses and PV yields.
- To develop a soiling map that illustrates PV soiling and correlates the PV yield considering soiling losses through optical losses with a PV yield with a constant soiling rate.
- To develop a mechanised cleaning and a self-cleaning coating on a coupon (low iron glass or acrylic plastic).
- To examine, evaluate, and correlate the performance of five soiling mitigation techniques in extreme outdoor conditions and provide a recommendation to enhance PV performance in the region.

1.5 Research questions

The following are the research questions this study attempted to answer:

- How can Nigeria bridge the gap between energy supply and demand in the country?
    - What are the challenges hindering PV penetration in the country?
    - How can PV penetration in the supply mix be increased in Nigeria?
    - Why is PV a viable option in Nigeria?

- How can solar PV failure be reduced in Nigerian?
  - What are the causes of PV failure in Nigeria?

- How is the impact of factors influencing soil to be determined?
  - What are the factors influencing dust accumulation on the PV surface?
  - What is the cause and impact level of each influencing factor?
  - What are the regional variations on each influencing factor?

- How can the impact of soiling on PV performance in Nigeria be determined?
  - What is the effect of seasonal variation on the performance and efficiency reduction of various PV types due to soiling?

- How can soiling rates across Nigeria be determined?
  - What are the effects of seasonal variation across regions?
  - What are the variances of soiling impact across the country?
  - What are the main parameters that could be used to predict PV soiling in the country?

- How can solar PV performance be prevented and/or restored from the effect of soiling in Nigeria?
  - What are the performances of various soiling mitigation techniques in Nigeria?
  - What is the most suitable cleaning technique and PV covering material to be adopted in the region?

1.6 Thesis contribution

Few soiling research studies have been conducted in sub-Saharan Africa, which lies within the Sun Belt and has a significant potential of unpredictable and extreme weather and environmental conditions. It is a region with a considerable energy supply deficit and striving to invest a massive percentage of its annual budget towards renewable energy. It is imperative and remains a prerequisite to investigate and report soiling losses, leading to identifying a cost-effective yet

appropriate mitigation technique to sustain PV performance at optimum yield across the region.

In this regard, this thesis provides comprehensive information on PV module soiling based on the most current research to stimulate the research community, PV system developers and installers on how dust can affect the PV performance in an area with high solar potential and less PV penetration such as Nigeria towards further research.

Chapter three of the thesis provides an approach illustrating optical and soiling loss rates of various dust particles considering seasonal variation and PV surface covering materials, which could be adopted for determining the extreme impact of a dust type on PV performance for a region with a similar airborne dust type.

Chapter four of the thesis highlights the impact of soiling, considering tilt angle as an influencing factor. It aims to resolve the threats of concern and attract potential investors and policymakers to finance PV projects, accelerating the technology's penetration and reducing greenhouse gas emissions. It has designed, developed and provided a unique, low-cost approach to determine soiling rates at different angles, different periods with their equivalent power losses and mass of accumulated dust that could be used by policymakers, PV companies, researchers, and potential PV investors. The results provided data could be used to estimate periods when soiling is causing significant PV performance and efficiency decrease in the region, and the data could be used to determine the type and frequency of mitigation required.

Chapter five of the thesis provides valuable first-hand in-situ PV performance information considering the effect of soiling on Bayero University Kano (BUK), Nigerian Government, PV soiling community, and scientists at large, highlighting the causes of PV performance reduction.

Chapter six of the thesis provides an innovative mapping approach by employing a low-cost technique to determine optical losses and illustrate them as soiling losses across the country's region. The development of a novel approach is

motivated by recent progress made by Global Solar Atlas (GSA) for providing solar energy information, which could be improved by adopting the method used in this thesis since it offered a low-cost soiling station that could be used to determine the actual regional soiling rates. The findings from this study may lead to a better understanding of soiling problems since the work highlights the significance of the effect of soiling, considering environmental differences as an influencing factor. The findings provided a more accurate and realistic soiling information rate for better PV installation and maintenance planning to achieve higher yields.

Chapter seven of the thesis has twofold novelties: first, developing and examining different mitigation approaches in the outdoor condition in a region with massive investment in solar PV. Secondly, investigating the system performance using a multivariable approach. The findings, if adopted, could prevent future unnecessary PV output losses due to soiling in the region. The study demonstrated a low-cost method to investigate the most suitable techniques for a region.

It is hoped that this document will provide PV engineers with adequate knowledge for planning and designing an advanced system that can address the effect of dust on the technology and which is correlated to the environment and human activities. This subsection of the thesis contributes to the body of knowledge in soiling on PV by providing unique approaches and can guide engineers in selecting solar farm sites and planning for adequate mitigation techniques for optimum yield. The findings could stimulate further research on sustaining PV performance. It could serve as a foundation to estimate the possible frequency and financial commitment for PV farm maintenance, enticing prospective stakeholders and governments to be confident about investing in the sector, knowing that investment would last longer and yield profit.

1.7 Thesis outline

This sub-section highlights the content of the study as illustrated in appendix 1, and the thesis is divided into eight sections with the following outlines:

Chapter two x-rayed Nigerian energy demand and supply status and highlighted all the available renewable energy resources. It provides a critical description of Nigeria's energy scenario showing the immediate requirement of renewable energy intervention based on the resource's availability and potentialities. The chapter concentrates on solar energy, highlighting its potential, penetration and barriers behind its low penetration into the country's supply mix. Several issues are presented, and a technical challenge (impact of soiling on PV) is selected and adequately investigated, and a comprehensive review is provided. Various factors influencing soiling on PV and their implications were identified and discussed. The effect of soiling on PV performance is reviewed, and some mitigation techniques are explored.

Chapter three provides a detailed investigation of dust accumulation's effect, focusing on dust particles and PV surface materials as influencing factors. 13 dust particles were employed to investigate the impact of soiling on optical transmittance and PV yield considering dry and wet deposition.

Chapter four explores the angular dependencies of dust accumulation: a low iron glass coupon is exposed on an in-house developed coupon holder at three positions horizontal, tilt (45°), and vertical considering annual, seasonal, and monthly variation to determine the position that promotes higher accumulation.

Four PV module's performances were examined in chapter five in a region with high solar energy potential, a wide gap between energy supply and demand, and incoming massive PV investment. The module's performances are initially determined under STC (standard test condition) and exposed to external conditions in a region with a high atmospheric dust pollution rate. The site's meteorological parameters are collected to allow a detailed analysis of how the various conditions influence dust accumulates on the PV surface, impacting its performance. Furthermore, glass coupons are also exposed, considering the time variation to determine the accumulation rate and identify particle morphology.

The effect of soiling on PV performance, focusing on environmental variables as factors influencing accumulation, were investigated in chapter five. Low iron glass coupons are exposed in seven locations across Nigeria at three positions; horizontal, tilt (45°), and vertical considering annual, seasonal and monthly variation. Optical loss data are collected and employed in developing a soiling map that can be used for PV installation planning and maintenance cost optimisation. The soiling map is compared with a map published on the Global Solar Atlas (GSA) website, and variations were presented. It examines the accumulated dust samples and identifies the mineral's diaphaneity. Also, the weather and air quality index (AQI) was employed for analysis purposes to determine the cause of accumulation on coupons in each region.

Chapter seven provides a comparative investigation on five main cost-effective mitigation techniques using two PV covering materials and considering seasonal variations in the arid region of Northern Nigeria. A manual cleaning using water/ squeegee and manual cleaning with a brush were employed as the manual approaches. Coupons are left without cleaning to represent natural cleaning. A mechanised platform was developed and engaged in performing automated or mechanised cleaning. At the same time, a hydrophobic coating was employed to represent a self-cleaning approach. The optical losses findings of the exposed coupon are used for the performance analysis of each technique. This is to establish the most suitable, cost-effective cleaning approach in the region.

2 Chapter Two - Review of Nigerian solar energy outlook

Grant and Booth (2009) provided an analysis of 14 types of reviews and their associated methodologies, and each was analysed against Search, Appraisal, Synthesis, and Analysis (SALSA). Among the review types provided, state of the art review was adopted since it addresses current issues and identifies areas requiring further research. This research employed search engines such as Google, Google scholar, science direct, researchgate, scoupus and Exeter learning environment as literature review sources. The keywords used were soiling, dust accumulation, dust formation, Nigeria, atmospheric dust, PV performance and mitigation techniques. A wide range of sources was considered, including papers from the early 1980s to 2021.

2.1 Renewable energy potential

Renewable energy is the energy that is replenishing and non-deplete-able. It can guarantee energy security, promote national development, reducing/ eliminating Green House Gas (GHG) emissions, and conserve non-renewable energy and eliminate or reduce their cost price (Okoye et al., 2016). The country has enormous potential for renewable energies, which are mostly unutilised. It has been established that Nigeria is blessed with abundant renewable energy such as biomass, hydro, solar and wind energy. The potential of these renewable energies is discussed in the subsequent section, and a summary is provided in Table 2.1.

Table 2.1: Summary of renewable energy potential in Nigeria.

Resources		**Potential Capacity**	**Utilisation**
Biomass	Agricultural Resources	697.15 TJ	43.4 million tonnes of firewood/yr.
	Municipal Waste	2.04 million m^3	
	Animal Waste	6.8 million m^3	
	Forest Resources	73,800 m^3	
Hydro	Large Scale	11,250 MW	1972 MW
	Small Scale	3,500 MW	64.2 MW
	Northern Part	25.2 MJ/m^2/day (9 hrs)	

Solar	Southern Part	12.6 MJ/m^2/day (3.5 hrs)	About 28 MW solar PV standalone across the country. No solar thermal electricity
Wind	Northern Part	4.0 to 5.12 m/s @ height of 10m	2 x 2.5 kW electricity generator; 10 MW wind farm in Katsina (Still under construction)
	Southern Part	1.4 to 3.0 m/s @ height of 10 m	

2.1.1 Biomass

Biomass is the non-fossil organic materials or any living matter derivable from sources such as plants and animals, including their by-products that can be used for the generation or formation of useful energy. Biomass is a chemical compound containing free energy, which can be in solid, liquid, and gaseous form. Electrical, mechanical, and heat energy can be generated when energy is released in breaking down the compound's molecule, generating heat. Nigeria possesses abundant Biomass resources, including but not limited to fuelwood, charcoal, shrubs, grasses, sawdust, forestry waste, crops, animal waste, aquatic wastes, municipal waste and industrial waste. These are categorised into agricultural, municipal solid waste, forestry resources and animal waste (Shaaban and Petinrin, 2014; Mas'ud et al., 2015; Akuru et al., 2017; and Aliyu et al., 2017). The potential of the various sources of biomass mentioned above is discussed in the subsequent section. It is noteworthy that the most utilised biomass in Nigeria is firewood (fuelwood). Monye et al. (2017) stated that about 90% of households in northern Nigeria use firewood for cooking and further estimated that about 72% of the population depend on fuelwood for cooking daily. Emodi et al. (2017) also supported this claim, stating that this is also the case for about 70% of the country's population. Shaaban and Petinrin (2014) reported that Nigeria has an estimated capacity of about 8 x 10^2 MJ of biomass resources, 13 million hectares of woody lands and 61 million tons per annum of animal waste crop residue.

The agricultural resource is categorised as either food crops or agricultural residue, and these resources are currently utilised either for domestic cooking or

industrial application. The various agricultural resources available in Nigeria include cassava, sugar cane, cornstalk, rice husk, palm kernel shell, coconut, cashew nuts, groundnut, sesame, jatropha curcas and castor oil. These resources have excellent potential for producing biofuel. Due to overdependence on conventional fossil fuel, the country has very few biofuel companies. It has been reported that Nigeria's agricultural resources potential is estimated as 697.15 TJ (Mohammed et al., 2013; Giwa et al., 2017; Sambo, 2009). This is a considerable amount and can be viable for practical energy generation.

Municipal solid waste resources are substances produced by human activities. Due to Nigeria's high population, the country has enormous potential municipal solid waste resources with a value of average per capita municipal solid waste varies between Nigeria's cities. According to Giwa et al. (2017), the country generates about 74,428.85 tons of municipal solid waste per day, producing 2.04 million m^3. The municipal solid waste can be converted to bioenergy through an anaerobic digester, steam boilers, burning resources, and gasification. A small number of private and government companies generate adequate energy amounts in the country from this source.

Animal residue implies animal waste products, dumps and remains. This chemical compound can generate energy using various methods and is a very efficient source of renewable energy. Nigeria access these resources through animal dumps from cattle, poultry (chicken, turkey and other domestic birds), goat, sheep, pigs, camels, horses, donkeys, and abattoir remains (consisting of blood, intestines, and other animal remains). Giwa et al. (2017) estimated that about 227,500 tonnes of animal waste are being produced daily, mostly in northern Nigeria, where energy poverty is exceptionally high. This amount of waste can be converted to about 6.8 million m^3 of biogas. This resource is not adequately utilised, with only a few companies using biodigesters were being identified in the country (Mohammed et al., 2013; Giwa et al., 2017; Sambo, 2009).

As earlier stated, firewood is the most used and most widely available biomass resource in Nigeria. The country has a large landmass, and it has been reported

that 12% of the land is mainly forest (Mohammed et al., 2013). In 2014, Nigeria had an estimated agricultural area of 70,800,000 ha and a forested landmass of 7,402,600 ha (FAO, 2018). The country's firewood potential was estimated to be about 73,800 $m^{3,}$ and the firewood used in the country is approximated at about 6 billion MJ in energy content (Giwa et al., 2017). Overdependence on firewood is continuously increasing due to the population rise and economic difficulties that led to excessive deforestation and causing the loss of about 300 000 ha landmass (Giwa et al., 2017). The use of forest resources such as firewood promotes deforestation and gas emissions, which is detrimental to human health and the environment.

2.1.2 Hydro

Hydropower energy generation is a process whereby energy is released to generate electricity using water body movement to rotate mechanical turbines. The amount of energy generated depends on the volume and falling rate of the water. The two major rivers in Nigeria are the river Benue and the river Niger. Hydroelectricity is the first renewable energy contributing to Nigeria's national utility grid's existing electricity energy supply mix. It has an installed capacity of 1,938 MW spread among three-generation plants Jebba Hydroelectric power (HEP) (578 MW), Kainji HEP (760 MW) and Shiroro HEP (600 MW) (Monyei et al., 2017). The country has a total exploitable potential of about 14,750 MW, with large hydro plants having the exploitable potential of about 11,250 MW while the small hydro plants have 3500 MW from 286 sites consisting of 86 small sites, 126 mini dams and 70 micro dams across the country (Vincent, and Yusuf 2014; Ikem et al. 2016). It has been established that Nigeria is an African country with the 9^{th} highest economic potential for hydropower. Several ongoing hydro projects in Nigeria are supported by the World Bank, African Development Bank, UNIDO (United Nations Industrial Development Organization) and the Chinese Government to boost agriculture and generate electricity. Figure 2.1 shows the hydro plant and potential sites across the country.

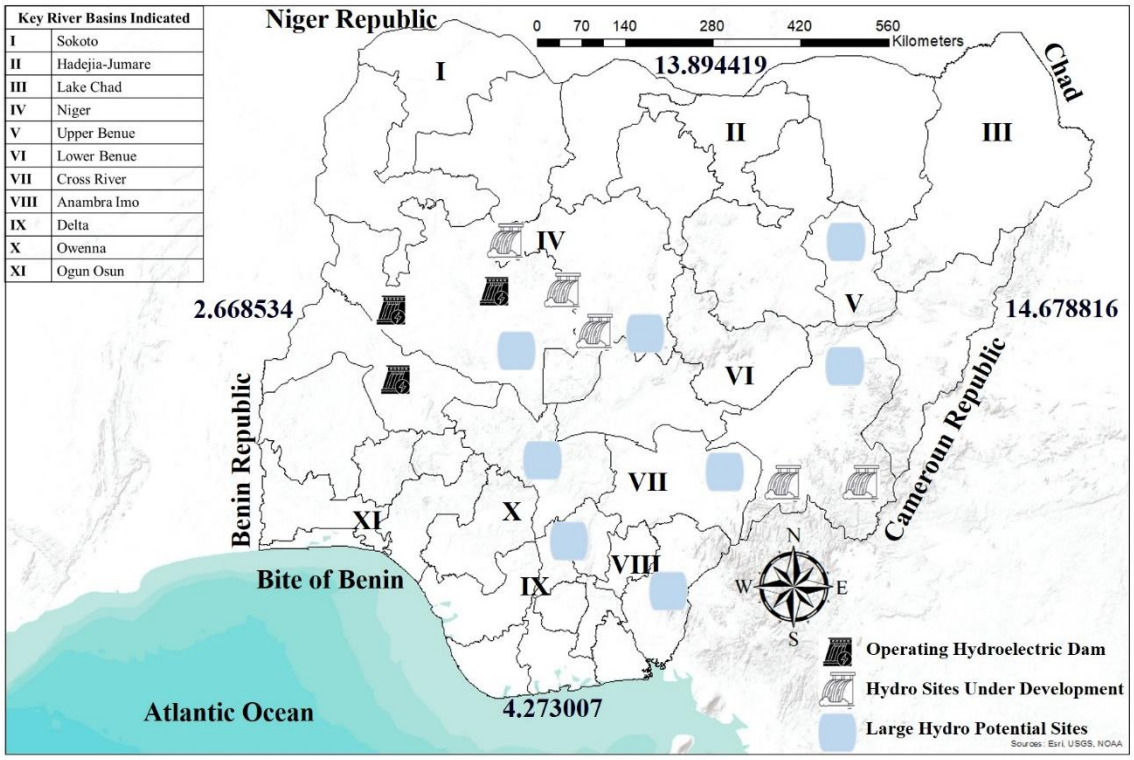

Figure 2.1: Hydropower sites in Nigeria, including operating, undergoing construction, and potential hydropower sites.

2.1.3 Wind

The wind is the movement of air masses triggered by differential heating of the earth's surface from the sun and its consequential pressure disparities. Wind energy is generated when kinetic energy is exploited. It causes the turbines' shaft to rotate (mechanical energy), thereby generating electricity (Akuru et al., 2017). Wind speed is the most crucial factor in wind energy, and the available wind speed in Nigeria varies with season and location. Many researchers have investigated the average wind speed in Nigeria, and most of them concluded that the available wind speed in the northern part of the country is viable for electricity generation. Ohunakin (2010) investigated the wind and its characteristics and reported that Nigeria has an annual average wind speed of 4.570 m/s in the Northern region and 2.747 m/s in the southern region at the height of 10 m. Similarly, researchers (Vincent and Yusuf, 2014; Ikem et al., 2016; Sambo, 2009) also report the wind potential, with an annual mean wind speed of about 4.0 m/s in the far North and about 2.0 m/s in the Southern coastal region at the height of 10 m. AKuru et al. (2017) also reported that the country has an annual mean wind

speed of 2 m/s in the southern coastal region and 8m/s in the far northern region at the height of 50 m.

On the contrary, researchers (Mas'ud et al., 2015; and Shaaban and Petinrin, 2014) reported slightly higher figures stating that Nigeria's wind speed ranges from about 1.4 to 3.0 m/s in the south to about 4.0 to 5.12 m/s in the far northern region. Figure 2.2 shows the average wind speed of various locations in the country, and it is evident that the Northern part of the country has exploitable wind potential. According to the ECN, cited by Mas'ud et al. (2015); Shaaban and Petinrin (2014), Nigeria has a wind energy reserve at the height of 10 m that varies from as high as about 97 MWh/yr in Sokoto (a northwestern state) and about 51 MWh/yr in Jos (a north-central state) to about 8 MWh/yr in Yola (a north-eastern state). These figures highlight the potential of wind in Nigeria.

Despite this abundant wind energy potential in the northern part of the country, wind energy does not contribute to the national supply mix. Few wind projects were recorded in the country, and the first and only sizeable notable wind farm project (10 MW project in Rimi village, Katsina State) that was meant to contribute to the national grid has been abandoned. The country's only successful, famous wind energy application is 0.75 KW in Dan Jawa Villiage of Sokoto State and 5 KW power generating station in Sayya Gidan Gada, Sokoto State (Akuru et al., 2017; Mohammed et al., 2017). Another unique method of wind energy utilisation in the country is water pumping installed in the Kano state during the colonial era.

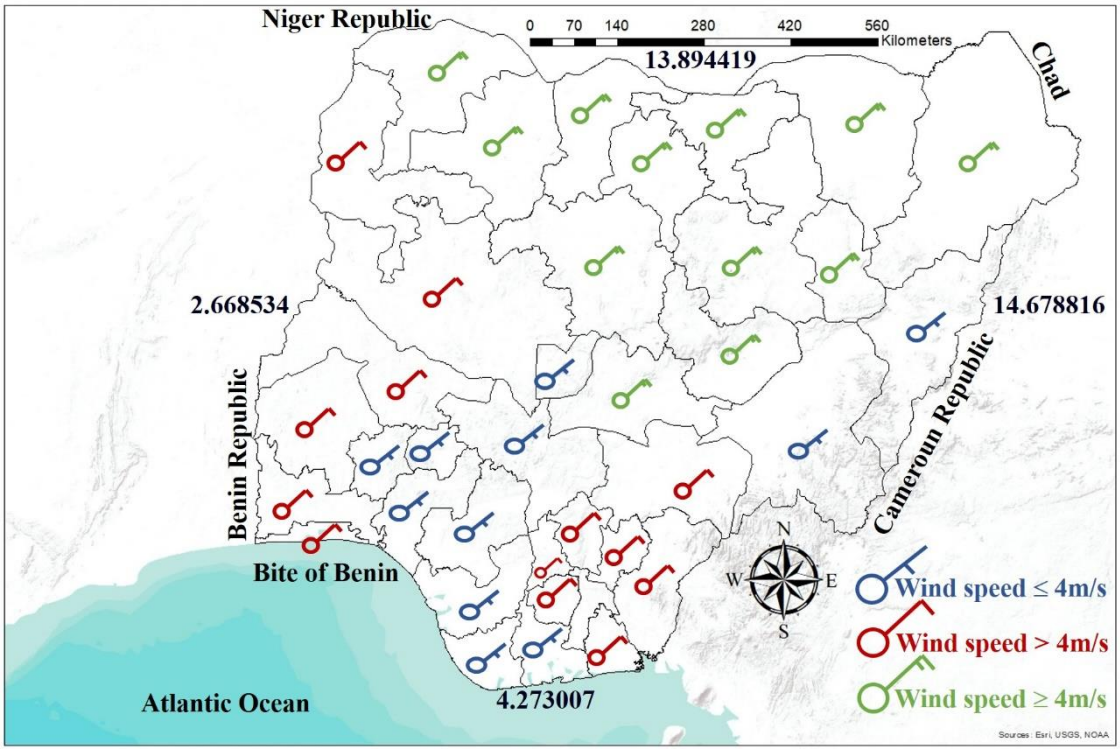

Figure 2.2: Variation of wind velocity across Nigeria.

2.1.4 Solar energy

Solar energy relies on nuclear fusion that emits from the core of the sun. Nigeria is situated in the equatorial region that exposes it to massive solar radiation. According to reports, Nigeria is endowed with intensive sunshine, with an average of 6.25 hours per day, ranging between 9.0 hours in the far northern boundary to about 3.5 hours in the coastal areas, meaning that Nigeria receives average solar radiation of about 12.6 MJ/m^2/day at the southern coastal latitudes and about 25.2 MJ/m^2/day in the far northern part of the country, giving the mathematical average as 18.9 MJ/m^2/day (Nnaji et al., 2010; Ilenikhena and Ezemonye, 2010; Ohunakin, 2010; Bala, 2012). This translates to an equivalent of 229.1667 W/m^2 in power terms (Ilenikhena and Ezemonye 2010; Ohunakin 2010; Mshelia n.d; Akuru et al. 2017; Ozoegwu et al. 2017). GSA. (2021) provided the details of direct normal irradiation across Nigeria, with an average of about 724 kWh/m^2 in the far Southern part and 1653 Wh/m^2 in the far Northern region. This translates into a PV power potential of 1248 kWh/kWp in the South and 1756 kWh/kWp, and this information is further illustrated in Figure 2.3 below. With a total land area of 923,786 km^2, Nigeria receives an impact of solar radiation of about 1500x109

MWh annually, with an annual average of 19 MJ m^{-2} day^{-1} (Ohunakin, 2010). An average of 6,372,613 PJ $year^{-1}$ (approximately 1,770x103 TWh $year^{-1}$) of solar energy received in the entire land area is 120,000 times the total of Power Holding Company of Nigeria (PHCN) electricity generating capacity of 2002, and this energy value was estimated at 115,000 times the electricity generated by PHCN and about 27 times the value of total fossil fuel resources in the country (Shaaban and Petinrin, 2014).

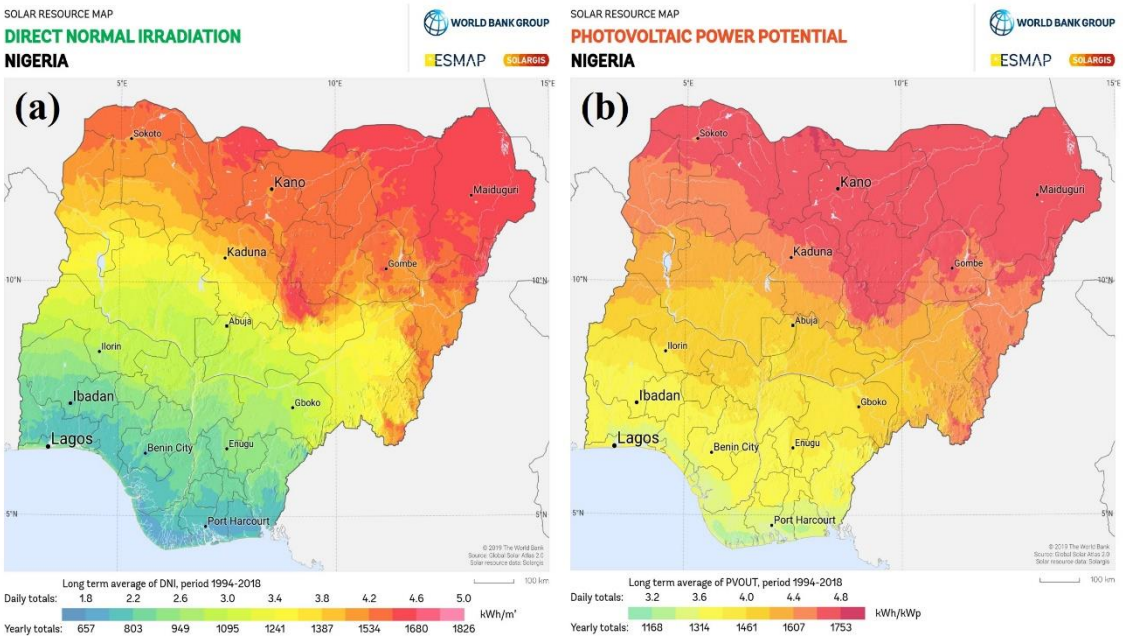

Figure 2.3: Direct Normal Irradiation and PV Power Potential (GSA, 2021).

2.2 Solar Energy Technologies

The Sun is a big ball of plasma composed of 92% hydrogen, 8% helium and other atoms and elements (Nelson and Starcher, 2016), with a diameter of about 1.4 million kilometres. The earth orbits around it at an estimated distance of about 150 million kilometres. The sun's centre can reach a temperature of about 1.5 million degrees Celsius, and the surface temperature is around 5,700°C (Leggett, 2009). Energy is radiated from the centre of the sun to space in all directions with a power of 3.8 x 10^{23} kW, the earth receiving a small portion of this massive energy which is 1.73 x 10^{14} kW (1.35 kW/m^2) (Sundaram et al., 2016; Monyei et al., 2017; Nelson and Starcher, 2016). At the earth surface perpendicular to the sun, the solar insolation is about 1.0 to 1. 2 kW/m^2 (Nelson and Starcher, 2016). The 99.9% of the sun's energy (irradiance) is transmitted between 250 and 2500

nm, where about 51% is near-infrared, 42% visible light and 6-7% ultraviolet light. These are highlighted in Figure 2.4 below.

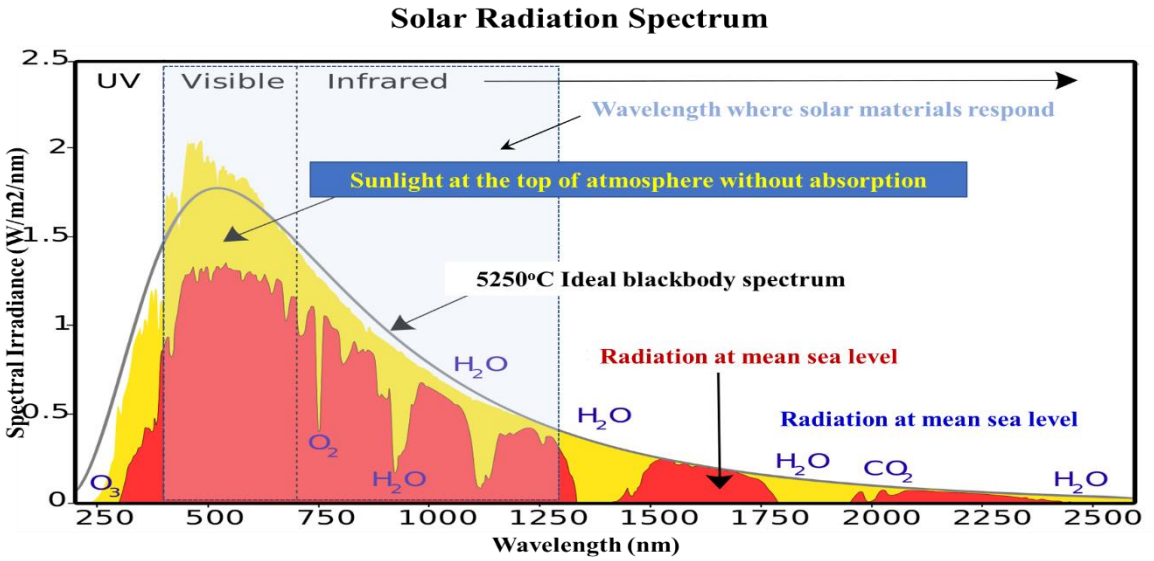

Figure 2.4: Solar Radiation spectrum (adapted from SunWindSolar, 2013).

This energy is inexhaustible, limitless and non-pollutant and can serve as a promising source for electricity generation. Despite this massive amount of solar energy striking the earth's surface, several developing countries such as Nigeria encounter difficulties harnessing the resources. According to Mohammed (2017), several developed countries have recorded electricity power supply stability after investing in solar. Investing in solar energy harvesting technologies can reduce or eradicate energy poverty in the developing world and promote the reduction of Green House Gases (GHG).

Solar energy technologies are devices that convert irradiance into a usable form of energy. There are three main approaches to convert solar energy into electricity: solar photovoltaic conversion, solar thermal conversion and concentrated solar power conversion. These technologies are briefly discussed in the subsequent section of this thesis, emphasising photovoltaic because it is the most utilised solar technology in Nigeria and worldwide.

2.2.1 Solar thermal

Solar thermal conversion is achieved by using the sun to heat a fluid to a certain steam level that can drive turbines to generate electricity. A solar thermal collector uses solar radiation to heat the fluid; then, the evacuating air is the steam that drives the turbines, and the heated fluid is transferred into a storage tank (Leggett, 2009). The required temperature for solar thermal depends on the intended application and the type of solar collector. Solar thermal has many other conversion techniques and can be used for various applications. In Nigeria, solar thermal is used to generate energy for solar cooking, crop drying, incubating, water heating for industries, hospitals, prisons and households (Aliyu et al., 2017). According to REN21 (2020), solar water heating collectors had a cumulative global installed capacity of about 479 GWth at the end of 2019, which is from a 1% decrease from the previous.

2.2.2 Concentrated solar power

This technology converts sunlight into energy using heat. It is designed to collect and concentrate sunlight to generate heat that drives energy generators such as turbines or solar cells to produce electricity (Green Rhino Energy, 2016). Devices such as lenses and mirrors are used to collect, focus, and concentrate solar radiation onto the photovoltaic cell to increase the device's generation and efficiency. This form of electricity generation requires immediate utilisation to protect against overheating in the system. It has been developed to reduce the photovoltaic system's cost by illuminating solar cells with a very high-intensity light using the lenses. Various methods in which concentrated solar energy generation can be accomplished, either trapping the light or utilising the refractive and reflective devices to increase sunshine intensity. The technology is in the market's introductory stage, and in 2019 it has an installed capacity of about 6.2 GW (IRENA, 2020). There is no record of the concentrated solar power technology installation in Nigeria.

2.2.3 Solar photovoltaic

This device uses photovoltaic effects when exposed to solar radiation to generate electricity. Photons become excited when exposed to solar radiation and then release electrons collected by wires to generate direct current electricity that most

needs to be converted to alternating current using converters (Leggett, 2009). The produced energy can be stored using a storage device such as a battery or transmitted to load for utilisation. The device continues to generate output as long as it is exposed to sunlight.

The photovoltaic effect was first discovered by a French scientist named Alexandre Edmund Becquerel in 1883. The scientist observed while experimenting with metal and electrodes. In the same year, the first photovoltaic cell from selenium wafers with about 1% efficiency was developed by an American inventor called Charles Fritts. In 1888, the first U.S. patent for the photovoltaic cell was received by Edward Weston, and in 1901, Nikola Tesla also received another U.S. patent for the technology and a methodology that was capable of utilising solar energy. In 1904, Albert Einstein published the theoretical basis of the photovoltaic effect, which earned him a Nobel Prize in 1923 (Akinyele, 2015). This important development was advanced by a Polish scientist called Jan Czonchralski in the mid-20th century, who developed the silicon cell with 11% efficiency in 1958 at an unaffordable price ($1000/W) (Akinyele, 2015; Kalogirou, 2019). Baurzhan and Jenkins (2016) reported that the Levelized cost of energy generated from the solar photovoltaic system was very high, but with the recent technological development, the price has been decreasing and will continue to decline. Also, Roche and Ifeanyi-Nwaoha (2017) stated that the solar photovoltaic system's cost drastically dropped by 60% between 2010 and 2015 and the technology cost is projected to drop further to 5.9% by the end of the same year. The low cost of technology was due to the higher appetite for the solar photovoltaic electricity harvesting system and massive production (Sundaram et al., 2016). With this rapid declination of PV module prices, there exists a promising future for the technology. However, despite this decline in photovoltaics cost price, some developing countries like Nigeria are yet to adequately utilise the technology's potential and continue to face energy starvation.

The photovoltaic effect occurs when an influx of solar energy hits a cell and gets absorbed by an atom's valence electron, creating pairs of electron holes. The level of electron energy increase according to the amount of photon absorbed.

When the photon's energy is greater than the semiconductor bandgap, the electron with excess energy will escape to the conduction band, where it will have freedom of movement. Therefore, the absorption of photon releases an electron that can be collected by employing an electric field across the cell's back and front (Kalogirou, 2014). When conductors are attached to this electric field with positive and negative terminals, it forms an electrical circuit and electrons are collected in the form of electrical current called photocurrent (I_{ph}). In the absence of illumination, the cell remains inactive and does not produce current. However, if the terminals are connected to a significant external voltage source, the yield is referred to as dark or diode current (R_{S}). Figure 2.5 illustrates the circuit diagram of an individual cell showing series resistance inside the cell and shunt resistance (R_{SH}) from the diode. Considering the aforementioned, the net current is given by Equation (2.1) provided by Kalogirou (2014).

$$I = I_{\mathrm{ph}} - I_D = I_{\mathrm{ph}} - I_O \left\{ exp\left[\frac{e(V+IR_S}{kT_C}\right] - 1\right\} - \frac{V+IR_S}{R_{SH}} \tag{2.1}$$

where I_O is the dark saturation current that strongly depends on ambient temperature, e is the electronic charge given as $= 1.602 \times 10^{-19}$J/V, V is the imposed voltage across the cell, k is the Boltzmann's gas constant given as $= 1.381 \times 10^{-23}$J/K, and T_C is the absolute cell temperature.

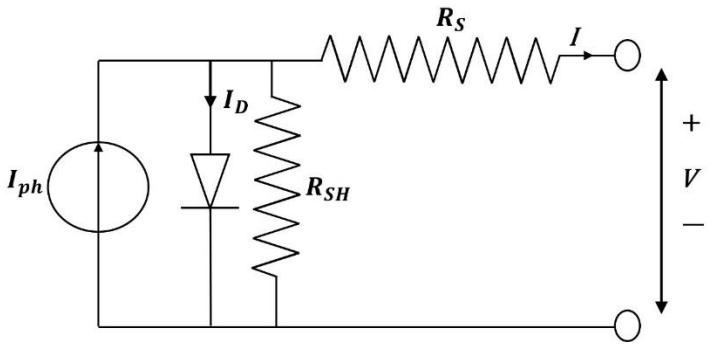

Figure 2.5: Circuit diagram of a typical solar PV cell.

Even though exposure to temperatures and other environmental factors such as dust formation generally reduce photovoltaic technologies' performance with time, the device is highly reliable and can last for an extended period. Bugaje

(1999) reported that a photovoltaic module has an average expected life span of 20 to 25 years. Conversely, a study by Sambo et al. (2014) shows that photovoltaic modules are expected to operate for a period of 30 to 35 years. Solar photovoltaic systems are grouped into first-generation solar cells, second-generation solar cells, and third-generation solar cells (Sundaram et al., 2016).

The first generation is based on silicon and accounts for more than 85% of the photovoltaic industry. Silicon is a natural resource that is abundantly available across the globe. This technology is used in generating electricity in GW. This category of photovoltaic is further divided into three types, according to the design and quality of the silicon, which are: (i) crystalline silicon (c-Si), (ii) polycrystalline (pc-Si), and (iii) thin film (a-Si). These technologies have a high-efficiency rate, with the mc-Si having about 25% efficiency and pc-Si having about 21.5% efficiency (Sundaram et al., 2016; Akinyele (2015). These technologies have been on the market for a long time, and their prices are rapidly declining.

The second generation is mainly based on thin films and were developed to optimise material consumption when designing a solar cell. These are thin layer semiconductors and consume less material when compared to crystalline photovoltaic. The conversion efficiency of these technologies is relatively lower than crystalline technologies. These categories include Copper Indium Gallium Selenide (CIGS), Copper Indium Selenide (CIS), Cadmium Sulphide (CdS/CdTe) and Cadmium Telluride (CdTe) (Sundaram et al., 2016; Akinyele, 2015). The lower efficiency conversion rate has limited the acceptance of the technology in the photovoltaic market.

Third-generation solar photovoltaic aims to reduce the cost of manufacturing by using materials that are more environmentally friendly. Due to the mechanical flexibility and materials used, these technologies have lower efficiency than the second generation. These technologies are undergoing intensive research across the globe to improve their conversion efficiency. The technologies under this category are Dye-sensitised PV, Organic and polymer photovoltaic, Nanomaterial-based PVs and Concentrated photovoltaic (Sundaram et al., 2016; Akinyele, 2015).

The categories of solar technologies mentioned above have been tested to generate electricity from free solar radiation, with no polluting (including air and noise pollution) effect during operation. It can also provide electricity to remote areas that are not economically viable to extend the grid network. Each type of PV system mentioned above responds to illumination in a wavelength range. Figure 2.6 illustrates the spectral response as a function wavelength for various PV types.

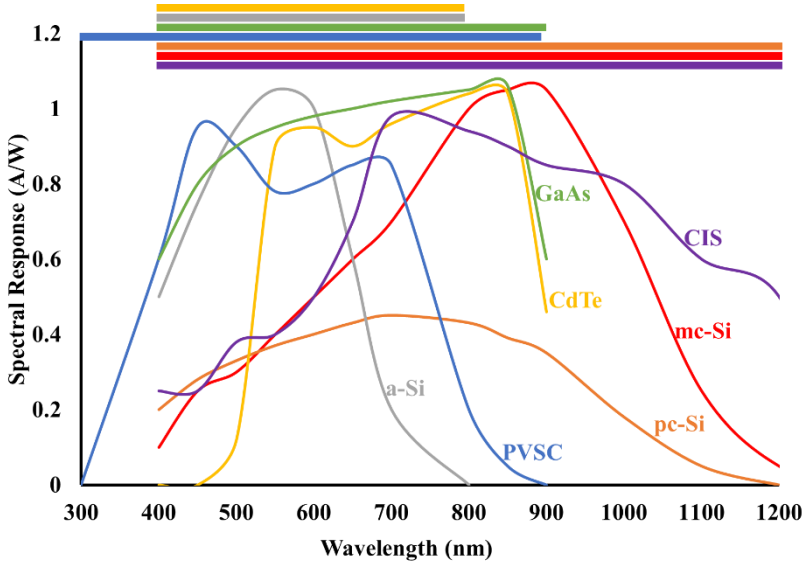

Figure 2.6: Variation of spectral response as a function of wavelength for various PV types.

With the abundance of solar irradiance potential in Nigeria, these technologies can be deployed to resolve the persisting energy crisis that has engulfed the nation for over two decades in rural electrification, residential and commercial buildings, water purification and pumping, street lighting, agricultural and industrial utilisation.

2.3 Solar energy penetration in Nigeria

The solar photovoltaic system is fast becoming the most reliable and promising clean energy technology in the world. Ohunakin (2010) stated that solar energy systems had been proved to be reliable for many decades in developed countries. According to REN21 (2020), in 2019, the global cumulative solar photovoltaic

capacity was about 627 GW and the net annual addition of about 115 GW of electricity in the same year. The yearly increments for a decade starting from 2009 to 2019 is illustrated in Figure 2.7. China alone accounts for 204.7 GW and has one of the largest solar PV plants (2.2 GWp with 202.8 MW/MWh storage) (IEA, 2020). Mohammed et al. (2017) and Ozoegwu et al. (2017) reported that most of Nigeria's available solar energy system installations are limited to simple load electricity appliances in households and street lighting.

In contrast, Sambo (2009) reported about 15 MW of isolated solar photovoltaic installations across the country. Also, many standalone installations of solar energy systems in the country are not adequately documented; this has resulted in the inaccurate data aggregation of solar PV penetration. Ozoegwu et al. (2017) stated that there are no accurate figures for the status of solar energy penetration in Nigeria, meaning there is no comprehensive statistical record such as a database for the deployment of solar energy technology in the country, which shows that the utilisation of solar energy is difficult to be ascertained highlighting that penetration might still be weak. Monyei et al. (2017) and Mohammed et al. (2017) concurred and supported this claim by stating that there is no exact and accurate data on the status of solar energy penetration in the country.

Nigeria's solar potential is very high but not adequately exploited. The Northern part of the country receives more solar radiation than the Southern region, and for that reason, it will be more suitable for solar electricity generation. If only 1% of the northern Nigeria land area is made available for electricity generation from a solar energy system using 5% efficiency, about 333,480 MW of electricity may be generated at a 26% capacity factor (Bala, 2012). As attractive as this may seem, the implementation concerns cannot be overlooked because it is practically impossible. Recently, in an attempt to integrate solar energy into the supply mix, the Federal Government approved a policy called National Renewable Energy and Energy Efficiency Policy (NREEEP), which intends to increase the percentage contribution of solar energy to the total energy supply mix to about 3% by 2020 and 6% by 2030 as the minimum contribution (NREEEP, 2015). Also, National Agency for Science and Engineering Infrastructure (NASENI) is a company that has been established to develop solar modules in

the country to promote and enhance the penetration of the technology. Aliyu et al. (2015) observe that solar energy penetration in the country is prolonged and further claimed that technology's cost is 20 times higher than conventional fossil fuel. A few years later, Mohammed et al. (2017) stated that solar energy technologies are now becoming relatively affordable as more households in the developed world are using the technology, and it is strategically vital for developing countries to adopt the technology as most of them are located around the Sun Belt in regions with high solar radiation.

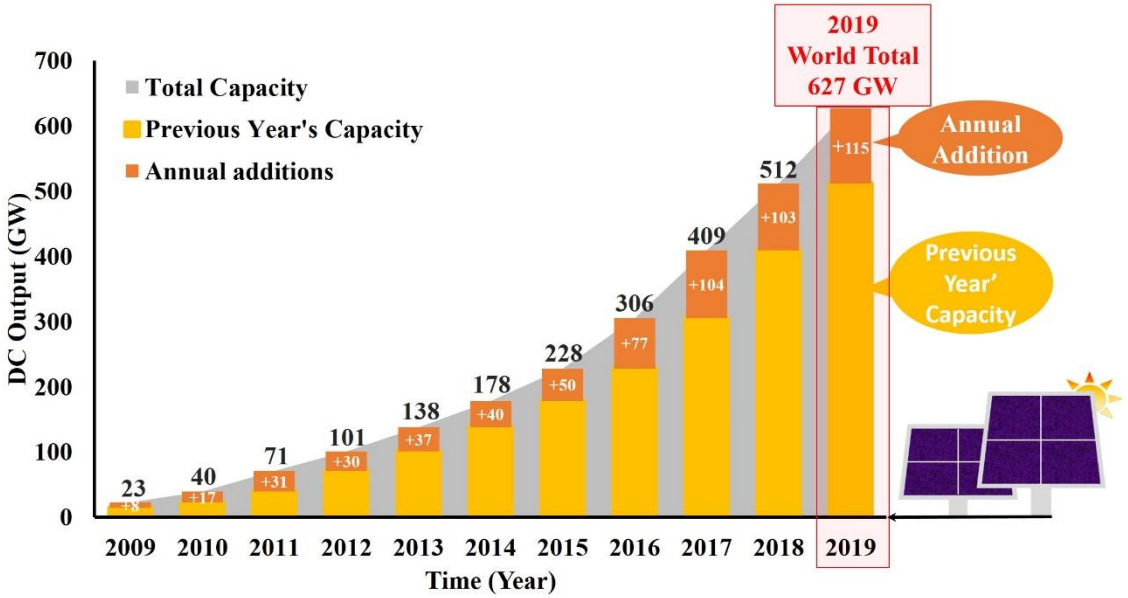

Figure 2.7: Solar Energy Installation (adopted from REN21, 2020).

Ozoegwu et al. (2017) stated that integrating solar energy systems into Nigeria's national grid in the past is nil, currently is also nil, and future status may only be seen on memoranda of understanding. In contrast, some large solar farms were recently commissioned: 1 MW in Bayero University Kano (Nigeria electricity hub, 2018), 7.1 MW in Bayero University Kano (Energy-storage, 2019), and 1.2 MW in Usman dam (Off-grid Nigeria, 2017), Abuja. Also, several solar farm projects are under construction, such as 100 MW in Sokoto, 50 MW in Nasarawa State, 100 MW in Katsina State, 100 MW in Kaduna State, and 100 MW in Bauchi State (Evwind, 2017). A total of 27.96 MW PV installations has been reported towards the end of 2019 (IRENA, 2020). However, the amount is meagre than other developing countries in the region, as illustrated in Figure 2.8. The countries with

less energy demand, a smaller population than Nigeria has high PV penetration rates even though Nigeria started using technology long before them.

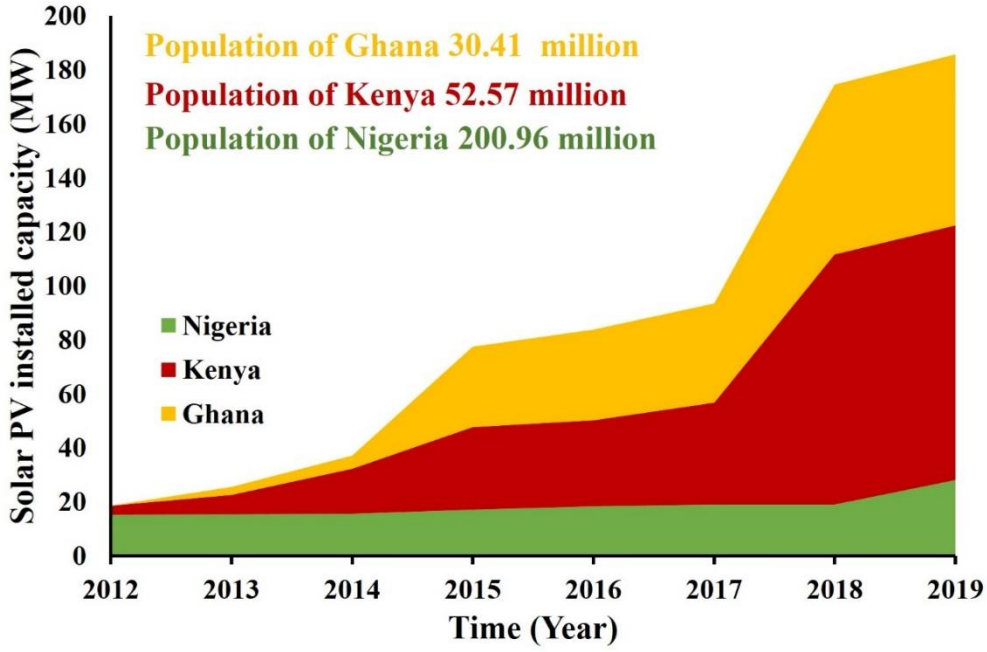

Figure 2.8: Variation of solar photovoltaic installation capacity among three sub-Saharan countries.

However, there are a large number of ongoing on-grid solar energy projects in the country, as earlier mentioned, and some additional ones are: 1 MW solar project, which the French oil company launched in Northern Nigeria (Aliyu et al., 2017); 58 projects embarked by the Energy Commission of Nigeria (E.C.N.), 3 MW of utility-scale solar photovoltaic (PV) projects by the Delta State Government; Zamfara State solar electrification, 600 projects by the Rural Electrification Agency; Niger State 300 MW solar power plant and the Anjeed Kafanchan 15 MW among others. The Nigerian government signed a memorandum of understanding (M.O.U.) with a United States-based company to provide 1200 MW electricity from solar PV projects within two years at the cost of over USD 2 billion (Mas'ud et al., 2015), the project is still at the documentation phase five years later.

The significance of solar energy development and integration into the supply mix is clear and well recognised. Aliyu et al. (2015) hold the view that solar energy

technology has an enormous advantage to resolve the energy poverty of small settlements in remote areas that are not connected to the national utility grid and provide other necessities such as rural clinic electrification, water supply, traffic lighting and school lighting. Ohunakin et al. (2014) also point out why solar energy should be integrated into the country's supply mix. These reasons are: solar energy can reduce the CO_2 footprint, provide energy security, improve supply, improve rural electrification and create job opportunities. Nigeria must bridge the gap between demand and supply by using renewable energy technology such as solar to overcome its present electricity crisis and pursue economic prosperity.

2.4 Challenges facing solar technology penetration in Nigeria

This thesis also highlights some challenges confronting solar energy penetration in the country, and without good penetration, sustainable development would be compromised. Ohunakin et al. (2014) highlighted the drivers and barriers of solar energy penetration in the country, such as lack of public awareness, government policy, theft, and vandalism. Furthermore, literature provided a number of these issues, which are summarised and categorised into three groups as follows:

2.4.1 Technical

2.4.1.1 The present level of research and development

There is no in-depth research on the challenges confronting solar energy penetration in the country, and most local research centres are neglecting this aspect. There is no state-of-the-art research on technological development related to solar energy in the country due to funding constraints; thus, the technology is yet to become widely available. The country has inadequate human capacity building and related training in solar energy development, installation, and maintenance (Mohammed et al., 2017).

2.4.1.2 Technology and equipment fabrication

Considering solar irradiance potential in Nigeria, the country has a low-level fabrication technology rating. As earlier mentioned, NASENI is the only indigenous establishment in the country recorded to be manufacturing solar

photovoltaic modules; otherwise, all other solar photovoltaic systems identified in the country were imported. Most of them are found to be substandard products.

2.4.1.3 Component failure

Several solar energy technologies in the country tend to drop in performance or become inefficient shortly after installation (Ikem et al., 2016). This component failure is mainly caused due to use of substandard technology and/or environmental and climate effects such as dust formation on the photovoltaic panel's surfaces (Oji et al., 2012). It makes the users turn away from using the devices and gives them a negative image.

2.4.1.4 Technical problem

Fundamental design problems such as suitable geographical site identification, load profile determination, intermittency of resources, and determination of the inclination angle are ignored by inexperienced personnel engaged in a solar installation across the country (Sambo et al., 2014). The country has few professionals capable of designing and installing the appropriate setup for residential, commercial, and industrial buildings but are principally engaged with other solar energy-related activities, allowing inexperienced personnel to handle the installations. There is insufficient technical knowledge of developing energy management systems that can integrate solar energy technology with the national grid.

2.4.1.5 Poor maintenance

Nigerians have a very poor maintenance culture. Many solar photovoltaic projects in the country fail because of low maintenance (Sambo et al., 2014). The solar photovoltaic installations around the country are not kept clean, and with dust particles, bird's droppings and other materials on top of the panel, the system's performance tends to decrease over time.

2.4.2 Economical

2.4.2.1 Affordability

As earlier stated, most Nigerians live below the poverty line, and most of them are residing in rural areas where electricity access is low; as such, most of them

cannot afford to acquire a complete home solar photovoltaic system setup because of the price. The price of solar energy technology and its installation cost is still considered expensive in the developing world, especially among the rural population (Giwa et al., 2017; Ikem et al., 2016; Mohammed et al., 2017; Oji et al., 2012).

2.4.2.2 Cost of generation

The initial cost of installing solar photovoltaic technology is very high compared with other energy harvesting systems such as diesel generators in the short run. However, the technology is far cheaper in the long term. The affordability issue by low-income earners will appear, as most people living without access to the national grid cannot afford the technology (Ikem et al., 2016).

2.4.3 Policy

2.4.3.1 Government policy

There have been policy implementation U-turns over the years by the Nigerian government regarding integrating solar energy in the national supply mix due to ignorance. The government has not yet initiated a substantial subsidy program, incentives and any other palliative mechanism to encourage and attract potential investors to the sector (Giwa et al., 2017; Ikem et al., 2016; Mohammed, 2017). There is a lack of importation taxation waivers in the power sector. According to Ohunakin et al. (2014), import duty for solar technology is about 21%, which is on the high side compared to petroleum and other oils products obtained from bituminous minerals, which is 5%.

2.4.3.2 Lack of awareness

The inadequate dissemination of information related to the enormous solar energy potential in the country and lack of awareness about immense solar energy benefit is leading to scepticism about the deployment of the technology for energy generation (Giwa et al., 2017; Ohunakin et al., 2014; Oji et al., 2012; Mohammed et al., 2017). There is also a lack of awareness regarding climate change and the consequences of GHG emission from fossil fuel utilisation in electricity generation.

2.4.3.3 Theft and vandalism

Solar energy technologies, most especially standalone systems, are prone to theft and vandalism (Mohammed et al., 2017). The region with enormous solar energy potential and high energy demand is more prone to theft and destruction of solar energy technologies due to insecurity and insurgency (Ohunakin et al., 2014).

Solar energy contribution to the nation's energy mix remains very negligible in the country when compared to its potential. This low penetration can be attributed to component failure, low awareness, technical problems, government policy, environmental factors and vandalism. However, many local research centres are making giant strides in technology's research and development to promote it to become a household commodity in the country (Ilenikhena and Ezemonye, 2010). The solar energy system's application to supplement fossil fuel technologies or become part of the supply mix will ensure sustainable energy development, which has enormous advantages.

2.5 Effect of soiling on the PV module

Photovoltaic (PV) materials are designed to convert photons into electricity, where emitted photons give their energy to valence electron and when the photon energy is greater than the bandgap of a semiconductor. The electron with excess would liberate and jump across the crystal to move freely (Kalogirou, 2014; Mekhilef et al., 2012). However, sometimes when the photons are emitted, and only a tiny percentages reach the solar cell because it could be transmitted, scattered, attenuated, absorbed or reflected by the airborne particles or material accumulated on the surface covering the PV cell, such as dust (Mekhilef et al., 2012). The ratio of light intensity that passes through a material to the light intensity that passes without any disturbance is known as light transmittance (Zaihidee et al., 2017). Areas within the global Sun Belt with the abundance of solar irradiance seems to suffer high concentration of atmospheric dust (Kazem and Chaichan, 2019) and this environmental condition (dust) has been identified as the prime degrading factor that causes a deleterious effect on the performance of the PV, particularly in the desert, arid and semi-arid regions such as Nigeria

(Chanchangi et al., 2020; Paudyal and Shakya, 2016). This degradation varies with location and exposure time (Tanesab et al., 2018; Said and Walwil, 2014).

The term dust is defined as a general term for any substance or particles matter of that exist in the atmosphere with less than 500 µm diameter (10 times smaller than the diameter of a human hair), including but not limited to solid inorganic and organic particles such as soil particles, smoke (including factory smoke, vehicular smoke and firewood smoke) volcanic vapour, bacteria, pollen, fungi, microfibers and eroded limestone (Darwish et al., 2015). MSHA (Mine Safety and Health Administration) define dust as finely solid particles that initially exist in the atmosphere without any changes to their physical and chemical properties other than the breakage (Darwish et al., 2015). These particles exist in different sizes, volumes, chemical concentrations and shapes. Also, particle types vary with geographical locations and their local activities. The term soiling refers to how dirt, dust, and contamination are deposited and accumulated on a solar PV module's surface.

Most locations with high solar potential worldwide are either arid or semi-arid, experiencing insufficient rain and pervasive dust, which is considered one of the primary mechanisms that significantly affect PV devices' overall performance (Al Shehri et al., 2016). The formation of dust on the PV module degrades the overall performance and reduces maximum yield during its expected operation period. The degree of performance degradation varies according to the number of influencing factors, which has prompted a significant research interest over the last few decades. Several review papers (Al Shehri et al., 2016; Costa et al., 2016; Costa et al., 2018; Kaczmarski et al., 2016; Darwish et al., 2015; Figgis et al., 2017; S. Ghazi, Sayigh and Ip, 2014; Maghami et al., 2016; Sarver et al., 2013; Sayyah et al., 2014), have highlighted various approaches to the impact of dust on the performance of the PV module and different mitigation methods. In 2016, 80% increased the number of research and development papers related to soiling than those conducted in 2015 (Costa et al., 2018).

2.6 Mechanism of soiling on PV

The soiling mechanism on PV includes dust particles from sources, entrained, transported (globally circulated), deposited to PV module. Figure 2.9 represents the entire soiling process starting from the generation process, including entrainment and transportation, to particle deposition on surfaces where some adhere, and others rebound or removed to become suspended again. This process is the entire life cycle of dust formation on PV, and subsection 2.6.1 to 2.6.3 explained all the phases from generation to re-suspension phase.

2.6.1 Generation of dust

Dust is generated from desert storms, volcanic eruptions, industrial emissions, construction debris, highway activities, vehicle emissions, microscopic organisms, pollen, plant material, dander (dead skin cells shed by animals) and other anthropogenic sources (Darwish et al., 2015). Some dust particles are generated and immediately deposited in the atmosphere, while other particles are initially generated and deposited to the ground surface, then later entrained in the atmosphere due to anthropogenic or natural activities (such as wind and storms). Dust concentration in the atmosphere depends on the local topography, climatic condition, industrial activities and agricultural activities and varies worldwide. Figure 2.10, Figure 2.11, and Figure 2.12 show the atmospheric dust concentration of various locations and their intensity, indicating the MENA (the Middle East & North Africa) region as the location with the highest concentration.

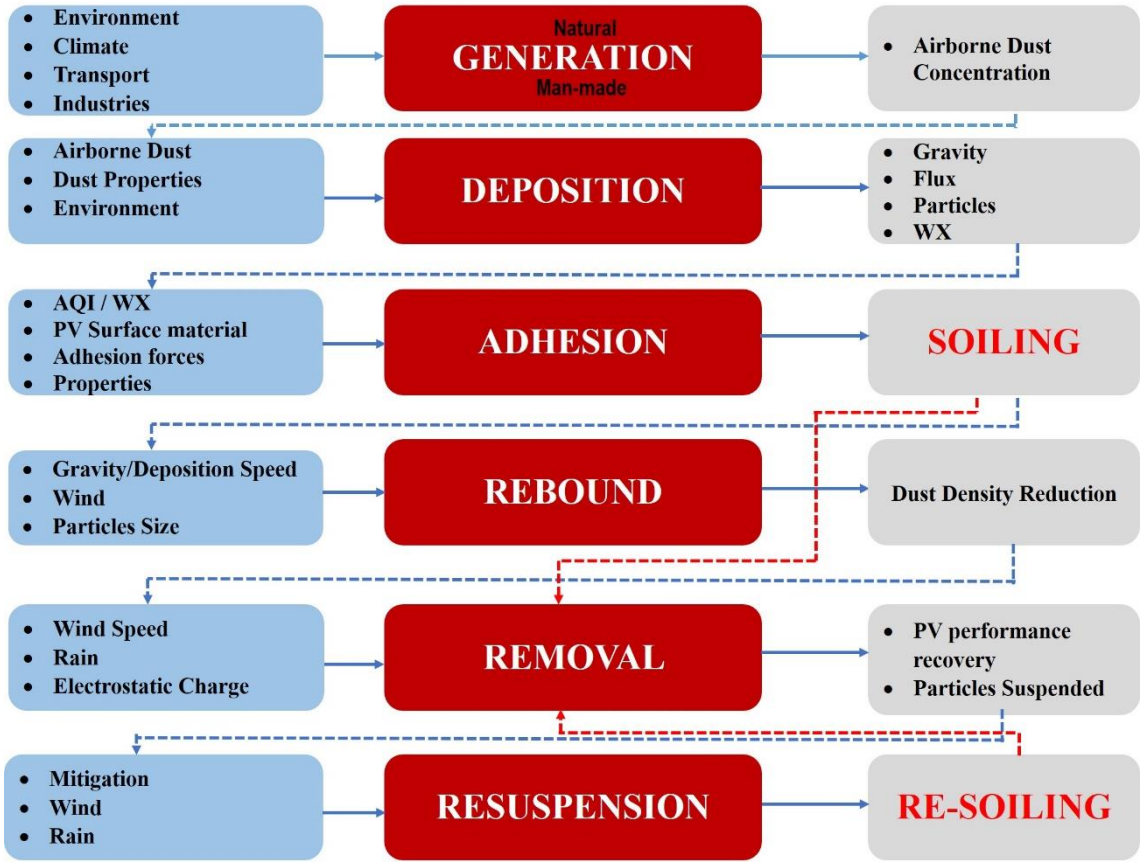

Figure 2.9: Mechanics and phases of soiling.

Arabian Peninsula, Central Asia, North Africa (Saharan and Sub-Saharan Africa), South Africa, Western and Eastern China, Northern and Southern America, and Australia (Longueville et al., 2010; Middleton, 2017; Tanaka and Chiba, 2006) regions are the primary sources of dust generations that contribute to global dust which originates from desert dust. However, these various regions do not have an equal active rate. According to Tanaka and Chiba (2006), the Saharan dust generates about 58% of the total global dust emission and is entrained and contributes about 62% of the total tropospheric dust, as shown in Figure 2.10 and Figure 2.11. Nigeria is located within the giant circle in Figure 2.10, and the country is also positioned within 0°-30°N and 0°-30°E in Figure 2.11, which shows it is within the region having the high loading of global atmospheric loading.

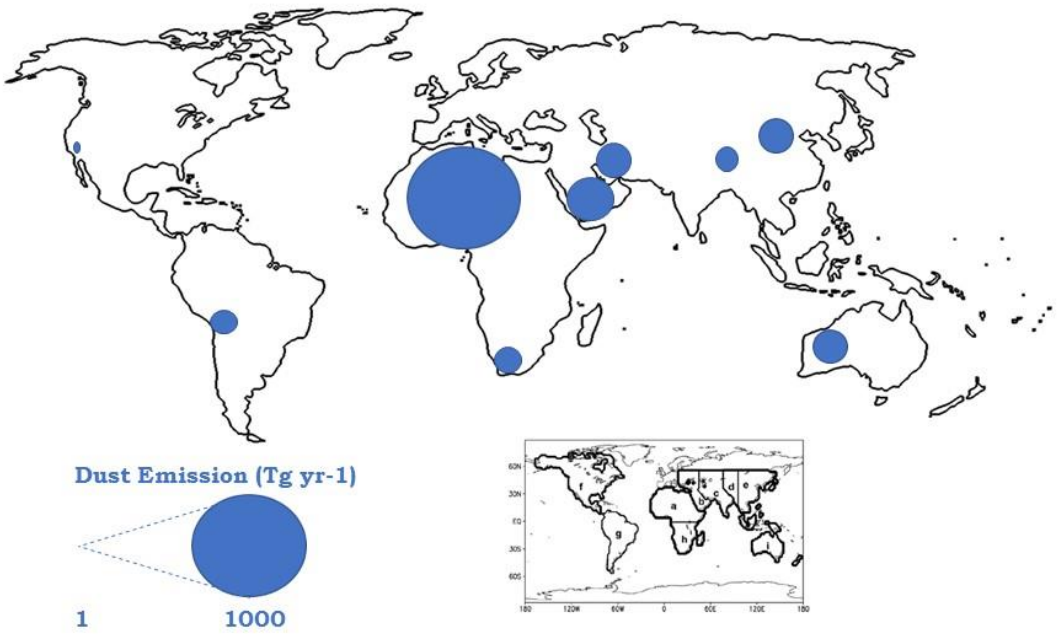

Figure 2.10: Sources and Geographical locations/Borders of dust emissions (Adapted from Longueville et al., 2010).

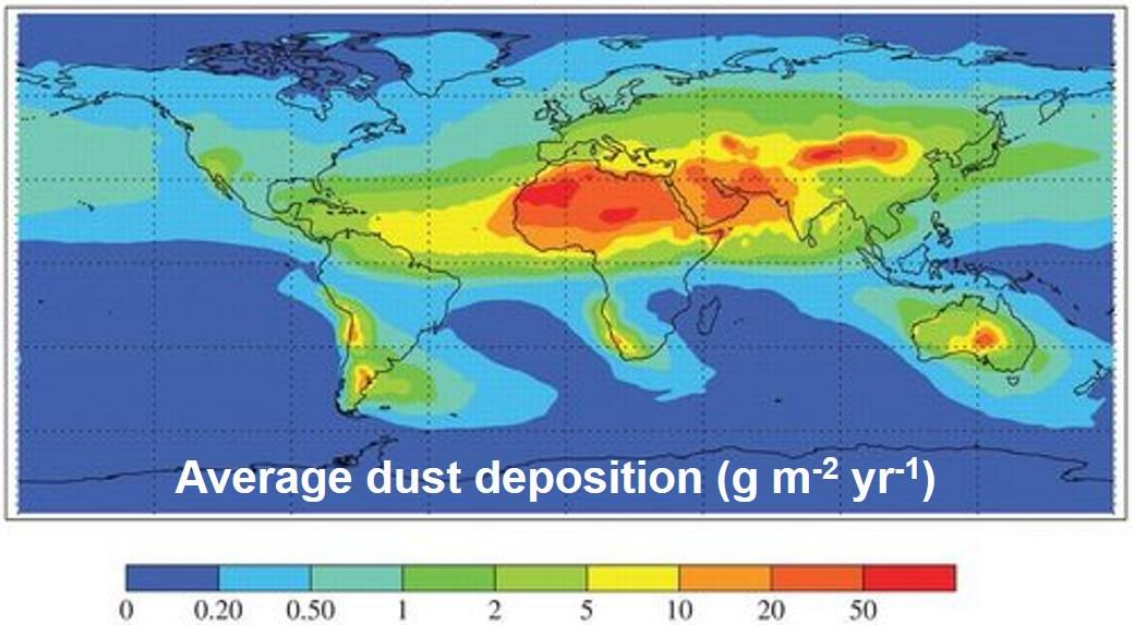

Figure 2.11: Geographical distribution of dust loading in the atmosphere (Jickells, et al., 2016).

There is disagreement regarding the contribution of losses due to the particle size; however, the particulate matter dimension between 0.1 μm to1000 μm with the majority (about 50%) is typical. Researchers (Ghazi and Ip, 2014; Picotti et

al., 2018; Sarver et al., 2013) reported that the diameter varies from a diameter <20 μm and further classified the dust particles according to size:

Deposited Particle Matter – this is any dust that drops from the atmosphere.
TSP (Total Suspended Particles) – particle matter with the size of 50 μm or less.
PM_{10} – particulate matter with the size of 10 μm or less.
$PM_{2.5}$ – particulate matter with the size of 2.5 μm or less (Ghazi and Ip, 2014).

The transportation of dust by air in the atmosphere depends on the shape, size, surface properties and weight of particles (Jamil et al., 2017; Zaihidee et al., 2016). Finer dust particles (with diameter <1 μm) have a greater tendency to uniformly cover the PV cell surface than the coarser (with diameter >5 μm) ones, causing a more significant decrease in solar radiation transmittance (Jamil et al., 2017). Figure 2.12 highlights the various locations with a fine concentration in the world. These properties vary with locations across the globe because of climatic conditions, topography, agricultural, industrial, construction and other human activities. This causes the determination of the actual dust composition to be fundamentally a location-based issue.

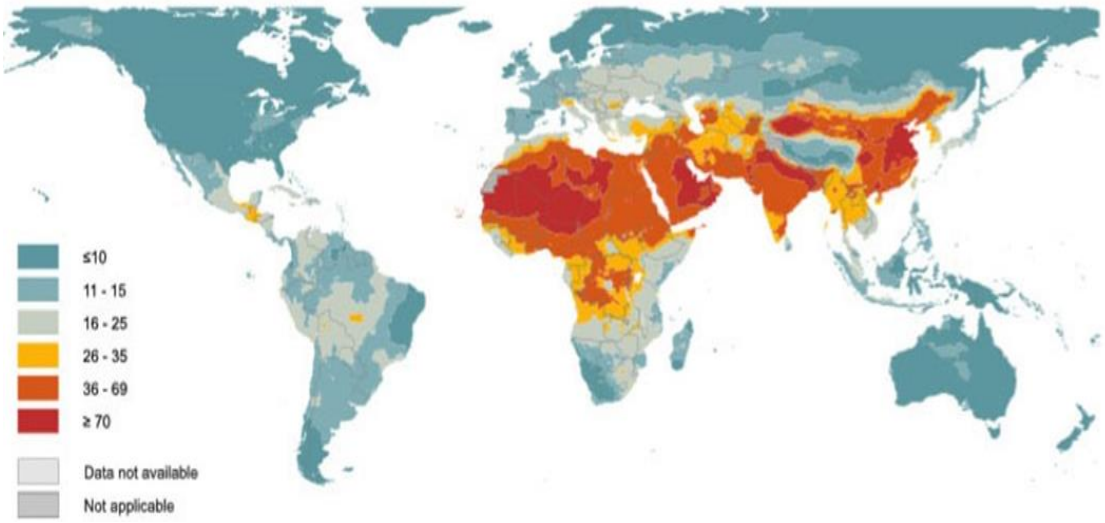

Figure 2.12: Global map with fine dust particles concentrations modelled based on the annual median concentration of $PM_{2.5}$ in $\mu g/m^3$ (Brenneman, 2016).

The threshold friction velocity and the vertical flux are the two major influencing factors for dust generation (Picotti et al., 2018). The generation phase includes the entrainment phase and the transport phase. In the entrainment phase,

particles from erosion, industrial and agricultural emissions are deposited into the atmosphere due to wind flow. Dust is sometimes entrained in the atmosphere through the aerodynamic lift, saltation through aggregate disintegration, while others are emitted from various other sources and become suspended (Picotti et al., 2018). The entrainment activity is dependent on geographical location, climatic conditions and human actions (Middleton, 2017). After generation and being suspended in the atmosphere, dust can be transported over long distances by wind. Middleton (2017) reported that dust from the Saharan desert had been transported through the troposphere over thousands of kilometres to Europe and Sub-Saharan Africa. In northeast Asia, dust is transported from the Gobi Desert to Beijing, Tokyo and Seoul. Dust movement is a transboundary activity that presents a significant challenge.

2.6.2 Deposition of dust on PV

This process involves the settlement of airborne dust particles on a surface. This phenomenon is strongly dependent on wind speed and particle matter (Boyle et al., 2016; Figgis et al., 2017). The deposition rate of dust particles is higher if it is closer to the generation source and declines with distance (Middleton, 2017). The dust deposition on PV is categorised into three groups based on their transport mechanism (Lay-Ekuakille et al., 2018), which are described below.

During the dry deposition process, airborne particles are transported to the PV surface without the water content. In a dry weather condition, dust atoms adhere to the PV module surface because of the adhesive forces (Kazem et al., 2014; Picotti et al., 2018). In a wet deposition, atmospheric dust is contaminated with various precipitations such as fog, rain and snow (Lay-Ekuakille et al., 2018). These precipitations are the transport mechanism that deposits the particles on the surface of the PV module. The shadow deposition mechanism is described as an “intermediary” between the dry and wet mechanisms. This process is when clouds and fog containing water droplets are mixed with dusty air before deposition (Lay-Ekuakille et al., 2018).

Dust accumulation or soiling is an unavoidable factor affecting solar PV module performance and is considered a significant factor after solar radiation and

temperature. A number of factors influencing dust accumulation on a PV module are represented in Figure 2.13 and explained in this thesis subsequent sub-section.

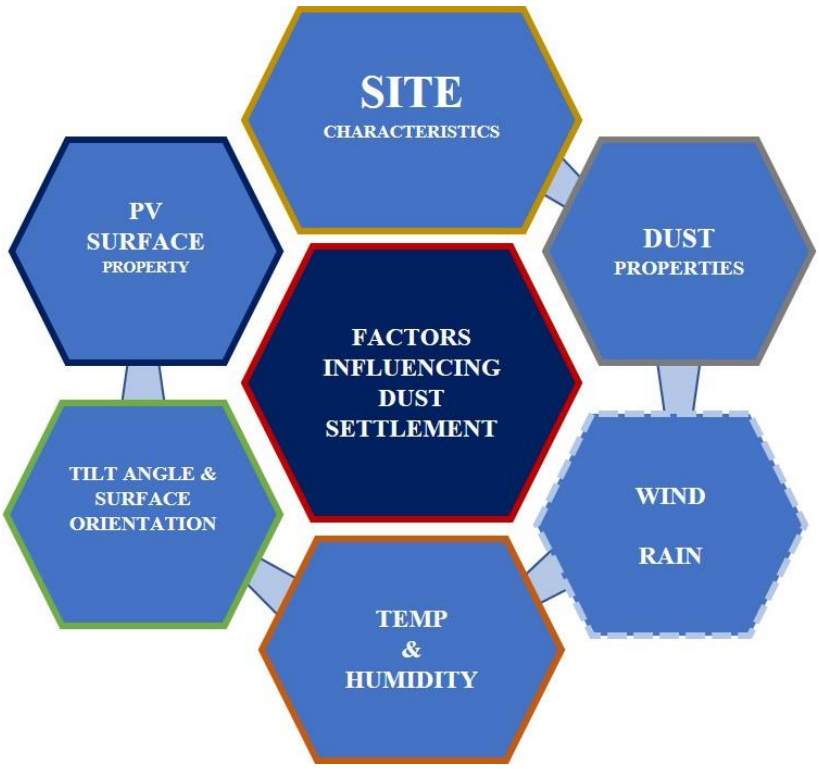

Figure 2.13: Factors influencing dust accumulation on a PV (adapted from Jamil et al., 2017; Mani and Pillai, 2010).

2.6.2.1 Dust Properties/Morphology of Dust

The shape, size, roughness and weight of particles can influence the extent to which light transmission is reduced. The diameter of dust grain includes fine-grain, which is less than 0.05 mm (predominantly clay and silt size), medium-grain, which is 0.05 – 2 mm (mostly sand size) and coarse grain, which can vary between 2 – 57 mm (mainly gravel) (Al-Shabaan et al. 2016; Picotti et al. 2018). The roughness of a dust particle can be fine or coarse. Fine dust particles have a higher tendency to adhesion than coarse dust particles, allowing them to be distributed uniformly over a PV surface causing higher light scattering and lower transmission (Tanesab et al., 2015). In addition, a porous layer allows more light transmittance than a smooth layer (Nirmal et al., 2014). Non-spherical and coarse particles have more potential to cause scattering than a spherical particle with a fine surface (Li et al., 2004). Diagonal or hexagonal particles have higher single

scattering albedo when compared to dust particles with spheroid and ellipsoidal structures (Mishra et al., 2015).

In contrast, Potenza et al. (2016) reported a finding that strongly conflicts with other studies' findings that non-spherical dust particles account for higher transmissivity than spherical. Tanesab et al. (2019) supported this claim and stated that dust structures that appear to have angular and diagonal shapes have better optical properties than spheroids or elliptical. Smaller dust particles have a stronger adhesion force and adversely impact larger particles since they occupy smaller spaces and attenuate light, whereas larger particles leave porous gaps where light can penetrate. Also, smaller dust particles have a stronger adhesion force than the lift force generated by wind and sometimes even more substantial than the lift force generated by rain, limiting the cleaning capacity of rainfall compared with large dust particles (Abderrezek and Fathi, 2017). A deposited dust particle with a greater mass reduces the voltage, ampere and power more than a dust particle of the lower mass (Kazem and Chaichan, 2016).

Characterisation of manual dust deposition on the PV surface has previously been performed within an indoor laboratory environment. The impact of the physical properties of six different types of dust collected from North Oman showed about 30% - 40% degradation of power output and that dust samples with the highest moisture content, specific gravity and plasticity index caused the most significant deterioration of PV performance (Kazem and Chaichan, 2016). An investigation into the effects of ash, sand, calcium carbonate, red soil, and silica on a pc-Si PV module's performance showed ash accounted for about 25% of PV voltage reduction and a more adverse effect on other samples (Kazem et al., 2013). Power output due to carbon, cement, and three classes of limestone deposition showed that finer dust particles could cause more PV performance degradation than coarse dust particles (El-Shobokshy and Hussein, 1993).

Performance degradation of PV due to fly ash, limestone and red soil showed that red soil accounts for the highest reduction in PV performance, followed by limestone and fly ash (Kaldellis et al., 2011). Sulaiman et al. (2011) investigated the effect of dust on PV performance using mud and talcum samples. The results

showed a power output of about 18%, with a 6% difference between the two samples. Wang et al. (2020a) reported high PV yield degradation. The researchers showed that the maximum power of a clean PV module degraded to about 82.1% from the original power after exposure, while a module that was earlier dirty and cleaned before testing degraded to about 46.7%. Their findings show that if a dirty module is subsequently cleaned, it becomes more prone to dust accumulation. Alnasser et al. (2020) examined the effect of dust accumulation on PV performance. Researchers showed that 100 g/m^2 of sand, ordinary cement, egg cement, gypsum, or industrial gypsum, caused 12%, 14%, 15%, 9% and 10% PV yield reductions, respectively. Adıgüzel et al. (2019) investigated the effect of coal on light transmittance and reported 62.05% degradation of PV performance when 15 g of tiny particles (38 µm) of coal were examined and 28.90% degradation when the larger particles (250 -500 µm) were used.

Desert areas are recognised as primary sources of dust as reported by Ilse et al. (2018) and are associated with airborne dust containing mineral compositions such as carbonates, feldspar, gypsum, illite, iron oxides, kaolinite, quartz and smectite. Ilse et al. (2018) reported that dust's mineral composition strongly influences the optical/transmittance behaviour when deposited on a coupon. Sarver et al. (2013) stated that mineral composition is vital to adhesion processes, especially when capillary force is activated.

Zaihidee et al. (2016) reported that PV performance degradation depends on dust deposition density. They further provide a result that shows a decrease of PV performance where short circuit current degrades by about 15 - 21%, open-circuit voltage by 2 - 6% and the efficiency by 15 - 35% when 20 g/m2 was deposited. Klugmann-Radziemska (2015) researched dust thickness and reported that dust thickness on PV is linear to PV efficiency decrease when it is less than 3 µm. Tanesab et al. (2019) confirm the effect of dust deposition density in a study that showed a linear reduction in light transmittance when PV surfaces were deposited with two types of dust which had densities of <0.3 mg/cm^2. Hachicha et al. (2019) investigated the effect of the morphology of dust samples on PV performance. Their result shows a linear relationship between dust density and

normalised PV power, reducing 1.7% per g/m^2. Their result also indicates a decrease in dust accumulation, increasing the tilt angle of 37.63%, 14.11%, and 10.95% concerning 0°, 25°, and 45° tilt angles.

Soiling rate varies with dust property; dust particles that are less than 1µm (finer dust particles) tend to settle and accumulate faster than those with a diameter greater than 5 µm (coarser dust particles) (Jamil et al., 2017). Similarly, particles with a larger diameter are easily affected by inertial and gravitational effects, while particles with a smaller diameter are affected by inter-particle forces such as Van der Waals forces, cohesive forces and electrostatic forces. Also, particles with charged electrostatic properties tend to accumulate faster and settle more than dust particles with neutral electrostatic properties due to coalescence (Sarver, 2013).

2.6.2.2 Surface Property

A PV module's surface property plays a significant role in influencing the dust accumulation rate, varying with various surface fabrications. A surface with a coated (hydrophobic or hydrophilic) layer has a lesser influence on dust settlement than an uncoated layer (Jamil et al., 2017). PV modules surface fabricated from tedlar, plastics, and epoxy tend to have a higher dust accumulation rate when compared to surfaces made from glass (Kalogirou et al., 2013; Zaihidee et al., 2016).

The widely employed PV covering materials based on plastic and glass is ineffective to avert dust accumulation on their own (Chesnutt et al., 2017; Sarver et al., 2013). Shaik et al. (2021) reported acrylic plastic and low iron glass as the commonly employed PV surface covering materials; however, the materials on their own are ineffective in terms of averting dust accumulation (Chesnutt et al., 2017; Sarver et al., 2013). Gupta et al. (2019) highlighted the research gap investigating PV surface covering material and the economic feasibility of various approaches.

2.6.2.3 Local Environment

Geographical site characteristics and their surrounding activities have a profound influence on dust accumulation on a PV module. Local site-specific factors such as human activities, natural topography, and regional development (urbanisation), vegetation and air pollution significantly influence dust accumulation. Cano et al. (2014) stated that site characteristic is the primary determinant of dust accumulation rate in a specific location concurrent with local human and natural activities such as sandstorms, volcanic eruptions, dust haze, bush burning, transportation system, constructions and industries. An area's population density also stimulates dust entrainment and can influence the dust settlement (Darwish et al., 2015).

Ghazi et al. (2014) carried out a preliminary study of environmental particles on solar flat surfaces in the United Kingdom (the UK) and concluded that dust accumulation is a complex phenomenon that varies according to location, environment and climate. Cano et al. (2014) support this claim that tilt angle and surface orientation have a less significant influence on soiling rate on a PV module, claiming that the surrounding environmental condition and activities are the key influencing factors.

As earlier provided in the literature in this chapter of the thesis, there is no uniformity in the soiling rate since it is dependent on the number of variables such as climatic condition, installation orientation, season (dry or wet), duration of exposure (daily, weekly, monthly or yearly), and regional human activities. The impact of soiling on PV performance has been extensively studied in the last two decades (Javed et al., 2017). However, some part of the mentioned region has received less attention over the years. Also, the soiling rate is site-specific, which was proved in research conducted by Micheli and Muller (2017), where daily soiling rates were determined for 20 different sites in the USA. Around the region of this study, Sanusi et al. (2012) reported a 20% reduction of the a-Si module's performance in Southern Nigeria during the Harmattan for two months in 2006 and 2008. Danjuma et al. (2016) reported a 12.46% power loss in Niamey and related reduced weather and dusty conditions in West Africa. Bernard et al. (2016) reported a 28.7% PV performance reduction and relate the loss to dust

accumulation caused by the Harmattan season. These findings were related to the Harmattan season, which adversely affected Northern Nigeria, but none of the studies provided a soiling rate for the region.

Adinoyi and Said (2015) reported a 50% loss of PV performance caused by dust accumulation over six months of exposure without cleaning in the Eastern region of Saudi Arabia. Emziane and Al Ali (2015) reported 84% of optical losses from exposed coupons in the Saudi Arabian desert. These two results are from the same region, yet some differences were recorded, confirming that soiling is explicitly site-specific. Mejia and Kleiss (2013) reported soiling rates averaging from 0.051%/day in the region of California, USA. In contrast, Kimber et al. (2006) reported about 1.5 - 6.2% annual losses in California. Zorrilla-Casanova et al. (2013) observed a daily loss of 4.4% in Spain and predicted the rate could increase to 20% during the dry season. Whereas, Piliougine et al. (2013) reported 12.5% I_{SC} degradation during summer in Spain. Both kinds of research were conducted in the same region of southern Spain city of Malaga. However, the variation has been recorded, which shows the importance of determining the various regions soiling.

Kimber et al. (2006) investigated the effect of soiling on an enormous grid-connected PV panel in the Southern-Western region of the USA and California. They reported 1.5 - 6.2% annual losses, depending on system location. Cano (2014) investigated soiling in the desert of Mesa, Arizona, USA, considering two tilt angles (23° and 33°). The researcher reported a short circuit loss of about 3.75% when the coupon is positioned at 23° and 3.45% at 33° tilt angles.

Liqun et al. (2012) investigated soiling in Taiyuan, China, by considering two tilt angles (0° and 45°) for two weeks. They reported a Pout reduction due to soiling of about 32.6% when the coupon is positioned at 0° and 18.2 % when at 45°. Guan et al. (2017) investigated the effect of soiling on PV in a rural area of Chang'an Xi'an, China, using glass coupons. They reported a 20.62% reduction of Pout when the coupon is positioned at a tilt angle of 35°.

Zorilla-Casanova et al. (2013) investigated the effect of soiling on the incoming radiation to PV in Malaga, Spain. They reported an average daily radiation loss of 4% in the short term and 20% in the longer term. Piliougine et al. (2013) investigated the effect of soiling for ten months during the Mediterranean hot summer in Malaga, Spain. They reported a short circuit reduction of about 12.5% when the coupon is positioned at a tilt angle of 21°. Kalogirou et al. (2013) investigated the effect of soiling on PV performance in Limassol, Cyprus, for ten weeks. They recorded PV performance degradation of about 13%. Pavan et al. (2011) investigated the effect of soiling on energy production for large-scale PV farm in Italy. They reported 6.9% losses when the plant was built on sandy soil.

Kazem and Chaichan (2016) investigated the effect of soiling on PV for three months in Oman. They reported a Pout loss of about 35%. Gholami et al. (2018) investigated the effect of soiling on PV using glass coupons for 70 days in Tehran, Iran. They reported a Pout reduction of about 21.47%. Alnaser et al. (2018) investigated the effect of soiling on PV performance in Bahrain. They recorded a Pout reduction of 55% in October and 63% in November. The annual Pout losses were 7% for a module that was cleaned once and 17% for a module that was never clean at all. Abdallah et al. (2016) investigated the performance of silicon heterojunction PV panels in Qatar. They reported a Pout reduction of about 15% due to dust accumulation on the PV module. Touati et al. (2016) also investigated solar PV performance in Doha. They reported the maximum power output of PV to degrade by 30% due to dust accumulation in five months.

2.6.2.4 Wind speed and direction

Wind speed/direction is one of the main factors influencing dust accumulation. It is the mechanism that transports dust particles over thousands of kilometres and deposits them on a surface. Wind influences dust accumulation in a negative way and also in a positive way by depositing and removing dust. The dust properties and wind velocity determine wind over dust accumulation, varying with location (Jamil et al., 2017). The dust accumulation rate is reduced on a PV module due to the wind blowing when positioned at a particular orientation and tilt angle (Hegazy, 2001). Said et al. (2018) reported that wind creates adverse effects on the soiling because it promotes the transferring and spreading of dust

particles in the atmosphere, leading to increased surface deposition. Goossens and Van Kerschaever (1999) researched the effect of wind velocity and PV surface orientation in relation to dust accumulation. Their results show that dust accumulation increases with an increase in wind speed. Hegazy (2001) investigated the dust effect on transmittance by measuring dust accumulation on glass coupons positioned at different tilt angles under various climate conditions in Egypt for one month and one year. The results show that the degradation depended on the tilt angle where the maximum degradation was observed at the horizontal position and the minimum at the vertical position. The researcher recommended a weekly cleaning of the PV module to avoid performance degradation.

Heydarabadi et al. (2017) studied the dust accumulation on a tilted PV panel considering a specific wind path. The findings revealed that the maximum deposition occurs at a tilt angle of 45° while the module faces southwards for larger particles (> 10 μm) and 90° for particles smaller than 10 μm. Figgis et al. (2019) investigated dust deposition and accumulation on coupons positioned in an axis perpendicular to wind in outdoor conditions and laboratories. Their outdoor result showed that maximum deposition occurred at angle 45°, but maximum accumulation occurred at 22° away from the incoming wind. It also shows that soiling can be easily reduced when PV modules are tilt towards maximum inflowing wind overnight for particle detachment.

The wind is reported to have influence when its velocity is strong and capable of removing particles on the PV surface and cooling it. It has a negative influence when it triggers dust movement from the various surfaces to the PV module.

2.6.2.5 Temperature and Relative Humidity

Temperature and relative humidity are conditions that can significantly influence dust settlement on a PV module. Relative humidity dust accumulation when the temperature is high, and it is low, which is a typical scenario in an arid or semi-arid location, such as Nigeria, which promotes easy transportation of dust particles by wind. Relative humidity usually becomes higher at night, increasing

water vapour content in the air and contacting a surface at lower temperatures; it condenses and forms water droplets. The capillary force will then create dust particles' adhesion on a PV module surface (Jamil et al., 2017).

Paudyal and Shakya (2016) stated that relative humidity is a secondary factor that influences dust accumulation because it only plays a role in long-term soiling to cause adhesion. However, the wind is considered the main element that causes dust entrainment and deposition. Said et al. (2018) stated that approximately 40% to 80% relative humidity increases adhesion to 80%. This clearly shows that relative humidity promotes dust particles' cementation, categorised as a secondary factor influencing dust accumulation. However, the water droplets that condense from vapour on PV module surfaces can attract and hold dust. Adinoyi and Said (2013) also stated that relative humidity promotes adhesion on module surfaces, requiring vigorous cleaning to restore PV module performance.

Mekhilef et al. (2012) investigated the effect of dust on a PV module considering humidity as the influencing factor. Their results show that atmospheric humidity significantly influences dust particle adhesion on a PV module, which degrades the technology's efficiency. Touati et al. (2017) experimented with dust on PV module performance, considering temperature and relative humidity as factors that influence dust accumulation on a PV in Qatar for two years. Their result shows that 50% degradation of power output was recorded due to an eight-month exposure without cleaning. Ramli et al. (2016) reported the effect of dust accumulation on a PV module considering Indonesia's environmental conditions. Their finding shows a reduction of 10.8% of PV performance in two weeks due to soiling being influenced by 52.24% humidity. Their outcome also reveals a PV performance reduction of 40% with a relative humidity of 76.32% during a raining condition.

Zorrilla-Casanova et al. (2013) studied solar radiation losses caused by dust accumulation on a PV module. Their results show that dust accumulation can reduce solar radiation by an average of 4% during rainy periods, while during summer, a daily reduction of about 20% was recorded. Ghazi and Ip (2014)

investigated the dust effect on PV, considering the weather effect as the influencing factor in outdoor and indoor experiments in Brighton, UK (United Kingdom). Their results from the laboratory (indoor) experiment show a reduction of 11% of light transmittance caused by fine dust particles, while results from the outdoor experiment show more severe degradation of the PV module performance, which was related to weather conditions. Ramli et al. (2016) investigated the dust effect on a PV module considering Indonesia's environmental conditions. Their results show a 10.8% reduction during the dry season, more than 40% during the rainy season, with an average relative humidity of 76.32% and 45% when the average relative humidity is 60.45%.

2.6.2.6 Tilt Angle and Azimuthal Orientation (PV Installation Design)

These are factors that have a significant influence on the dust accumulation rate. The inertial dust deposition on a PV module is influenced by the tilt and azimuth angle of the PV module, while the surface’s tilt angle influences the sedimentation. When considering the surface orientation as a factor, dust accumulation is highest if the PV module surface is horizontally positioned and is moderate when tilted. When considering tilt angle as a factor, sedimentation is highest at a horizontal plane and reduces when tilted towards the vertical plane. The azimuth angle influence depends on the wind, and degradation occurs similarly to the tilt angle (Figgis et al., 2017).

The tilt angle is a crucial factor that determines the PV module's production capacity, whereas the deposition of dust is an unavoidable external variable to be considered (Xu et al., 2017). The optimum tilt angle of a location differs for various variables, such as time of use, geographic latitude, temperature, atmosphere and other ambient influences, such as dust and emissions. According to Asl-Soleimani et al. (2001), optimum tilt angle depends on several parameters: the type of application, maximisation of solar energy absorption, and site climatic conditions (such as sand storm, dust haze, snowfall, or Harmattan haze). Several methods were employed to determine the optimum tilt angle of sites (Mani and Pillai, 2010; Xu et al., 2017), where the calculation was based on local latitude alone. However, due to a number of factors mentioned above, it is challenging to deploy a mathematical model to determine a particular site's actual

optimum tilt angle, but it can be estimated considering all the factors. Conceiç~ao et al. (2019) provided a model that makes it possible to calculate the optimum tilt angle for a soiled PV module since the inclusion of soiling provides an accurate result for different tilt angles being used in the absence of cleaning; rather than using an optimum tilt angle solely based on irradiance.

Elminir et al. (2006) researched the dust effect on light transmittance using 100 glass samples. Findings show transmittance reduction with dust deposition and revealed that dust deposition varies with a tilt angle from 15.84 g/m^2 to 4.48 g/m^2 with a tilt angle from 0° to 90°, and the corresponding transmittance reduces approximately from 53% to approximately 12% respectively. Ghazi et al. (2013) conducted an experiment that investigated the effect of dust on glass transmittance, considering six different tilt angles (0° – 90°) for three months under the United Kingdom conditions. Their results show a low reduction of transmittance of about 5–6%. Cano et al. (2014) conducted a study on dust on PV modules at Arizona State, focusing on tilt angle as an influencing factor. The result shows that about 2.02% degradation was observed when a PV module was positioned at a 0° tilt angle, with a 1.05% reduction at 23° and 0.96% at a 33° tilt angle. Hachicha et al. (2019) investigated the effect of dust on PV performance in Sharjah, UAE. Their result shows a linear relationship between the increase in dust density and the reduction in PV performance. Their result shows that dust accumulation is a function of tilt angle where a high accumulation of dust was recorded on a horizontal plane, and the accumulation reduces at a tilt angle of 25° and continues to reduce towards 45°. Semaoui et al. (2015) investigated the impact of soiling on the PV module glazing in the Algerian desert area. The modules were exposed at a tilt angle (32°), and the tests revealed a loss of around 8%.

Xu et al. (2017) analysed the influence of tilt angle in dust formation. They provided an inverse correlation between the tilt angle and dust deposition density. They also presented a method to calculate the optimal tilt angle of a soiled PV module to provide maximum power output, and this was validated using Matlab simulation. Qasem et al. (2019) investigated the effect of dust on spectral

transmittance. Their results indicated that transmittance losses variations were higher around angle 30° with a non-uniformity of 4.4% compared to 0.2% around the 90° angles.

2.6.3 Adhesion

Dust is initially deposited on the surface due to gravitational force; however, adhesion forces such as Van der Waal forces, electrostatic forces and capillary forces are the active force that causes adhesion on a surface. These adhesion processes are described in Figure 2.14, starting with the equation describing gravitational force where R is the radius of a dust particle, ρ is the density of the material, and g is the gravitational acceleration constant (Isaifan et al., 2019). Due to Van der Waals force, small dry dust particles adhere over a dry surface (Picotti et al., 2018). This is considered the dominant force between a solid platform and a dry particle under dry ambient conditions (Isaifan et al., 2019). The Van der Waals forces are always present between surface and particles and act within a short range since they originate from two surfaces in contact with interacting dipoles (Ilse et al., 2018). The equation in Figure 2.14 represents the dry spherical dust particle on a flat surface where R is the radius, *A* is the Hamaker constant, and Z is the distance between the flat surface and particle (Isaifan et al., 2019).

Capillary force is attributed to the air's moisture content (RH-Relative Humidity) and on the surface. The capillary forces act when two wet bodies meet. Water vapour condenses in fine particles, thereby bridging the dust particles' gap on a PV module surface, resulting in adhesion (Figgis et al., 2017). Capillary force is more active if RH is below the saturation point, but once it reaches saturation (RH is 100%), adhesion force will reduce. Capillary force combines two force components: the strength due to pressure between water meniscus and air and the force due to surface tension (Isaifan et al., 2019). The equation in Figure 2.14 representing the capillary force describe the adhesion of spherical dust particle on a flat surface where R is the radius, γ is the surface tension of water and θ is the contact angle between the substrate and the water (Isaifan et al., 2019).

Some dust particles have chemical compositions that cause them to be conductive or dielectric, and these properties usually control their interaction with the PV module surface. The electrostatic force causes adhesion when charges are present using two approaches; when the surface is wet and when particles are close to each other (Ghazi and Ip, 2014; Picotti et al., 2018). This electrostatic force can be either repulsive or attractive (Ilse et al., 2018). Dust particles tend to acquire electric charges in the atmosphere by colliding with one another and through other means, and these charged particles tend to attract positive charges on the surface, which induces a coulomb force. PV surface such as low iron glass, which is non-conductive, surface charges can come through triboelectrification. Materials become charged when they have frictional contact with different materials. The interaction is described in Figure 2.14, where q is the charged particle, ε is the dielectric constant, εo is the permittivity of free space, l is the separation distance equal to 2R (Isaifan et al., 2019).

A notable and catastrophic soiling mechanism that promotes adhesion using the types of force mentioned above (capillary force) is called cementation and is a process of bonding that originated from the dissolution of the soluble matter of wet deposited dust particles during condensation or dry particles on the damp surface, to form a strong solid bond with the surface upon drying (Figgis et al., 2018; Picotti et al., 2018). This process usually occurs during evaporation and condensation (Figgis et al., 2018) and possess severe consequence to PV performance. Dew formation is another phenomenon that appears on the PV surface due to radiative cooling glass surface at night. This can serve as a mechanism that promotes particle adhesion on PV surfaces (Ilse et al., 2018). Particles are further rearranged, agglomerated, and compacted together on surfaces to form particles caking, which is another severe form of cementation that can cause scattering and absorption effect of solar radiation, leading to reduced PV performance.

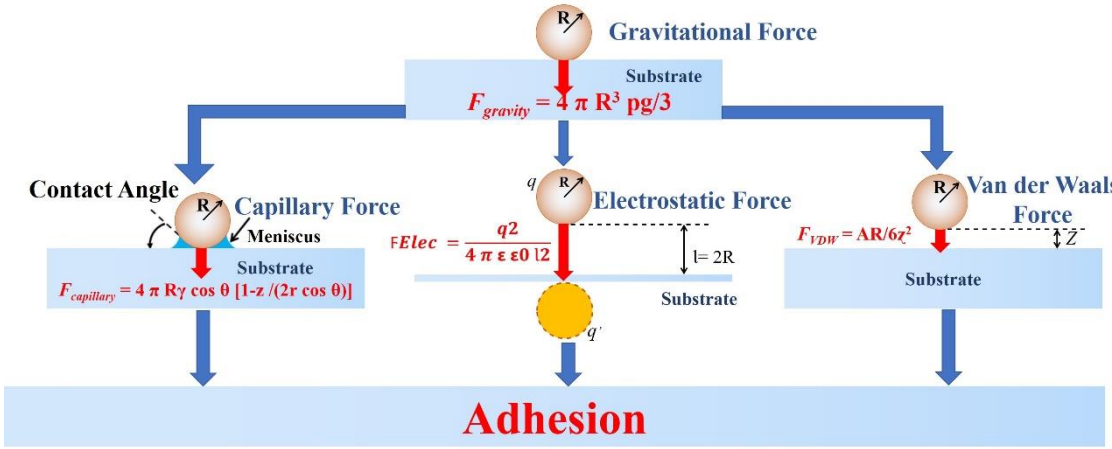

Figure 2.14: Adhesion Forces (adapted from Isaifan et al., 2019).

2.7 Impact of dust on PV modules

In 2017, the PV technology had a global annual net addition installation of about 93.653 GW, summing up to the global cumulative installation of 385.674 GW (IRENA, 2017). However, 243.715 GW was recorded as the cumulative generated capacity in the same year. This is due to factors such as dust that degrade the performance of the technology.

PV module performance is significantly affected by atmospheric and accumulated dust. A solar cell of a PV module cannot respond to wider spectrum sunlight because photons with lower energy than the solar cells cannot be absorbed, causing a material bandgap; thus, 100% solar energy conversion cannot be achieved (Al-Shabaan et al., 2016). Therefore, efficiency degradation should be avoided wherever necessary to achieve optimum performance.

As stated above/previously in this thesis, dust is a global occurrence that negatively influences the PV module performance by scattering, absorbing, reflecting and attenuating the solar radiation from reaching photovoltaic solar cells. Suspended dust in the atmosphere tends to reduce the PV module's performance; however, this has a lesser effect than the dust that settles on the PV surface. These occurrences interplays to diffuse solar rays from reaching the solar cells, thus reducing the amount of light transmittance to the solar cells to perform efficiently and causing a substantial loss in energy production (Khanum et al., 2016). Dust accumulation tends to degrade the PV module's performance

significantly, and this has been established from several sources cited in the subsequent section of this thesis.

2.7.1 Degradation of performance

The presence of atmospheric dust and the high deposition of dust on a PV module negatively affect PV solar cells' performance. The degradation rate of PV's performance varies with dust particles, location and climatic condition. According to Zaihidee et al. (2016), PV module performance degradation caused by dust is linear with dust deposition density. The rapid increase of solar PV technology installation across the globe and the underperformance of the technology caused by dust has prompted considerable research interest. Salim et al. (1988) conducted a study on the effect of dust on PV module performance for eight months near Riyadh, Saudi Arabia, their results showing a 32% reduction of PV output. Tanesab et al. (2015) conducted a study on the effect of dust on a PV module's performance exposed for almost two decades (18 years) without cleaning in Perth, Australia, their results showing the degradation of 8-12%. Sanusi (2012) investigated the amorphous silicon PV module in southern Nigeria under dust haze (Harmattan season) for three months without cleaning, which showed a 20% degradation of PV performance. Klugmann-radziemska (2015) investigated the PV power performance degradation in Poland, focusing on the current-voltage characteristic, chemical and physical characteristics of dust. The results showed a maximum loss of 0.8% per day of 370 tilted panels. The researcher also identified an average annual PV module performance degradation of 25.5% and 3% power losses. Sarver et al. (2013) document a comprehensive review of the impact of dust accumulation on PV modules, highlighting its detrimental effect on PV performance. Similarly, Costa et al. (2016) and Costa et al. (2018) presented review papers with comprehensive listings and references for research related to dust accumulation on solar energy harvesting systems. Also, Darwish et al. (2015) presented a critical review that challenges the research questions that have been used in investigating the impact of dust accumulation on solar PV performance.

An indoor experiment revealed that coarser particles have a lesser impact, while finer particles significantly impact solar cell efficiency (El-Shobokshy and

Hussein, 1993). An experiment performed on a rooftop in Athens showed a 19% degradation of PV module performance for red soil deposition, 10% for limestone and 6% for ash (Kaldellis et al., 2011). Mani and Pillai (2010) investigated the effect of dust on PV module efficiency, focusing on the influence of dust particles' physical characteristics. It was found that finer dust particles of about 2 mg/cm^2 reduced the PV output by about 30%, while deposited coarser particles of about 8 mg/cm^2 reduced production by 10%. Sulaiman et al. (2011) conducted a laboratory experiment using a light simulator to investigate the effect of dust on the PV module's performance (monocrystalline silicon). Their results showed an 18% reduction in PV module performance when a dust sample was deposited on it. Kazem et al. (2016) investigated the effect of dust (artificial) on PV modules using samples of dust (sand, ash, red soil, silica and calcium carbonate) of 5 to 10g. It was documented that ash has the highest degradation effect on a PV module than the other dust particles. Ash reduced open-circuit voltage by 40%, while sand reduced it by only 4%. Kazmerski et al. (2016) investigated the interaction between dust particle adhesion on a PV module’s surface, focusing on the chemical and morphology of dust particle accumulation. Their results show that adhesive force is highly dependent on the chemical bonding of dust particles.

Jiang et al. (2011) investigated the effect of dust on three photovoltaic modules (monocrystalline silicon PV with a glass surface, polycrystalline silicon panel with an epoxy surface, and thin-film amorphous silicon). The results show that efficiency degradation varies from 0% to 26% when the dust deposition density increases from 0 to 22 g/m^{-2}. Their results also show that polycrystalline exhibits more significant efficiency degradation while monocrystalline PV module efficiency degradation was less than the amorphous silicon surface. In another similar research, Kalogirou et al. (2013) reported the dust accumulation effect on three types of PV modules: monocrystalline, polycrystalline, and amorphous silicon. Their results show that polycrystalline and monocrystalline efficiency was significantly reduced compared to amorphous silicon PV modules. Alnaser et al. (2018) conducted outdoor research where monocrystalline silicon modules were exposed for 100 days without cleaning. They recorded a 10% degradation, and they further recommended that PV modules be cleaned at least once a month.

2.8 Removal of dust from PV

A wide range of variations of the effect of dust accumulation on PV was reported in the literature, ranging from 0.51% in the USA (Mejia and Kleiss, 2013) to about 98% in an indoor study (Chanchangi et al., 2020a). However, no study has provided a permanent cleaning rate to mitigate PV soiling (Gupta et al., 2019). The use of conventional cleaning approaches tends to have a significant financial implication in some regions (Fathi et al., 2017).

Deb and Brahmbhatt (2017) stated that airborne dust particles in the path of an incident radiance of a PV device and deposited impurities on PV covering surfaces act as barriers to the impending solar radiation in areas with massive solar energy potential such as arid and semi-arid regions. It decreases the light transmittance, leading to power losses (Piliougine et al., 2013). Its rate widely varies with location, surface covering material and seasonal variation (Chanchangi et al., 2020b; Deb and Brahmbhatt, 2017; Tanesab et al., 2019). Similarly, there is variance in property of the deposited particles requiring different cleaning approaches and cycle's frequency (Bunyan et al., 2016).

Mitigating the problem of dust accumulation on PV covering surfaces is vital for the penetration and sustenance of renewable energy in the developing world. Therefore, the scientist has put a massive effort to develop a mechanism that can prevent soiling losses or restore optimum PV output performance, and several techniques were reported by Chanchangi et al. (2020b), Gupta et al. (2019), and Jamil et al. (2017). Each technique presents a different level of performance concerning the environmental condition of the location it has been deployed and the type of PV cover surface it is cleaning. However, some techniques have a long list of drawbacks, such as cost and uncontrolled water requirement supply, known as the primary concerns for the region in focus (Quan, 2017; Sayyah et al., 2017). This subsection of the thesis briefly highlights the main soiling mitigation approaches in the subsequent paragraph.

This detachment process removes dust particles from the PV module surface (Picotti et al., 2018). Removal processes include artificial and natural, automated and self-cleaning, as shown in Figure 2.15.

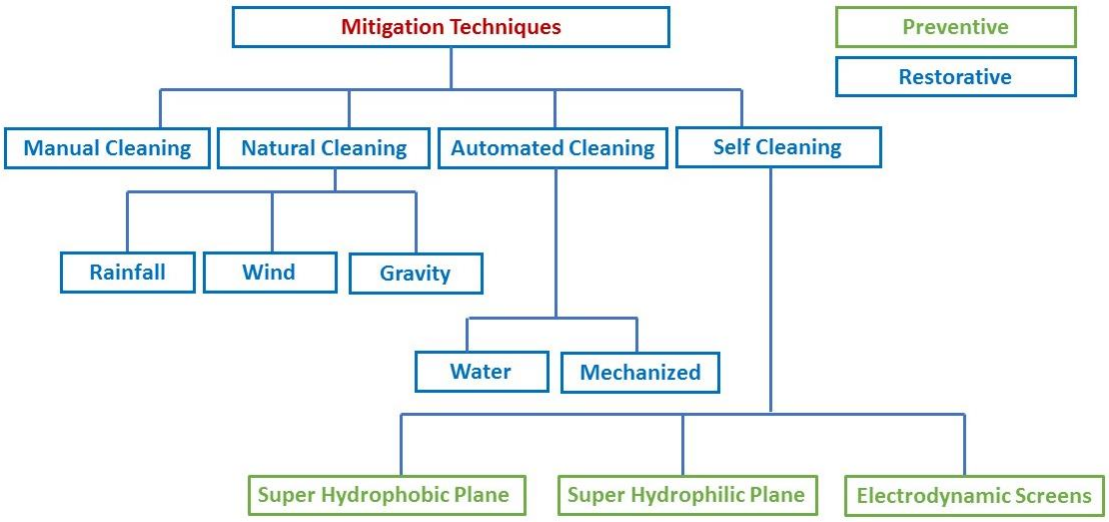

Figure 2.15: Mitigation Techniques.

2.8.1 Natural removal

Rebound and re-suspension are the two natural types of dust removal from PV surfaces. For the rebound process, the adhesion force is lesser than the dust particle's kinetic energy. Thus, the dust particle immediately bounces off from the PV module surface upon deposition and becomes re-suspended/re-entrained in the atmosphere (Figgis et al., 2017). Therefore, it becomes difficult to attract the particles and for them to become stacked on the surface. The rebound process is influenced by factors such as the size of particles and deposition velocity, PV module surface orientation, surface roughness, surface moisture, relative humidity and wind.

This is the re-suspension of dust particles into the atmosphere after detachment from a PV module's surface. This process is divided into two approaches; the energy re-suspension approach and the force re-suspension approach. The former occurs when adhesion tends to break due to sufficient energy from vibration or rocking, and the latter occurs when the aerodynamic force is higher than adhesion forces (Figgis et al., 2017). Particles are detached through lift-off

motion, sliding and rolling. The amount of particle re-suspension is the function of the velocity flow. Wind speed plays a vital role in dust particle re-suspension. The dust particles size is another factor that promotes re-suspension, where a large sizeable particle is proportional to re-suspension force while the adhesion force is linear to small dust particles (Figgis et al., 2017). It makes small particles immune to removal due to wind, while large particles are easily removed and re-suspended into the atmosphere by wind (Figgis et al., 2017).

2.8.2 Cleaning

2.8.2.1 Natural Cleaning

The natural cleaning technique is a restorative approach of cleaning where rainfall, wind and gravity are expected to remove accumulated particles from the PV surface and restore their potential performance (Ghazi et al., 2014). It is the low-cost approach and sometimes tends to be significantly effective (Sarver et al., 2013), while sometimes it could cause more damage by influencing more accumulation (Kimber et al., 2006).

Rainfall, wind and gravity are the natural cleaning mitigation process of dust from a PV module (Ghazi et al., 2014) stacked on the surface by moisture due to the capillary force (Deb and Brahmbhatt, 2017). Rainfall is considered the most effective natural cleaning process, and it improves efficiency by cleaning the PV module surface; however, the water droplets that remain on the PV surface tend to create adhesiveness on the surface (Kalogirou, 2013). Light rain has a negative impact because it collects airborne dust particles and deposits them on the surface, leaving sticky dirt patches, which can cause a sudden decrease in PV module performance (Kimber et al., 2006). Rainfall is a natural phenomenon and, as such, cannot be relied on, most especially in arid and semi area areas.

High wind speed can partially clean a PV module surface, and this depends on factors such as wind direction and the tilt angle of a PV module (Mekhilef, 2012). The wind is also a natural occurrence similar to rain and, as such, cannot be depended upon. Low wind velocity also tends to drop suspended atmospheric dust particles on the PV module, which can cause degradation of its performance.

2.8.2.2 Water-based Cleaning

Water-based cleaning is an effective and widely used method of mitigating the dust effect on a PV module. The pressurised water is used in cleaning the surface, and sometimes cleansing solutions such as detergent are also added to improve cleaning efficiency. This is considered one of the most efficient approaches. However, some areas, such as arid and semi-arid locations with high solar energy potential, have water scarcity, and employing pressurised pumping machines can lead to the loss of a large quantity of water. The use of water in cleaning an electricity-generating component also tends to cause thermal shock. However, appropriate planning and cleaning schedules can resolve this problem (Deb and Brahmbhatt, 2017; Jamil et al., 2017).

2.8.2.3 Manual Cleaning

Manual cleaning is the traditional analogue strategy used in cleaning a PV module, a similar approach to the one used in cleaning windows and glasses. Brushes and rags are used in scrubbing and washing the module surface to restore the cleanliness of the PV module surface. It is also efficient in removing cementations and hard soiling. The manual cleaning with squeegee and water technique is another integral approach that is highly labour intensive. It requires personnel to employ small tool squeegee, wipes or towels to remove accumulated particles on PV surface through simultaneous scrubbing and washing, including water addition (Deb and Brahmbhatt, 2017; Jamil et al., 2017). In addition, detergents and other cleaning chemicals are sometimes employed to enhance cleanliness. This approach is among the effective and reliable cleaning methods that could restore PV performance (Mohamed and Hasan, 2012). However, since brushes and other materials are directly used on the PV module surfaces, there is a (strong) likelihood of an abrasive effect. This method is also considered an expensive approach in the developed country as it is labour intensive and requires additional equipment for cleaning (Deb and Brahmbhatt, 2017; Jamil et al., 2017).

2.8.2.4 Mechanised Cleaning

This automated approach uses some techniques for cleaning the PV module's surfaces, including mechanical wiping, mechanical brushing, blowing,

vibrating/shaking, and robotic cleaning. This method eliminates labour intensity by deploying automation. The vibration technique uses the piezoelectric effect to create ultrasound vibration that cleans the PV module surface. This technique can restore about 95% of a solar PV module' efficiency (Williams et al., 2007). However, a decade later, Deb and Brahmbhatt (2017) and Jamil et al. (2017) stated uncertainty on the efficiency and thoroughness of cleaning capacity of all mechanised cleaning and its high initial and maintenance cost. Wiping and brushing techniques use the electromechanical approach, consisting of a programmable logic controller and a microprocessor to operate the wiper and brushes to move on the PV surface (Ghazi et al., 2014). Blowing employs an air nozzle with a vortex generator attached to a brush or wiper to rotate across the PV surface (Sarver et al., 2013).

Automated/robotic cleaning is an effective restorative technique that could clean the entire PV surface and be operated manually or automatically with accuracy and flexibility. This technique is sometimes categorised under a mechanised approach. It is configured according to requirement and comes with sensors, controllers and wiper or brushes. The system is designed to act with fast response, high stability, and operate independently (unmanned), low power consumption, and reduced labour cost (Jamil et al., 2017). Although it reduces the labour in the cleaning module, it has a very high initial cost and requires periodic cleaning. It could also cause abrasion and can be unreliable in some cases (Deb and Brahmbhatt, 2017). This approach is recently widely adopted and undergoing intensive research at different institutions globally (Makmee et al., 2021). Azouzoute et al. (2021) reported a robotic cleaning device developed by SOL Bright Technology to eliminate about 99% of accumulated dust and improve the 7-15% performance output of a large solar farm. However, this comes at a high cost and required monitoring.

These approaches require a considerable amount of energy and are relatively expensive because of the devices' initial and continuous maintenance cost. The technologies' cleaning efficiency is still uncertain as some dust requires a thorough cleaning (Deb and Brahmbhatt, 2017; Jamil et al., 2017).

2.8.2.5 Self-cleaning

The self-cleaning technique is a preventive and restorative passive approach that resist dust accumulation on PV surfaces through repelling achieved by PV surface modification, coating (hydrophobic or hydrophilic layer), and electrodynamic screen (EDS).

2.8.2.5.1 Super-hydrophobic plane (SHOP)

This preventive approach employs a self-cleaning concept that utilises a chemical or screen layer that requires no energy to repulse dust particles back to the atmosphere using the lotus effect. This self-cleaning technology has a surface with low wettability, which can prevent water droplets from stacking on the PV surface, assisting the removal of soiling with rainfall to improve cleanliness and sustain efficiency (Jamil et al., 2017). However, the technology's lifespan is short, and it can easily break when exposed to high-level ultraviolet radiation.

Hydrophobicity uses the lotus effect to prevent or remove dust from PV surfaces using a nano-structured layer (Son et al., 2012). The coating resists the adhesion of dust particles to the PV surface but requires water to eliminate it. However, this technique is expensive on a large scale (Jamil et al., 2017), and its optimum efficiency only lasts between 3-4 years (Mitdal and Jelle, 2013) and two years, according to Gholami et al. (2017). As mentioned above, the techniques have the individual capacity to reduce dust. Still, no flawless approach has been recommended for the region in focus.

2.8.2.5.2 Super-hydrophilic plane (SHIP)

This is another preventive approach with a self-cleaning technique. The term hydrophilic expresses the diffusion of water on a surface. It is the exact opposite of hydrophobicity, where this hydrophilicity attracts water, the other repels it. This technology used nano-pattern fabrication and was developed using Titanium dioxide (TiO_2), described as a low cost, high light transmittance, non-toxicity, chemically stable and highly durable material. However, it causes more soiling

when the surface coating begins to deteriorate due to prolonged exposure to ultraviolet rays and requires washing and drying after rainfall (Deb and Brahmbhatt, 2017; Jamil et al., 2017).

Nundy et al. (2020) investigated hydrophilicity using Zinc oxide (ZnO) and achieved a 2.8° (super hydrophilicity) wet contact angle depositing the microspheres (M-ZnO) on an Indium Tin Oxide (ITO) glass substrate. The compound's morphology shows an average 41.5 nm crystallite size with a bandgap value calculated from the ultraviolent to visible (UV-VIS) absorption spectrum found to be 3.1 eV.

2.8.2.5.3 Electrodynamic screens (EDS)

This is a preventive approach where the electrodynamic screen is placed on top of the PV module to prevent dust deposition by repelling it using an electrostatic field. It operates in dry ambient conditions with the capacity of detaching and restoring over 90% of PV module performance in two minutes (Jamil et al., 2017). However, it has been reported that it is inefficient in mitigating cementation and small dust particles (Jamil et al., 2017). The device also requires a high voltage supply of electricity to generate the electric field on the PV module surface, reducing generation capacity by 15% (Deb and Brahmbhatt, 2017; Jamil et al., 2017).

The EDS removes using electrostatic forces to repel dust particles when an electric field is established on surfaces of the covering material (Sayyah et al., 2017). It is reported to restore 90% of PV output performance by removing 80% of accumulated dust (Mazumder et al., 2013). However, Guo et al. (2019) examine the technology's performance in outdoor conditions and reported efficiency degradation from 40% to 14% over four days.

2.9 Nigerian context

Nigeria is a sub-Saharan country located in West Africa on the Gulf of Guinea, with Niger and Chad to the North and Atlantic Ocean to the South. Its topography varies from semi-desert and savannah in the northern part to tropical forest and

coastal swamp in the Southern region. The atmosphere in the Northern part of Nigeria is affected by desert dust emanating from the Sahara in Northern Africa, Bodélé Depression, Bilma-Faya Largue in part of Chad and Niger Republics due to proximity. Simultaneously, the Southern part is affected mainly by the same dust and soot from oil exploration activities in the Niger Delta and offshore region when the wind direction changes, dependent on Inter-Tropical Displacement positioning (ITD). It is caused by the Coriolis effects that direct the movement of the wind. Figure 2.16 depicts some locations with high dust concentrations in the atmosphere.

There are many dust sources across the globe, including industrial pollution, mining, agricultural pollution, cosmic dust, volcanic, sea salt, desert dust and dust storms. Several studies reported that Saharan desert dust is the largest source, with about 50% – 58% of the total global dust (Longueville et al., 2010; Middleton, 2017; Tanaka and Chiba, 2006). According to Longueville et al. (2010), sub-Saharan (West African) is the area of the world that is most affected by the dust from the Saharan region due to wind movement and proximity. The North-easterly winds usually blow off the Saharan dust and converge with the South-westerly wind to form the Inter-Tropical Convergence Zone (ITCZ) in West Africa (Doherty et al., 2014). It has a tremendous effect on seasonal variability, which sometimes causes an influx of a high concentration of dust in the region's atmosphere. Doherty et al. (2014) stated that the ITCZ primary mechanism drives the regional climate in West Africa because it plays a significant role in controlling wind direction. Middleton (2017) further supported this claim by stating that the long-range transportation of desert dust mainly depends on the wind path that differentiates seasonal variations. This high concentration of dry dust in the air transported by wind from the Sahara through West Africa to the Gulf of Guinea is called the Harmattan season, usually from November to March. Meindinyo et al. (2017) describe Harmattan as a strong, hot, dry and dusty northeasterly trade wind that emanates from the Sahara and blow across West Africa.

The Harmattan season is associated with a deterioration of visibility due to the high concentration of dust particles (natural and anthropogenic sources) in the atmosphere. The visibility can drop to less than 1000 m, and Harmattan dust is

categorised as Thick Dust Haze (TDH), which is when visibility ≤ 1,000 m (VX ≤ 1,000 m), and Light Dust haze (LDH) when the visibility range from >1,000 m to ≤ 5,000 m (Ochei). Dust pollution with reduced visibility below 1000 m is also considered dust (Anuforom, 2007). This season lasts for six months in Nigeria, and as such, it can affect the country's PV system's performance. The quantity of dust in the air is higher in the northern areas and reduces when moving towards the south (Longueville et al., 2010). The dust particles vary, and therefore, optical properties would also vary. The difference in the optical properties of dust depends on the regions and the source's distance since particles are added and released during the transport phase (Tanaka and Chiba, 2006). Some can be opaque, and others translucent capable of causing a reduction of light transmittance. Middleton (2017) reported that dust could degrade PV's performance from about 15% to 30% in moderate dusty conditions, and if cementation occurs, it can reach up to 100%.

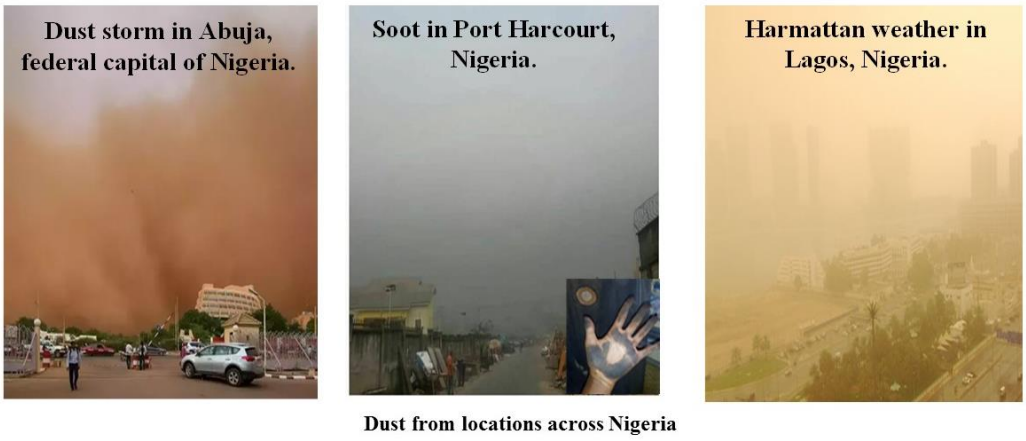

Figure 2.16: Dust from locations across Nigeria (Adapted from Environ News Nigeria, 2018).

This Saharan desert dust injection is mobilised by Bodélé low-level jet (North Easterly wind), which transports about 60% of the particles southward towards the Gulf of Guinea, having the highest effect on Northern Nigeria, 12% northward affecting the Northern African and Southern Europe and 28% goes west to the Equatorial North Atlantic (Afeti and Resch, 2000; Anuforom, 2007). The low-level wind generates sandblasting and saltation across the region during the Harmattan season, causing dust outbreaks leading to solar radiation's

attenuation (Tulet et al., 2008). The wind is most active in January (Washington and Todd, 2005). Harmattan dust aerosol granulometry depends on the distance from the initiation region, wind velocity that decreases with distance (Southward), and increased atmospheric humidity (Anuforom, 2007). Aerosol optical thickness (AOT) can be greater than five at peak period (Tulet et al., 2008), and texturally, the Harmattan dust particle is classified as silt and abrasive. However, other different particles, such as heavy metals, are injected by anthropogenic sources during the transport phase, making them hazardous (Uduma and Jimoh, 2013). The average Thick Dust Haze (TDH) duration of the Harmattan season ranges from about six days in the dry northern part of Nigeria to about a half-day in the southern coastal region (Anuforom, 2007). It is mainly attributed to proximity to the primary emission source.

Anuforom (2007) reported that the shrinking of the Lake Chad basin due to drought increases the concentration of dust levels in the troposphere during the Harmattan season. The high concentration of dust in the atmosphere has a negative impact on incoming solar radiation by causing absorbing and scattering effect on a significant fraction of solar radiation leading to radiative imbalance, optical and electrical properties modification and changes of microphysical properties of clouds (Anuforom, 2007; Tulet et al., 2008).

Documented evidence shows that soil in Northern Nigeria is mainly attributed to Harmattan dust from Aeolian suspension and saltation deposition (dune sand) (McTainsh, 1983). Structures such as Zaria and Funtua loessic in Northern Nigeria have particle texture with morphology and mineral characteristics similar to those obtained from Harmattan dust, while particles from Northern mantles are predominantly identical particles from the dune sand (Goudie and Middleton, 2017; McTainsh, 1983). The Southern part of the country's soil is mainly attributed to higher erosivity and can be easily entrained into the wind's atmosphere; however, it has enormous vegetation with low wind velocity (Oduola, 2010). The high possibility of soil erodibility and erosivity in Northern Nigeria is a potential source for dust entrainment, where a large volume of dust is injected into the troposphere, influencing the changes in the global radiation budget by directly

scattering and absorption of solar radiation reducing the photovoltaic effect reaching PV technology (Ogunjobi et al., 2008; Washington and Todd, 2005).

Nigeria is categorised as a developing country, and the level of air pollution in the country is expected to be low due to few industrial activities. However, the country is blessed with abundant mineral resources, leading to several legal and illegal mining activities across the country, causing massive injection of heavy metals and minerals into the atmosphere to cause air pollution and other hazards (Aigbedion and Iyayi, 2007). Mining activities generally come with a substantial positive economic benefit; however, it always has some consequences. Olujimi et al. (2015) reported a high Geo-accumulation index rate, indicating mining site contamination in Northern Nigeria with a high-risk cancer level for adults and children. The negative impact of mining-related to this study is the emission of heavy metals into the atmosphere, absorbing and scattering solar radiation effects. Large-scale dust is generated from various mining activities such as oil and gas, cement, quarry, and other minerals. These industries generate a significant amount of dust during the mining of raw materials and generate another large volume during the utilization phase.

The oil and gas industry in Nigeria generates the highest air pollution as it is the country's primary source of revenue. Apart from oil spillage, illegal refineries are also generating unaccountable emissions from the sector. Nigeria is the 6th largest natural gas flaring country, with approximately 180 gas flaring sites generating toxic gases into the atmosphere (Fluenta, 2019). According to Aigbedion and Iyayi (2007), large endless burning flames are common sites in Nigeria's oil-producing region, flaring an enormous volume of hazardous gases to the environment.

Nigeria has a good number of cement companies producing locally for domestic consumption. These companies obtained their primary raw materials locally from limestone mining in the country, thereby generating a large volume of dust daily at all stages (Aigbedion and Iyayi, 2007). Maina et al. (2013) stated that dust generated during cement production in Nigeria is enormous, and some dust particles are also generated in various forms such as gas emission, leakages,

clinker dust, raw mills and precipitator dust. Researchers also stated that soil around the factory's vicinity had been polluted with many heavy metals. In the cement industry, dust is mainly discharged into the atmosphere at various stages during the production process, such as crushing, grinding, blending materials by cranes, crushers, mills, rotary kiln and packaging processes (Ibanga et al., 2008; Mojiminiyi et al., 2007). These dust particles can be entrained and transported to cause a disturbance in the PV industry and other environmental and health issues.

The quarry industry generates a large volume of dust across the country due to high demand from the road and construction industry. Particles are generated during stone crushing or production processes and entrained in the atmosphere, then transported by wind. According to Ugwu (2008), quarry operation discharged many particles to the atmosphere ranging from 1.0 microns to 2.5 microns and transported over by wind over a significant distance.

Anthropogenic activities using old or poorly maintained vehicles, petroleum and diesel generators, combustible biomass, forest fire, construction, and demolitions generate enormous dust in Nigeria (Shinggu, 2014). An old or poorly maintained vehicle is another source of air pollution in Nigeria due to inadequate emission control contributing additional particles to the atmosphere. According to Akan et al. (2013) and Kanu et al. (2015), heavy metals containing toxic elements are discharged from poorly maintained vehicles all over the country as a result of oil leakages, fuel burning, tyre wearing, substantial exhaust particle emission and other mechanical non-exhaust emissions such as breaking and road abrasion. Ogunsola et al. (1993) stated that vehicle emissions causing air pollution are most likely aggravated by poor vehicle and road maintenance and lack of emission management technologies such as catalytic converters. Fossil fuel generators and combustible biomass are widely used to complement the electricity supply, thereby generating toxic gases in the atmosphere. These gases are entrained and transported over a long distance to cause environmental and health issues. Construction and demolition activities are happening worldwide and can generate enormous dust, which causes air pollution in Nigeria that generates both fine and coarse dust particles on-sites (Mafuyai et al., 2014).

The wood industry generates an enormous amount of wood dust daily in the country. The application of outdated tools and machines in processing wood leads to the generation of significant by-product, which is poorly controlled due to a poor working environment (Tobin et al., 2016). It is then entrained in the atmosphere and transported over a distance. This anthropogenic emission is mostly higher in large cities (such as Lagos, Port Harcourt, and Kano) with high population density across the country where emitted particles are visible, causing strong turbidity, awful smell and eye irritation (Baumbach et al., 1995). Suspension of toxic particles in the atmosphere with these characteristics will have a negative effect on the PV performance.

2.10 Discussion

This review section of the thesis has highlighted generic mechanics in which the soiling process occurs on the PV surface, and a section was provided to highlight the sources of dust in Nigeria. Dust is generated from various sources in the country. However, there is an excessive influx of dust from the Saharan dust causing severe impacts on PV performance during the Harmattan period. Other dust sources were described, which provide additional constituents to the atmospheric dust and promote further negative consequences of attenuating solar radiation by scattering and absorbing the rays. The wind is a factor that plays a vital role in triggering the advection activity where particles are made to entrain and are transported in the atmosphere. The reduction in wind speed with distance also promotes the deposition of dust on surfaces within the region. The country's particle adhesion depends on the significant active forces (electrostatic, Van der Waals and capillary force) earlier highlighted. During the country's Harmattan season, humidity is low, causing the Van der Waals force and electrostatic force to be very active, whereas the capillary force will be significantly less or completely inactive. However, the capillary force can be triggered by light rain, dew or high humidity at the beginning of the rainy season due to the introduction of the South-Westerly wind (monsoon influx) caused by the migratory repositioning of the Inter-tropical discontinuity (ITD) (Afeti and Resch, 2000; Tulet et al., 2008). It will initially cause cementation due to the

mixture of dust particles and light rain on a surface, causing the most considerable PV performance degradation, but the heavy rain will later arrive and serve as a mitigator to clean and restore the PV performance. However, enormous energy potential will be lost due to the low harvesting performance caused by soiling during the period.

The incident radiation received by solar cells inside a PV module is lower than radiation falling on the extreme top of the module surface. The transmittance coefficient of the cover glass is critical for the performance of the device as the other factors such as tilt angle and orientation, and temperature (Gholami et al., 2017) since it has an influence on the influx of light that reaches the solar energy collectors (Elminir et al. 2006). The leading causes of this energy loss are PV surface materials (mainly low iron glass and acrylic plastic) and accumulated dust on the module surface (Cano et al., 2014). The first has a more negligible effect, which is always less than a 9% transmission reduction, as reported by Chanchangi et al. (2020), while the second could cause a significant effect on the performance of the technology. In addition, Conceiç~ao et al. (2019) stated that soiling on PV decreases the actual radiance absorption by solar cells and, consequently, reduces the power output to as much as about 50% in some regions. Dust accumulation provides a shielding effect that causes a decrease in light transmittance, causing the wastage of abundant solar energy resources. Determining local soiling would be significantly valuable for PV installation since it can increase energy generation and reduce cleaning tasks (Conceiç~ao et al., 2019). In certain situations, economic implications cause consideration of the trade-off between maintenance costs (cost of mitigating the dust) and energy production, thus, contributing to negligence or inadequate maintenance (Conceiç~ao et al. 2019; Tanesab et al. 2016). It is recommended that there is a need for continuous research on soiling in the target region with high solar energy potential and proposing large PV installation to avoid possible wastage and stabilise energy production that could improve penetration (Gholami et al., 2017; Abdolzadeh and Nikkhah, 2019; Chanchangi et al., 2020a).

Jaszczur et al. (2019) reported that PV modules are widely neglected and not adequately maintained with appropriate cleaning after installation, which leads to soiling, causing a deteriorating effect on the system performance.

Many studies presented above extensively reported that dust formation on PV has a tremendous effect on the technology's performance. However, only two studies were identified: Sanusi (2012) conducted in the Southern region and Sambo et al. (2019) in the Northern part. The study does not consider many significant factors influencing the dust formation on PV and does not mention other research challenges. Dust formation is site-specific. Most of the studies presented in this thesis were not conducted in Nigeria or focused on Nigerian conditions; however, this thesis has provided general information on dust on PV performance and specific information about the region to guide further research. Investigating the significant factors influencing dust formation on PV highlighted above can play an essential role in understanding PV's soiling for a particular location. This research can provide information on the appropriate mitigation techniques for a specific region with high PV potential and low penetration.

A carefully documented section for dust mitigation techniques was provided above to demonstrate various ways to prevent this serious problem (dust formation on PV) or restore the technology's performance after dust accumulation. No evidence of implementing any techniques in Nigeria was reported in the literature, but it was observed that manual cleaning with brushes is employed in some installations. However, with or without implementing any method, the natural cleaning technique (rain, wind and gravity) will be active on the PV installation once exposed to outdoor conditions across the country. This highlight a research gap to investigate the availability and efficiency of mitigation techniques used in the country to provide information to the research community and potential investors for future development.

A good number of research gaps were identified in this study, which can adequately address the required information to promote the technology's penetration to achieve sustainable development goal seven, aiming to ensure the provision of clean, modern, sustainable and reliable energy for all.

According to Ochei and Adenola (2018), dust across Nigeria has a significant influence in reducing visibility due to the suspended elements in the troposphere, and this can lead to an absorbing and scattering effect on solar rays. Similarly, if dust accumulates on a PV module platform, it can also reduce transmittance, promote reflectance, and reduce PV performance. Dust movement and deposition is a natural phenomenon and cannot be eradicated but can be mitigated. Some mitigation techniques were highlighted above, and there is a need to identify the particular dust properties in Nigeria and conduct an experiment to determine the appropriate mitigation techniques to be used in the country. Natural cleaning is considered ineffective during the dry season. While manual cleaning might be cheaper due to the cost of labour in Nigeria, all the other mentioned mitigation techniques are expensive and might increase the cost of generating clean energy.

This dusty wind movement across countries has influenced the formation and accumulation of dust particles on objects exposed to outdoor conditions. Solar PV is a technology that requires installation outdoors and without any obstruction to receive maximum solar radiation, and this will make it prone to dust formation and accumulation, which has a deteriorating effect on the performance of the technology. In order to promote PV system penetration and sustainability, PV research must identify the soiling status of various regions with high potential and design PV systems with efficient and sustainable dust mitigating capacity.

Despite the success of the reports presented above and in the literature, it is notable that none of the research attempted to investigate more than two numbers of sites in a region, considering the difference of environmental factors that could influence dust settlement on the surface. The literature presented varied results from studies conducted in the same region, which support the claim that dust accumulation is location-dependent and soiling value of each region should be determined. When conducting an extensive literature review, it was observed that most soiling losses were recorded on a single location, during a particular season or few weeks to a month and reported, which makes it extremely difficult to know the soiling losses rates of a country or region. It was

also observed that some of these studies position coupons or PV modules on a single angle which would limit their analysis and predictions level. There has been an increased recognition that more attention needs to be put on soiling in various regions with high potential and less PV penetration to scale up the application of renewable energy (RE) technology and reduce the gas emission that promotes climate change.

Furthermore, Micheli and Muller (2017) stated the annual losses of the region such as the United States was reported with a range from 0-6%; meanwhile, the PV soiling data rate is not readily available for most of the regions categorised as highly polluted regions such as Nigeria. Some findings of outdoor soiling experiments that recorded significant losses are provided in the literature since outdoor soiling losses were reported to range from as low as 0.5% reduction of daily PV soiling rate (Sulaiman et al., 2015) to about 63% bi-annual soiling losses (Alnaser et al., 2018). Fouad et al. (2017) reported rates of publication related to percentage considering the factors researchers are focusing on, with 50% on environmental, 35% on installation, 20% on PV systems, 18% on PV system degradation, and 5% on PV systems on cost.

Few of the aforementioned studies presented soiling research in sub-Saharan Africa, a region that lies within the Sun Belt and has a significant amount of irradiance and extreme weather and environmental conditions. A region with a significant energy supply deficit striving to invest a massive percentage of its annual budget towards renewable energy. It is imperative and remains a prerequisite to investigate and report soiling losses across the region, leading to identifying a cost-effective yet appropriate mitigation technique to sustain PV performance at optimum yield.

2.11 Case Study

Selected case studies have been provided in this thesis in the research context and its importance for the studies carried out in Nigeria. The following case studies are identified, researched and adapted for the relevance of this study. Although a large number of case studies are available in the literature, only

selected case studies are provided below. This subsection provides a global, regional summary that shows a variation of soiling impact caused by different dust particles having various properties under harsh climatic conditions. It is observed that some regions have natural activities such as denudation, erosion and storms that generate enormous dust into the atmosphere due to the texture of its ground surface. In addition, some regions come with a high soiling rate during certain seasons while others don't, which is also related to anthropogenic causes.

2.11.1 Africa

The following studies were conducted in Africa; Dajuma et al. (2016) investigated the impact of weather and dust on PV performance. Authors highlighted that increasing energy demand and solar energy potential prompted an investigation of PV efficiency, sensitivity to dust and weather over West Africa. An in-house made mini mc-Si module (15 W) was deployed in the tropical region (Abidjan, Côte D'Ivoire: 5°N 4°W) for twenty-four days (from 19 Jun to 12 Jul 2015), and Sahel arid region (Niamey, Niger republic: 13°N 2°E) for thirty-one days (from 22 Jul to 22 Aug 2015) to examine the influence of weather, and effect of dust accumulation on PV performance. Findings reveal that an increase in temperature above 33°C reduces the performance efficiency of the module in both regions. In contrast, dust accumulation was recorded to reduce PV output by about 12.46% in Niamey, Niger Republic, after twenty-one days of exposure. The study recommended a more comprehensive approach with a longer duration to determine the effect of seasonal variation. The study also suggested a two-week cleaning frequency for Niamey, Niger, to mitigate PV soiling (Dajuma et al., 2016). The recommendation might be inadequate as a mini-module with 15W capacity is too small to determine the impact of soiling in a region, particularly when assuming the frequency of cleaning for a larger installation.

In Northern Africa, Semaoui et al. (2020) investigated the effect of soiling on PV performance to determine the rate of losses so that prospective investors can manage it. Algeria Government adopted the renewable energy (RE) generation program by employing a solar photovoltaic system with a capacity of about 13

GW in a distributed pattern estimated to cover around 90 km^2 across the country. The experimental site (coastal region of Northern Algeria 36.8N, 3E) is reported to have an average solar energy potential capable of producing about 2580 kWh/m^2 when positioned at an optimum angle (36°). However, the region is characterised by soot (black carbon emissions), dust particles and high humidity, which cause PV soiling and affect the system's performance. Therefore, six mc-Si were deployed to investigate the impact of soiling on PV power output by cleaning some modules and other left unclean. The findings reported that an average decrease of the I_{SC} was recorded after one month of exposure. Losses are observed during the daytime and are directly related to the accumulation of PV surfaces, preventing light from reaching the solar cells. The study recommended that soiling losses be adopted when sizing the region's PV installation and forecast output (Semaoui et al., 2020).

2.11.2 America

The rapid increase of PV installation in California, which account for 47% of total USA installation, has prompted an investigation that quantifies the region's technology's conversion efficiency performance. About 186 installation sites, including residential and commercial, were observed during the dry season in 2010. Weather data were collected from a nearby weather station. The findings show an average soiling loss of 0.051% per day, with higher losses recorded on installations positioned at tilt angles less than 5°. It also shows that lower losses of about 0.1% were recorded from 26% of the sites. The study recommended a schedule for manual cleaning and automated cleaning, where the first technique was predicted to have restored an annual average from 0.81% to about 4% if it was conducted halfway through the drought period. The latter was predicted to have a yearly average efficiency restoration capacity of 9.8% (Mejia and Kleiss, 2013).

Micheli and Muller (2017) attempted to establish soiling rates using influencing factors in the USA. The apparent impact of soiling on PV performance prompted research to determine various parameters used in predicting the soiling rate. Data were collected from 20 sites in the USA, with each station having a minimum of

two modules and a pyranometer. All modules or solar cells in all stations are regularly cleaned, except one or two are left uncleaned. Operational exposure periods vary, ranging from seven to forty months, between 2013 and 2016. The findings reveal that PM data and precipitation patterns are the two primary parameters with significant correlations with the soiling metrics. The result from quantifying the strength of the annual daily average of correlation between environmental factors and soiling shows PM_{10} and $PM_{2.5}$ to be the best parameter for determining soiling losses of a site, with both having a high coefficient of determination (R^2) 0.82. PM emission between 30 – 50 km radius reduces the R^2 to about 0.45 and 0.55. When additional variables such as rainfall and wind direction were added to PM data, the R^2 of 50km radius shows 0.73 for PM_{10} and 0.90 for $PM_{2.5}$. The study recommended extending the research to determine secondary parameters that could significantly predict the soiling rate (Micheli and Muller, 2017).

2.11.3 Asia

Economic and environmental benefits of PV incited Paudyal et al. (2017) to conduct a study on the effect of soiling on PV performance in Kathmandu valley, Nepal (27° 40' 54.6132" N, 85° 17' 6.3168" E) solar radiation potential of about 3.83 kW/m^2 per day. This study investigated transmittance losses that cause PV power output reduction. Two pc-Si modules with 40W ratings were exposed at a 27° tilt angle from August 2015 to January 2016. Also, 150 slides (with having a dimension of 25.1 mm × 75.2 mm × 1.2 mm) were exposed to determine transmittance losses and mass of accumulated dust. PV output is measured and stored on a data logger where the P_{max} is calculated from 9 am to 3 pm every day. Slides were subjected to optical transmittance measurement using a spectrometer. The mass of accumulated dust was examined in an electric balance. Weather parameters were collected from a nearby meteorological station. The findings show that accumulated dust significantly obstructs the potential light to reach solar cells to generate electricity. The deposition density ranges from 0.1047 to 9.6711 g/m^2. About 69.06% of transmittance loss was recorded over five months, which causes approximately 29.76% of power

reduction. The study recommended using a carefully selected cleaning technique to reduce the soiling rate (Paudyal et al., 2017).

PV systems potential and availability of massive solar irradiance stimulated Ullah et al. (2020) to investigate the effect of soiling on power output losses. Nine pc-Si modules with each having a 10 W rating were exposed in Lahore, Pakistan (latitude 31.47° N and longitude 74.41° E) for 120 days from October 2018 to January 2019. Eight modules were positioned at fixed angles 0°, 15°, 30°, 45°, 55°, 65°, 75° and 90°, while the remaining one is not fixed and is always cleaned. Four bifacial modules were emulated using a set of eight mono facials with the same rating mentioned above. Two of the bifacial modules were positioned at 90°, and another two at 30° tilt angle with one from each group is cleaned and the other left uncleaned. Manual and automated soiling mitigation techniques were employed to optimise performance. Electrical output such as I_{SC} and V_{OC} were recorded three times per day (9 am, 12 pm and 3 pm) using Fluke115 meter. Shimadzu AX200 analytical balance was employed to determine the mass of accumulated dust, while FEI Nova NanoSEM 450, equipped with Oxford Inca X-Act energy dispersive X-ray detector, was used to determine the mineral morphology and composition. The findings reveal an average daily soiling rate ranging from about 1.11% for PV module positioned at 0° tilt to ~0.11% for PV module at 90°. The result further shows an average daily soiling rate of 0.84% on the PV position at a 30° tilt angle, closest to the site's optimum tilt angle. The bifocal module exposed on a 30° tilt angle shows an average daily reduction of about 1.12% and 0.22% for 90°. The accumulated dust's mass density was recorded to range from 0.21 mg/cm^2 when positioned at the tilt of 0° to about 0.00354 mg/cm^2 at 90° tilt angle for one week. Particle characterisation shows carbon, oxygen and silica to be the main elements of the modules. The study recommended manual cleaning weekly on modules exposed at 30° and once in three weeks for modules exposed at 90° tilt angle (Ullah et al., 2020).

2.11.4 Australia

Ghiotto et al. (2016) attempted to develop the performance prediction model after observing the operational performance data and acquiring PV installation

experience. The prediction of the performance of three large major solar farms was validated theses solar plants are: Greenough River, solar farm with 10 MW located in the Geraldton; Western Australia (WA), Nyngan solar plant with a capacity of 102 MW located in Nyngan; New South Wales (NSW), and Broken Hill solar plant with capacity 53 MW located in Broken Hill, NSW. All plants were developed using Cadmium Telluride (CdTe). The study investigated First Solar's modelling guidelines meant to improve the viability of future installation in Australia. The plants' performance was investigated using an approach where the plants' actual performance data were aligned with an energy prediction software output (Plant Predict). Parameters that significantly impact PV performance, such as spectral shift, temperature, and soiling, were collected from the various sites. Both PlantPredict and PVSyst software were employed to compare the predicted performance. Findings show an average soiling rate of about 0.31% Green river, 0.27% for Nyngan, and 0.14% for Broken Hill solar plant. The validation parameters demonstrated the performance reliability of the modelling guidelines. The study recommended determining the accuracy of any prediction model to reduce contractual performance risk (Ghiotto et al., 2016).

The influence of seasonal variation on PV performance stimulated Tanesab et al. (2016) to conduct a soiling study in Perth, Western Australia (32.0680° S, 115.8352° E) considering its temperate climate. The study investigated the effect of dust on the PV modules degradation in the area. Three PV types (mc-Si, pc-Si, and a-Si) were deployed to quantify the impact of dust on the PV performance over twelve months, considering the seasonal variation with the expectation of natural cleaning by wind and rain. The findings show decreased PV performance towards summer and spring while improving performance was observed towards autumn and winter. The study recommended that natural cleaning by the rain is sufficient for the region (Tanesab et al., 2016).

2.11.5 Europe

As reported through satellite images, the influx of Saharan dust from Northern African during February and March 2017 has prompted a significant concern on PV installation performance in Southern Europe, particularly Portugal. Therefore, Conceição et al. (2018) investigated the impact of dust accumulation on

transmittance in two experimental sites (Évora – 38°34′0.01″ N; 7°54′0.00″ W and Alter do Chão – 39°12′3.39″ N; 7°39′37.09″ W) using of 25 glass coupons each (dimension: 110 mm x 90 mm x 3.2 mm thickness). The samples were grouped based on six coupons positioned at 15° inclination intervals per surface orientation (North, East, South and West) at approximately 1.5 m above the ground. The mass of accumulated dust was determined using microbalance weekly, and particle characterisation is performed using SEM/EDX. Two mc-Si PV modules' performance was earlier measured using Eurotest PV Lite MI 3109 when exposed at a tilt angle of 30° in each site. A maximum of ≈1067 mg/m^2 was recorded in Évora, which was the highest recorded from all sites in a week, while only ≈402 mg/m^2 was recorded from Alter do Chão. The imaging analysis shows high pollen due to olive trees that acted as a barrier to the travelling dust. The PV performance measurement finding shows a maximum power output reduction of about 8% and a short circuit reduction of 3%. The study recommended the need for a long-range forecast of dust movement and its potential impact. It also urged the development of low-cost self-cleaning such as anti-soiling coating.

Dust and dirt particles play a significant role in determining PV performance. Norwegian climate and the regions' isolation conditions could provide ample opportunity for PV penetration, which has started attracting massive interest. Pedersen et al. (2016) investigated PV soiling losses using sixteen low iron glass coupons with 2 mm thickness with eight having an anti-soiling layer, all exposed on a rooftop at a tilt angle 45°. The mass of accumulated dust was determined using a high precision balance. The optical transmittance was characterised using an in-house setup. The collected particles were characterised using an SEM. The findings reveal a transmittance reduction of about 0.09% for uncoated coupons and 0.11% for coated coupons per 10 mg/m^2. Approximately 40 mg/m^2 of saturated dust density was recorded after heavy rainfall, making rain an imperfect cleaning approach. The study recommended a further investigation of soiling using a full-sized module glass in the region.

2.11.6 Middle East

The effect of environmental conditions on PV yield causes significant concern for penetration of the device in Qatar. Abdallah et al. (2016) conducted a

comparative study on PV performance between conventional diffused junction n-type mc-Si PV and Si Heterojunction (SHJ) under a harsh environmental condition in Doha, Qatar (25.33° N and 51.43° E). 150 kWp installation with different PV types including mc-Si, pc-Si, a-Si/μc-Si, CdTe and CIGS was developed in at the Solar Test Facility, Qatar Science and Technology Park, Doha (25°.19.5207'N and 51°26.2458'E). All PV modules were positioned at a 22° tilt angle in Southern orientation. IV characteristic of PV strings was collected on a one-minute interval. Similarly, PV temperature was collected using a thermocouple. Weather data, such as radiance, temperature, and wind speed, were collected. Findings reveal that SHJ shows higher output compared with conventional arrays. The results show that PR drops by about 15% when modules are left uncleaned. The study recommended regular cleaning, particularly after the sand storm and schedule cleaning during the wet season.

The fluctuation of fossil fuel prices led an oil-producing country to develop solar PV installations. This development prompted Kazem and Chaichan (2019) to conduct a feasibility study on the impact of weather and soiling factors that could affect the region's PV performance. Two identical mc-Si PV modules with 125 W rating each were installed in six sites across Oman (16° 40′ and 26° 20′ N and longitudes 51° 50′ and 59° 40′ E) with three in an industrial area (Liwa, Sohar, and Muscat) and others far away from industrial areas (Al-Khabourh, Suwaiq, and Shinas). One module is cleaned, and the other is uncleaned for twelve months, from 1 Nov 2017 to 31 Oct 2018. Digital Voltmeter-Ammeter was used to collect voltage and current data. A whole year of weather data, including wind speed and direction, humidity, rain, temperature, and irradiance for six locations, were collected. Nine manual cleaning approaches were used in cleaning the module. The findings reveal a failure to cleaned modules resulted in about 50% or more PV performance reduction in regions with one month. The result shows a maximum efficiency decrease of 18% in the Liwa site, and the lowest was 5.5% in Al-Suwaiq and Al-Khabourah. The wet season provided natural cleaning for all regions. However, it was observed that it is more effective in Al-Khaburah, Shinas, and Al-Suwaiq and less effective in the other three sites since accumulated particle composition is related to PM_{10}, magnesium and calcium

oxides and NaCl from the refinery and industrial emission. The sodium detergent is found to be effective in removing all the minerals. The study recommended continuous cleaning of PV modules in the region with proximity to refineries and industrial sites.

2.11.7 South America

The Atacama Desert has been reported to be one of the regions with the highest solar irradiance potential globally. However, windblown dust is massive during the summer period, negatively impacting the PV systems' performance. Cordero et al. (2018) investigated soling losses by comparing twenty-four pc-Si modules over one year from January 2017 to January 2018 in five sites (Arica, 18.47° S 70.31°W; Iquique, 20.24°S 70.14°W; Calama, 22.49S 68.9°W; Copiapo, 27.26°S 70.78°W; La Serena, 29.92°S 71.2°W; Santiago, 33.45°S 70.68°W). Each site has four modules where two of the modules were cleaned using a manual washing approach, and the others left uncleaned. Each module is connected to an inverter that registers input every fifteen minutes. Findings have revealed 0.75% (Arica) - 0.05% (Copiapo) daily soiling losses during spring to summer and 1.12% (Arica) to 0.03% (Calama and Copiapo). The maximum annual energy loss of 39% was recorded in Arica, followed by an 18% loss in Iquique, while the lowest loss was about 1% was recorded in Copiapo. The study recommended a cleaning cycle for PV in Arica to be performed every 45 - 75 days and 3 - 4 months in Iquique.

Chile has become one of the countries where PV penetration is massively growing. However, environmental parameters such as climate and soiling seem to be affecting the predicted lifespan of the technology. Urrejola et al. (2016) investigated the annual PV degradation over two years at the Pontifical Catholic University of Chile, Santiago, Chile (3.50°S, 70.61°W) from December 2013. The performance of an array of mc-Si modules with a total capacity of 1590 Wp, pc-Si array with 1410 Wp, and a-Si/μc-Si array with 1380 Wp were analysed when modules were exposed at a 32° tilt angle. Climate data such as temperature (PV and ambient), relative humidity, irradiance, wind speed, the rain was collected using individual sensors. The findings reveal daily PV performance degradation

between 0.13% and 0.56% and an Annual degradation of 1.29% for the pc-Si array, 1.74% for the mc-Si array, and 2.77% for a-Si/μc-Si. It shows that the performance ratio highly depends on temperature. The study recommended a periodic cleaning cycle to be conducted after every 45 days, regardless of cost. It also recommended further research to conduct particle characterisation of dust in the region.

2.12 Summary and conclusion

This chapter presented a summary of Nigeria's renewable energy potential and penetration. It highlighted solar PV as the most viable to overcome its energy deficit based on a number of recommendations presented in the previous chapter and this chapter of the thesis. However, several challenges that severely affect the technology's penetration were identified in the literature and presented. Besides, it was observed that a critical issue such as the impact on PV performance that is globally recognised as a local environmental factor that has a detrimental effect on PV performance had not been rigorously and thoroughly studied in the literature. Therefore, the section further presented a review on the effect of dust on PV systems in Nigeria, describing the generic global source and operational mechanics of dust, underlining the factors that influence its formation on PV surface and its potential impact. It also presented local dust sources with seasonal and regional variation across the country and illustrated some mitigation techniques that could be adopted to restore or maintain the technology's performance. Finally, case studies on the effect of dust on PV performance worldwide were presented considering seven continents. Subsequent chapters presented findings of the investigation of factors influencing dust accumulation and their possible impact.

3 Chapter Three - Indoor assessment of dust properties and PV surface material as factors influencing dust accumulation

3.1 Introduction

Factors influencing PV soiling, such as dust properties, have been investigated by several researchers, as reported earlier in the literature but, only a few dust samples were examined. This section of the thesis studied many dust samples and considered other parameters such as comprehensive investigation and analysis of morphological and chemical/mineral composition that were overlooked or not adequately considered in previous work. The most commonly used PV surface materials (acrylic plastic and low iron glass) were among the parameters investigated. Findings contribute to the body of knowledge in the field of soiling on PV and serve as a guide to engineers to select solar farm sites and plan for adequate mitigation techniques. It highlights the significance of soiling issues and provides a sound foundation that can further research mitigation approaches.

3.2 Method

Zaihidee et al. (2016) stated that conducting an indoor experiment includes the comfort of selecting an appropriate dust sample to be used. For this research, 13 dust samples were collected from Nigeria, measured and quantified. The rationale behind selecting these samples was to include all possible constituents of PM_{10} and $PM_{2.5}$ identified in the literature review around the region. Figure 3.1 is the digital image showing all the samples. Each sample was loaded into a 40 ml bottle and weighed using a ME204 Mettler Toledo sensitive digital scale. The weight of each sample is documented in Table 3.1 below. Each sample was deposited using two approaches (dry and wet) on two different materials (low iron glass and Acrylic plastic). The materials were selected because of their high-level transmittance properties, and they are widely accepted and used materials in the PV industry. Each low iron glass and acrylic plastic had a dimension of 130 x 130 x 4 mm. A mini-module with an active area of 1208.4 mm was developed using four mc-Si cells, with dimensions 52 mm x 52 mm.

Table 3.1 shows the initial average weight of samples used for both depositions. All samples are dry except bird droppings, which had particles in semi-solid form. It was observed that tipping of the coupons and wind effects also caused blowing off, rolling, and sliding particles. Particle weight was not measured after deposition; therefore, the exact weight of deposit particles that remained on the coupons was not measured. The wet deposition might have had additional weight since water was added, but the weight was not measured.

Figure 3.1: Digital images of dust Samples.

Table 3.1: Dust samples.

Sample	**Weight**
Ash	21.8 g
Bird droppings	16.2 g
Carpet dust	10.3 g
Cement	33.2 g
Charcoal	15.6 g
Salt	48.1 g
Sand - Coarse	54.4 g
Sand - Laterite	41.0 g

Soil - Clay	44.3 g
Soil - Loamy	50.9 g
Soil - Sandy	40.3 g
Stone dust	46.5 g
Wood dust	10.3 g

3.2.1 Samples preparation and deposition

Determining an appropriate way to simulate the dust deposition for an indoor experiment is a critical task. Injection and fan mixing (Jiang et al., 2011), spraying sample with water content (Kaldellis et al., 2011), using a wind tunnel and manually discharging samples from a dust cloud producer (Goossens and Van Kerschaever, 1999), using a diffuser integrated with a sandblaster (Al-Hasan, 1998) and by manual sieving and free fall from a tube (Beattie et al., 2012; Qasem et al., 2011) are the reported methods for this work. All these methods resulted in different cluttering patterns and uniformity on the platform. However, natural dust depositions are not the same around the world. This research adopted the manual and free-fall approach reported by Beattie et al. (2012) and Qasem et al. (2011) based on its simplicity to achieve natural positioning, initial bouncing, and re-suspension particles that occurred in the natural deposition. However, this approach does not provide an accurate representation of natural dust accumulation. It only permits experimenting with extreme soiling conditions to highlight degradation that could occur during severe weather such as a sand storm, volcanic eruption, wildfire, tornado, hurricane, windstorm and other natural disasters.

Samples were deposited using an in-house developed dispenser, made using a 3D printer with thermoplastic Polyurethane. The dispenser was designed only to allow particles less than or equal to 2 mm to fall. The dispenser was initially used to sieve samples to eliminate particles greater than 2 mm. It was later used to spread out a bottle (40 ml) of each sample on each coupon (low iron glass or acrylic plastic). The inertial force was applied based on the design of the dispenser where the upper part has a wider opening, and the lower part is narrowed down to only allow particles less than or equal to 2 mm to pass through,

enabling Brownian diffusion to take place where particles collide with one another to settle on a coupon. Particles become adhered to one another due to Van der Waals forces that make small dry particles stick to one another. Samples were deposited and allowed to settle for about 24 hours to promote sedimentation. Then the coupons were tilted to about 45° to allow the gravitational effect to remove particles that have not adhered.

Furthermore, coupons were tilted to 90° and subsequently exposed to a table fan which generated wind at a 4 m/s to simulate its effect. (See, Figure 3.2 for dry deposited samples). This approach is used to represent the dry season dust deposition.

Said and Walwil (2014) stated that when water exists between the dust particles, creating capillary bridges between the particles dust and between particles and the surface. It has been reported by Isaifan et al. (2019) stated that capillary forces proliferate when the relative humidity is above 70%. Natural relative humidity and dew were avoided in order to prevent biasing the parameters.

The wet deposition is used to represent the dew and rainy season dust deposition. The same dispenser was used in spreading the same amount of dust on the surface area of the coupons. Coupons were sprayed with 20 ml water before and after sample deposition and were allowed to dry for about 24 hrs. The initial 20 ml water spray was to simulate dew. The spraying after the deposition was to simulate light rainfall so that diffusiopherisis will allow cementation of particles considering the capillary bridges created by the water (see Figure 3.3 for wet deposited samples). Coupons were tilted to about 45° and 90° to allow gravitational effects and exposed to a table fan that generated wind at 14 km/hr (~4 m/s).

The wind velocity used in this study falls within the ranges of wind speed in Nigeria. Argungu et al. (2019) reported that average wind speed at the height of 10 m in the North ranges from 4.0 to 5.12 m/s and 1.4 - 3.0 m/s in the southern part. The blowing of wind towards the coupon is an attempt to remove some particles using a natural mitigation approach. Kazem and Chaichan (2019) stated

that whenever the wind direction faces a PV module's surface, the air movement removes a certain amount of accumulated dust particles. Gholami et al. (2017) stated that the critical levels determining the dust accumulation on the PV module are average wind speed above 4 m/s and relative humidity below 50%. This figure was determined in Iranian dry, hot conditions but could be adopted when examining dust samples with similar properties. Higher wind velocity might occur during the wet season, but the wind speed used here could illustrate extremities of accumulation pattern.

Figure 3.2: Dry deposition illustrating 13 samples deposited on acrylic plastic and low iron glass where all samples on the left sides are acrylic plastic except clay where it is positioned on the right.

Figure 3.3: Wet deposition illustrating 13 samples deposited on acrylic plastic and low iron glass where all samples on the left sides are acrylic plastic.

Several attempts were made to acquire natural bird droppings deposition by placing coupons in strategic locations where birds were usually found but were

not achieved. Bird droppings were collected in semi-solid and solid forms and were preserved in bottles to maintain freshness. During both depositions, samples were poured over the coupon surfaces without using the dispenser.

3.2.2 Procedure

This subsection provides detailed step by step procedures employed in data collection. The subsection is divided into three categories, including spectral, imaging and PV yield characterisation. A flowchart illustrating the various steps through the research methodology of this subsection of the thesis is provided in Appendix B – Figure 0.3.

3.2.2.1 Spectral test

The optical characterisation was conducted to determine the transmittance deterioration level caused by each dust sample on various coupons using the Perkin Elmer Lambda 1050 UV/VIS/NIR spectrometer. Clean low iron glass and acrylic plastics were first tested to identify and confirm the coupons' actual transmittance levels. Each sample from the various deposition methods was then subjected to spectral transmittance evaluation. UV (Ultraviolet), VIS (Visual) and NIR (Near Infra-Red) transmittance level of each sample was measured, ranging from 250 nm to 1250 nm wavelength. This was to investigate the dust samples' transparency, considering the wavelength within which the used PV technology (monocrystalline solar cells) responds, as mentioned earlier. The transmittance results are validated using the following Equation (3.1), where S(λ) is the relative spectral distribution of solar radiation, T(λ) is the spectral transmission, and Δλ is the change in wavelength.

$$\tau_{solar} = \frac{\sum_{\lambda=300nm}^{1250nm} S(\lambda)T(\lambda)\Delta\lambda}{\sum_{\lambda=300nm}^{1250nm} S(\lambda)\Delta\lambda} \quad (3.1)$$

The spectrometer's schematic diagram is provided below in Figure 3.4 to illustrate how the transmittance was measured.

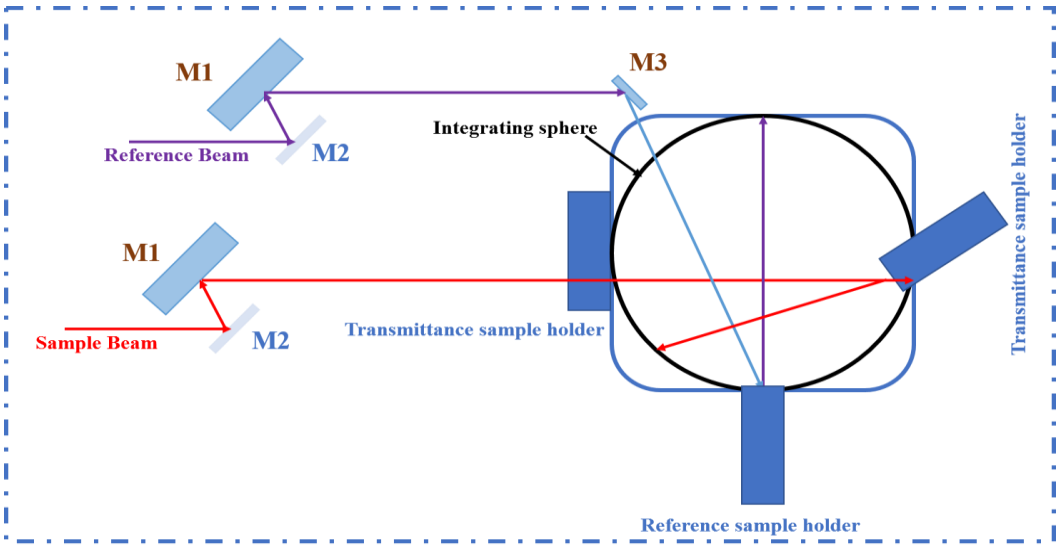

Figure 3.4: Schematic diagram of Perkin Elmer® Lambda 1050 UV/VIS/NIR spectrometer illustrating the transmittance test procedure.

3.2.2.2 Image Analysis

Image characterisation was conducted to determine the morphology and chemical composition of each dust sample. Samples were carbon prepared using an Em-tech low profile pin stub with a diameter of 25 mm and a conductive carbon tab. Samples were carbon-coated using the Emi-Tech K950 carbon coating machine before they were subjected to image scanning using the SEM (S) Quanta FEG 650, which was equipped with an EDX (Energy Dispersive X-ray). Each sample's morphology was characterised using the shape and size of the backscattered electrons (BSE) and the secondary electron (SE) images. Each sample's chemical composition was identified using the EDX results and further analysed using specific information such as diaphaneity and mineral density from online mineralogy databases such as webmineral.com, mindat.org and minerals.net. Surface roughness was observed and analysed by comparing SEM images obtained in this research and SEM images reported in the literature mentioned above.

The size and shape of the particle were analysed using SEM images and equations provided in the literature. The surface diameter and area were measured and estimated from the SEM images. Aïssa et al. (2016) provided Equation (3.2) and Equation (3.3) which were adopted for analysing the SEM

images using the aspect ratio and particle shape. Shapes were determined using SEM images that present a 3D view of the dust particle, where *A* is the cross-sectional area of the dust particle, *Lproj* is the most extended dust particle's length, and where P is the perimeter of the dust particle in Equation (3.3).

$$(\boldsymbol{Aspect\ ratio}) = \frac{\pi(L_{proj})^2}{4A} \tag{3.2}$$

$$(\boldsymbol{shape}) = \frac{P^2}{4\pi A} \tag{3.3}$$

Kalashnikov and Sokolik (2004) also provided Equation (3.4) to estimate the surface radius. This research adopted the equation since all parameters can be measured and estimated, and it was achieved using Equation (3.4), where R is the radius and surf is the surface of the particle. Figure 3.5 illustrates the image characterisation procedure conducted on each of the samples. The estimated dimensions were obtained from the SEM images. All estimations were presented in Table 3.3.

$$\boldsymbol{R_{surf}} = \sqrt{\boldsymbol{S}}/\boldsymbol{4\pi} \tag{3.4}$$

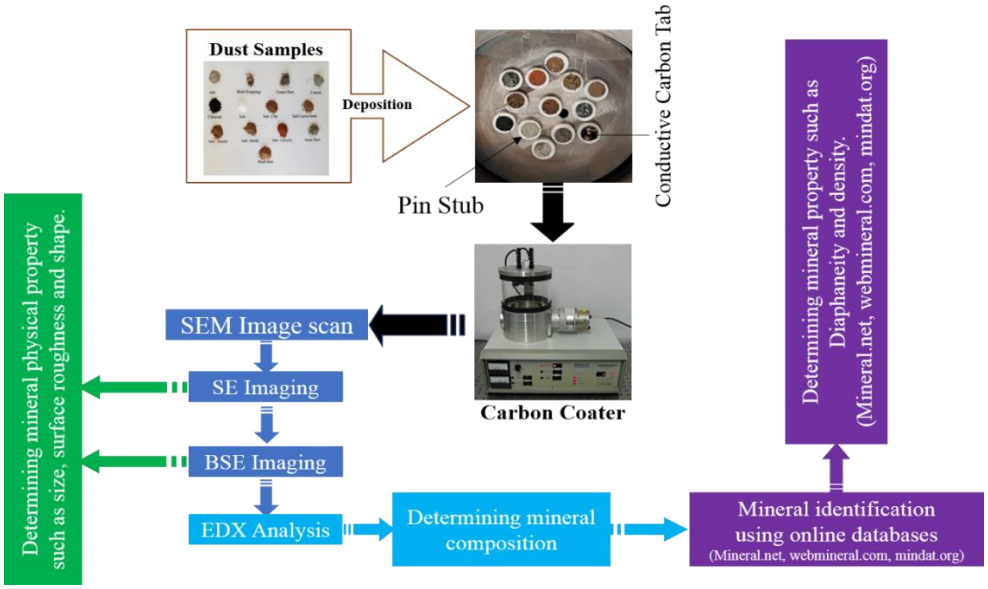

Figure 3.5: Image characterisation.

3.2.2.3 PV Performance Measurement

The mini module's performance was tested using a Wacom continuous solar simulator at a controlled temperature of 25°C and was subjected to several tests using thirteen dust samples deposited on the two types of coupons, as mentioned in section 3.2. The module was initially tested without surface covering to obtain baseline performance data of the module. Then modules were individually tested with a covering of clean acrylic plastic and low iron glass coupon. The device was further tested by covering the active area with each of the dust samples from the two deposition methods highlighted above. Current and voltage data were generated, and the power data were computed to plot the I-V/P-V (current-voltage / power – voltage) curves for analysis. The air vacuum effect between the solar cells and the coupons used was ignored since the experiment focused on dust on short circuit current reduction. Therefore, modules were not exposed to light for an extended period to avoid temperature excitement that could lead to voltage degradation, affecting the device's overall output. Thermophoresis was prevented during the experiment since the ambient temperature and the PV temperature are equal throughout the period. The results obtained allow easy data analysis and highlight the power degradation caused by the various dust samples deposited on the different surface materials. A schematic diagram representing the procedure of PV performance measurement is illustrated in Figure 3.6 below.

To verify the results, mathematical equations provided by Hachicha et al. (2019) and Kalogirou (2009) were adopted. Equation (3.5) was used in determining the degradation of PV performance caused by dust accumulation using normalised electrical PV characteristics such as voltage, current and power, where φ represents the PV electrical output parameters (voltage, current and power).

$$\boldsymbol{\varphi}\ \mathbf{normalised} = \frac{\boldsymbol{\varphi}\ \mathbf{dusty}}{\boldsymbol{\varphi}\ \mathbf{clean}} \tag{3.5}$$

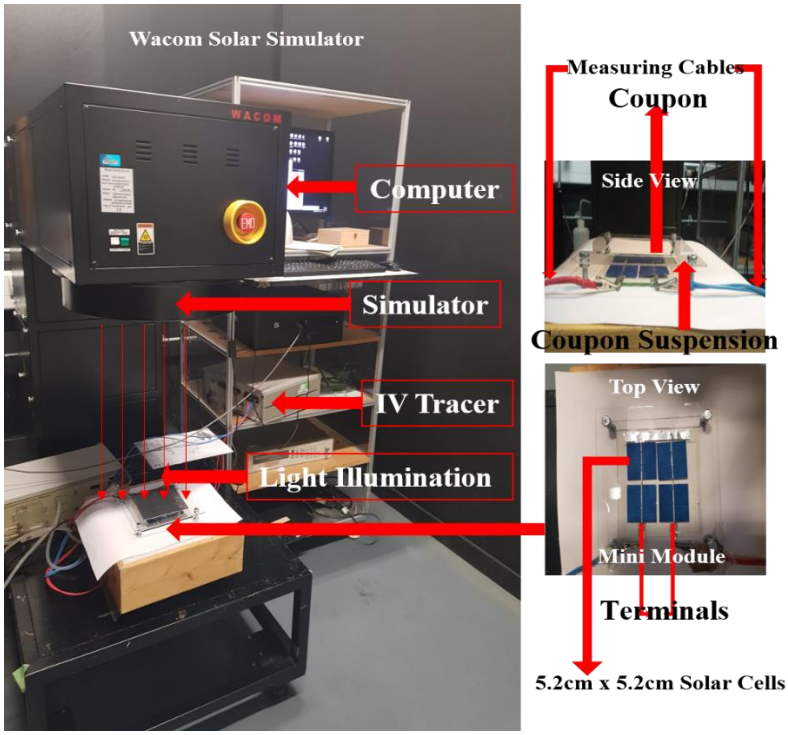

Figure 3.6: PV performance characterisation procedure using a Wacom continuous solar simulator.

This is further calculated using soiling Equation (3.6), relative to a clean surface, where SL_{PV} is PV soiling, P_{max} is the maximum power that passes through the maximum power point when the load resistance is optimum. The dissipated power to the resistive load is maximum, $P_{max,clean}$ represents the maximum power output of a clean module and $P_{max,dusty}$ represents a module with dust accumulation.

$$\mathbf{SL_{PV}} = \frac{P_{max,clean} - P_{max,dusty}}{P_{max,clean}} \tag{3.6}$$

The P_{max} equation is explained using Equation (3.7), where I_{max} is the load current which maximises the output power, and V_{max} is the voltage that maximises the power output, and P_{max} can also be represented using Equation (3.8), where I_{SC} is the short circuit current, V_{OC} open-circuit voltage, and FF is the fill factor obtained from the IV tracer. The FF can be calculated using Equation (3.9).

$$\mathbf{P_{max}} = \mathbf{I_{max}}\,\mathbf{V_{max}} \tag{3.7}$$

$$P_{max} = I_{sc}V_{oc}FF \tag{3.8}$$

$$FF = \frac{P_{max}}{I_{sc}V_{OC}} = \frac{I_{max}V_{max}}{I_{SC}V_{OC}} \tag{3.9}$$

Table 3.2: Mini module's parameters.

Parameter	**Value**		
Type	Monocrystalline Solar Module		
Surface Material	Clear	Acrylic Plastic	Low Iron Glass
Maximum Power (P_{max})	1.62 W	1.55 W	1.5 W
Output Tolerance	0 ~ ± 5%		
Maximum Voltage (V_{mpp})	2.0 V	2.0 V	2.0 V
Maximum Current (I_{mpp})	0.82 A	0.77 A	0.76 A
Open Circuit Voltage (V_{OC})	2.5 V	2.45 V	2.44 V
Short Circuit Current (I_{SC})	0.95 A	0.90 A	0.89 A
Weight	229.4 g	310.0 g	392.6 g
Fill Factor	0.7	0.704	0.703
Dimensions	150 mm x 150 mm		
Test Conditions	1000 W/m^2, AM 1.5, T = 25°C		

3.3 Results and analysis

This section presents the results of all the experiments mentioned above. PV performance results, spectral results, and SEM images of each dust type are presented to describe the individual sample's effect. The mini module's IV/PV (current and voltage/ power and voltage) curve is initially introduced in Figure 3.7 to show the system's optimum performance and its IV and PV characteristics.

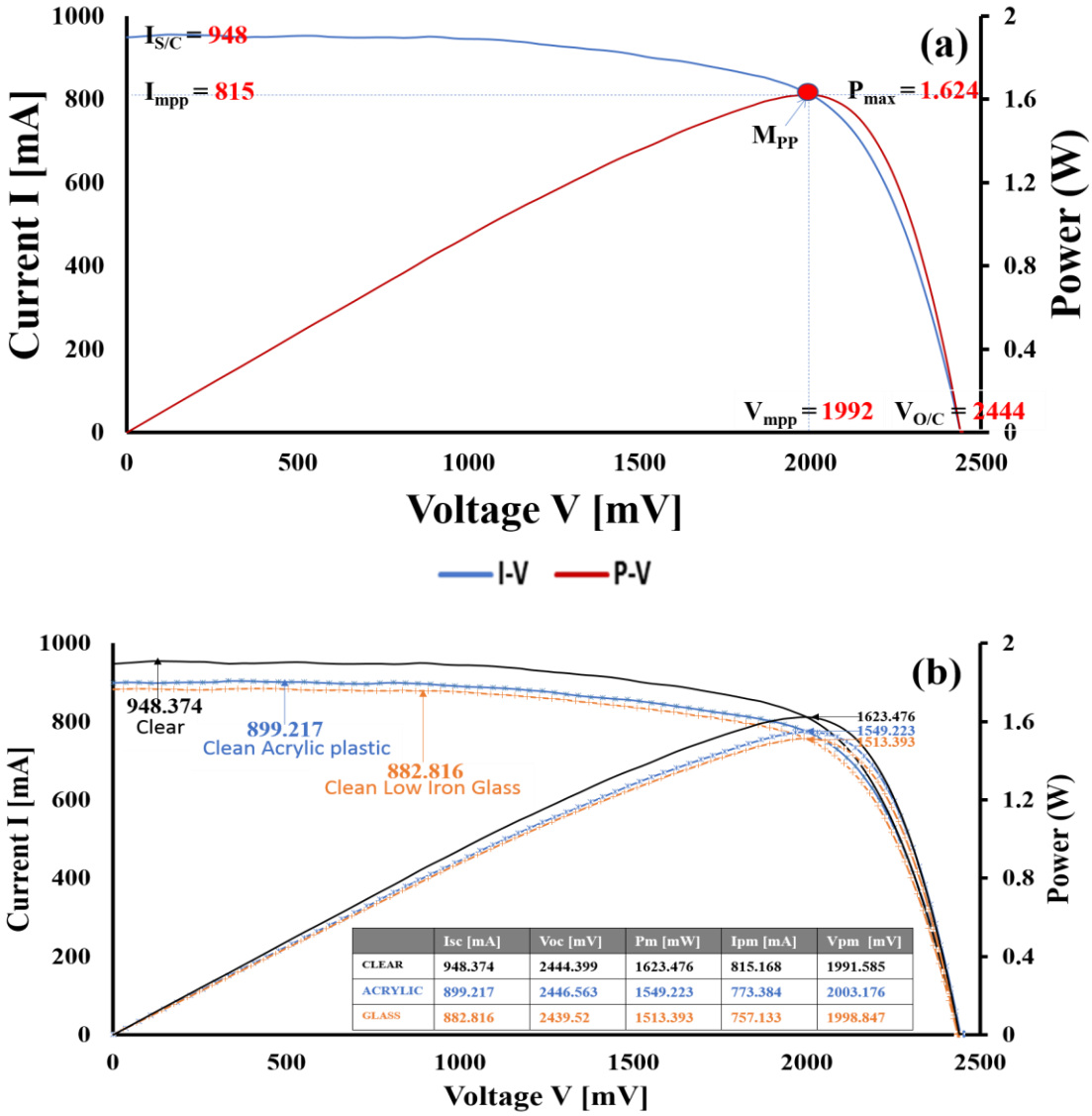

Figure 3.7: Mini module's IV/PV curve (a) clear, (b) clear, clean acrylic plastic and clean glass.

3.3.1 Ash

The sample ash is also known as fly ash and is a fine by-product of burnt dry wood, a common source of dust in developing countries due to farm by-products to generate energy. Combustion of materials such as wood in high temperatures leads to both fly and bottom ash production. The fly ash can be transported by wind. Results from the various experiments show that when ash is considered as a source of dust, it has a detrimental effect on the PV performance because it obstructs the photovoltaic effect from reaching the solar cells of a PV module (Kazem et al., 2013; Kaldellis et al., 2011) and Figure 3.8 confirms this assertion.

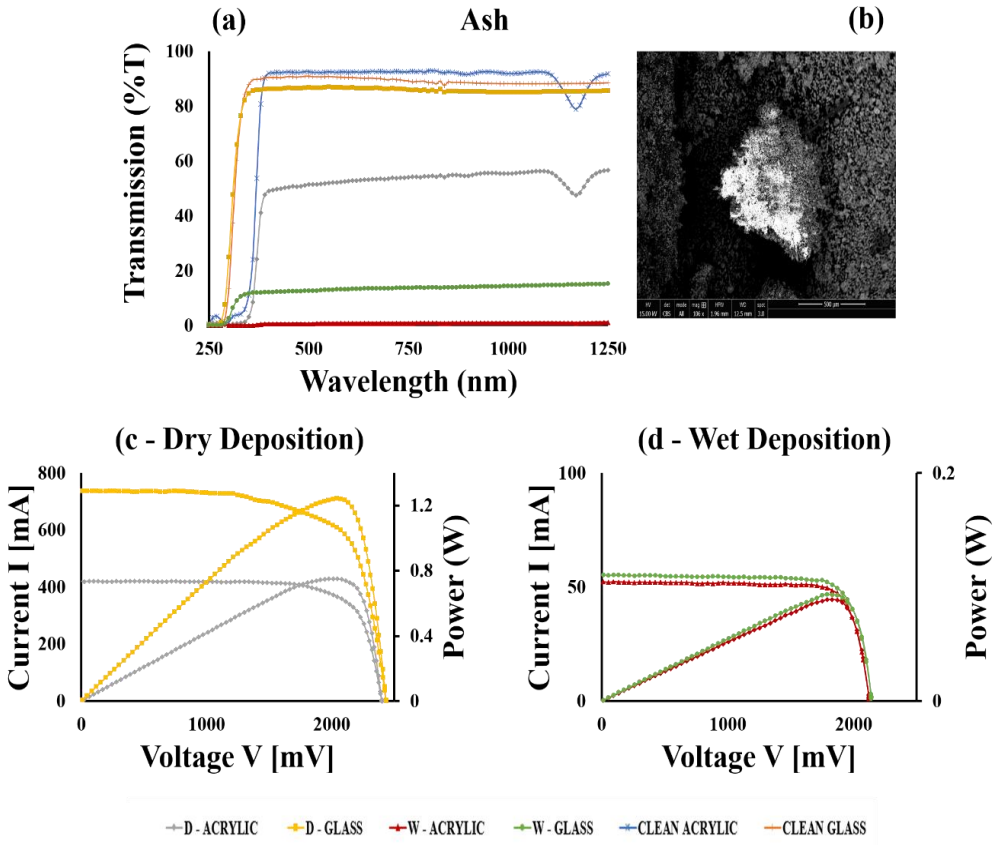

Figure 3.8: Ash - (a) Spectral transmittance (b) SEM imaging (c and d) PV performance.

Figure 3.8 shows the spectral transmission, SEM and PV performance while coupons (acrylic and glass) were deposited with ash. The light transmission reduction was recorded when ash was dry deposited on coupons with a 55% reduction for acrylic and 4% for low iron glass. On the other hand, a very high radiation reduction was recorded when it was wet deposited, where acrylic plastic had 99%, and low iron glass has 87% degradation. The image characterisation shows that ash dust particles appear to have minerals that seem opaque, angular in structure, small in size (µm), dense and have a coarse surface. The short circuit current (I_{SC}) degraded by about 56% when ash was dry deposited on acrylic plastic and about 22% on the low iron glass. It also shows that about 94% of I_{SC} degraded when the ash sample was wet deposited on the acrylic plastic and similarly on the low iron glass.

3.3.2 Bird droppings

This is the faeces of flying birds, which is a combination of liquid and semi-solid materials. Faeces comprise a mixture of three components, depending on the bird's consumption; uric acid, which comes in the liquid form, the green material and whitish parts, which are semi-solid. These materials are always opaque. Bird droppings have a devastating effect on light transmittance, reducing a module's Pmax (maximum power). The results below highlight the effect of soiling caused by bird droppings on PV performance.

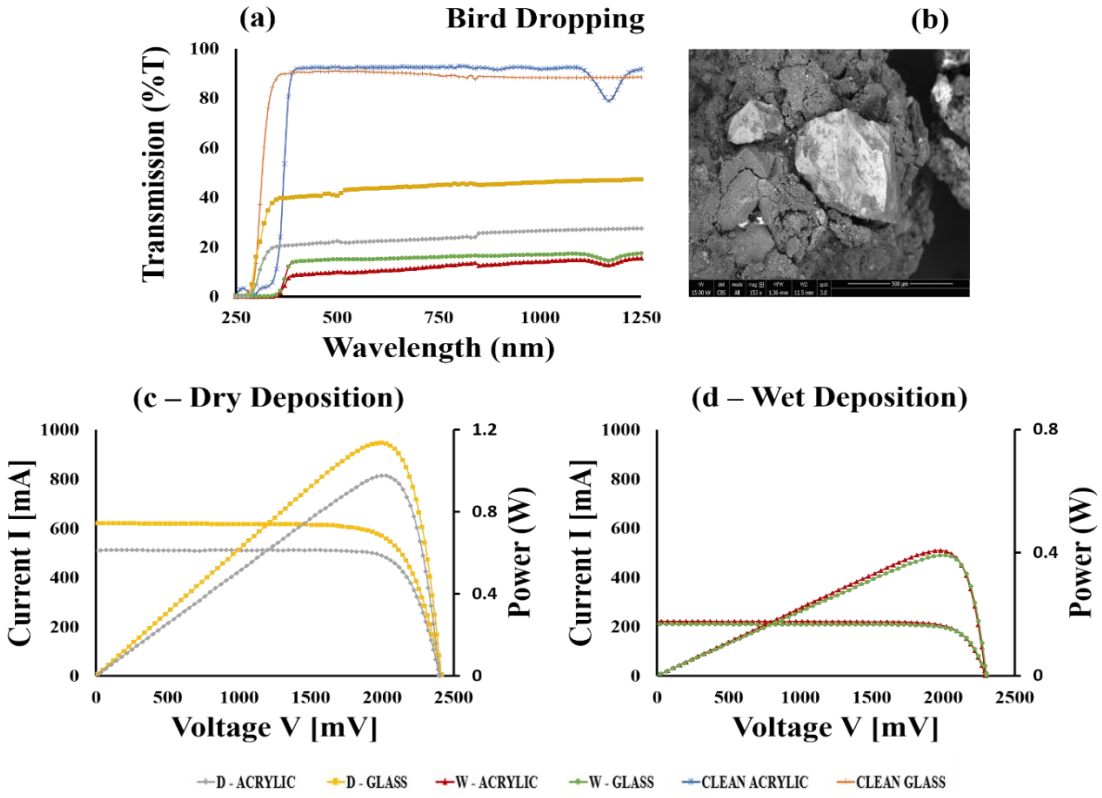

Figure 3.9: Bird droppings - (a) Spectral transmittance (b) SEM imaging (c and d) PV performance.

Figure 3.9 shows the spectral transmission, SEM and PV performance when coupons (acrylic and glass) were deposited with bird droppings. The very high transmission reduction was recorded when bird droppings were deposited onto coupons with acrylic reaching 90% and low iron glass 54%. On the other hand, when the bird droppings were wet deposited, a reduction of about 87% was recorded on acrylic plastic and 75% on the low iron glass. Image characterisation shows that bird droppings comprising many different minerals appear to be

transparent, translucent, and opaque, which reduces the penetration of light. The density of the materials observed would slow flux intensity and can cause light absorbance. The surface of the particle was found to be fine and smooth, which promotes light scattering. Sample shape appears to be aggregated, and the sizes were not uniformly distributed because some parts appeared to be large while others were tiny. Light can penetrate through the areas with larger particle deposition because they are porous. Also, due to lack of a urinary bladder, bird droppings come with a percentage of liquid (uric acid), and this promotes capillary bridges that can lead to the closure of small gaps and porous areas, disrupt light penetration and further promote cementation. The PV performance results show that the short circuit current degraded by about 46% when bird droppings were deposited on the acrylic plastic and about 35% on the low iron glass. Further degradation was observed when more water was added to various coupons to simulate light rain and dew. An almost two-fold deterioration was observed, with I_{SC} reduction of 87% on acrylic plastic and 74% on the low iron glass.

3.3.3 Carpet dust

These are particles stored in carpets, and some are visible while others are not. These particles can be anything, including volatile organic compounds. According to Becher et al. (2018), carpets are the repository for indoor air pollutants such as dust particles, biological contaminants, dirt and allergens. Some of these materials can be emitted into the air and transported by the wind in the atmosphere and, when deposited on a PV module, can cause light transmittance disturbances. The results below highlight the effect of soiling due to carpet dust on PV performance.

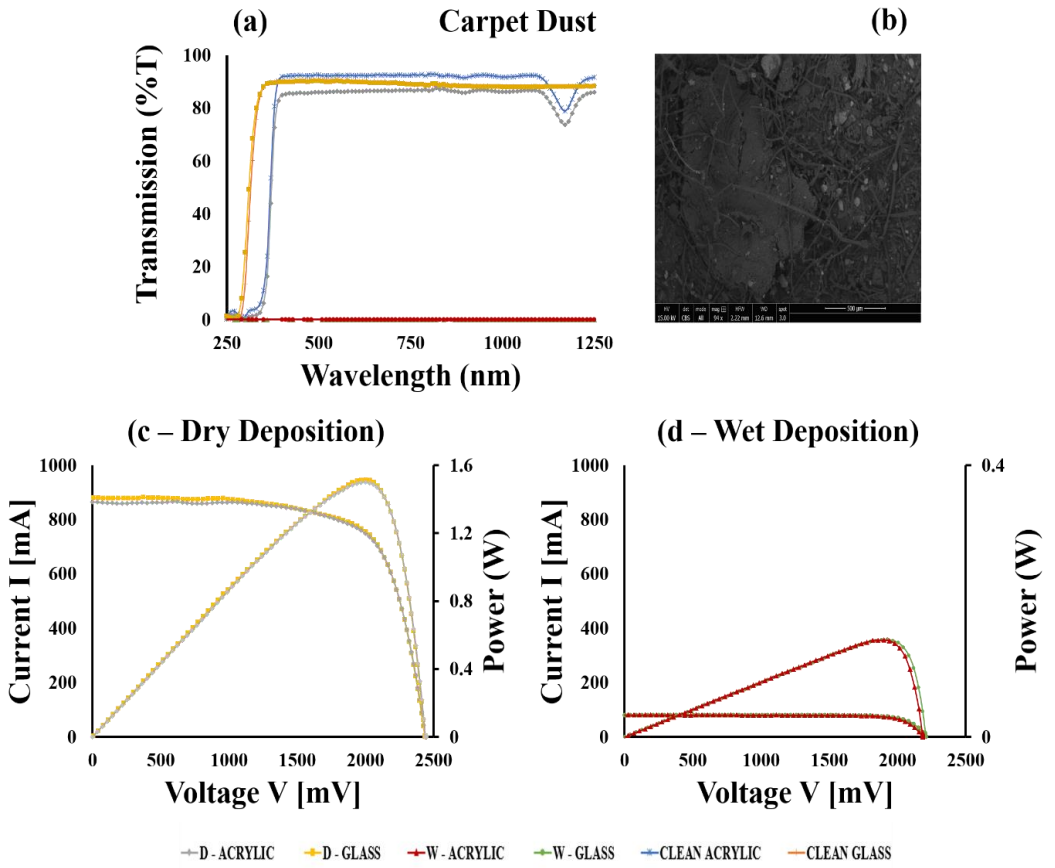

Figure 3.10**:** Carpet dust - (a) Spectral transmittance (b) SEM imaging (c and d) PV performance.

Figure 3.10 illustrates the spectral transmission, SEM and PV performance when coupons (acrylic and glass) were deposited with carpet dust. Meagre light transmission reduction was recorded when carpet dust was dry deposited on the coupons, with acrylic plastic showing about 8% and low iron glass just 1% reduction. On the other hand, the high reduction was recorded when carpet dust was wet deposited on coupons where almost 100% decrease was documented on both coupons. Image characterisation shows that ash carpet dust combines a wide range of minerals, and the sample used for this research appears to be translucent and opaque, which can attenuate light transmittance. Minerals appeared to have a high mineral density, which can slow down the flux intensity of light. The surface of the particles was observed to be coarse and might possess good light transmittance qualities. Particle sizes appear to be a combination of tiny invisible and large visible particles, but all particles were very light in weight. Sample shape appears to be a bent angular/triangular channel-like structure representing a better optical property and can promote light penetration. Even

though the carpet dust possesses some positive light transmittance qualities, the negative qualities surmount. The PV performance result shows that the short circuit current degraded by about 9% when carpet dust was dry deposited on the acrylic plastic and 7% on the low iron glass. An alarming increase was observed when the sample was wet deposited on the various coupons, with a 91% loss on acrylic plastic and 92 % on the low iron glass.

3.3.4 Cement

This is a fine complex mixture of several compounds using high temperatures of >1400^{0}C and building material (Taylor, 1992). Various compounds are used to produce cement; each cement type's chemical components depend on the company. Cement is light in weight and can be transported by the atmospheric wind from one location to another. Moreover, when deposited on a PV, it can reduce or obstruct light transmittance. The results below highlight the effect of soiling caused by cement on PV performance.

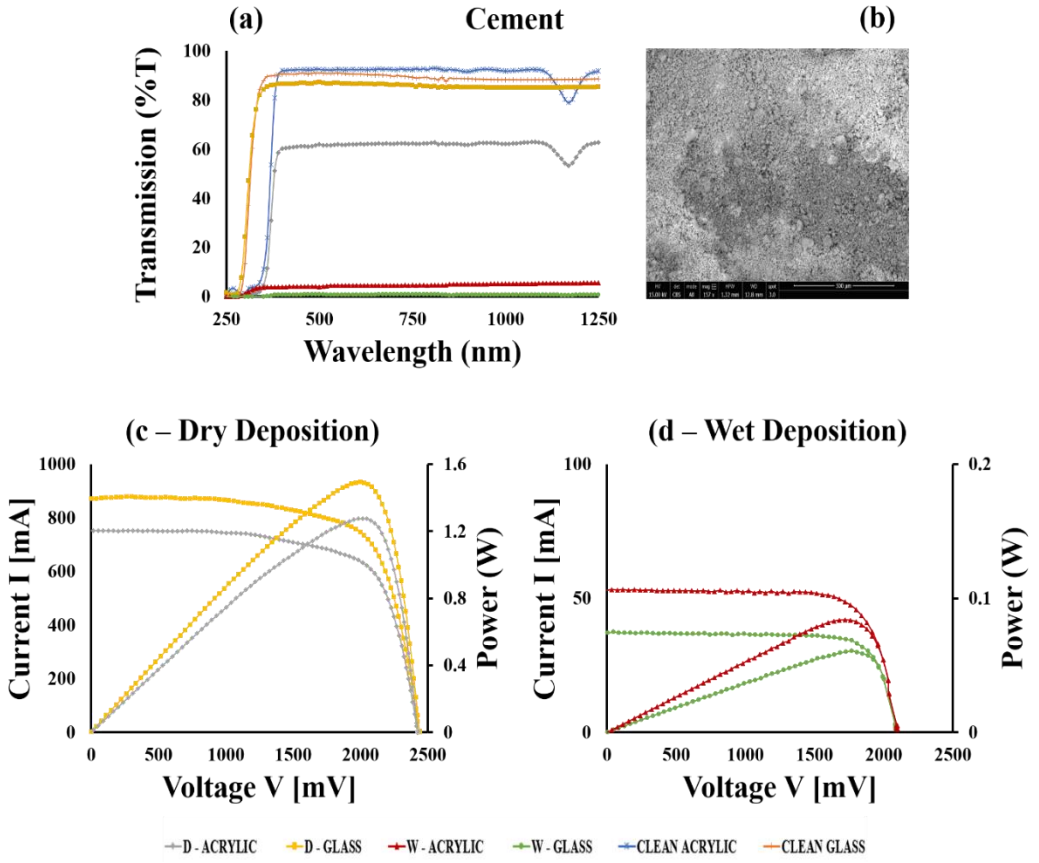

Figure 3.11**:** Cement - (a) Spectral transmittance (b) SEM imaging (c and d) PV performance.

Figure 3.11 illustrates the spectral transmission, SEM and PV performance when coupons (acrylic and glass) were deposited with cement. When the cement was dry deposited on coupons, the light transmission was reduced by about 34% on acrylic plastic and 4% on the low iron glass. On the other hand, the high reduction was recorded when cement was wet deposited on coupons with an acrylic plastic recording about 95% and low iron glass about 99% reduction. The image characterisation shows that cement particles appear to be opaque with the capacity of attenuating light. These minerals appear to have high density, which can slow the light's flux intensity, resulting in light absorbance. Particle surfaces are coarse, which present good quality of light transmittance. The particles are tiny in size, and this can attenuate the light. An angular flattened shape was observed, promoting minerals' optical property and allowing more transmittance of light. Even though the sample has some good optical qualities, the negative qualities surmount. The PV performance result shows that the short circuit current degraded by about 21% when cement was dry deposited on acrylic plastic and 8% on the low iron glass. A high increase in degradation was observed when the cement sample was wet deposited on the various coupons, where degradation of about 94% on acrylic plastic and 96% on low iron glass were recorded.

3.3.5 Charcoal

This is a by-product of agro and forestry-based residue generated using a small amount of oxygen. The charcoal powder's quality or composition depends on the original material and can have various chemical characterisations; however, most of them are interrelated with pure carbon content. The charcoal itself is big and heavy, but the mechanical process breaks it down and produces a powder-like material that settles at the bottom. During transfer or movement, these fine particles escape into the atmosphere and are transported by wind to another location. This material is opaque, and when deposited on PV, it will decimate light transmittance to PV cells. The results below highlight the effect of charcoal powder accumulation on PV performance.

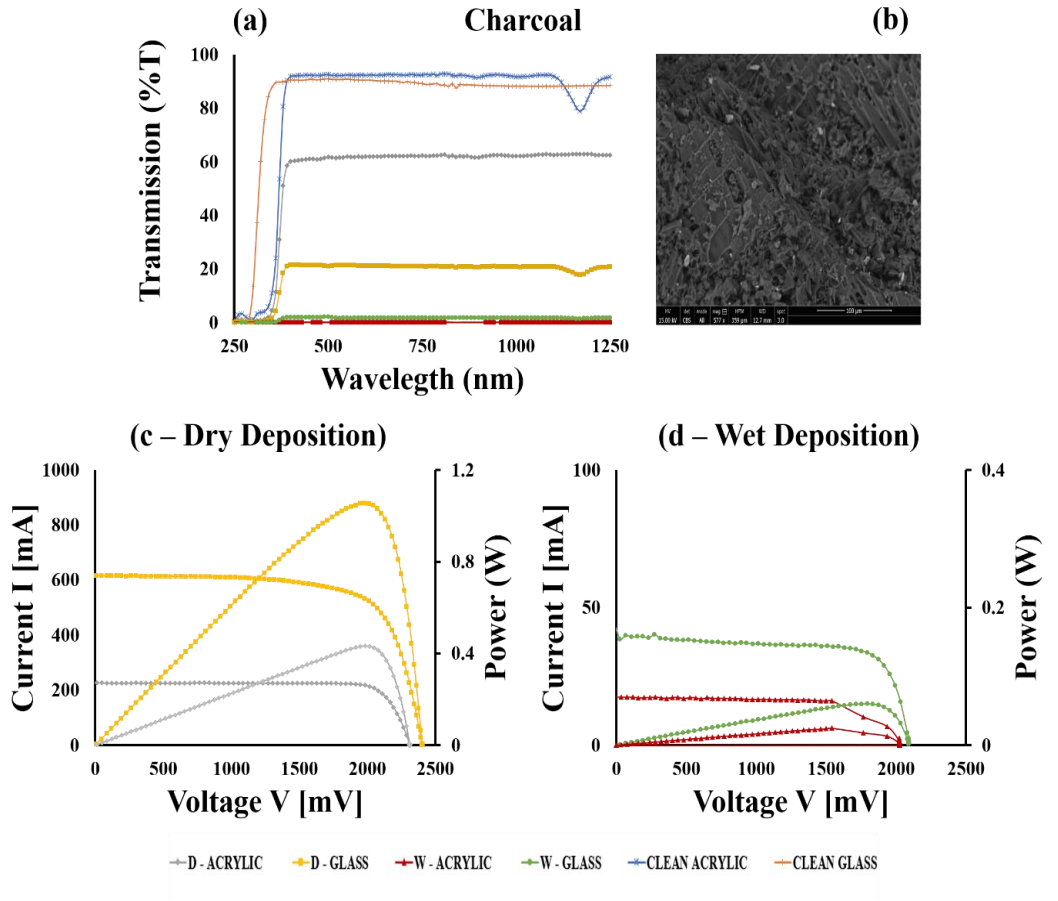

Figure 3.12**:** Charcoal - (a) Spectral transmittance (b) SEM imaging (c and d) PV performance.

Figure 3.12 shows the spectral transmission, SEM and PV performance when coupons (acrylic and glass) were deposited with charcoal. A decrease in light transmission was recorded when charcoal dust was dry deposited on coupons of about 77% on acrylic and 35% on the low iron glass. On the other hand, the high reduction was recorded when charcoal was wet deposited on coupons with an acrylic plastic recording about 98% and low iron glass almost 100% reduction. The image characterisation shows that charcoal is a dark compound characterised with opaque minerals with absorbance, scattering and attenuation effects on light. These minerals appear to have a high density and are capable of slowing flux intensity. Mineral surfaces seem to be coarse, smaller in size with a few medium sizes, which can cause light attenuation. The particles appear in flaky aggregated triangular glassy like structures and are very light in weight. The PV performance result shows that the short circuit current degraded by 76% when the charcoal sample was dry deposited on the acrylic plastic and about 35% on

the low iron glass. A substantial increase in degradation was observed when the charcoal sample was wet deposited on the various coupons, where about 98% of degradation was recorded on acrylic plastic and 95% on the low iron glass.

3.3.6 Clay

Clay is comprised of minuscule particles with high cohesion, dilatancy and plasticity and low permeability. When particles are dry, it becomes solid, but when wet, it becomes sticky because of its high-water retention. Tiny silicates are the main minerals found in clay soil. They are light in weight and can be transported by the wind in the atmosphere to PV surfaces, which can cause a reduction of light transmittance to PV cells. The results below highlight the effect of clay formation on PV performance.

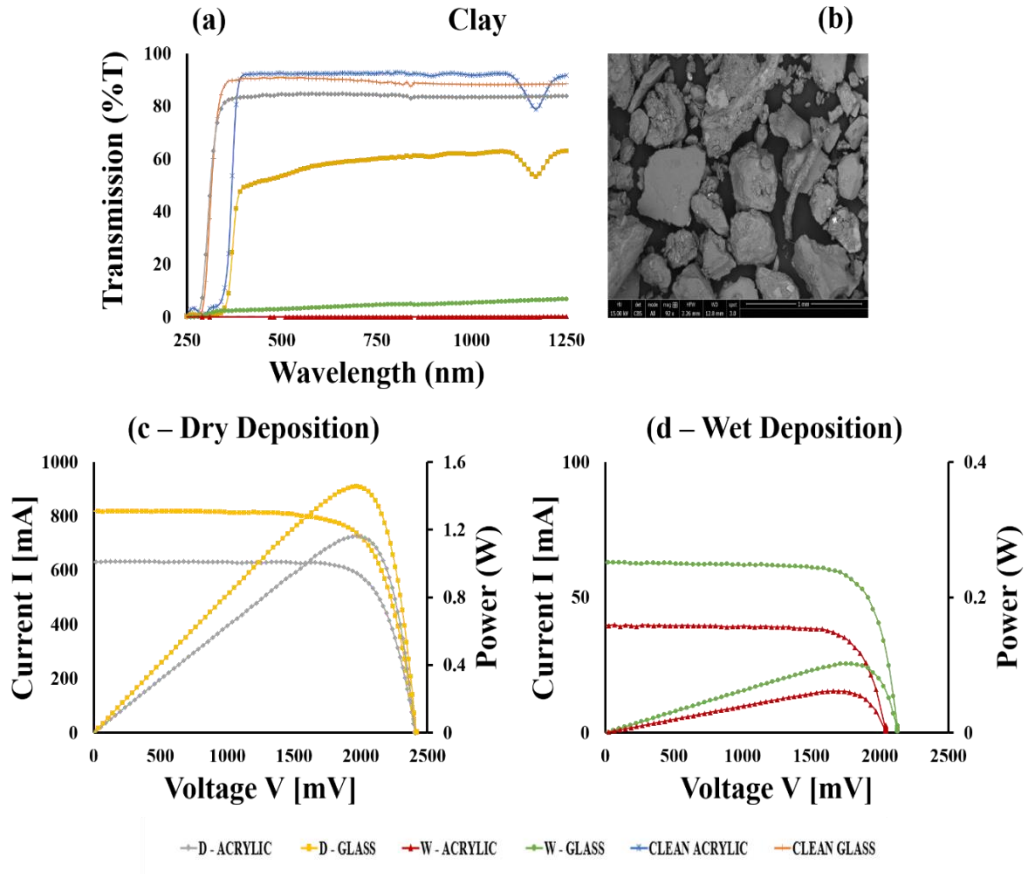

Figure 3.13**:** Clay - (a) Spectral transmittance (b) SEM imaging (c and d) PV performance.

Figure 3.13 shows the spectral transmission, SEM and PV performance when coupons (acrylic and glass) were deposited with clay. The reduction in light transmittance was recorded when clay was dry deposited on coupons of about 43% on acrylic plastic and 8% on the low iron glass. On the other hand, a high reduction was documented when clay was wet deposited on the coupons, with the acrylic plastic recording about 100% and low iron glass a 77% reduction. The image characterisation shows that the clay comprises fine minerals that exhibit plasticity and low permeability and appear to be partially translucent and opaque, which has an attenuation effect on light transmittance. Minerals density appears to be high, which can result in reduced flux intensity, causing light absorbance. Particles have smooth and fine surfaces, which can promote scattering, and the shape seems to be a flaky rounded crust structure, resulting in light reflection or attenuation. Particles are very tiny and heavy but can be blown by the wind or gravitational effects, causing rolling, sliding and lift-off. The PV performance result shows that the short circuit current degraded by about 33% when clay samples were dry deposited on acrylic plastic and 14% on the low iron glass. A high increase in degradation was observed when the clay sample was wet deposited on the various coupons, where about 96% was recorded on acrylic plastic and 93% on the low iron glass.

3.3.7 Coarse sand

This is soil mixed with larger grit pieces that are heavy, cannot be transported by wind, and hardly stick together even when wet. Coarse sand is described with secondary fraction, larger grain shape, mass structure and density. This material has poor permeability and can hardly settle on a surface. It is difficult to transport, deposit and cement to the surface of a PV module. However, it can be transported and deposited on the module's surface during sandstorms or strong wind, reducing light transmittance to PV cells. The results below highlight the effect of coarse soil formation on PV performance.

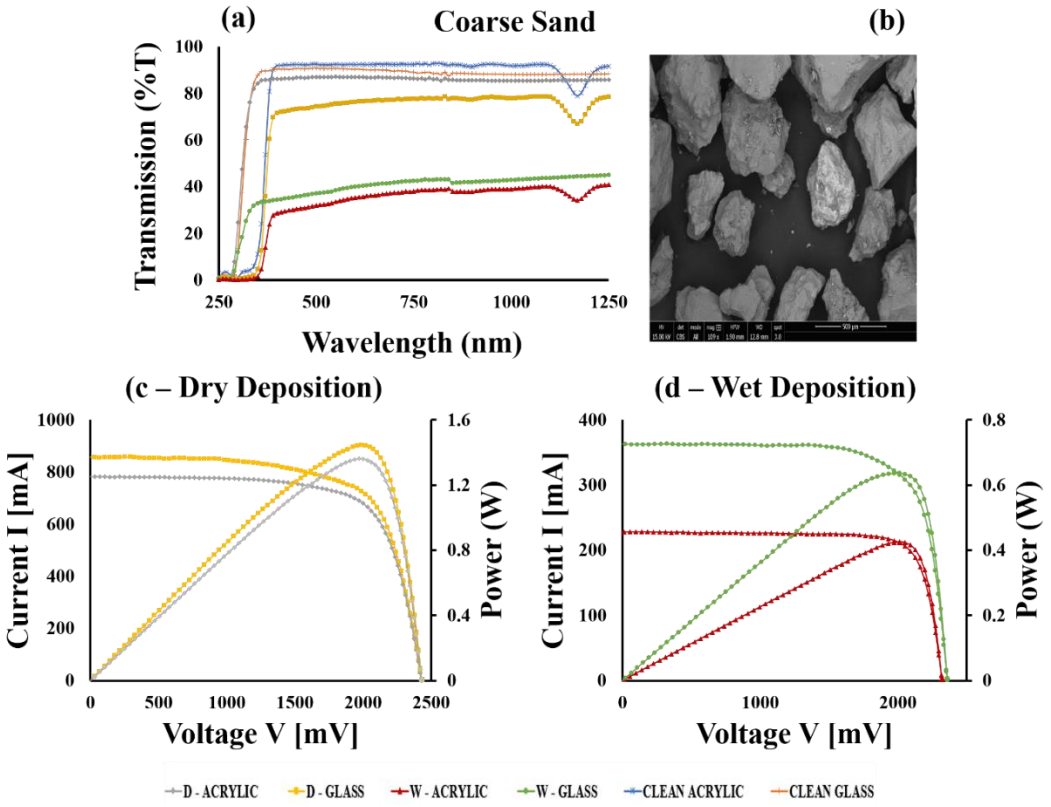

Figure 3.14**:** Coarse sand - (a) Spectral transmittance (b) SEM imaging (c and d) PV performance.

Figure 3.14 shows the spectral transmission, SEM and PV performance when coupons (acrylic and glass) were deposited with coarse sand. The reduction in light transmittance was recorded when coarse sand was dry deposited on coupons, by about 33% on acrylic plastic and 4% on low iron glass was documented. The reduction was when coarse sand was wet deposited on coupons with acrylic plastic was about 74%, and low iron glass was about 63%. Image characterisation shows coarse sand comprising broken rock particles with translucent and sub translucent minerals, which allows a certain percentage of light to pass through. The minerals' density appears to be high, slowing the flux intensity, resulting in light absorbance. Particles seem to be heavy and appear to have a spherical and/or quadrangular structure with a partial coarse surface, which offers favourable optical properties. Although the particles possess some excellent optical properties, the negative properties surmount. Also, during both depositions, particles bounce off or roll off the coupons. The particles are large, meaning this type of dust is porous, and light can pass through the spaces. Also, large dust particles can be affected by gravitational forces and light wind effects.

The PV performance result shows that the short circuit current degraded by about 17% when the coarse sand sample was dry deposited on the acrylic plastic and about 10% on the low iron glass coupon. An increase in degradation was observed when the rough sand sample was wet deposited on the various coupons, where about 76% loss was recorded on acrylic plastic and 62% on the low iron glass.

3.3.8 Laterite

This is a reddish, yellowish and/or dark brown soil found in semi-arid or savannah regions with warm air temperatures, dry periods and abundant rainfall such as West Africa and comes in different forms because of the iron oxide content. It is used for road construction across the West African region and possesses a high aluminium and iron level, which could harden to form a rock. When mixed with water on a surface, it can rapidly dry up, forming cementation. This soil is affected by wind erosion and could be lifted and transported to the module's surface, reducing light penetration to PV cells. The results below highlight the effect of lateritic soil formation on PV performance.

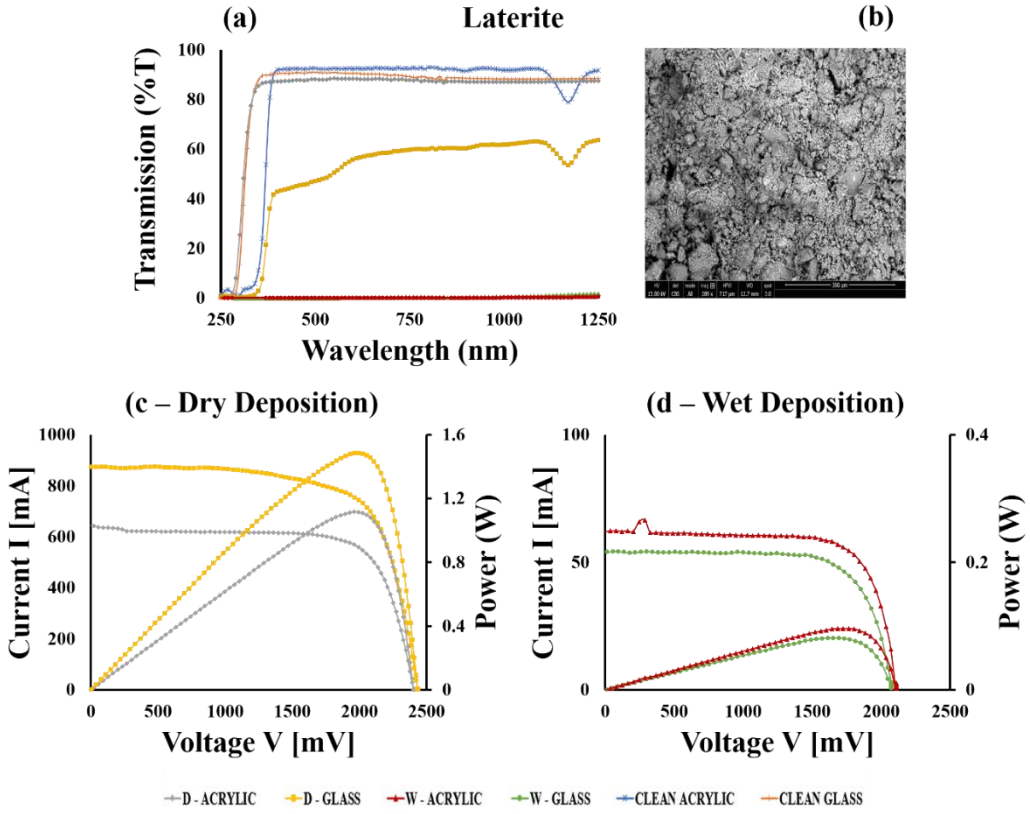

Figure 3.15**:** Laterite - (a) Spectral transmittance (b) SEM imaging (c and d) PV performance.

Figure 3.15 shows the spectral transmission, SEM and PV performance when coupons (acrylic and glass) were deposited with laterite. The light transmittance reduction was recorded when laterite was dry deposited on coupons with acrylic plastic showing about 55% and low iron glass 3% reduction. On the other hand, the extreme reduction was documented when laterite was wet deposited on the coupon, with both reaching almost 100% reduction. Laterite is a reddish or brownish compound with high levels of aluminium and iron. The image characterisation shows that the mineral content appears to be opaque, translucent and sub translucent, and this characteristic can cause light attenuation. Mineral density was high, which can slow down flux intensity and result in light absorbance. Most of the laterite particles used are tiny, heavy and spherical, which can cause light attenuation, reflection and scattering. Few larger particles bounce off the coupons during deposition. The PV performance result shows that the short circuit current degraded by about 32% when laterite samples were dry deposited on the acrylic coupon and 8% on the low iron glass. An alarming increase in degradation was also observed when laterite samples were wet deposited on the various coupons, where about 96% decrease was recorded on acrylic and about 94% on the low iron glass.

3.3.9 Loam

This is a type of soil containing organic components, nutrients and moisture. Loam soil comprises sand, silt and clay in different proportions (clay content is minimal). It has better water content managing capabilities because it retains a certain amount of water and allows unwanted water to drain. This soil is less affected by wind erosion. However, it can be lifted and transported by strong wind and storms in the atmosphere and later to the PV module's surface, reducing light transmittance to PV cells. The results below highlight the effect of loam soil formation on PV performance.

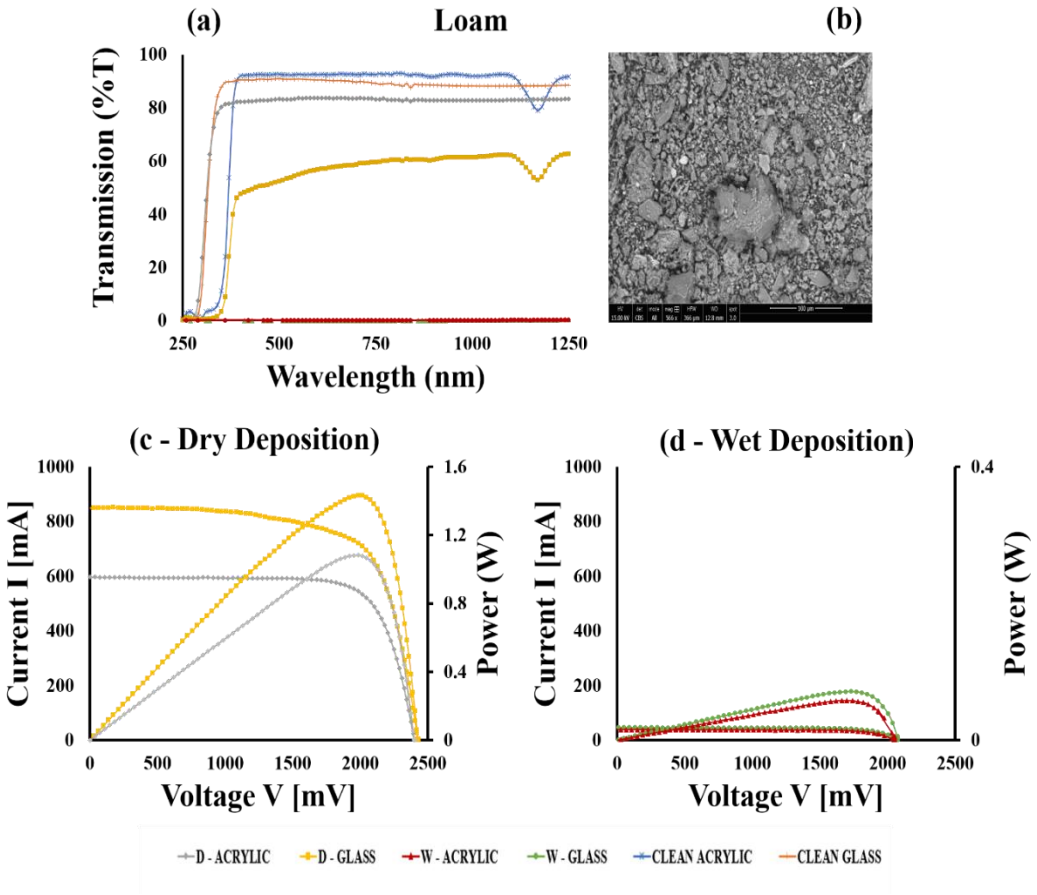

Figure 3.16: Loam - (a) Spectral transmittance (b) SEM imaging (c and d) PV performance.

Figure 3.16 shows the spectral transmission, SEM and PV performance when coupons (acrylic and glass) were deposited with loam. The light transmittance reduction was recorded when loam soil was dry deposited on coupons with levels of about 55% for acrylic and 3% for low iron glass. On the other hand, the extreme reduction was documented when loam soil was wet deposited on the coupon, with both having almost 100% reduction. The image characterisation shows that loam is a compound comprised of various minerals, and some were observed to be opaque and translucent, which can cause light attenuation. Minerals were also found to have a high density, reducing the flux intensity, causing light absorbance. Particles vary in size; some appear to be very tiny while others are large; this will cause light attenuation because the smaller particles tend to fill up the porous areas left by the larger particles. These particles are heavy, angular and quadrangular, with a coarse surface. The PV performance result shows that the short circuit current degraded by about 37% when loam soil was dry deposited

on acrylic plastic and about 10% on the low iron glass. An alarming increase in degradation was observed when loam soil was wet deposited on the various coupons, with about 96% recorded on the acrylic plastic and 95% on the low iron glass coupon.

3.3.10 Salt

This is a hygroscopic compound that deliquesces to a gaseous state when the relative humidity is low and becomes droplets when relative humidity is high. This compound can be transported from the sea to the module's surface by wind, and during the transport phase, other dust particles can be incorporated. Sea salt particles adhere to PV surfaces when they become dry, reducing light transmittance to PV cells. The results below highlight the effect of soiling due to sea salt accumulation on PV performance.

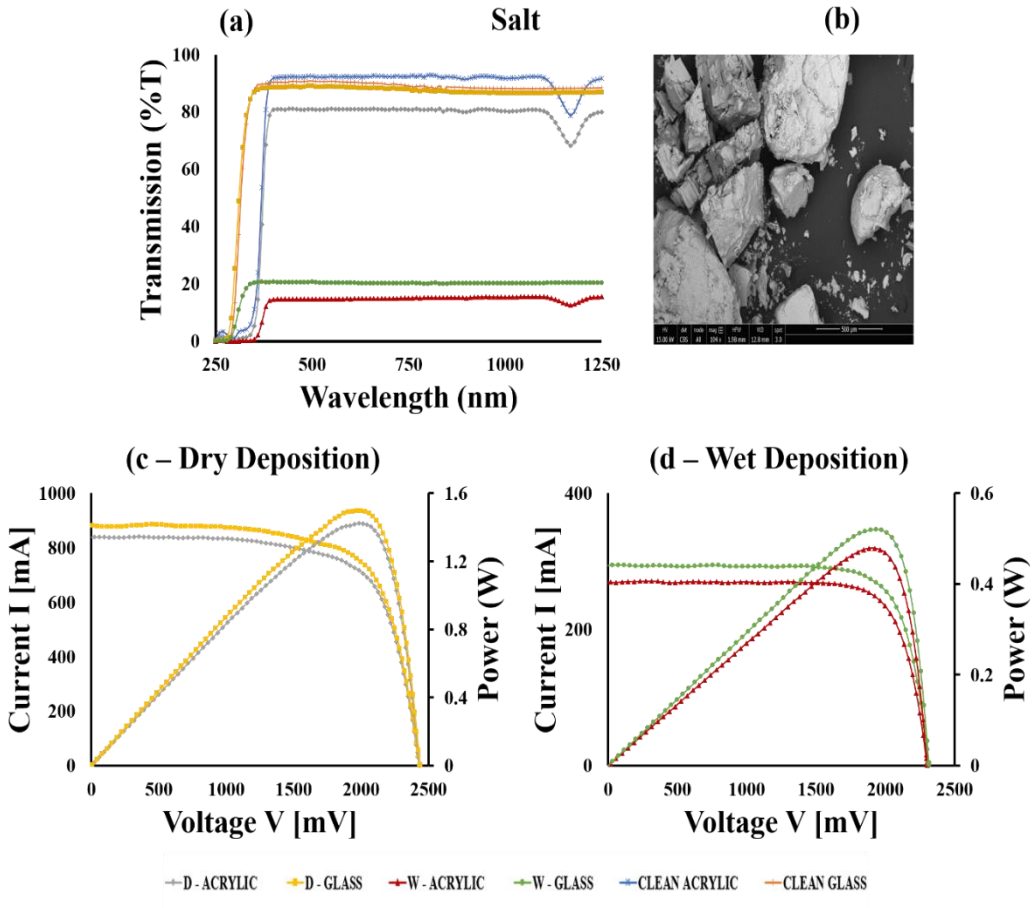

Figure 3.17: Salt - (a) Spectral transmittance (b) SEM imaging (c and d) PV performance.

Figure 3.17 shows the spectral transmission, SEM and PV performance when coupons (acrylic and glass) were deposited with salt. Low light transmittance reduction was recorded when salt was dry deposited on coupons with acrylic plastic showing a 24% and low iron glass a 2% reduction. On the other hand, a high reduction was documented when salt was wet deposited on coupons with acrylic plastic recording 87% and low iron glass 77% reduction. The image characterisation shows that salt is a transparent, crystalline mineral with reasonable mineral density, which presents good optical quality since flux intensity will not be affected. Particle size ranged from medium to large, which makes it porous, allowing more passage of light. It appears to be a quadrangular layered structure, and its roughness seems coarse, which also presents good optical properties since better transmittance can be achieved. Despite the good optical quality salt possesses, negative qualities surmount due to how it accumulates in layers. The PV performance result shows that the short circuit current degraded by about 12% when salt is dry deposited on acrylic plastic and about 7% on the low iron glass. An increase in degradation was observed when salt was wet deposited on the various coupons where about 72% was recorded on the acrylic plastic and about 69% on the low iron glass coupon.

3.3.11 Sandy soil

Fine sand particles are used in combination with other materials for plastering or rendering the exterior of a building or structure, found from river beds and riverbanks. It allows water to settle and has less reduced permeability, is easy to compress and lift when completely dry. This type of soil is affected by wind erosion and can be lifted and transported to the PV module's surface, reducing light transmittance to PV cells. The results below highlight the effect of sand soil formation on PV performance.

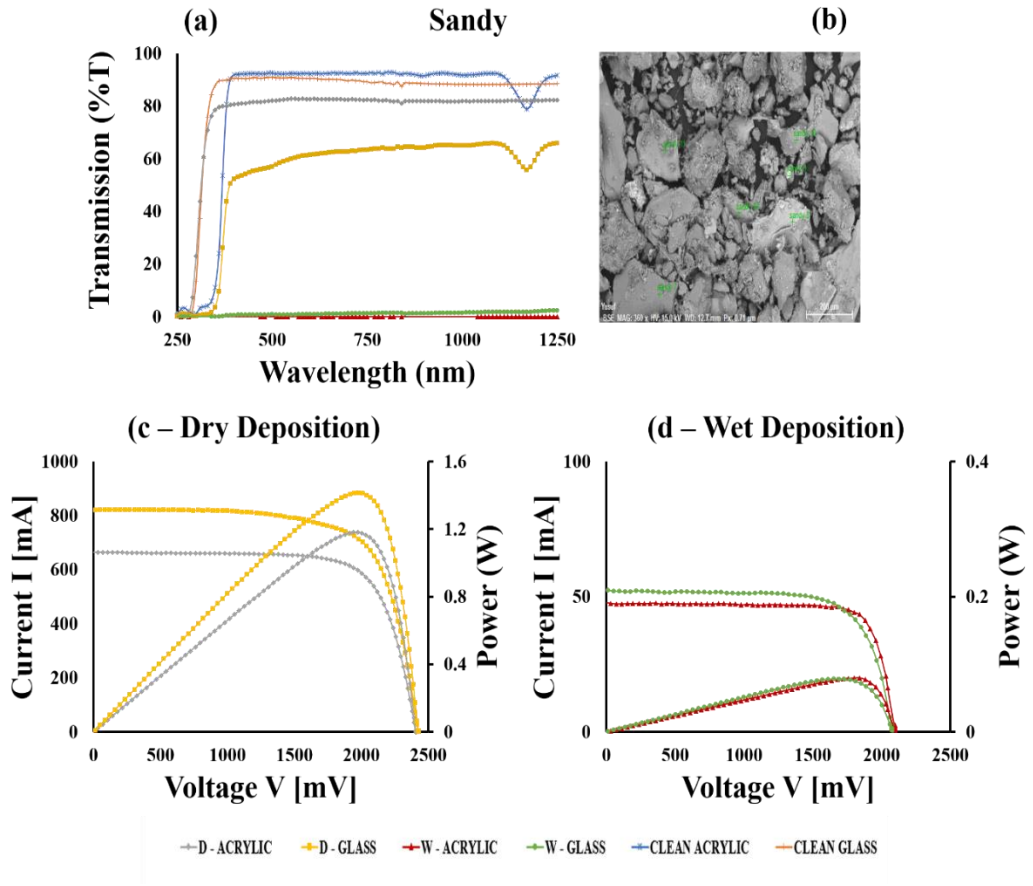

Figure 3.18: Sandy - (a) Spectral transmittance (b) SEM imaging (c and d) PV performance.

Figure 3.18 shows the spectral transmission, SEM and PV performance when coupons (acrylic and glass) were deposited with sand. The light transmittance reduction was recorded when sand was dry deposited on coupons with 51% on acrylic plastic and 11% on the low iron glass. On the other hand, a higher reduction was recorded when sand was wet deposited onto coupons, with both recordings at around 99% reduction. Image characterisation shows that the sand sample was opaque and partially sub translucent. Minerals were found to have a high density, which can slow flux intensity. Particle sizes range from small to medium, which can cause light attenuation. The particle structure appears to be aggregated and euhedral; therefore, it can absorb light. The surface appears to be smooth, causing light scattering. It is also heavy, which means it will readily settle and accumulate on a platform. The PV performance result shows that the short circuit current degraded by about 30% when sand was dry deposited on acrylic plastic and about 13% on the low iron glass. A high increase in

degradation was observed when sand was wet deposited on the various coupons, with about 95% degradation recorded on acrylic and about 94% on the low iron glass.

3.3.12 Stone dust

This is a quarry industrial by-product known as quarry dust; it is grey and can be refined or coarse depending on the crusher's holes and screening traps. It is used for road construction, pavement, tiles and bricks due to its highly reduced permeability. Fine stone dust was selected and used in this research since wind can lift and transport it. Heavier and larger particles are difficult to transport, deposit and cement on the PV module's surface. However, during sandstorms or strong wind, it can be transported and deposited on the module and can reduce light transmittance to PV cells. The results below highlight the effect of stone dust formation on PV performance.

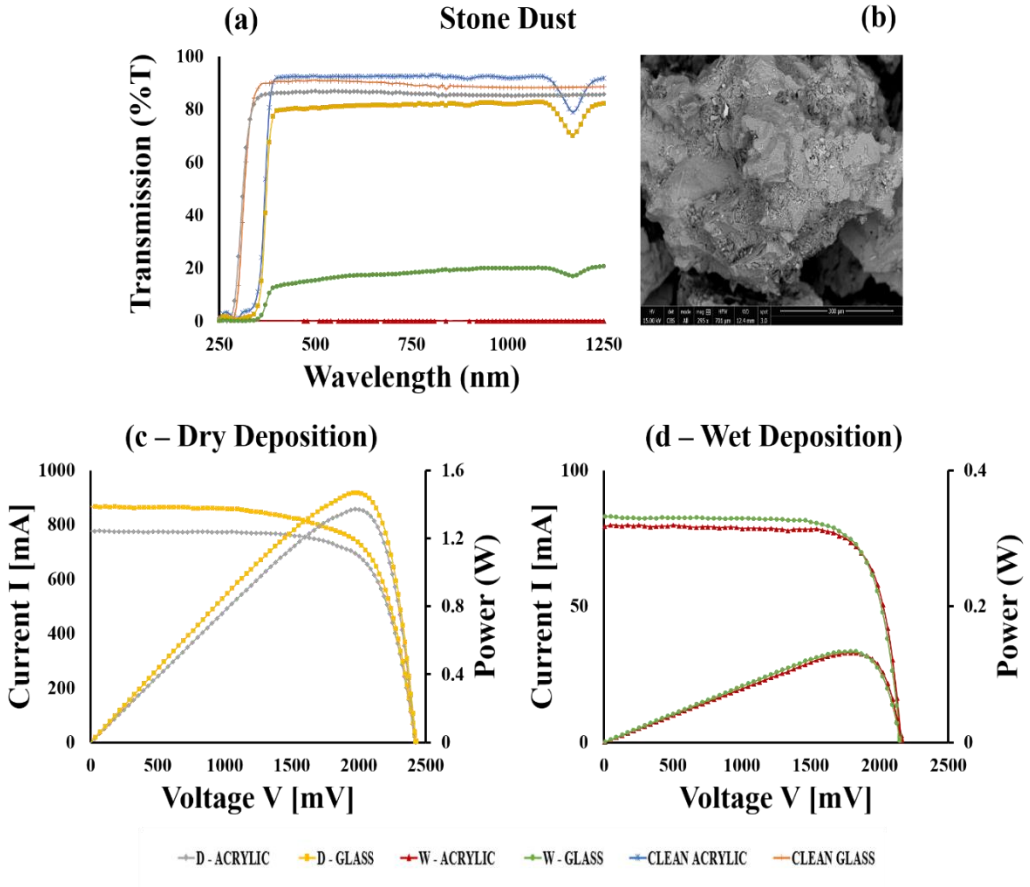

Figure 3.19: Stone dust - (a) Spectral transmittance (b) SEM imaging (c and d) PV performance.

Figure 3.19 shows the spectral transmission, SEM and PV performance when coupons (acrylic and glass) were deposited with stone dust. Low light transmittance reduction was recorded when stone dust was dry deposited on coupons with acrylic plastic showing about 16% and low iron glass 5%. On the other hand, a higher reduction was recorded when stone dust was wet deposited on coupons with acrylic plastic, recording 87% and low iron glass as high as 100% reduction. The image characterisation shows that stone dust comprises minerals found to be opaque and translucent, which have attenuation and reflection effects on light and have a high density, reducing the flux intensity, resulting in light absorbance. Particle surfaces appear to be coarse. The structure seems to be an aggregated layer, which can have a scattering effect on light. The stone dust sample used appears to be small and medium-sized with low light porosity. It is also heavy, which means it will readily settle and accumulate on a platform but can roll, slide and lift-off due to wind and/or gravitational effects. The PV performance result shows that the short circuit current degraded by about 18% when sand was dry deposited on acrylic plastic and about 9% on the low iron glass. A high increase in degradation was observed when sand was wet deposited on the various coupons, with about 92% degradation recorded on acrylic plastic and about 91% on the low iron glass.

3.3.13 Wood dust

This is a by-product of wood known as sawdust, generated from the carpentry industry when machines are used in cutting, drilling, sawing, milling, roughening and shaping wood. It is a bio-polymeric composite, and some of the fine wood dust become particles immediately suspended in the atmosphere as they are generated, while others are affected by gravitational forces before a strong wind suspends them in the atmosphere. These particles can be transported to the module's surface, reducing light transmittance to PV cells. The results below highlight the effect of wood dust formation on PV performance.

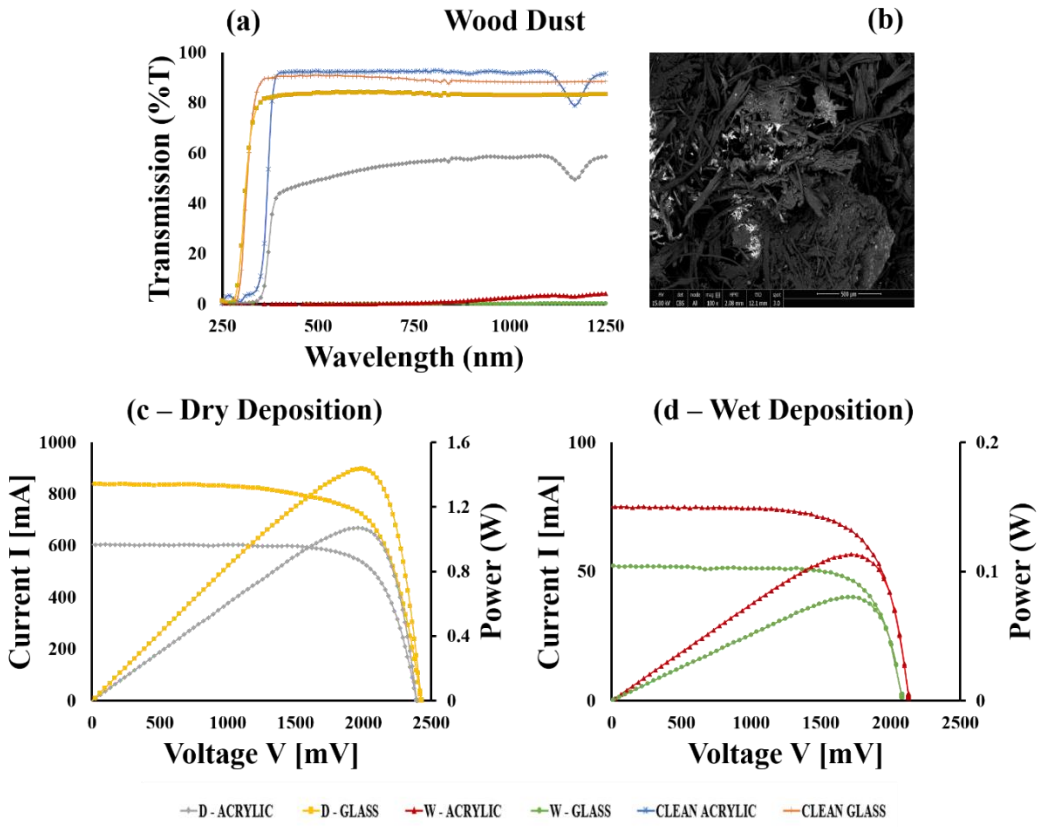

Figure 3.20: Wood dust - (a) Spectral transmittance (b) SEM imaging (c and d) PV performance.

Figure 3.20 shows the spectral transmission, SEM and PV performance when coupons (acrylic and glass) were deposited with wood dust. The light transmittance reduction was recorded when wood dust was dry deposited on coupons with acrylic plastic showing about 56% and low iron glass about 9% reduction. On the other hand, a high reduction of light transmittance was recorded when wood dust was wet deposited, with both coupons recording about 100% reduction. Image characterisation shows that wood dust (also known as sawdust as mentioned above) comprises minerals found to be opaque and translucent, which have an attenuation effect on light and a high density, reducing flux intensity resulting in light absorbance. Particle shape appears to be a flaky elongated rectangular structure with a fine surface, which can cause a scattering effect. Particles are light in weight and range from small to medium size, which resulted in an attenuation effect. The PV performance result shows that the short circuit current degraded by about 36% when sand was dry deposited on acrylic plastic and about 12% on the low iron glass. A high increase in reduction was

observed when sand was wet deposited on the various coupons, with about 92% degradation recorded on acrylic plastic and about 94% on the low iron glass.

3.3.14 Summary of results

Figure 3.21 illustrated the power performance when different dust types were deposited onto the PV surfaces. Table 3.3 illustrates the short circuit current degradation of each sample, power degradation, transmission losses, and results from image characterisation.

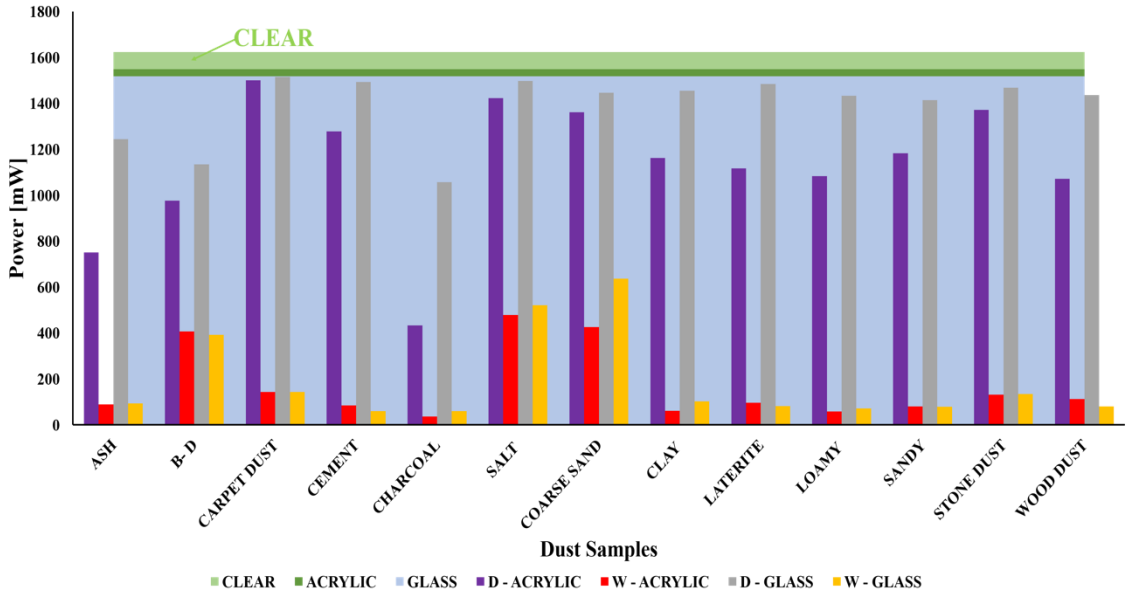

Figure 3.21: Summary of results (power output).

Table 3.3: Summary of results.

	I_{sc} Degradation				Power Degradation				Transmission Degradation				Image Characterisation						
	Acrylic		Glass		Acrylic		Glass		Acrylic		Glass								
	Dry %	Wet %	Dry %	Wet %	Dry %	Wet %	Dry %	Wet %	Dry %	Wet %	Dry %	Wet %	Size (μm)	Weight (g/m^2)	Shape Structure	Surface Roughness	Composition	Diaphaneity	Density
ASH	56	94	22	94	54	95	23	94	55	99	4	87	0.5-80	1289.94	Angular	Coarse	Fairchildite	Transparent	2.45
																	Manganese	Opaque	7.01
B-D	46	87	35	74	40	75	30	76	90	87	54	75	0.1-400	958.58	Aggregate	Fine	Amphibole (Richterite)	Translucent	3.09
																	Silica	Opaque	2.13
																	Xenotime	Transparent	
CARPET	9	91	7	92	8	91	7	91	8	100	1	100	<1->1000	609.47	Bent angular/triangular channels	Coarse	Olivine (monticellite)	Translucent	3.13
																	Calcite	Opaque	2.71
CEMENT	21	94	8	96	21	95	8	96	34	95	4	99	<1-150	1964.50	Angular flattened	Coarse	Hatrurite	Opaque	3.02
																	Brownmillerite	Semi Transparent	3.76
																	Calcite	Opaque	2.71
CHARCOAL	76	98	35	95	73	98	35	96	77	98	35	100	<1-100	923.08	Flaky aggregated triangular glassy like	Coarse	Ankerite	Sub Translucent	3.05
																	Calcite	Opaque	2.71
																	Charcoal	Opaque	
CLAY	33	96	14	93	28	96	10	94	43	100	8	77	<2-<60	2621.30	Flaky rounded crust	Fine	Beryl	Translucent	2.76
																	Stilpnomelane	Opaque	2.86
																	Anxite	Translucent	3.28
COARSE	17	76	10	62	16	74	11	61	33	74	4	63	50-2000	3218.93	Rounded and quadrangular structure	Coarse	Allanite	Translucent	3.93
																	Chlorite (Chamosite)	Sub Translucent	3.2
																	Prehnite	Translucent	2.87
LATERITE	32	93	8	94	31	94	9	95	55	100	3	100	>50-150	2426.04	Aggregated angular and rounded layered	Coarse	Schorl	Opaque	3.15
																	Chlorite (Chamosite)	Sub Translucent	3.2
																	Bauxite	Opaque	3.5
LOAMY	37	96	10	95	33	96	12	96	55	100	9	100	<2-2000	3011.83	Angular and quadrangular	Coarse	Feldspar (Labradorite)	Translucent	2.69
																	Stilpnomelane	Opaque	2.86
																	Anxite	Translucent	3.28
SALT	12	72	7	69	12	70	8	68	24	87	2	77	50-500	2846.15	Quadrangular layered	Coarse	Halite	Transparent	2.17
SAND	30	95	13	94	27	95	13	95	51	99	11	100	15-500	2384.62	Aggregated euhedral	Fine	Mica (Biotite)	Opaque	3.9
																	Beryl	Translucent	2.76
																	Stilpnomelane	Opaque	2.86
STONE	18	92	9	91	16	92	10	92	16	87	5	100	75-250	2751.48	Aggregated layered	Coarse	Mica (Muscovite)	Translucent	2.82
																	Staurolite	Opaque	3.71
																	Leucite	Translucent	2.47
WOOD	36	92	12	94	34	93	12	95	56	100	9	100	10-100	609.47	Elongated flaky rectangular like	Fine	Calcite	Opaque	2.71
																	Beryl	Translucent	2.76

Table 3.4: Results from similar research.

Authors	Particles samples	Quantity	Output Percentage Reduction	Transmittance Reduction
Alnasser et al (2020)	Sand	100 g/m^2	12%	40% @ 35 g/m^2
▪ Power reduction (%)	Normal Cement	100 g/m^2	14%	45% @ 35 g/m^2
▪ Transmittance reduction (%)	White Cement	100 g/m^2	15%	55% @ 35 g/m^2
	Normal Gypsum	100 g/m^2	9%	50% @ 35 g/m^2
	Technical Gypsum	100 g/m^2	10%	52% @ 35 g/m^2
Kaldellis et al (2011)	Red soil	0.35 g/m^2	0.75%	
▪ Efficiency reduction (%)	Limestone	1.51 g/m^2	0.95%	
	Fly ash	3.71 g/m^2	1.5%	
Kazem et al (2013)	Red soil	10 g/m^2	7%	
▪ Power reduction (%)	Ash	10 g/m^2	25%	
	Sand	10 g/m^2	4%	
	Calcium Carbonate	10 g/m^2	5%	
	Silica Gel	10 g/m^2	4.5%	
Appels et al (2013)	White sand	60 g/m^2	14.74% and 13.76%	15.03
▪ Power reduction (%)	Clay	60 g/m^2	48.77% and 47.21%	48.42
▪ Transmittance reduction (%)	Cement	60 g/m^2	64.16% and 65.68%	66.66
Abderrezek and Fathi (2017)	Ash	1.02 g/m^2		73.71%
Transmittance reduction (%)	Cement	1.01 g/m^2		74.62%
	Gypsum	1.01 g/m^2		65.52%
	Salt	1.2 g/m^2		62.79%
	Soil	1.02 g/m^2		20.02%
	Sand	1 g/m^2		19.11%
El-Shobokshy and Hussein (1993)	Carbon	28 g/m^2	90%	
▪ Power reduction (%) @ 195W/m^2	Cement	73 g/m^2	80%	
▪ I_{sc} reduction (%) @ 195W/m^2	Limestone (50 µm)	125 g/m^2	80%	
	Limestone (60 µm)	168 g/m^2	78%	
	Limestone (80 µm)	250 g/m^2	94%	
Wang et al. (2020)	Sand	2.199 g/m^2	5.296%	
▪ Efficiency reduction (%)		6.29 g/m^2	12.027%	
		17.37 g/m^2	34.332%	
		21.067 g/m^2	38.981%	
		30.18 g/m^2	43.216%	
Sisodia and Mathur (2019)	Bird Dropping		23.8% @ 0^0	31% @ 0^0
▪ Reduction in power (%) with tilt angle β			23.8% @ 10^0	28% @ 10^0
▪ Reduction in transmittance (%) with tilt angle β			21.0% @ 20^0	27% @ 20^0
			11.5% @ 25^0	15% @ 25^0
			10.8% @ 30^0	14% @ 30^0
			10.5% @ 40^0	13% @ 40^0
			10.8% @ 50^0	14% @ 50^0
			10.8% @ 60^0	15% @ 60^0
			15.8% @ 70^0	18% @ 70^0
			16.0% @ 80^0	21% @ 80^0
			16.5% @ 90^0	24% @ 90^0
Adıgüzel et al. (2019)	Coal Dust 38 µm	15g	62.05%	
▪ Power reduction (%)	Coal Dust 38 - 53 µm	15g	55.78%	
	Coal Dust 53 - 75 µm	15g	50.83%	
	Coal Dust 75 -106 µm	15g	44.12%	
	Coal Dust 106 -250 µm	15g	36.97%	
	Coal Dust 250 -500 µm	15g	28.90%	

3.4 Discussion

Alarming results were highlighted in the previous section, showing almost 100% degradation of performance. Several parameters were considered to characterise and analyse each variety of dust particles and how and what promotes its degradation effect on PV cell performance. This section provides an in-depth discussion of the analysed results from the various experiments.

This research investigated two materials (acrylic plastic and low iron glass) used in the PV industry to encapsulate solar cells and allow adequate light transmittance for the functioning of the technology. These materials were

selected since they possess excellent transmittance quality. Acrylic plastic has a transmittance of about 92%, and low iron glass has a transmittance of 91%. These materials have many other advantages that have made them a practical option in the industry. Findings from literature and laboratory experiments show that acrylic plastic possesses a higher transmittance capability than low iron glass. However, results also show that acrylic plastic attracts and accumulates more dust during depositions. This is due to the electrostatic discharge (ESD) of the material, which attracts the particles. This claim is supported by Zaihidee et al. (2016) and Jiang et al. (2011), who stated that plastic and epoxy materials could accumulate more dust than glass. This result is comparable with a report provided by Nahar and Gupta (1990), where acrylic plastic was found to accumulate a more significant amount of dust when compared to a glass surface. A report provided by Kalogirou et al. (2013) also confirmed that glass was found to accumulate less dust compared to Tedlar.

The image analysis comprising morphological and mineral characterisation of particles describes the size, weight, shape, surface roughness and mineral composition (including their diaphaneity and density). These properties vary with minerals, and most samples comprise more than two minerals, excluding salt. However, the negative properties surmount the positive ones and influence light transmittance due to accumulation.

Our result revealed that larger particles create wider gaps between them that could allow light penetration, but small and uniformly spread particles would not have enough spaces that light can penetrate. Adıgüzel et al. (2019) investigated the effect of different coal dust particles on PV performance. Their results showed that the most significant power losses were observed when the smaller coal dust particles were deposited compared to larger particles. They also proved that increasing the weight of accumulated dust particles further reduces the yield of the technology. A micro or nano-sized particle can prevent a tiny fraction of solar radiation from reaching the solar cell, which is essential for its operation, thereby degrading the technology's overall performance. The results presented in Table 3.3 are compatible with other experimental studies highlighted in Table 3.4, which shows that certain dust particles cause a significant reduction of transmittance

and a decrease in PV output. It should be noted that the actual quantity used by other researchers presented in Table 3.4 was minimal. In contrast, a large quantity was used in this experiment, an informed decision based on an observation made in an ongoing study and other outdoor soiling experimental publications.

Al-Ammri et al. (2013) investigated the effect of bird droppings deposition on PV performance and reported that bird droppings deposition had a more significant effect than dust. On the contrary, our study found that a dust sample (charcoal) deposition had a more significant effect on PV performance when compared to bird droppings. Also, El-Shobokshy and Hussein (1993) reported that carbon particles absorb more solar radiation than limestone and cement. Similarly, this research also shows that samples with carbon particles (charcoal) absorbed more light than cement.

It is observed that particles were rolling, sliding and lifted off the coupons when exposed to artificially generated wind velocity and gravitational effect (when coupons were tilted). The results show that the wind and gravitation effect has a more significant impact on the dry deposited dust when compared to the wet deposited samples.

The effect of dust particle deposition (dry and wet) processes have been compared, and the results are highlighted in the diagrams above. Our results illustrate how wet deposition can affect light transmittance. It was observed that during the dry deposition on the coupons (acrylic plastic and low iron glass), a small quantity of tiny sample particles adhered to the coupons. Theoretically, it has been established that Van de Waal forces are always present between the particles and the surface, which can act together when the interacting dipoles are within a short range (Ilse et al., 2018). This factor can influence the adhesion of dry dust on both coupons. The electrostatic force that is always present on the acrylic plastic is another factor that can attract the dust during dry deposition, leading to more dust accumulation resulting in more significant PV performance degradation than that of the low iron glass. Figure 3.22 illustrates how the Van der Waals and Electrostatic force acted between particles and the surface.

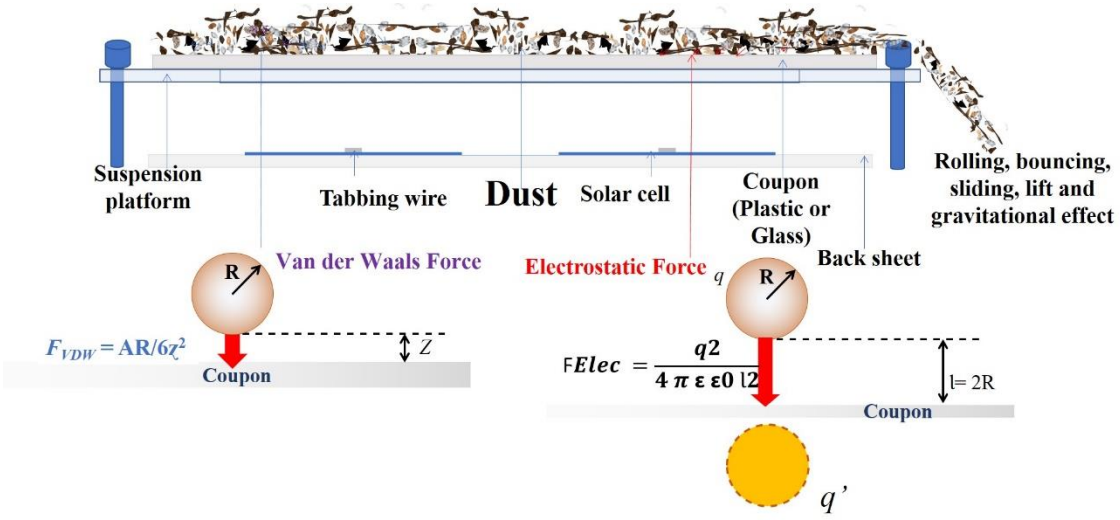

Figure 3.22: VDW and Electrostatic force promoting dust particles accumulation, where R represents the radius of dust particles, ρ is the material density, *q* is the charge of a particle, A is the Hamaker constant, ʐ is the distance between the particle and coupon, l is separation distance, ε is the dielectric constant that exists between the surface and particles, εo is the free space permittivity (Isaifan et al., 2019).

The adhesion caused during the dry deposition due to the gravitational, electrostatic and Van der Waal forces was compatible with Isaifan et al. (2019). On the contrary, the main active forces causing adhesion during the wet deposition were gravitational, capillary and Van der Waal forces. This result is compatible with those presented by Isaifan et al. (2019), where the researchers stated that capillary force accounts for about 98% of the forces acting during the humid condition (wet deposition), while 2% was due to Van der Waal forces.

The electrostatic force could promote inter-particle adhesion during a deposition where charged particles collide with one another or the surface, inducing a coulomb force and attracting each other due to opposite charges. When a coulomb force is triggered, it may attract or repulse, depending on the dust particle's polarity. It was observed that the adhesion is higher between particles compared to the PV surface and particles. Hassan et al. (2016) confirmed that electrostatic charges could cause tiny particles to adhere to the large ones. Also,

Kazmerski et al. (2016) reported that the adhesion force between particles and PV surfaces is lower when compared to the inter-particle adhesion force.

On the other hand, it was observed that additional forces increase the adhesion during the wet deposition of samples. The main forces that promoted adhesion on acrylic plastic during this deposition were the capillary and electrostatic forces. The electrostatic forces attracted particles to remain on the coupon's surface, while the capillary forces created bridges that caused mechanical interlocking of the particles and surface. On the other hand, the adhesion force that acted on the low iron glass was capillary. As mentioned above, it created capillary bridges between the particles and coupons, causing entanglement/mechanical interlocking. Furthermore, since the particles were allowed to settle over a long period, cementation, caking and capillary ageing occurs. More PV degradation was observed during wet deposition on the acrylic plastic, except for a few samples (such as carpet dust, cement, laterite and wood) that caused slightly more significant PV performance degradation on low iron glass than the acrylic plastic. Figure 3.23 illustrates how the capillary force acted on dust particles when water was introduced.

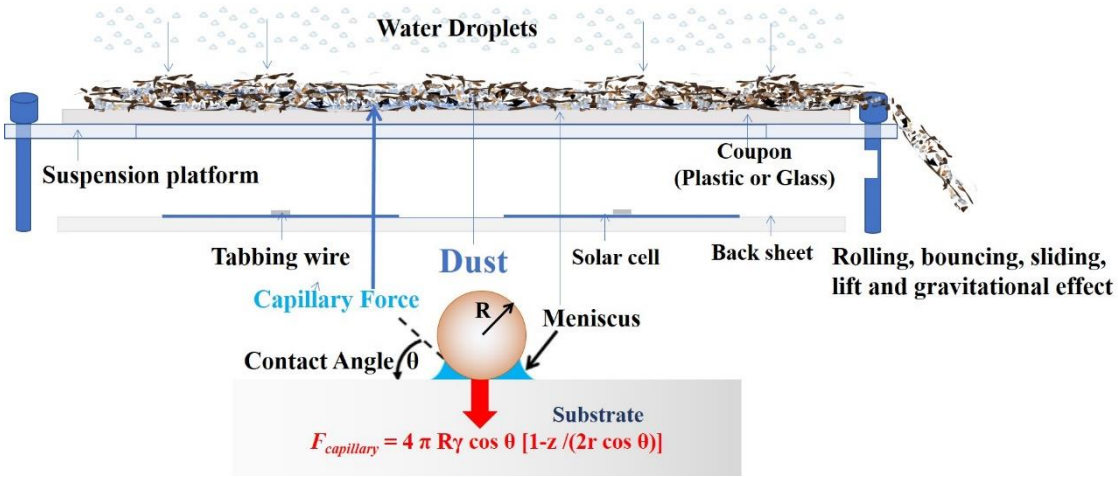

Figure 3.23**:** Capillary force promoting dust particle accumulation, where γ is the surface tension, and θ is the contact angle between the moisture and coupon (Isaifan et al., 2019).

The overall results show that the presence of water on the PV surface promotes bonding and adhesion potency both between particles and also between particles

and module surface materials due to triggering of capillary forces, preventing the sliding, bouncing off, lift and rolling off of particles which leads to retention of more particles on the module surface. Light rain, high relative humidity and dew are ways of depositing water droplets with dust particles on the PV surface, and the dew could occur in the early hours of the morning. After sunshine, the particles will dry up and become firmly adhered to each other. The module's surface (cementation) makes it very difficult to clean and depositing water before/after in the wet deposition, leading to a massive increase in PV yield degradation and creating a stronger adhesion between both particles and the coupons. Ilse et al. (2018) confirmed this by stating that dew enhances the adhesion of accumulated dust on the PV module's surfaces, and some particles might improve the strength of the adhesion depending on the chemical composition. Also, Said and Walwil (2014) stated that water between the dust particles creates capillary bridges both between the particles and between dust particles and the surface.

Exposing accumulated particles to the wind shows a significant removal effect on dry accumulated dust, but a more negligible effect was observed when wet deposited particles were subjected to wind. As earlier stated, Gholami et al. (2017) reported that dust particles' density was reduced when accumulated dust particles are subjected to an inward wind. We also observed that large particles (such as coarse sand) were removed when coupons were tilted and exposed to the wind, and the microscopic particles remained on the surface. Jiang et al. (2018) reported that the wind effect is more significant to larger dust structures than smaller ones. Tanesab et al. (2019) also reported that it is challenging to remove the tiny layer of dust particles on a PV module that is horizontally positioned.

PV performance relies on solar irradiance, and this research observed that the short circuit current is influenced by dust accumulation, reducing the PV yield. Overall, the PV performance results show that the short circuit current is significantly affected compared to open-circuit voltage since the short circuit current depends on light illumination while voltage is affected by temperature. The highest reduction of short circuit current was observed when the charcoal sample was wet deposited on acrylic plastic, while the lowest reduction was when

salt was dry deposited on the low iron glass coupon. These reductions in short circuit current resulted in a similar reduction in the mini-module overall power output. The result obtained from the transmittance test was used in validating the losses that were observed. Dust accumulation on the PV surface reduces the system's conversion efficiency since the accumulated particles can scatter, absorb, and attenuate the incident light from reaching the solar cell. All the samples used in this research, reduced or prevented light from reaching the solar cell and decrease the system's conversion efficiency. However, this report shows that physical and chemical characteristics play a significant role in determining the level of degradation a dust particle can cause. The results highlight that reductions in PV yield performance observed were related to the amount of deposition and the dust particles' physical and chemical properties. This has also been confirmed by Kazem and Chaichan (2019) and Sarver et al. (2013). Hachicha et al. (2019) stated that physical and chemical composition is an essential factor determining how particles interact with each other and with PV module's surfaces.

Previously, researchers have also stated that it would be beneficial to determine the most effective technique to mitigate dust accumulation. Gupta et al. (2019) stated that there is no recommended cleaning rate since dust accumulation depends on several variables. Several mitigation techniques such as manual cleaning, the natural method by wind and rain, mechanical and robotics and self-cleaning using the electrodynamic screens, superhydrophobic and super hydrophilic coating were provided (Chanchangi et al., 2020). These approaches are location dependent, and each one has its limitation. Therefore, it is imperative to conduct another research using specific environmental conditions to determine an efficient, practical approach for a particular location.

3.5 Summary and conclusion

In summary, this section of the thesis presented a detailed indoor experimental study of 13 dust samples on PV performance considering two different PV covering surfaces using two deposition approaches. Findings showed a significant PV performance loss of 98% when the charcoal powder was wet

deposited on acrylic plastic. The result shows acrylic plastic accumulates a higher quantity of dust than low iron glass and the wet deposition (representing dew or light rain) promotes the retention of more particles on a surface compared to dry deposition. This study provides a thorough analysis of the effect of dust properties on PV performance and could be used for site selection and planning solar PV farm design. The findings could also be used in choosing suitable mitigation techniques according to the location and consideration of other factors. The asperity of degradation observed in this study cannot be overlooked, and therefore proper mitigation techniques must be provided to prevent the soiling of PV surfaces.

4 Chapter Four - Angular dependencies of soiling loss on photovoltaic performance in Nigeria

4.1 Introduction

In recent times, solar energy systems are widely utilised in different forms and in different applications such as BIPV (Building Integrated PV), BAPV (Building attached/applied PV), VIPV (Vehicle integrated PV), solar farms (large grid), isolated solar micro, and mini-grid, car parking roofing and interior decoration (Ghosh 2020; Ghosh 2020a; Reddy et al., 2020). Some of these applications allow the positioning of PV absorbing surfaces at a location-specific optimum angle, while others do not allow due to their kind of application. The positioning of PV module in an angle other than the site-specific optimum angle could lead to angular losses due to a reduction of solar irradiance reaching the solar energy collectors, causing an unwanted wastage of resources that could lead to a decrease in the performance of technology (Tanesab et al., 2018; Martin and Ruiz, 2001). According to Conceiç~ao et al. (2019), the angular losses coefficient has a dependency on the transmittance ratio.

As reported earlier in the literature, a number of researchers have investigated the PV tilt angle as an influencing factor in dust accumulation. However, the approach used in this research is scarce, and this provides improved information on how the tilt angle influences the accumulation of dust in areas with enormous solar energy potential and less penetration by considering a number of factors, such as reduced light transmission, reduced PV energy generation, and mass of accumulated dust (deposition density) using a low-cost approach. There is a shortage of systematic approaches for exposure of coupons considering the weather and period variability to the consequences of dust deposition influence by tilt angle when reviewing relevant literature. Furthermore, many publications mentioned above presented time dependency results and may not be usable in the same region at a different time. The study investigated the influence of angular positioning in promoting soiling on PV considering transmission coefficient losses, the mass of accumulated dust on surfaces, and potential PV output losses. However, since soiling is location-specific and PV technology is

recently used for wider application varieties, it restricts it from being positioned at a specific angle. The study developed a soiling station that investigated dust accumulation considering monthly, seasonal, and annual formation that determines the effect of dust on PV performance at all tilt angles (0° – 90°) using interpolation as provided in the subsequent section.

To date, studies on the influence of tilt angle on dust accumulation for Nigeria is relatively unexplored, even though the country has enormous solar energy potential, and the government is making a considerable investment towards solar energy installation. The study has the novelty of presenting a low-cost approach that could determine the regional influence of tilt angle on PV soiling. It would resolve the threats of concern, such as the influence of angular position on PV soiling, which hinders the acceptance of technology in the region and presents a cost-effective and straightforward approach to determine angular soiling rates and their peak period. This will enable an optimal maintenance schedule and reduce operational costs to achieve a higher yield. Moreover, once PV performance yield could be sustained over its life cycle duration at an optimum rate, there is a high possibility of attracting potential investors and policymakers to finance PV projects, accelerating the technology's penetration and reducing greenhouse gas emissions. This section of the thesis contributes to the body of knowledge in the field of soiling on PV by providing a unique approach to determine the level of soiling at different angles, different periods with their equivalent power losses and weight of accumulated dust which can serve as a guide to engineers for planning installation and determining the required optimum maintenance. It also provides a valuable substance that can motivate further research on prevention and restoration techniques to ensure optimum performance of PV technology is sustained. This work highlights the significance of the effect of soiling considering tilt angle as an influencing factor with the following subsection of the thesis provides background and methodology used in the research, results and then discussion.

4.2 Background

4.2.1 Tilt angle (β)

Tilt angle is the angle between the horizontal plane and the PV module plane. It varies from 0° to 90°, and it is positive when positioned towards the azimuth angle direction (Akhlaghi et al., 2017; Ullah et al., 2019).

4.2.2 Declination angle (δ)

Declination Angle is the angle between the equator (earth's axis) and the perpendicular plane to a line between the earth and the sun (Akhlaghi et al., 2017; Ullah et al., 2019). Declination varies annually from 23.45° north to 23.45° south due to the earth's orbit around the sun (Al Garni et al., 2019). The declination can be estimated using Equation (4.1) below, where *n* is the n^{th} day of the year and can be 31st December, meaning n = 1.

$$\delta = \frac{23.45\pi}{180}\sin\left(\frac{2\pi(284+n)}{365}\right) \tag{4.1}$$

4.2.3 Solar hour angle (ω)

The solar hour angle is the angle between a longitude of a location on the earth's surface and the longitude parallel to the sun's ray (Akhlaghi et al., 2017; Ullah et al., 2019). The hour angle is negative in the morning, zero at noon, and positive in the afternoon. Since the earth orbits every 24 hours, the hour angle is estimated using Equation (4.2) below.

$$\omega = \frac{360^0}{24h} = 15° \text{ per hour} \tag{4.2}$$

4.2.4 Sunrise (ω_{sr}) and Sunset angles (ω_{ss})

The sunrise and sunset occurred when the sun was positioned at the horizon when the zenith becomes null.

4.2.5 Zenith (θ) and Azimuth angle (γ)

The zenith angle can be described as the sun's angle relative to a vertical line to the earth's surface (Akhlaghi et al., 2017; Ullah et al., 2019). The angle is directly

related to the angle of the solar elevation. The zenith angle can be estimated using Equation (4.3) below, where φ is the latitude of a particular location. The azimuth angle is the sun's relative position with respect to the north and south axis, which varies from -180° to 180°.

$$\cos\theta = \sin\varphi \sin\delta + \cos\varphi \cos\delta \cos\omega \quad (4.3)$$

4.2.6 Solar altitude angle (α)

The solar altitude angle is the angle between the horizontal surface and the sun's rays and can be estimated using Equation (4.4) below (Kacira et al., 2004).

$$\alpha = \cos^{-1}\varphi \cos\omega \cos\delta + \sin\varphi \sin\delta \quad (4.4)$$

The parameters mentioned above, such as the tilt angle, declination angle, latitudes, solar altitudes, zenith and azimuth angle, are illustrated in Figure 4.1 (a) and (b) below.

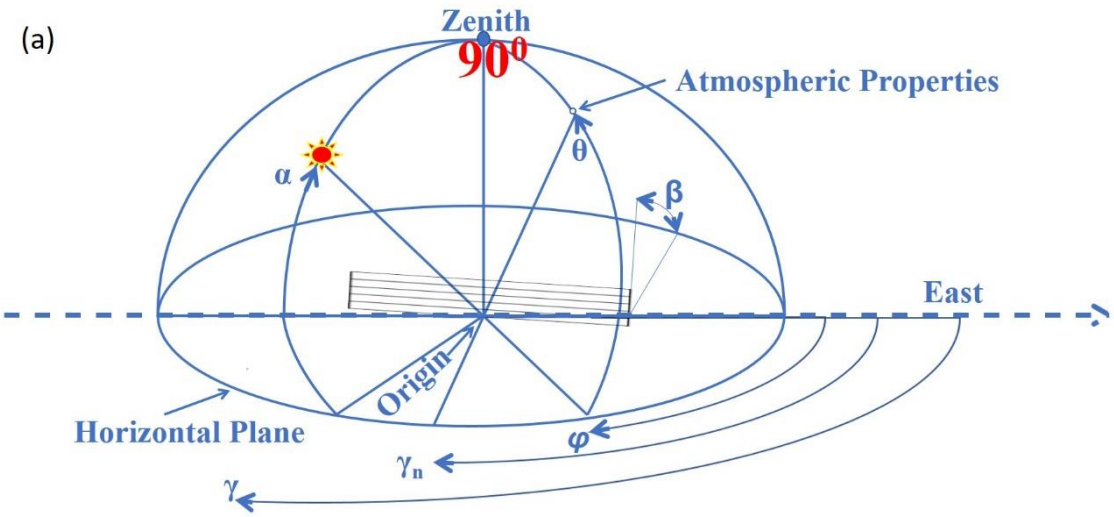

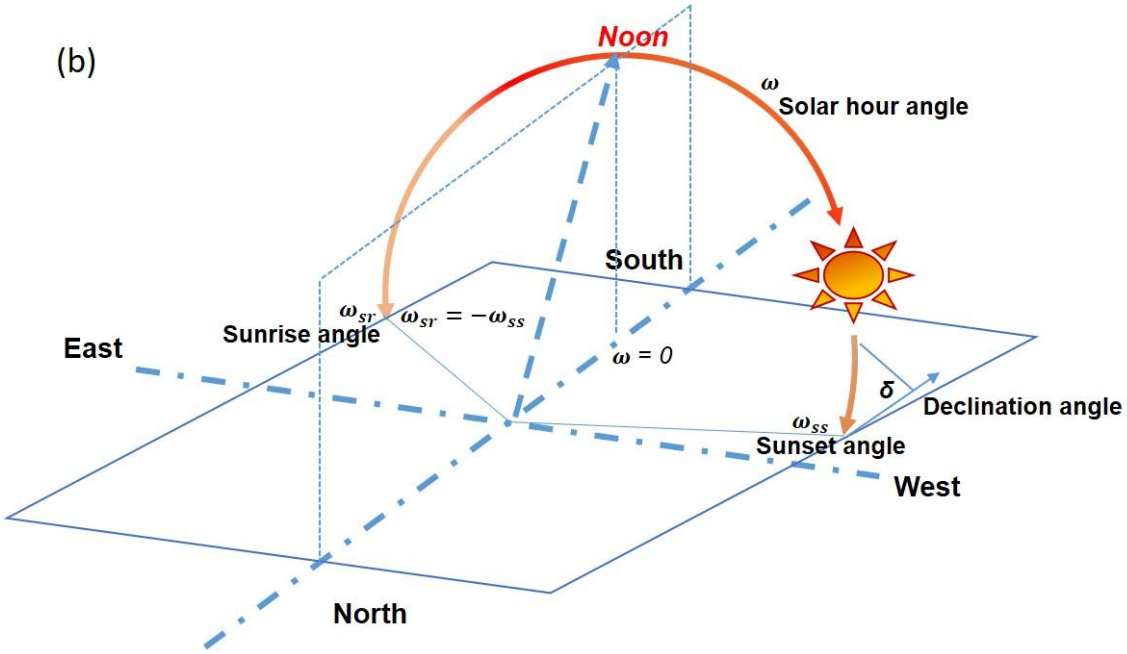

Figure 4.1: (a) Latitude, tilt, zenith and azimuth angle, (b) schematic definition of angles relative to sun path illustrating solar hour angle, declination angle, sunrise angle and sunset angle.

4.2.7 Global (H_G), beam, diffuse and reflected radiation

Global solar radiation consists of three components, including direct (beam) solar radiation, diffuse solar radiation, and reflect solar radiation (see Equation (4.5)). All these components are elaborated and further illustrated in Figure 4.2 below.

$$H_G = H_B + H_D + H_R \tag{4.5}$$

4.2.8 Direct (beam) radiation (H_B)

Direct solar radiation is incident solar radiation directly from the sun reaching the earth's surface without having significant interference or scattering. The direct solar radiation received on a PV module can be calculated using Equation (4.6), where H_b the direct solar radiation on a horizontal surface and R_b is the ratio of the direct solar radiation incident on a surface tilt to the one reaching the horizontal surface.

$$H_B = H_b R_b \tag{4.6}$$

R_b is considered as a tilt factor, positive in the southern hemisphere and negative in the northern hemisphere. R_b can be estimated using Equation (4.7).

$$R_b \frac{\sin(\varphi \pm \beta)\ \omega_{ss} \sin\delta + \sin\omega_{ss}\ \cos\delta \cos(\varphi \pm \beta)}{\omega_{ss} \sin\delta \sin\varphi + \cos\delta \cos\varphi \sin\omega_{ss}} \quad (4.7)$$

4.2.9 Diffuse radiation (H_D)

Diffuse solar radiation reaches the earth's surface after being scattered by clouds or other atmospheric suspended particles. The diffuse radiation can be estimated using Equation (4.8) below, where H_d represent the diffuse radiation on a horizontal surface and R_d is the tilt factor described as the ratio of solar radiation reaching a tilted surface to that of the radiation received on the horizontal surface.

$$H_D = H_d R_d \quad (4.8)$$

R_d Equation (4.9) can be estimated if the sky is considered an isotropic radiation source (Ullah et al., 2019).

$$R_d = \frac{1 + \cos\beta}{2} \quad (4.9)$$

When the sky turns out to be cloudy or dusty, an anisotropic model such as the Hay model can be used to estimate the ratio using Equation (4.10) as provided by Ullah et al. (2019), where H_o is the extra-terrestrial daily incident solar radiation on the earth's horizontal surface.

$$R_d = \frac{H_g - H_d}{H_O} R_b + \frac{1}{2}(1 + \cos\beta)\left[1 - \frac{H_g - H_d}{H_o}\right] \quad (4.10)$$

4.2.10 Reflected radiation (H_R)

The reflected radiation is the reflected solar radiation that reaches the PV module's surface after reflecting from terrain or other reflective surfaces. The estimated reflected solar radiation can be calculated using Equation (4.11) below, where $H_g$the global solar radiation incident on a horizontal surface and R_r is the tilt factor for reflected solar radiation, which is the reflected solar radiation ratio

between the horizontal surface and a tilted surface. It can be estimated using Equation (4.12) below as provided by Ullah et al. (2019), where ρ is the surface albedo, which further described below.

$$\mathrm{H_R} = H_g R_r \tag{4.11}$$

$$R_r = \rho \frac{1-\cos\beta}{2} \tag{4.12}$$

4.2.11 Surface albedo (ρ)

Surface albedo (ρ) is the radiance ratio reflected from the terrain to the irradiance received by a PV module surface. It can be determined by the spectral angular distribution of solar radiation received at the earth's surface and the reflecting surface property. It can vary from 0.9 for fresh snow to 0.04 for new asphalt (Ullah et al., 2019).

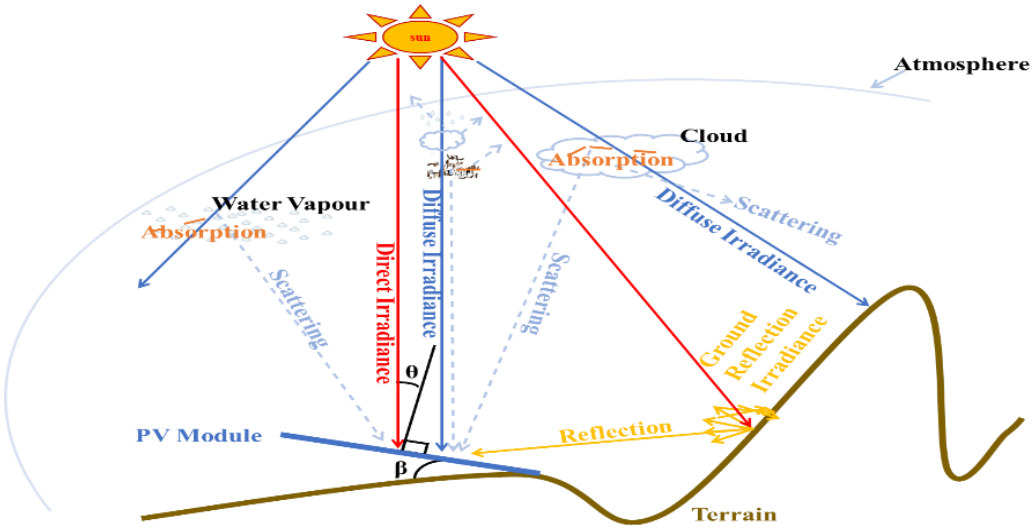

Figure 4.2: Components of global solar radiation.

4.3 Methods

Forty-five pieces of 50 mm x 50 mm x 4 mm low iron glass coupons were exposed to outside weather conditions in Abuja (09°03'N, 07°30' E), Nigeria's federal capital territory. These coupons were exposed in three groups considering the period of exposure (monthly, seasonally and yearly), where 36 coupons were used monthly, 6 for seasonal (3 for dry and 3 for wet season) and 3 for annual. Also, each group of coupons was placed in three positions; horizontal (0°), tilt

angle (45°) and vertically (90°) using an in-house developed research jig shown in Figure 4.3. The research jig design using solid works and was fabricated using a Stratasys uPrint SE 3D printer with a P430XL ABS (Acrylonitrile Butadiene Styrene) material. This material was selected for its properties would not be transferred to the coupon surface during extreme weather conditions such as rainfall, high temperature, or dry-dusty wind. It has good thermal conductivity and remains stable at temperatures between -20°C to + 80°C. Samples were labelled on the 4 mm part of the glass with information such as location, period, and exposure position. Monthly coupons are exposed on the first day of the month and removed on the first of the following month, marking the expiration period for monthly coupons of the previous month. Seasonal coupons are exposed when the weather varies for over two weeks towards the end of the season. Annual coupons were exposed in January 2019 and were removed in January 2020. These dates were analysed at the beginning of the experiment to avoid been biased. All coupons were removed at the expiration of their exposure period and returned to the University of Exeter solar laboratory for detailed characterisation. A flowchart illustrating the various steps through the research methodology of this subsection of the thesis is provided in Appendix B – Figure 0.4.

A crate was carefully designed using solid works and fabricated with the above-mentioned 3D printer, which was employed in transporting the samples. The crate was designed in two parts container (main container and the cover) to prevent movement, shaking, and breakage. Then the crate was placed in a sample Fisherbrand SureOne 02-707-411 container and filled with Eco-Flo biodegradable packing peanuts or bubble wrap packaging. The container is further wrapped with bubble packaging before shipping. On delivering the sample, each crate was examined to determine if the deposited sample was removed from the container by placing a plain white paper underneath the container before opening and when removing the samples. A very tiny quantity of samples was observed, and it would have any significant impact on the study's findings; as such, it was deliberately disregarded. Therefore, It was assumed that the formation pattern was not distorted during transport.

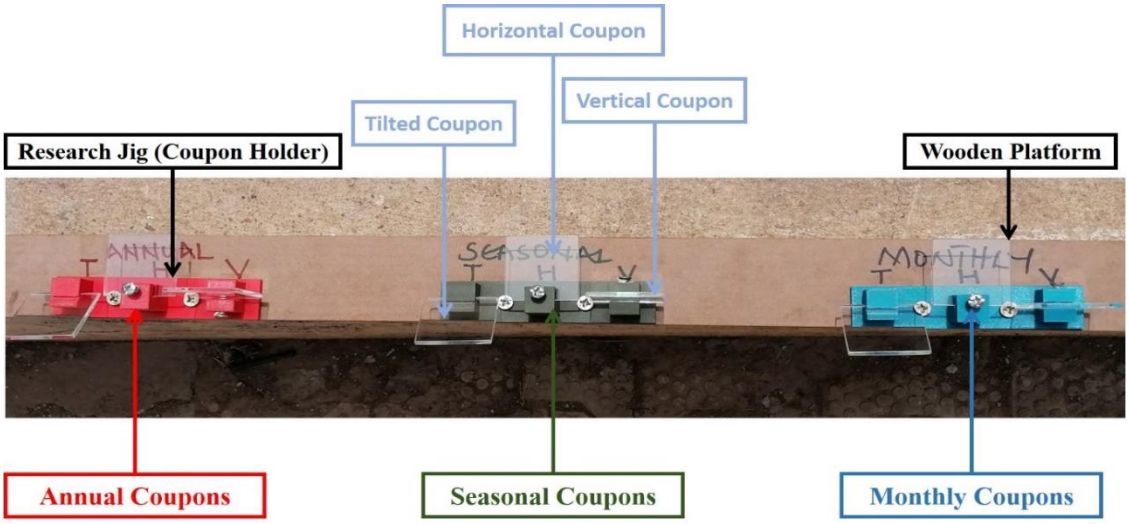

Figure 4.3: Digital image of coupons and research jig installation.

4.3.1 Site

Details about the site of exposure are documented in Table 4.1. This location was carefully selected because of its excessive energy demand (where 43.5% of the population does not have electricity access, and the remaining populace has an epileptic supply) and high interest in PV installation (World Bank Group, 2020).

Table 4.1: Site information.

Abuja Municipal (AMAC), Federal Capital Territory, Nigeria			
Longitude	Coordinates	09°03'00"	North
Latitude		07°30'00"	East
Time	Time zone	UTC+01	[WAT] - Lagos
DNI	Direct normal irradiation	1116	kWh/m^2
GHI	Global horizontal irradiation	1888	kWh/m^2
DIF	Diffuse horizontal irradiation	1052	kWh/m^2
GTI opta	Global tilted irradiation at an optimum angle	1927	kWh/m^2
OPTA	The optimum tilt of PV modules	13/180	^{0}
TEMP	Air temperature	26.6	^0C
ELE	Terrain elevation	498	m
PV_{OUT_total}	Total photovoltaic power output and Global tilted irradiation	0.004	MWh per day
PV_{OUT_total}	Total photovoltaic power output and Global tilted irradiation	1.449	MWh per year
PV_{OUT_total}	Total photovoltaic power output and Global tilted irradiation	1919	kWh/m^2 per year

The average weather condition of Abuja was provided for analysis purposes of the dust accumulation on various coupons. Weather data were obtained from World Weather Online (2020). Figure 4.4 includes temperature, humidity, cloud, precipitation and wind speed during exposure.

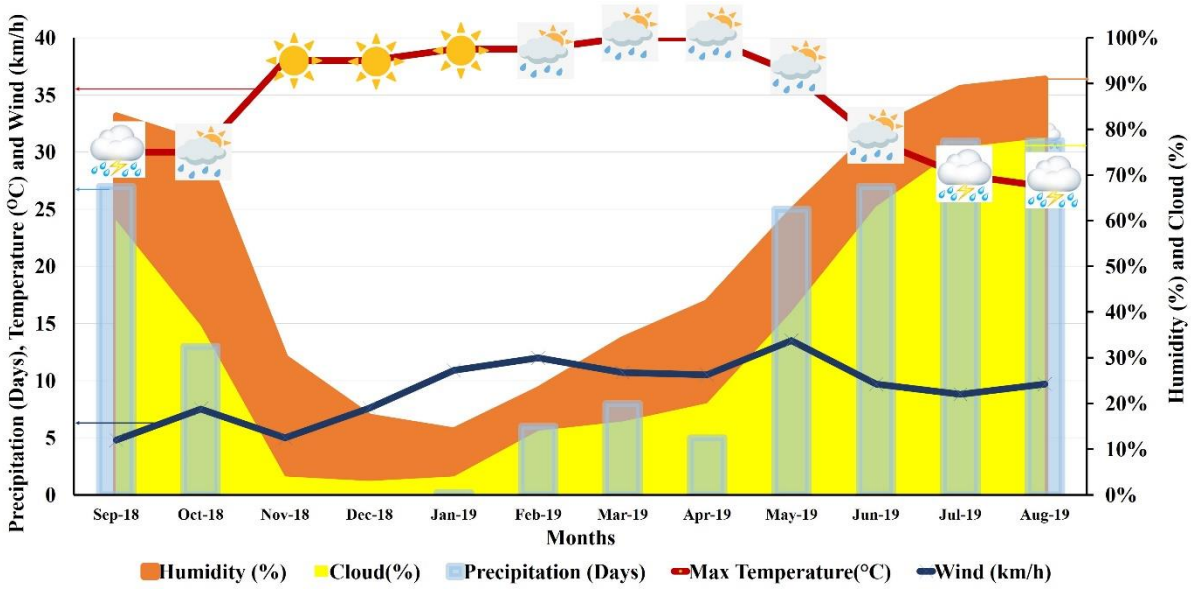

Figure 4.4: Monthly weather condition variation in Abuja during the period when coupons were exposed.

4.3.2 Optical characterisation

Optical degradations of coupons were examined using the Perkin Elmer Lambda 1050 UV/VIS/NIR spectrophotometer. A clean coupon was initially tested to establish the optimal transmittance level of low iron glass, and subsequently, all the exposed coupons were also subjected to the same test where UV (Ultraviolet), VIS (Visual) and NIR (Near Infra-Red) transmittance levels were measured ranging from 200 nm to 1200 nm wavelength. The spectrum accommodates all the existing PV technologies available in the market. The results obtained were calculated using Equation (4.13) below for verification purposes, where T(λ) is the spectral transmission, Δλ is the change in wavelength and S(λ) is the relative spectral distribution of solar radiation.

$$\tau_{solar} = \frac{\sum_{\lambda=200nm}^{1200nm} S(\lambda)T(\lambda)\Delta\lambda}{\sum_{\lambda=200nm}^{1200nm} S(\lambda)\Delta\lambda} \quad (4.13)$$

Changes in transmittance of various coupons were calculated to determine the percentage difference using Equation (4.14) below, where Δ is the change, τ_x is transmittance data of a coupon positioned at an angle relative to a horizontal surface, τ_{clean} is transmittance data of a clean coupon.

$$\Delta\tau_x = \frac{(\tau_{clean} - \tau_x)}{\tau_{clean}}(\%) \tag{4.14}$$

Transmission data on Abuja's PV installation's optimum angle was interpolated using Equation (4.15) below, where $\tau_{\beta_{(optimum)}}$ is the calculated light transmittance reduction of a coupon considering the PV optimum angle of Abuja (13°) in percentage, $\tau_{\beta_{(0)}}$ is transmittance reduction data in percentage from a coupon that was horizontally positioned (90° from the vertical plane) and $\tau_{\beta_{(45)}}$ is transmittance reduction from coupons that were positioned at 45° angles.

$$\tau_{\beta_{(optimum)}} = \tau_{\beta(45°)} + \frac{(\tau_{\beta(0°)} - \tau_{\beta(45°)})(\beta_{(optimum)} - \beta_{(0°)})}{(\beta_{(45°)} - \beta_{(0°)})} \tag{4.15}$$

4.3.3 PV output losses

The global solar atlas is the only reliable free online source that provides solar energy and PV potential in Abuja, Nigeria. This atlas provides easy access to global solar energy resources and PV potential data. The World Bank funds the platform to support countries and provides information to scale up global solar energy penetration. PV output data of Abuja were provided by GSA (2020), considering 13°/180° as the optimum tilt angle and azimuth for PV installation. PV output specific data for a small residence with an installed capacity of 1kWp was used to illustrate PV output reduction caused by soiling influenced by various tilting coupons' positioning. The PV output was determined using the global irradiation falling on the optimum tilt plane by calculating the global horizontal irradiance, direct irradiance, terrain albedo, sun position, diffuse irradiance, and angular reflected radiance (GSA, 2020). In addition, Global Solar Atlas considered several parameters in calculating and generating PV power output. Some of these are PV field self-shading, nominal operating cell temperature, inverter Euro efficiency, DC soiling losses**,** DC cable losses, DC mismatch losses,

AC transformer losses, AC cables losses and availability. It should be noted that PV power output is for the optimum tilt angle (13°) and remains the same for all the various tilt angles in this research. Soiling losses considering the PV installation capacity, as mentioned above, were calculated for various angles using Equation (4.16) to Equation (4.19) below, where β the angle of exposure measured from the horizontal plane, τ_t is transmittance data of a coupon positioned at 45° from the horizontal plane, τ_h is transmittance data of a coupon positioned at horizontal plane and τ_v is transmittance data of a coupon positioned at 90° from the horizontal plane.

$$PV\_out\ _{(\beta_{(90)})} = PV_{(Total\ \ PV\ Output)} * (1 - \Delta\tau_v) \quad (4.16)$$

$$PV\_out\ _{(\beta_{(45)})} = PV_{(Total\ \ PV\ Output)} * (1 - \Delta\tau_t) \quad (4.17)$$

$$PV\_out\ _{(\beta_{(0)})} = PV_{(Total\ \ PV\ Output)} * (1 - \Delta\tau_h) \quad (4.18)$$

$$PV\_out\ _{(\beta_{(Optimum)})} = PV_{(Total\ \ PV\ Output)} * \left(1 - \Delta\tau_{optimum}\right) \quad (4.19)$$

PVSyst was employed to generate the horizon and sun path of the experiment's site (shown in Figure 4.5), showing the high potential of solar energy in the region. The location has high potential throughout the year, with a bit of change during the wet season. This and the other hourly average of PV output data was used to calculate the hourly PV performance degradation caused due to dust accumulation. Equations (4.16), (4.17), (4.18), and (4.19) were used in calculating the soiling losses of the various angles.

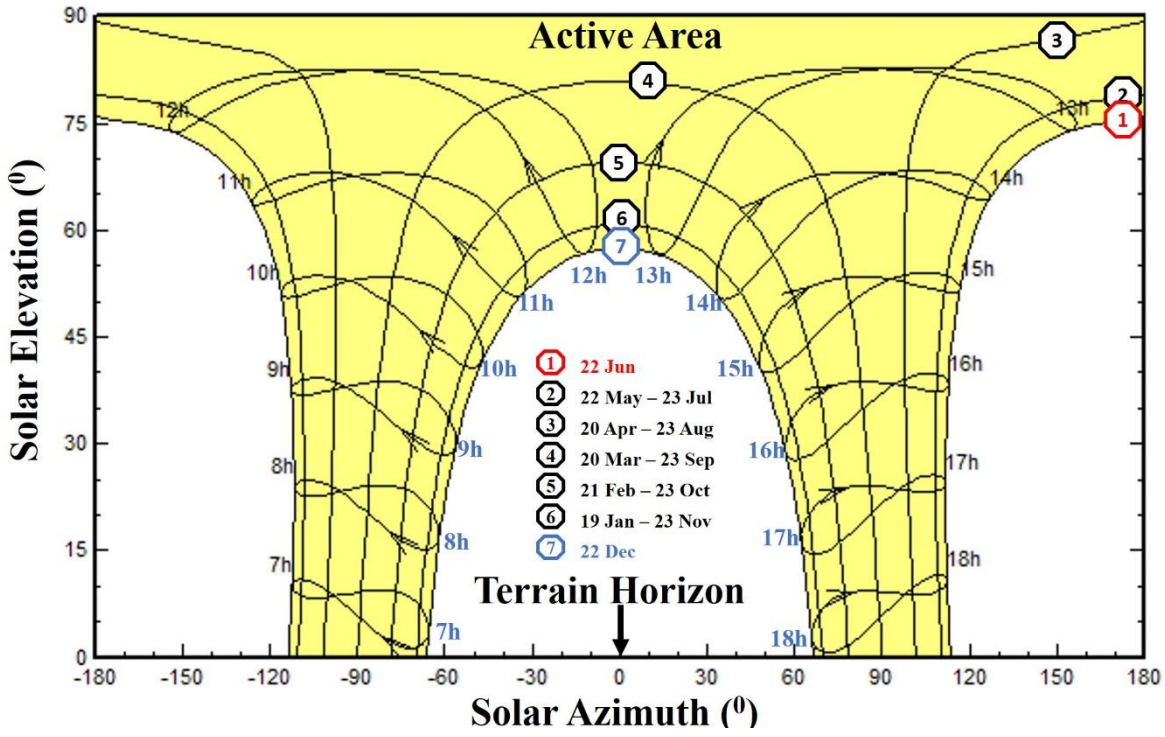

Figure 4.5: Abuja's horizon and sun path (obtained from PVSyst) indicating daily sun hours for various months.

4.3.4 Mass measurement

Sample weights were measured using Mettler Toledo ME204 that provides accurate and reliable weighing results, as shown in Figure 4.6. Soiled coupons were initially weighed and documented. Then each coupon was washed using water and soap, cleaned with acetone, dried with a hand dryer, and weighed again. The variation of weight between a soiled and a washed coupon is the accumulated dust weight, calculated using Equation (4.20), where ρ_d is the deposited dust density, $\rho A \rho d C$ is the area density of a soiled coupon, $\rho A C$ is the area density of a coupon after cleaning (clean coupon), and 10^6 is the conversion factor g/mm^2 to g/m^2 since the coupon area is 50 x 50 mm.

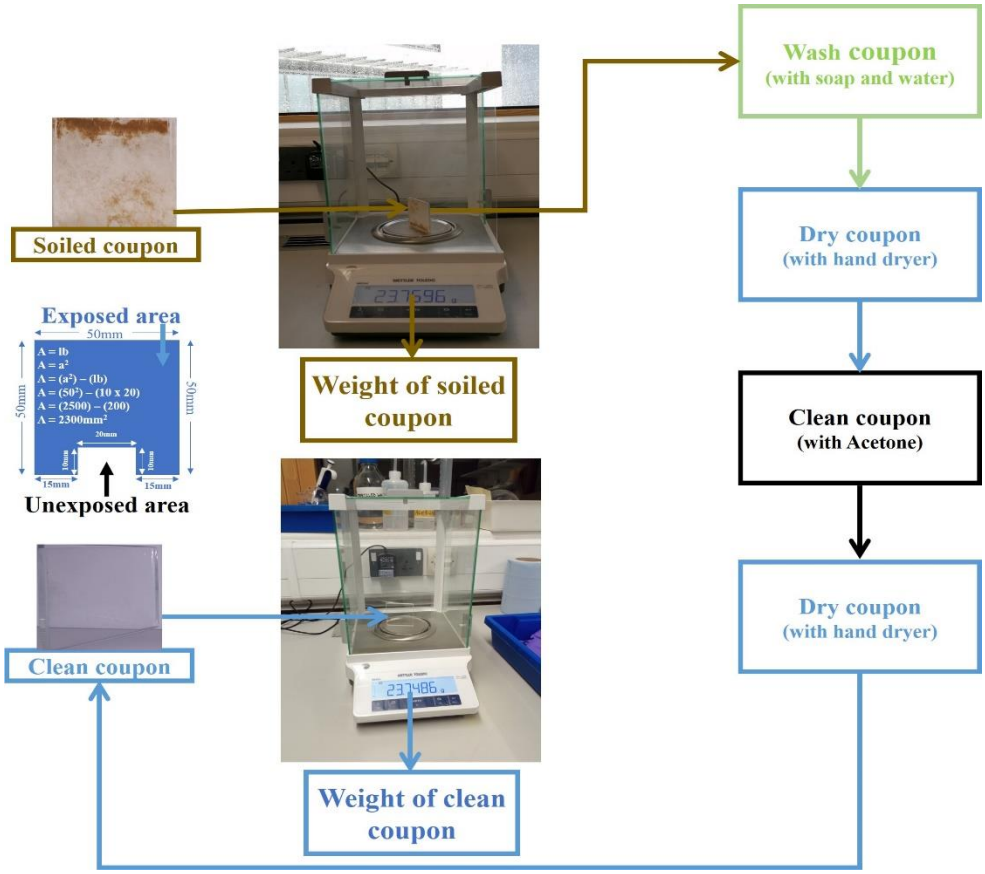

Figure 4.6: Schematic for the measurement of the weight of accumulated dust on coupons.

$$\rho_d(g/m^2) = \rho A \rho d C_{(g/mm^2)} \times 10^6 - \rho A C_{(g/mm^2)} \times 10^6 \quad (4.20)$$

4.4 Results

4.4.1 Transmission losses

Transmission losses on coupons were determined, and the results were categorised and presented according to their period of exposure (monthly, seasonally, and annually). Subsequent paragraphs present all other results and their analysis.

4.4.1.1 Monthly transmission reduction due to dust accumulation

Average transmission losses due to dust accumulation were determined considering different tilt angles. The monthly reduction is presented in Figure 4.7 and Figure 4.8. Figure 4.8 shows that coupons exposed in a horizontal position cause higher transmittance reduction. The highest transmittance reduction of

about 38% was observed in February for a horizontally positioned coupon. Simultaneously, the result presented the most negligible transmittance reduction of approximately 1% in September for a vertically positioned coupon. This result shows that horizontally exposed coupons always accumulate more dust, followed by tilted coupons (at 45°), and then vertically positioned coupons have a minor accumulation. The observed pattern of accumulation is due to the wind effect and the gravitational force that allows the dust to settle on a flat horizontal platform. The wind effect tends to have a more negligible effect on the accumulated particles on the horizontal surface than a tilted one (45°), resulting in more accumulation. The gravitational force allows more dust to gravitate and settle on a horizontal and tilt platform (45°) compared to a vertical position platform.

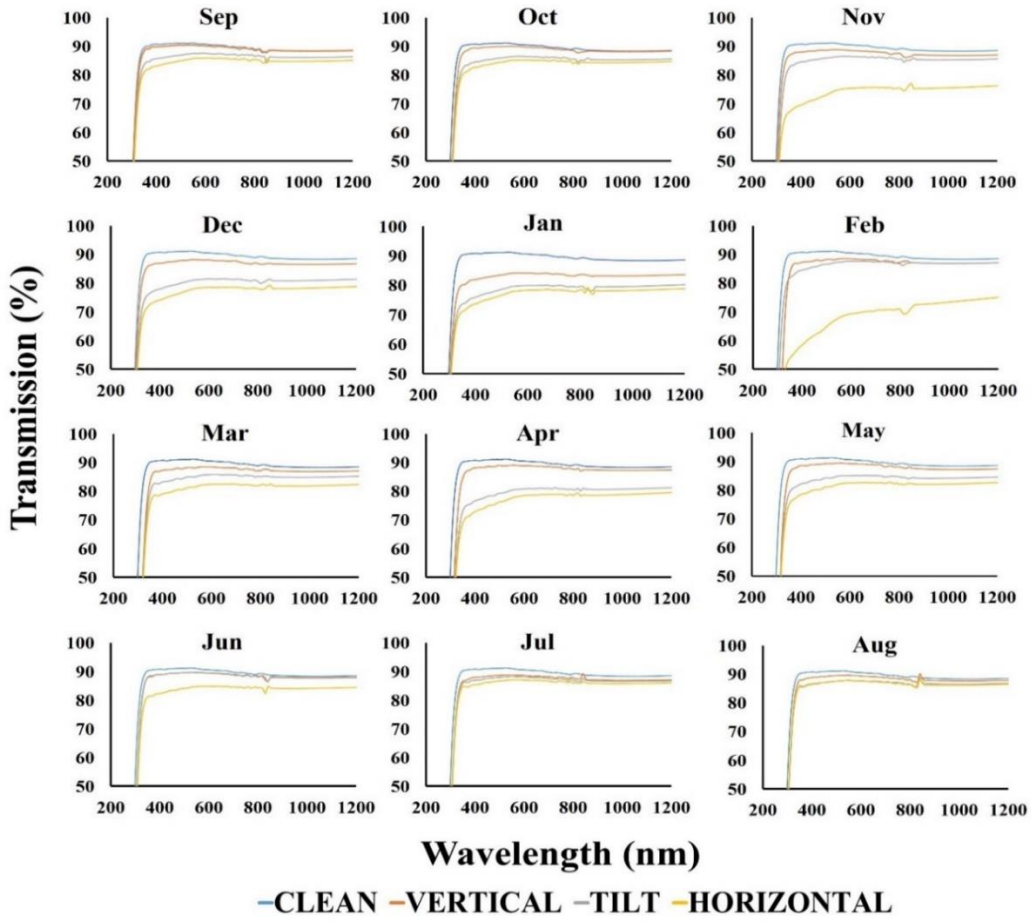

Figure 4.7: Monthly optical transmission variation for clean, vertical, 45° tilt and horizontal surface of the coupons recorded through optical characterisation by employing spectrometer to measure both direct and total transmittance.

The optimum tilt angle based on transmission data was calculated for Abuja by employing Equation (4.15), and it was found to present alarming optical losses, as shown in Figure 4.7 and Figure 4.8. The highest loss was recorded from the horizontal coupon, followed by an optimum tilt angle calculated using the interpolation technique. The most significant loss based on the calculation used in determining optimum tilt angle losses was recorded for February with about 17% reduction, and the lowest was recorded for June and August, with both having a 5% reduction. Figure 4.8 presents the calculated monthly losses and other losses obtained from exposed coupons.

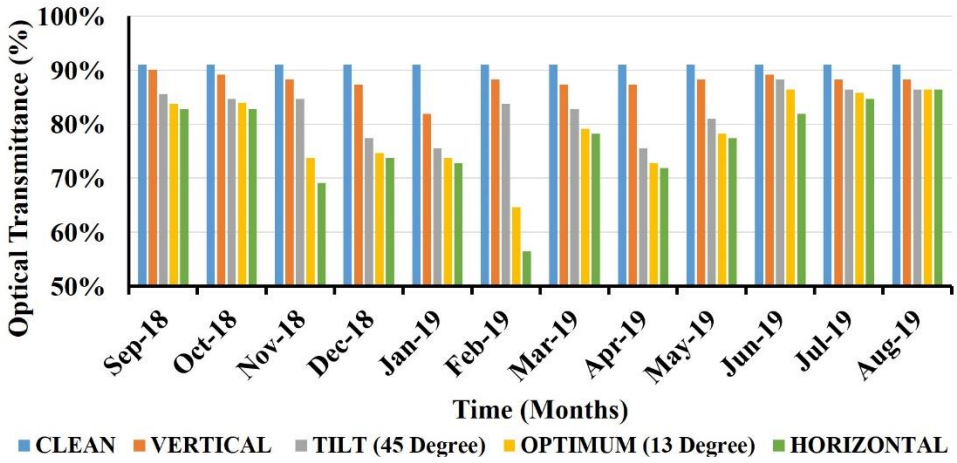

Figure 4.8: Monthly variation of optical transmission reductions for different orientations with calculated optical losses of Abuja's optimum tilt angle (13°).

4.4.1.2 Seasonal transmission reduction due to dust accumulation

The seasonal transmission reduction shows that both seasons have a severe dust accumulation, affecting the light transmission, with the dry season having the most devastating effect. The result from Figure 4.9 shows that during the dry season, a horizontal position coupon accumulates dust that causes about 88% reduction, 24% for a tilted (45°) coupon, while a vertical position coupon is about 14%. On the other hand, coupons exposed during the wet season presented a reduction of about 37% when positioned on a horizontal plane, 19% for a tilted (45°) coupon and about 15% for a vertically positioned coupon. These significant reductions of light transmittance due to dust accumulation can cause a devastating effect on PV technology's performance. The lower amount of dust accumulation during the wet season is due to the rain that provides natural

cleaning to the coupons. However, the figures are still higher and can cause a significant decrease in PV performance. The higher transmittance reductions observed during the dry season are due to a Harmattan season that blows low-level jet wind spreading dry dust across the country and lack precipitation, as highlighted in Figure 4.4.

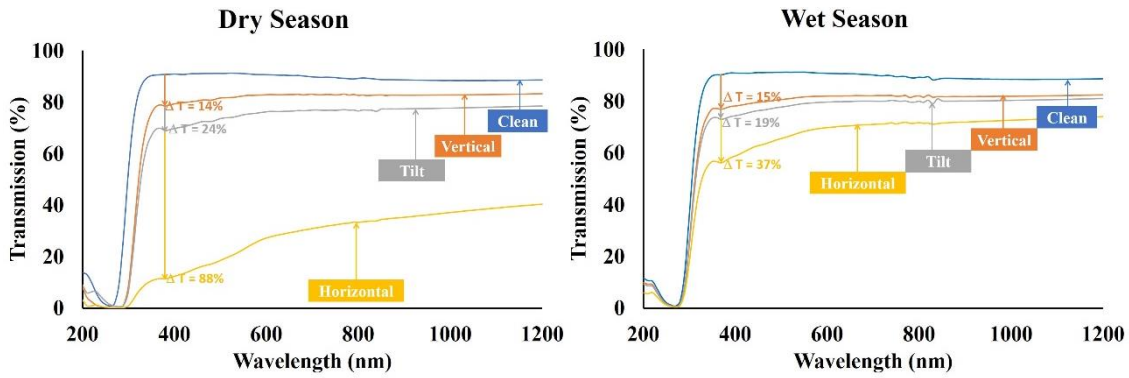

Figure 4.9: Variation of optical transmission losses for different coupon angular orientations exposed during the wet and dry seasons.

4.4.1.3 Annual transmission reduction due to dust accumulation

The result obtained from the coupons exposed for a one-year duration shows that light transmission reduction varies with exposure positioning. Figure 4.10 shows that the average transmission of a horizontally positioned coupon reduces by about 59% and 42% for a tilted (45°) coupon, while the vertical position coupon is 34%. The result shows a massive accumulation of all the coupons due to the long duration of subjection to outdoor weather.

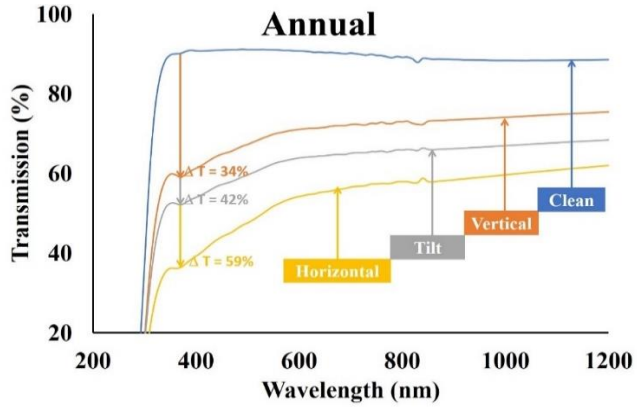

Figure 4.10: Variation of optical transmission losses for different coupons orientations that were exposed for one year in Abuja.

4.4.2 PV Performance reduction considering dust accumulation influenced by the tilt angle

The PV output used in this research is a temporal aggregation, provided by GSA (2020) for a particular tilt angle (13°) which is the optimum tilt angle for the research site. The optimum tilt angle (13°) was selected based on GSA's annual average irradiance data. PV power output parameters remain the same for other angles, even though more or less power can be achieved at some times of the day for the other angle. However, this section of this research highlights and demonstrates the influence of tilt angle in dust accumulation and its effect on PV performance.

4.4.2.1 Hourly PV Output Losses

Hourly PV performance data were collected from GSA (2020) considering 1 kWp installed capacity, and the monthly transmission losses from the glass coupon were used to calculate the hourly power reduction. The result shows that significant power losses occurred when PV installation tends to generate high output. Figure 4.11 shows those months with higher outputs (November, December, January, and February) have high losses during the peak output hours compared to other months. The results also show that coupons exposed in vertical positions tend to have less power degradation than tilt (45°), optimum tilt, and horizontally positioned coupons. However, the power output used was based on the optimum tilt angle (13°) as such power output of other angles such as vertical, tilt (45°), and horizontal might differ with the lower value of output. The values were intentionally used since this section's objective illustrates how various angles can accumulate dust and cause severe hourly power losses.

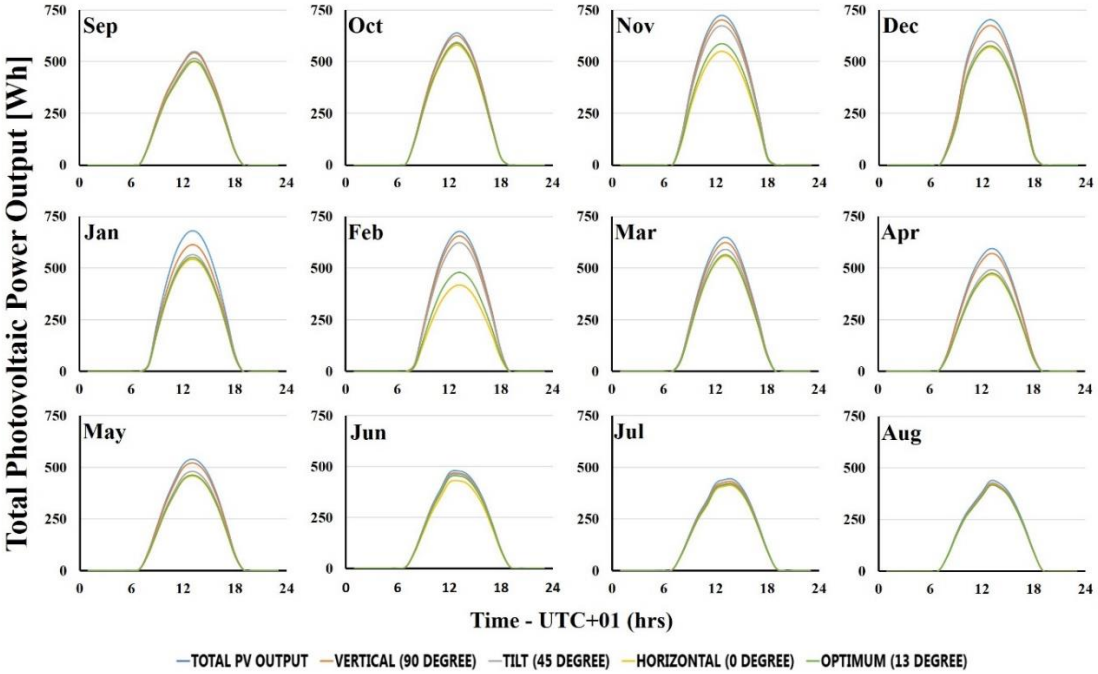

Figure 4.11: Hourly photovoltaic power output variation of 1 kWp rating installation and soiling losses based on optical transmission losses recorded from coupons exposed on Abuja's various orientations.

4.4.2.2 Monthly PV output losses

The monthly PV output losses were determined using power output provided by Global Solar Atlas (2020), considering 1kWp-installed capacity and transmission losses obtained from the exposed monthly coupons. Results show a higher degradation of PV power output on horizontally positioned coupons, and the power output improves when the angle is being tilted towards the vertical position. Results in Figure 4.12 show that reductions were significantly higher during November and February, with November having 35.7 kWh/kWp losses and February having 47.1 kWh/kWp for the horizontal position coupon. Less reduction was observed on coupon exposed at an optimum tilt angle where the power degraded by about 28.3 kW/kWp for November and 35.9 kWh/kWp for February. It is observed that the degradation reduces on tilted (45°) and vertically position coupons for the two months compared to coupon on horizontal and optimum tilt with the tilted (45°) having a reduction of 10.4 kWh/kWp for November and 9.9 kWh/kWp for February while the vertical position coupon degraded by 4.5 kWh/kWp for November and 3.7 kWh/kWp for February.

The lowest PV output degradations were recorded during August due to high rainfall that clean all the coupons and restore the PV's power output considering all the various tilting positions. Figure 4.13 shows that reductions are similar to various tilting positions. The result shows that 5.0 kWh/kWp reduction was recorded for horizontal, optimum tilt and tilted (45°) angle coupons while the vertically positioned coupon degraded by 3.0 kWh/kWp. Figure 4.4 shows that rainfall was experienced for 31 days, and according to World Weather Online (2020), a cumulative rainfall amount of 628 mm for the month was recorded. The high amount of rain can restore a PV surface's cleanliness but cannot be relied on since we can observe some can still record some soiling losses.

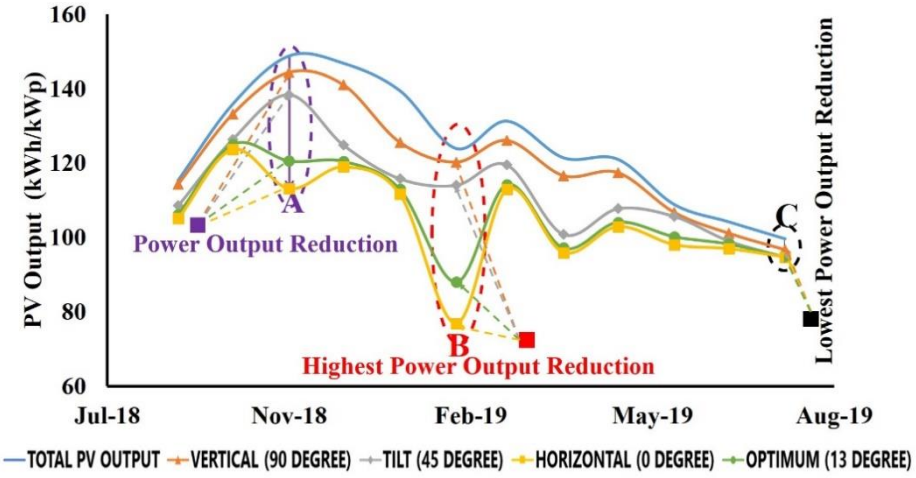

Figure 4.12: Monthly photovoltaic power output variation of 1 kWp rating installation and soiling losses based on monthly optical transmission losses recorded from coupons exposed at various angular orientations in Abuja.

4.4.2.3 Seasonal PV output losses

The seasonal PV output losses were determined by taking the average power output in the months of a particular season as provided by the GSA (2020), considering 1 kWp-installed capacity and transmission losses obtained from the seasonal coupons that were exposed. The result from Figure 4.13 shows that the summation PV output for the wet season is 937.93 kWh/kWp and the soiling losses resulted in degradation of about 141 kWh/kWp when the coupon is exposed in a vertical position, 178 kWh/kWp at a tilt angle (45°), 300 kWh/kWp at an optimum tilt angle (13°), and 347 kWh/kWp at a horizontal position. On the

other hand, Figure 4.13 shows that the summation of PV output for the dry season without soiling losses is about 559.07 kWh/kWp and it also presented soiling losses which caused degradation of about 78 kWh/kWp when positioned on a vertical plane, 134 kWh/kWp when on tilt (45°), 391 kWh/kWp when on optimum tilt and 492 kWh/kWp when placed in a horizontal position. The result shows that the high average degradation on both seasons was recorded when coupons were exposed to extreme conditions on a horizontal plane, with the dry season having the most alarming degradation.

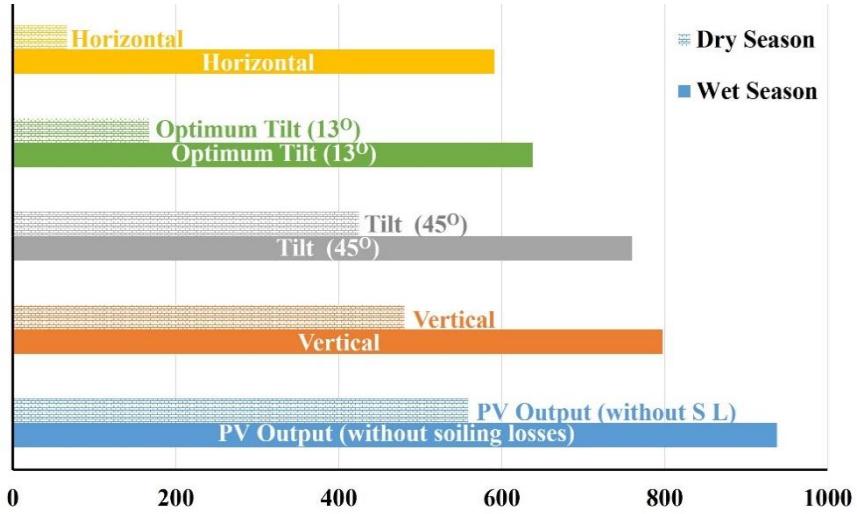

Figure 4.13: Wet and dry season photovoltaic power output variation of 1kWp rating installation and various soiling losses based on optical transmission losses recorded from coupons exposed on three orientations in Abuja and a calculated optical loss for the optimum tilt angle orientation.

4.4.2.4 Annual PV output losses

The annual PV output losses were determined using power output provided by Global Solar Atlas (2020), considering 1 kWp-installed capacity and transmission losses obtained from the exposed annual coupons. The result from Figure 4.14 shows that an average of 1.50 MWh/kWp per year could be recorded with a PV installation having 1 kWp. The result shows about 0.81 MWh/kWp per year loss is estimated due to soiling when PV is installed at an optimum tilt angle, 0.51 MWh per year for vertically position installation, 0.63 MWh/kWp per year for a tilted (45°) installation, and 0.88 MWh/kWp for a horizontal position installation.

These numbers are very high, and without cleaning in just a year, soiling caused a very alarming degradation of PV performance.

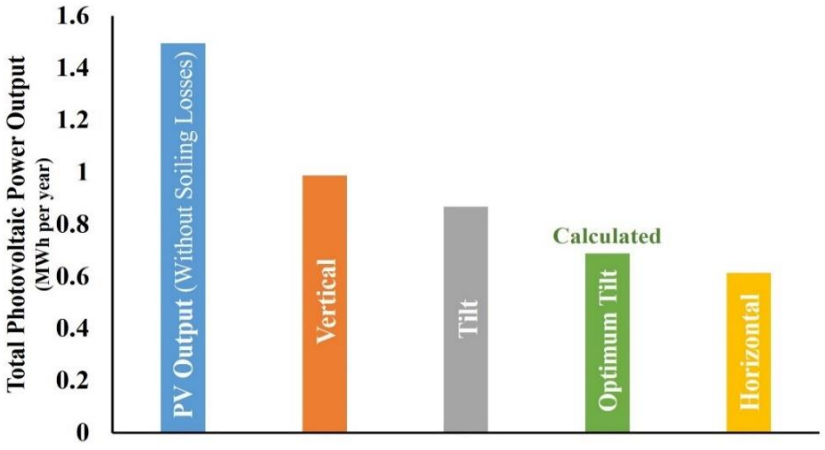

Figure 4.14: The annual photovoltaic power output of 1 kwp rating installation with various soiling losses based on optical transmission losses recorded from coupons exposed on three orientations in Abuja and a calculated optimum tilt angle optical loss.

4.4.3 Mass of accumulated dust

The weight of accumulated dust as a function of tilt angle has been analysed in this section. Results obtained clearly show how the tilt angle influences accumulation on the platform.

4.4.3.1 Monthly mass of accumulated dust

Results from monthly coupons show various weights concerning the positioning and the period of exposure. The highest accumulations were recorded on horizontal position throughout the twelve months of the year, followed by a tilt (45°) and vertical consecutively. The horizontal coupon from February tends to accumulate more dust with about 4.16 g/m^{2,} but the minor accumulation was recorded from the vertical coupon exposed during September with about 0.2 g/m^2. Figure 4.15 shows all the months and their corresponding dust accumulation mass and exposed position.

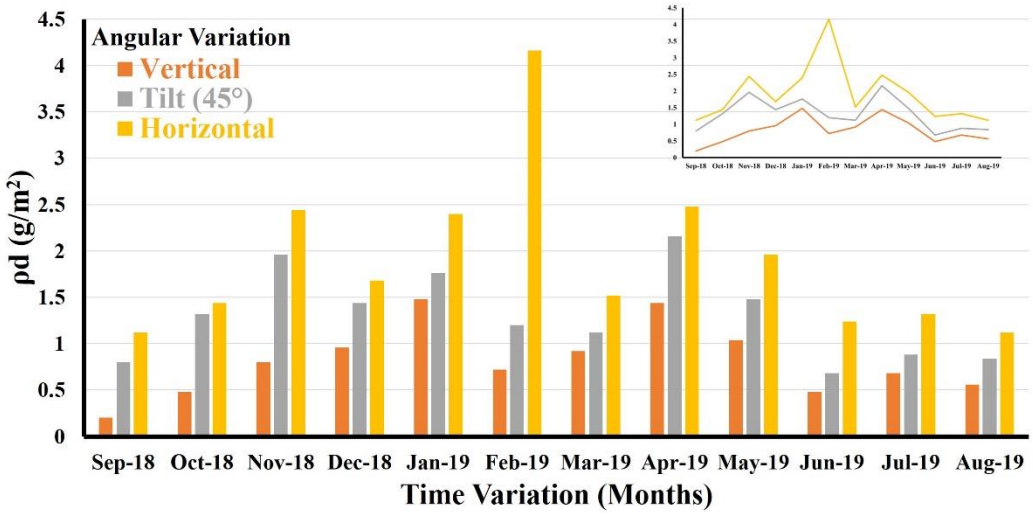

Figure 4.15: Monthly variation of the mass of accumulated dust for the three orientations (vertical, 45° tilt and horizontal).

4.4.3.2 Seasonal mass of accumulated dust

Dust accumulation considering season (wet and dry) was evaluated, and the results obtained highlighted an alarming weight. Figure 4.16 shows dust accumulation mass during the dry season exposed in a horizontal position, having a frightening accumulation of about 12.56 g/m^2, 2.44 g/m^2 for the tilt (45°), and 1.88 g/m^2 for vertical position. On the other hand, the result from Figure 4.16 shows a lower mass of accumulated dust for coupons exposed during the wet season with the coupon placed on a horizontal position, having 3.4 g/m^2, 2.2 g/m^2 for tilt (45°), and 1.76 g/m^2 for vertical position.

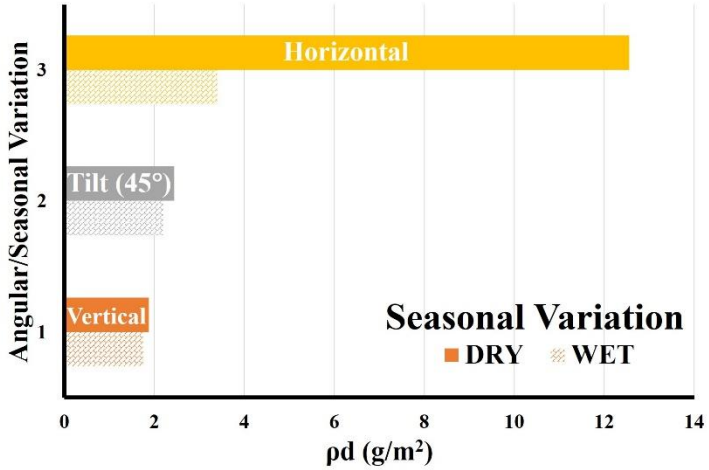

Figure 4.16: Seasonal variation of the mass of accumulated dust.

4.4.3.3 Annual mass of accumulated dust

The mass of accumulated dust from coupons exposed for one year is shown in Figure 4.17, where the result shows that the horizontally positioned coupon is having the highest accumulation with about 8.52 g/m^2, followed by the coupon exposed on tilt (45°) position with about 3.84 g/m^2, and the least is the vertical position with about 3.24 g/m^2.

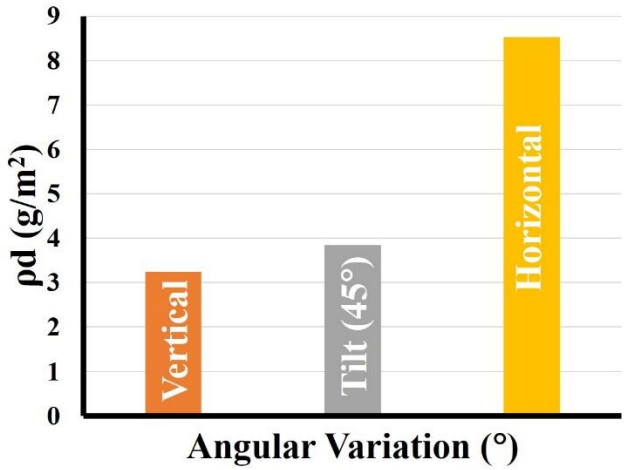

Figure 4.17: Variation of the mass of accumulated dust for one year.

The high mass of accumulated dust on coupons exposed in the horizontal position presented above is related to gravitational forces and weather conditions. The transmission coefficient loss in correlation with the weight of accumulated dust on the coupon was presented in Figure 4.18. Moreover, illustrating how the reduction in transmission continues to increase as the weight of accumulated dust increases.

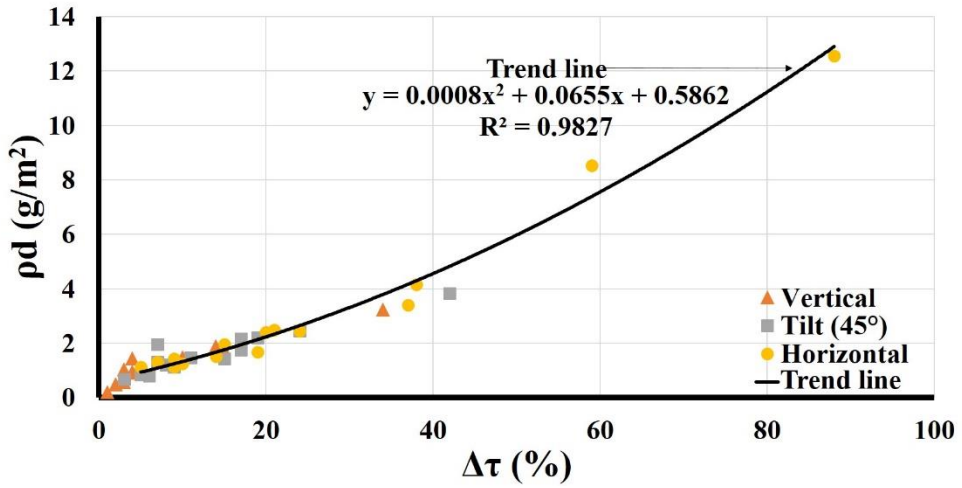

Figure 4.18: Transmission coefficient losses verse mass of accumulated dust.

Dust accumulation as a function of the tilt angle is presented in Figure 4.19. They furthermore illustrate how the influence of tilt angle plays a significant role in dust accumulation. The result shows that when coupons are positioned on a horizontal plane, they tend to have a higher mass than tilt (45°) and vertical position, with vertical being the one with less weight. Similarly, this pattern of accumulation occurs on all the coupons for various exposure periods.

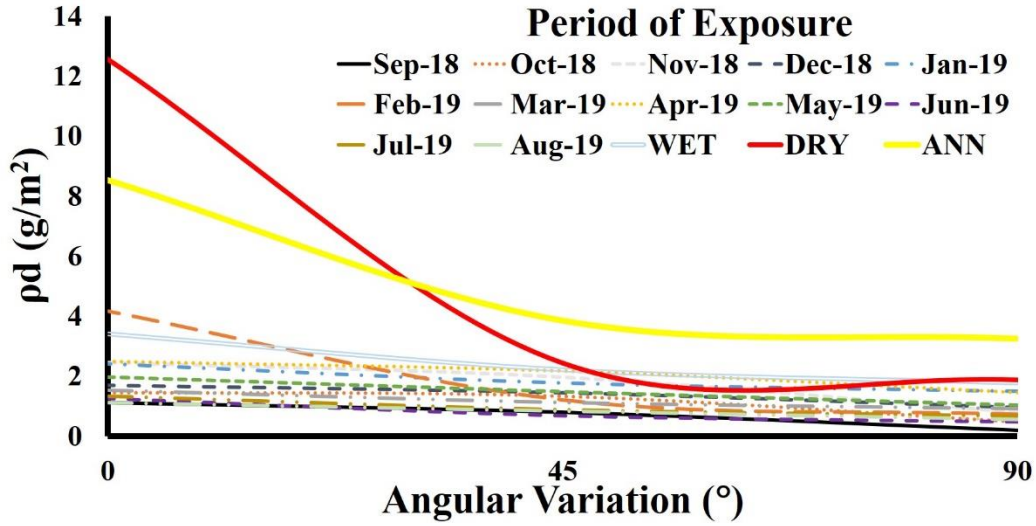

Figure 4.19: Variation of the mass of accumulated dust as a function of tilt angle.

The result obtained from the mass of accumulated dust validate our transmission and power output reduction result presented above and corroborated with the result presented in literature from other similar studies mentioned above.

4.5 Discussion

Transmittance reduction was recorded on all the exposed coupons with a higher reduction on the horizontally positioned coupons, gradually increasing with tilt angles (45°) towards the vertically positioned coupons. Considering the weather data provided in 2, it is clear that there is less or zero precipitation during the dry season months and low wind velocity. It is observed that the highest accumulation was recorded on the horizontal position coupon during February. Another reason is the light rain that occurred and promotes capillary bridges between dust particles to cause more adhesion on the coupons, thereby resisting the wind effect. The positioning also contributes by reducing the sliding and rolling of particles to retain more particles on the surface.

A variation was observed on some wavelengths in Fig 5, with a more noticeable decrease around UV wavelength attributed to the different types of accumulated dust particles, their morphology (precisely size), chemical composition, and deposition pattern. The majority of the existing PV technology's spectral response is from hundreds of nanometres, as such a particle with a diameter of around less than a micron could cause light attenuation. As earlier provided, the AQI parameters recorded in the region showing a higher concentration of PM_{10} and $PM_{2.5}$ and related to dust particles characterisation provided by Chanchangi et al. (2020a). It was assumed that the variation is due to broader particle diameter and the decrease in wavelength since UV wavelength could be easily affected by a tiny particle. It is also related to the natural deposition that is usually non-uniform. Gholami et al. (2017) stated that whether using PV devices or solar collectors, solar radiation needs to pass through the covering material, mainly glass or plastic, before exciting the technologies to generate heat or electricity. Therefore, the transmittance coefficient of the PV covering material is vital for device performance and anything that affects it could cause performance degradation.

Figure 4.9shows a broader variation during the dry season, especially on horizontally position coupons compared to other orientations in the same season and also compared to the wet season. A similar variation was observed in Figure

4.8; this time, the seasonal variation effect was sub-divided into months. The disparity is related to weather and gravitational force during the dry season, where dominant inward wind flow has more effect on accumulated particles on the vertical and tilt orientation, causing re-suspension of a significant amount. When the wind velocity drops and the weather tends to be calm, the relative humidity sometimes builds up to develop water droplets at specific points or dew build-up, and these could quickly settle on a horizontal surface compared to other orientations. Furthermore, during the daytime, when the relative humidity is dropping and the temperature rises, dry, dusty weather comes and mix with the water droplets, cementation would occur to retain a significant amount of particles. Figure 4.4 shows a slight increase in precipitation and humidity at the beginning and towards the end of the dry season, which plays a vital role in causing cementation. When cementation and capillary ageing occurs on a surface, it is challenging for the wind to cause rolling, lifting and sliding since the incoming wind would have less access to an acting force (capillary force) and nearly no access to another acting force (Van de Waal force). This corroborates with Hee et al. (2012), where they demonstrated how an inward wind reduces accumulation on a facing coupon and more reduction in rainfall. Also, higher mass was recorded on coupons exposed during the dry season wet season, as shown in Figure 4.16.

Figure 4.11 shows wide gaps between potential PV output and output losses during peak hours in months with higher PV outputs (November, December, January, and February) and higher transmittance losses. The illustrated wider gaps or losses are directly related to the increase in solar irradiance, which does not penetrate the accumulated particles on the coupon. The months comes with high solar irradiance, less cloud and zero - less precipitation, but the soiling rate is higher, as shown in Figure 4.4. Therefore, accumulated dust would tend to have a higher impact on high solar irradiance since more obvious losses can easily be observed. When using a constant soiling rate, it would be observed that the transmittance losses tend to increase as the irradiance level increase.

The wind effect tends to have a more negligible effect on the accumulated particles on the horizontal surface than a tilted one (45°), resulting in more

accumulation. Vertically positioned coupons were observed to have less accumulation on all the setup. It is due to less exposure to the angle of attack of the wind flow. The airflow sometimes tends to contact the coupon at a right angle, causing a high increase in dust particle detachment. On a vertically positioned, the rain has no platform to settle as such washes of particles on the coupons. Figgis et al. (2019) stated that a high increase in dust particle detachment could be observed by fast near-wall flow (air or water). Tilted (45°) positioned coupons were observed to have moderate accumulation on all the setup due to the obtuse angle created and facing the wind that promotes high deposition and detachment of particles. It was observed that horizontally positioned coupons accumulated more dust compared to others. As earlier stated, it is due to gravitational effects. These coupons also retain more water on their surface after rain and, when they become dry, they tend to form strong cemented material on the surface. Cano et al. (2014) have confirmed this observation by stating that platform tilted at angles less than 15° retains a higher amount of water on their surface after rainfall. In addition, coupons are not exposed to maximum airflow; therefore, the wind tends to have a lesser detachment effect on particles, which can cause detachment of particles. Figgis et al. (2019) stated that airflow tends to have a more negligible effect on the coupon on the steeper tilting angle, reducing particles' detachment. It was observed that average monthly wind velocity at the experiment site tends to be greater than 4 m/s and Gholami et al. (2017) stated that wind velocity above 4 m/s could play a critical role in determining the accumulation rate on surfaces. Ilse et al. (2018) show that detachment could occur due to wind velocity of 10m/s through rolling, sliding, and lift-off, but the angular position of the surface was neglected, which could play a vital role. It is assumed that a significant amount of dust has been re-suspended due to direct contact with an inflow of high wind speed and particles/adhesion forces acting on them.

The gravitational force allows more dust to gravitate and settle on a horizontal and tilt platform (45°) compared to a vertical position platform. The particles mentioned and the air quality data presented above show large particles size, and the gravitational force tends to significantly influence particles with a wider diameter and higher mass. However, it is negligible when the particle's diameter

is small. Ilse et al. (2018) provided an illustration and simulation of how particles greater than 2.5 µm could be influenced to settle on a horizontal surface due to gravity.

According to Air Plume Labs (2020), the region's air quality index shows a significant concentration of PM_{10} in the atmosphere and appears to be the greatest. Similarly, many of the accumulated particles appear larger and have angular shapes with almost flattened tops. Air Plume Labs (2020) reported that the air quality index for February is the highest, indicating 194 AQI categorised as unhealthy and harmful to some sensitive groups. Main pollutant are categorised as $PM_{2.5}$ = 164AQI, PM_{10} = 194AQI, NO_2 = 14AQI, and O_3 = 32AQI while $PM_{2.5}$ = 96µg/m^3, PM_{10} = 231µg/m^3, NO_2 = 28µg/m^3 and O_3 =70µg/m^3. These figures clearly show the reason why high accumulation was recorded during the month. Based on the PM of the accumulated dust is assumed to have a high concentration of coarse sand and loamy soil from construction sites, agriculture and windblown dust. These kinds of particles tend to settle quickly on a flat surface rather than a tilted or vertical platform due to gravity acceleration influenced by their weight.

It was observed that coupons appear to have a non-uniformity pattern of deposition, and the disparity rate varies with angular positioning. It was observed that some homogenous pattern of accumulation tends to occur on vertically positioned coupons, but it was not 100% similar. These coupons have small accumulations, and the difference was hardly detected easily with bear eyes. The tilted (45°) and horizontally positioned coupons have areas on their surfaces with an aggregated pattern of accumulation and were observed on the coupons with higher accumulation (November, February, dry season and annual coupons). The horizontally positioned coupons for the annual and dry season show a multi-layered and sectional aggregated accumulation pattern.

The results obtained from this study was compared to other similar studies. Table 4.2 compares transmittance results with other studies (Hegazy, 2001; Elminir et al., 2006; Abdolzadeh and Nikkah, 2019) that have similar reductions. It also

shows that higher transmittance reduction was found on the horizontal position coupon, with a gradual increase in light transmittance as the tilt angle increases towards a vertical position, except for research presented by Gholami et al. (2017). The study shows that the highest transmittance reduction was recorded on the tilt angle, followed by horizontal and then vertical when coupons faced the opposite side of the dominant incoming wind direction.

Table 4.2: Comparison of transmittance results with published works.

Research	Location	Period of Exposure	Vertical	Tilt	Horizontal
Hegazy (2000)	Minia, Egypt	**30 days**	4%	40^0 = 12% 50^0 = 15%	27%
Elminir et al. (2006)	Cairo, Egypt	**7 Months** (Dec –Jun)	13%	45%	52.54%
Qasem et al. (2011)	Safat, Kuwait	**30 days**	0.21	1.00	1.98
Said and Walwil (2014)	Dhahran, Saudi Arabia	**45 days**	2%	7.5%	10.5%
Gholami et al. (2017)	Isfahan, Iran	**70 days** (May – Aug)	West = 24%	West = 24.7 %	West = 24.6%
Sisodia and Mathur (2019)	Jodhpur Rajasthan, India	**Annual**	24%	13%	31%
Abdolzadeh and Nikkhah (2019)	Kerman, Iran	**Monthly**	June = 8%	June = 11.5%	September = 15%
		Seasonal	Winter = 3.4% Spring = 4% Summer = 8% Autumn = 5.9%	Winter = 4.5% Spring = 6.5% Summer =11.5% Autumn = 10%	Winter = 5.2% Spring = 7% Summer =13.5% Autumn = 15%
This work	Abuja, Nigeria	**Monthly**	January = 10%	April = 15.5%	February = 38%
		Seasonal	Dry = 14% Wet = 15%	Dry = 24% Wet = 19%	Dry = 88% Wet = 57%
		Annual	32%	42%	59%

PV tilting position influences its power output reduction due to dust accumulation. The results above demonstrate reductions in PV power output in a location with high solar energy potential and atmospheric dust activity. The result also demonstrated how angular variation causes a disparity in PV output with the horizontal position, having the highest degradation rate followed by an optimum tilt angle, tilt angle (45°), and vertical angle the lowest. Other research (Elminir et al. 2006; Hachicha et al., 2019; Sisodia and Mathur, 2019; Abdolzadeh and Nikkah, 2019) highlighted in Table 4.3 confirmed that the tilt angle influence dust accumulation, which causes PV performance degradation.

Table 4.3: Comparison of PV performance reduction results with published works.

Research	Location	Period of Exposure	Vertical	Tilt	Horizontal
Elminir et al. (2006)	Cairo, Egypt	**7 Months** (Dec –Jun)	5 mW	20.5mW	35 mW
Hachicha et al. (2019)	Sharjah, United Arab Emirates	**6 Months**	N/A	10.95%	37.63%
Sisodia and Mathur (2019)	Jodhpur Rajasthan, India	**Annual**	16.5%	10.5%	23.8%
Abdolzadeh and Nikkhah (2019)	Kerman, Iran	**Monthly**	November = 6.7%	June = 10.9%	September = 12.6%
		Seasonal	Winter = 2.4% Spring = 3.2% Summer = 6.8% Autumn = 6.6%	Winter = 3.2% Spring = 4.6% Summer =9.6% Autumn = 9%	Winter = 3.8% Spring = 6% Summer =12.6% Autumn = 12.6%
This work	Abuja, Nigeria	**Monthly**	January = 10%	April = 15.5%	February = 38%
		Seasonal	Dry = 14% Wet = 15%	Dry = 24% Wet = 19%	Dry = 88% Wet = 57%
		Annual	32%	42%	59%

The weight of accumulated dust based on angular dependencies shows an increment with a change of angle from vertical towards the horizontal position. It is recorded that the weight of accumulated dust decreases as the tilt increase towards the vertical position. As presented in the result section, the increment of accumulated dust's weight is directly proportional to light transmittance reduction; as the weight increases, the light penetration reduces. The highest accumulated dust weight was recorded on a horizontally positioned coupon, while the lowest was recorded on a vertically positioned coupon. These results were validated considering other publications (Hegazy, 2000; Elminir et al., 2006; Said and Walwil, 2014; Gholami et al., 2017; Abdolzadeh and Nikkah 2019) highlighted in Table 4.4.

Table 4.4: Comparison of the weight of accumulated dust obtained with other published works.

Research	Location	Period of Exposure	Vertical	Tilt	Horizontal
Hegazy (2000)	Minia, Egypt	**30 days**	0.5 g/m^2	2.45 g/m^2	7 g/m^2
Elminir et al. (2006)	Cairo, Egypt	**7 Months** (Dec –Jun)	5 g/m^2	14 g/m2	15.84 g/m2
Said and Walwil (2014)	Dhahran, Saudi Arabia	**45 days**	0.8 g/m^2	4.5 g/m^2	6.5 g/m^2
Gholami et al. (2017)	Isfahan, Iran	**70 days** (May – Aug)	5 g/m^2	5.5 g/m^2	5.2 - 6 g/m^2
Abdolzadeh and Nikkhah (2019)	Kerman, Iran	**Monthly**	2.2 g/m^2 – June	2.7 g/m^2 - September	4 g/m^2 - September
		Seasonal	2.2 g/m^2 – Summer	2.7 g/m^2 - Autumn	4 g/m^2 - Autumn
This work	Abuja, Nigeria	**Monthly**	Jan – 1.4 g/m^2	Apr – 2.16g/m^2	Feb - 4.16 g/m^2
		Seasonal	Dry – 1.88 g/m^2 Wet – 1.76 g/m^2	Dry – 2.44 g/m^2 Wet – 2.2 g/m^2	Dry – 12.56 g/m^2 Wet – 3.4 g/m^2
		Annual	3.24 g/m^2	3.84 g/m^2	8.52 g/m^2

Table 4.2 shows an increase of optical losses with an angular increase towards the horizontal plane. However, these findings demonstrate the potential superiority of considering additional variables (three exposure periods) over established methods. Furthermore, this approach employs low-cost techniques to provide findings compatible with those obtained from standard techniques. Optical losses findings reported by Elminir et al. (2006) and Hegazy (2020) are relatively similar to the result obtained with Hegazy providing monthly results comparable with this finding and Elminir et al. (2006) providing seven months results comparable with annual results and some seasonal results considering angular positioning. These studies were conducted around the region that is the closest to the site of this research. The increment of optical losses and power degradation related to angular variation is comparable to findings from literature in Table 4.2 and Table 4.3. Similarly, an increase in dust density relative to angular positioning is comparable to findings from literature in Table 4.4.

Vertically positioned coupons were observed to have less accumulation on all the setup. This is due to less exposure to the angle of attack of the wind flow. The airflow tends to contact the coupon at a right angle, causing a high increase in dust particle detachment. On a vertically positioned, the rain has no platform to settle as such washes of particles on the coupons. Figgis et al. (2019) stated that a high increase in dust particle detachment could be observed by fast near-wall flow (air or water). Tilted (45°) positioned coupons were observed to have moderate accumulation on all the setup due to the obtuse angle created and

facing the wind that promotes high deposition and detachment of particles. It was observed that horizontally positioned coupons accumulated more dust compared to others. As earlier stated, it is due to gravitational effects. These coupons also retain more water on their surface after rain and, when they become dry, they tend to form a strong cemented material on the surface. Cano et al. (2014) have confirmed this observation by stating that platform tilted at angles less than 15° retains a higher amount of water on their surface after rainfall. Also, coupons are not exposed to maximum airflow; therefore, the wind tends to have a lesser detachment effect on particles, which can cause detachment of particles. Figgis et al. (2019) stated that airflow tends to have a more negligible effect on the coupon on the steeper tilting angle, reducing particles detachment.

Evidently, the results obtained show a substantial reduction of transmittance due to dust accumulation when coupons were exposed to Abuja's outdoor condition. The dust accumulation rate on a surface is related to coupon positioning (Tilt angle) with the highest dust density at horizontal and gradually decreases as the angle is tilted towards the vertical position. However, although findings show that the angular orientation has a significant influence on dust accumulation rate, there are other parameters such as weather condition (wind speed and direction, humidity and temperature), particles, PV covering materials (such as acrylic plastic and low iron glass), location, and period of exposure. These parameters could significantly influence deposition and accumulation, and some might be more sensitive than angular orientation. Whichever tilt angle the PV devices are being installed on, the technology cannot be left unattended. Considering the result obtained and other published research works in Table 4.2, Table 4.3, and Table 4.4. It is confirmed that tilt angle is an influencing factor for dust accumulation in Abuja and every location around the world, which requires continuous maintenance even during the wet season when a certain level of cleaning is naturally provided by precipitation. Since results highlight periods of high soiling in Abuja, the information could predict soiling activities in the region and provide guidance for maintenance where the optimal timing for mitigating dust on PV can be performed. Chanchangi et al. (2020a) provide some mitigating

soiling methods, which could be used to prevent or restore the PV performance capacity.

4.6 Summary and conclusion

To sum up this section, it has been demonstrated that the tilt angle of PV installation plays a vital role in influencing dust accumulation in Abuja (capital of Nigeria; 9.06° N, 7.46° E), as it has been previously reported in other locations by researchers. The findings show that the horizontal position could cause dust accumulation leading to transmission reduction from 5% to 38% for one month, 45° tilted position is from 3% to 17%, while the vertical position from 1% to 10%. The seasonal results indicate an 88% transmission reduction for a coupon exposed on a horizontal plane during the dry season and 37% during the wet season. For the 45° tilt position, 4% was recorded during the dry season and 19% for the wet season, while the vertical position is 14% for the dry season and 15% for the wet season. The annual results indicate a similar dust accumulation trend showing transmission reduction of about 59%, 42%, and 34% for horizontal, tilt (45°) and vertical position, respectively. The results illustrated how the PV tilt angle influences dust accumulation density, with higher mass recorded on coupon exposed to extreme conditions on horizontal position than tilt (45°) and vertical. In conclusion, the soiling rate is attributed to PV surface positioning (tilt angle) with the horizontal position accumulating more, and the density slowly decreases as the angle becomes inclined towards the vertical direction and it is even more significant when the PV is not facing an inward bound wind or during a calm period with low wind velocity. However, other parameters such as weather condition, particles characteristics, PV covering materials, location, and exposure period could significantly influence the accumulation, and some might be more sensitive than angular orientation

5 Chapter Five - Impact of soiling on PV performance influenced by weather parameters in Northern Nigeria

5.1 Introduction

Some weather parameters such as wind, rain, temperature, and humidity are considered omnipresent factors which significantly influence dust accumulation on PV surfaces, as provided in the previous section of the thesis (Chanchangi et al., 2020). These variables influence soiling interdependently and synergistically affect the system; therefore, to predict PV soiling in a region, there is a need to consider and investigate all.

The Nigerian government has invested vast amounts of money to commission two solar farms (1 MW and 7.1 MW) (Nigeria Electricity Hub, 2018 and Energy Storage News, 2019) sited in the Northern Nigerian city Kano based on the immense potential of solar irradiance in the region throughout the year. However, significant discrepancies between actual and predicted regional soiling have been observed (Ghazi and IP, 2014). Javed et al. (2017) recommended that it is essential to understand the cause of PV performance degradation due to soiling as a function of certain input variables. Therefore, it is imperative to investigate the soiling losses of a region with millions of pounds in investment in PV installation and recommend the appropriate mitigation technique that would sustain it and show the prospective investor its potential in the sector.

This section of the thesis investigates the effect of dust accumulation on the performance of four PV types in a region with high solar energy potential, a wide gap between energy supply and demand, incoming massive PV investment. Module performances were initially determined under STC (standard test condition) and exposed to external conditions in a region with a high atmospheric dust pollution rate. The site's meteorological parameters were collected to allow a detailed analysis of how various conditions influence dust accumulates on the PV surface, impacting its performance.

Furthermore, glass coupons were also exposed, considering the time variation to determine the accumulation rate and identify particle morphology. This thesis

chapter investigated the level of soiling effect in the region, considering time variation and identifying when most performance losses are encountered so that a periodic frequency for a suitable, cost-effective cleaning technique would be determined. It provides valuable first-hand information that could stimulate research on the PV soiling community and scientists. The results would provide data that could be used to estimate periods when soiling is causing PV performance and efficiency decrease in the region, and the data could be used to determine the type and frequency of mitigation required. The findings would entice prospective stakeholders and governments in other regions to be comfortable investing in the sector, knowing full well that investment would last longer and yield profits.

5.2 Method

This subsection provides detailed step-by-step procedures for data collection subdivided into three categories: characterisation of optical losses variation, dust density, accumulated particle, indoor, outdoor initial, monthly PV yield, and weather parameters. A flowchart illustrating the various steps through the research methodology of this subsection of the thesis is provided in Appendix B – Figure 0.5.

5.2.1 Site

The old site of Bayero University Kano is the home of the first 1 MW solar farm in Kano state, Northern Nigeria (11°59'02.1"N, 8°28'52.5"E) is the business capital of Northern Nigeria, and it is the most populated city in the region with a population of about 3,999,000 in 2020 (Macrotrends, 2020). Kano was carefully selected for this research since it has high solar potential (GSA, 2020), very high AQI (air quality index) (Air plum lab, 2021) and is the only location with an institution having a working MW solar farm (with the capacity of 1 MW) in the region at the beginning of the study. GSA (2020) provided the following data: direct normal irradiation (DNI) is estimated to be about 1518 kWh/m^2, global horizontal irradiation (GHI) is about 2126 kWh/m^2, diffuse horizontal irradiation (DHI) is about 1005 kWh/m, and the global tilted irradiation at an optimum angle (GHI_{opta}) is about 2188 kWh/m^2. The terrain elevation is about 489 m with a 12° optimum angle, and 180° surface orientation was obtained from Waziri and Usman (2014) and Abdullahi et al. (2019). Figure 5.1 present's horizon and sun

path generated using PVSyst software and was further modified to highlight the sunrise and sunset for various months in the region.

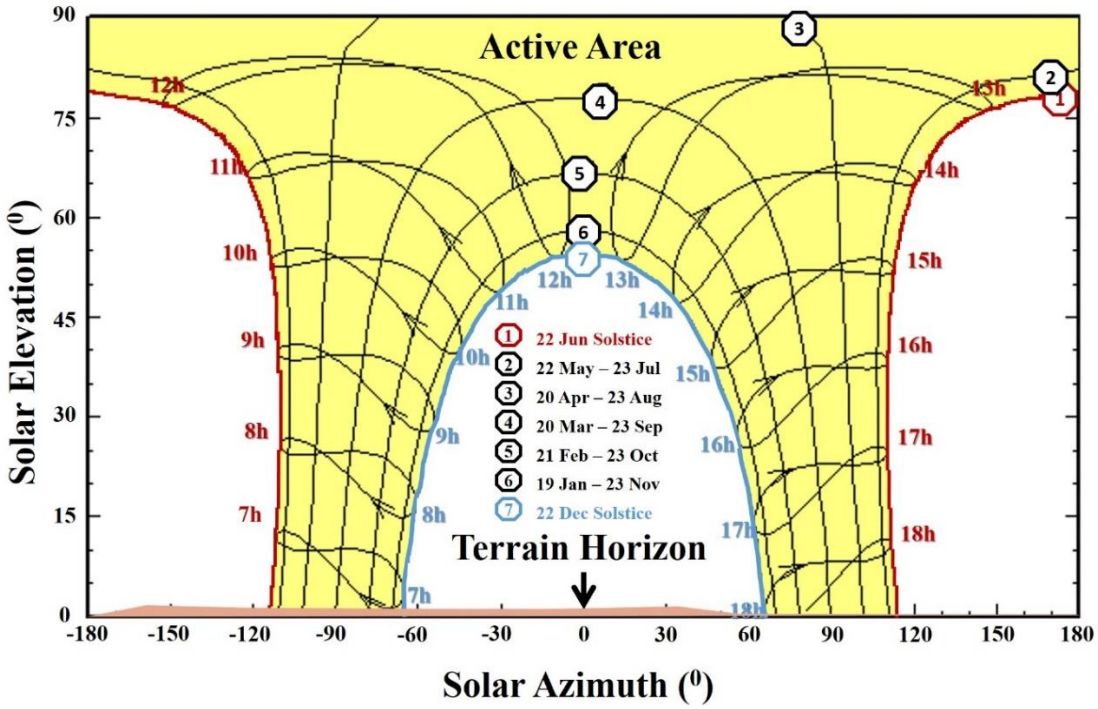

Figure 5.1: Sun path and Horizon line with an elaborated sketch highlighting sun availability in Kano, Nigeria (11°59'02.1"N, 8°28'52.5"E).

5.2.2 PV types

Monocrystalline Silicon, polycrystalline Silicon, Cadmium Telluride, and amorphous Silicon were the four different PV modules employed for the experiment. Ratings of each module are shown in

Table 5.1 below. The modules vary in size. The a-Si (amorphous Silicon) module has the most expansive active area with 1300 mm x 1100 mm and the highest rating, followed by the CdTe (Cadmium Telluride), about 1200 mm x 600 mm. However, monocrystalline (mc-Si) and polycrystalline (pc-Si) Si modules have the same dimension of 1030 mm x 700 mm with about the same rating. The result from the initial laboratory PV performance measurement was recorded using the PASAN software. It was analysed with Microsoft Excel to plot the graph in Figure 5.3 to establish a baseline for all the PV modules' optimum performance at various irradiance levels.

In addition, the performance of a 1 MW solar farm at the same site of the experiment, developed using 3080 pc-Si modules, with each having P_{max} (maximum of power) of about 325 W, was investigated. The set-up has been configured in parallel mode with 20 modules making a string, 11 strings going to an inverter, 14 inverters making the total output. A single module's characteristics are V_{mpp} (voltage at maximum power point) is 37.6 V, I_{mpp} (current at maximum power point) is 8.66 A, V_{OC} (open-circuit voltage) is 46.7 V and I_{SC} (short circuit current) is 9.10 A. Performance data from the solar was used to illustrates the possible impact of soiling in the region.

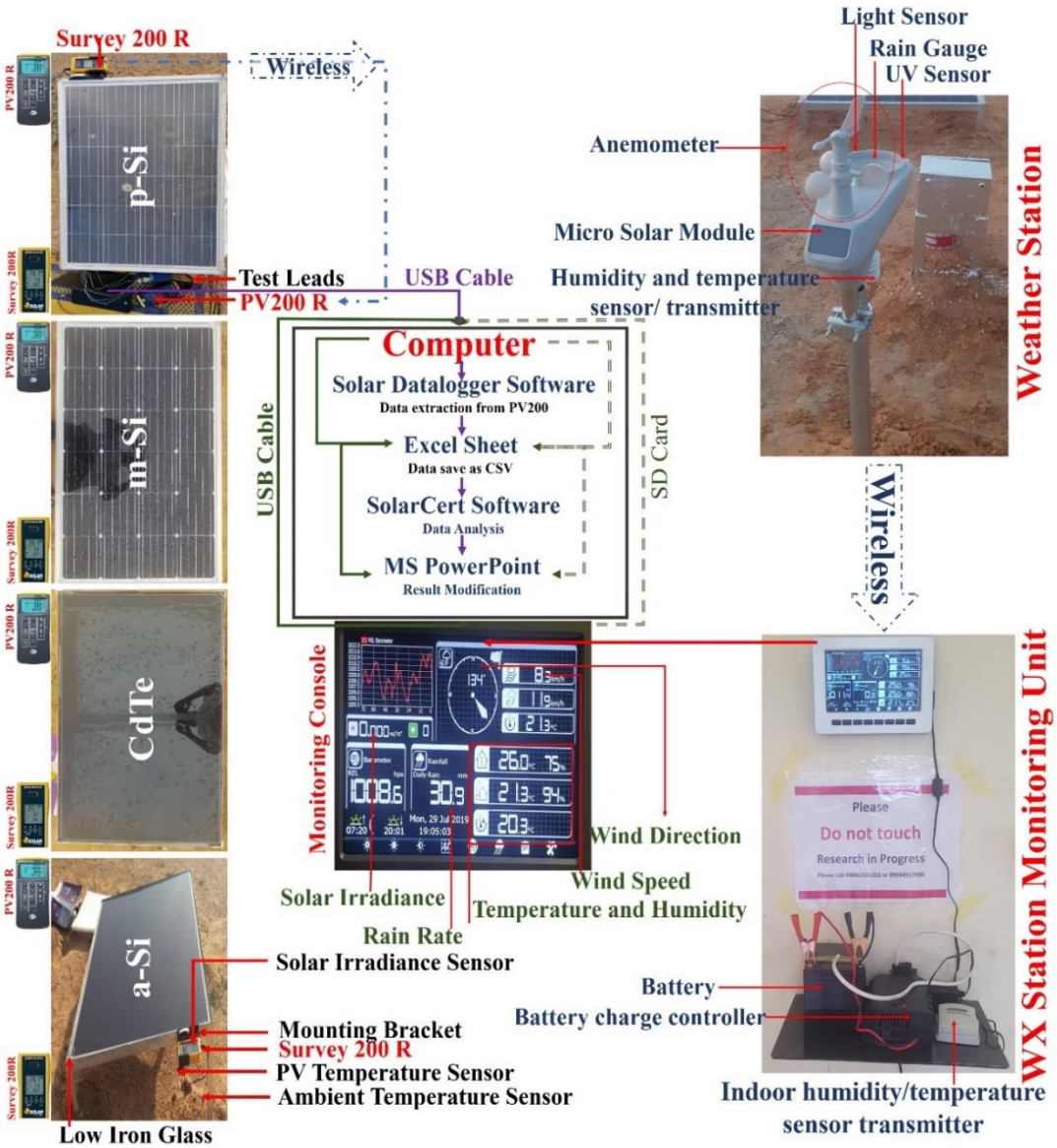

Figure 5.2: Schematic illustration of all exposed modules, PV200 and Survey R, and weather station installation with its various components, including data collection/analysis procedure.

5.2.3 PV yield measurement

5.2.3.1 Initial laboratory PV yield measurement

The PV modules were subjected to initial measurement using a PASAN flash Solar Simulator (A+A+A+) at the University of Exeter solar laboratory, where the series of the mask were deployed to reduce the intensity of the irradiance level from 1000 W/m^2 to various levels (700 W/m^2, 500 W/m^2, 400 W/m^2, 300 W/m^2, 200 W/m^2, and 100 W/m^2). The inputs are determined using equations that estimate the maximum slope that the device could tolerate under test since the simulator uses split flash. The following equations were used to determine the input values for the PASAN PV module and cell measurement software:

The start voltage was determined by employing a negative value for direct mode measurement. The usual typical value used is either (- 3 V) or (- 4 V), and the positive value of a reverse mode measurement is applied to determine it using Equation (5.1) below, where $V_{OC\ is}$ the open-circuit voltage.

$$\text{Positive Start voltage} = \text{Voc1} + 20\ \%. \tag{5.1}$$

For the end voltage, the positive start voltage is employed as direct mode measurement and Equation (5.1) is negative for the reverse mode measurement.

The maximum positive current (A) is determined using Equation (5.2) below, and the maximum negative current is the corresponding minimum negative current value of the device under testing, where I_{SC} is the short circuit current.

$$\text{Maximum positive current (A)} = \text{Isc} + 5\% \tag{5.2}$$

The V_{OC} series resistance regression starts current of the PV module (A) is the first point of linear regression on the current and voltage graph (IV curve), and the value is determined by Equation (5.3), where the I_{mpp} is the current at maximum power.

$$= \text{Impp2}\ /3. \tag{5.3}$$

The V_{OC} series resistance regression end current of the module is the last point of the linear regression on the current and voltage graph (IV curve) which is typically = 0

I_{SC} series resistance regression starts voltage of the module is the first point of linear regression on the current and voltage graph (IV curve) determined by Equation (5.4), and I_{SC} series resistance regression end voltage is the last point of linear regression on a graph which is = 0.

$$= \mathrm{Vmpp3}\ /2. \tag{5.4}$$

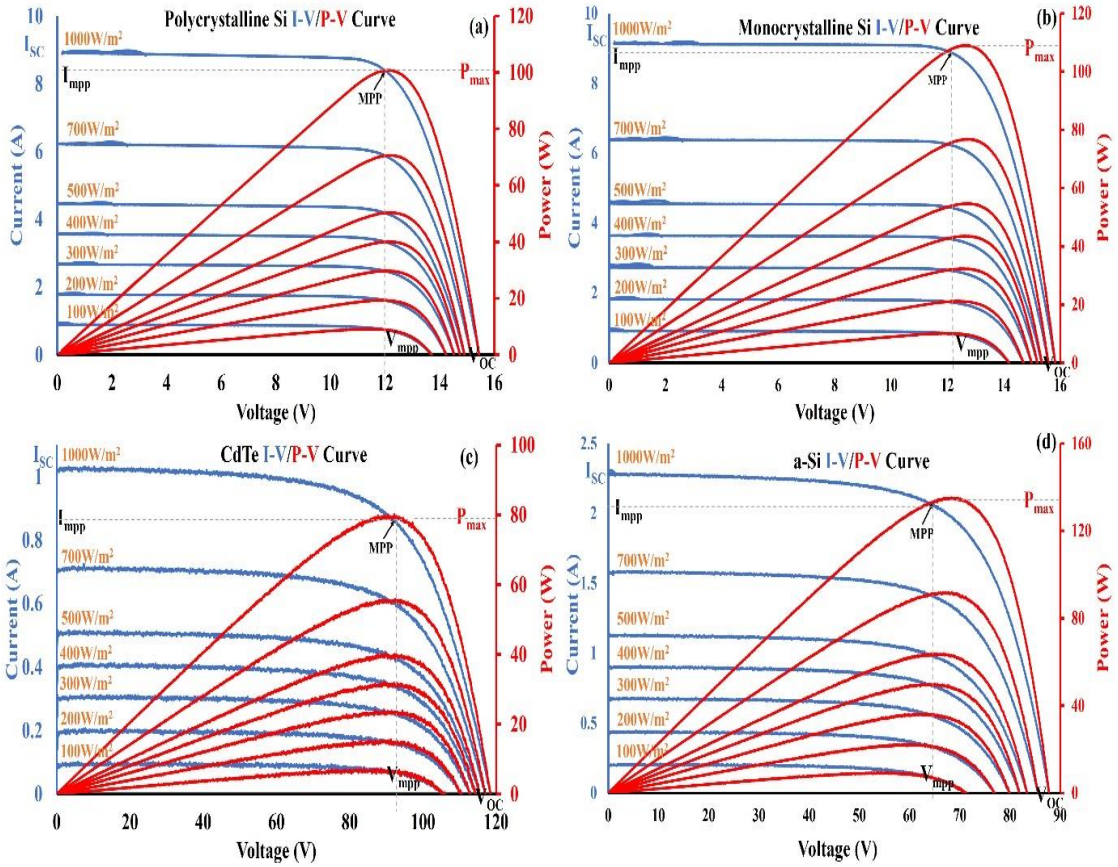

Figure 5.3: IV and PV characteristics showing the optimal capacity of (a) pc-Si module, (b) mc-Si, (c) CdTe, and (d) a-Si at various irradiance levels under standard conditions.

All the results obtained from the initial measurement are presented below in Figure 5.3 and

Table 5.1. These values allow establishing the module's maximum capacity at an absolute irradiance under standard conditions, which would help identify the soiling losses caused due to outdoor exposure.

Table 5.1: Summary of maximum output characteristics of all the PV modules under standard test conditions.

Parameter	**Value**			
PV Type	**pc-Si**	**mc-Si**	**CdTe**	**a-Si**
Pmax	100.7 W	108.97 W	79.431 W	135.85 W
I_{sc}	8.95 A	9.2 A	1.02 A	2.28 A
V_{oc}	15.459 V	15.84 V	118.3 V	88 V
I_{mpp}	8.32 A	8.626 A	0.88 A	1.98 A
V_{mpp}	12.109 V	12.626 V	90.459 V	68.747 V
η	14.3%	16%	11%	9.4%
Active Area	1030 x 700 mm	1030 x 700 mm	1200 x 600 mm	1300 x 1100 mm
Test Condition	1000 W/m^2, AM 1.5, T = 25°C			

5.2.3.2 On-site initial PV yield measurement

The initial in-situ measurement was conducted by employing the PV200 and Survey 200R. These are handheld IV (current and voltage) tracing devices used in PV installation and PV yield performance measurement developed by Seaward. The PV200 measure V_{OC} and I_{SC}, I_{mpp}, V_{mpp}, and fill factor (FF). While the Survey 200R measures the real-time irradiance, PV temperature, ambient temperature and could be used to determine the optimum tilt angle and surface orientation. The two devices communicate with each other using a wireless signal, where data on the Survey 200R are transmitted and stored in the PV200, which could be downloaded by connecting a USB cable to a computer device or using NFC (Near-Field-Communication) to a mobile device. The device was employed to conduct an hourly measurement from sunrise to sunset, highlighting the PV modules' outputs at various times of the day considering irradiance. The measurement was conducted on 27 July 2019 at the solar farm old site campus

of Bayero University Kano, Nigeria. The results of this measurement are presented in the results section.

5.2.3.2.1 Monthly PV yield

The monthly PV yield measurement was conducted using the PV200 and Survey 200R, where every week, the PV systems are measured and sometimes measured twice a week. The data obtained were analysed using the SolarCert software and measurement where the highest irradiance was selected for each month, and the results were presented, showing an IV curve for various months. This is because modules were cleaned after the first five months to start an annual reading from January 2020 to January 2021. Soiling affects the I_{SC} since accumulated particles could block the absorption of photons. The measured I_{SC} recorded on all the modules was converted to I_{SC} under the STC (standard test conditions) and presented in the subsequent section. The conversion was achieved by employing the SolarCert software when optimum module performance parameters under standard conditions are provided.

Optimal performance values were automatically generated during the initial state as earlier presented. The outdoor real-time performance measurement was recorded weekly, aggregated and presented as a monthly outdoor measurement. The efficiency was determined using Equations (5.5) and (5.6) provided by Kalogirou (2014), Hachicha et al. (2019) and Mekhilef et al. (2012). Gupta et al. (2019) stated that PV system efficiency significantly depends on solar radiation getting to solar cells. Therefore, it is imperative to determine PV efficiency losses using the parameters recorded during a series of experiments. I_{SC}, V_{OC}, FF, I_{max}, V_{max}, and P_{max} were recorded during all the relevant experiments.

$$\eta_{max} = \frac{P_{max}}{P_{in}} = \frac{I_{mpp}V_{mpp}}{AG_t} \tag{5.5}$$

Or

$$\eta = \frac{P_{max}}{A \times G} \times 100\% \tag{5.6}$$

where I_{mpp} represents the current at the maximum power point depending on the I-V tracer, V_{mpp} is the voltage at the maximum power point, A is the active area of

the PV module, and G is the incident solar irradiance. Then Equation (5.7) was employed to determine the outdoor efficiency losses.

$$\Delta\eta = \frac{\eta_{Clean\ PV} - \eta_{Soiled\ PV}}{\eta_{Clean\ PV}} \times 100\% \quad (5.7)$$

Furthermore, the performance ratio was determined using Equation (5.8) provided by Hachicha et al. (2019) and Mekhilef et al. (2012), where P_{rated} is the power output under STC, E is the actual incident radiance, and G is the irradiance used under STC (1000 W/m^2).

$$PR = \frac{P_{max}/P_{rated}}{E/G} \quad (5.8)$$

5.2.4 Optical losses

Fifteen pieces of 50 mm x 50 mm x 4 mm low iron glass coupons were deployed to obtain monthly, seasonal (dry and wet) and annual optical losses from the experimental site. The monthly coupons were exposed on the first day of the month and removed/replaced on the first day of the following month. The seasonal coupons were exposed at the beginning of the season and removed/replaced towards the end of the season when weather conditions changed for more than two weeks. The annual coupon was exposed on the first day of installation and removed on the final day when the monthly coupon was removed. The coupons were exposed by the edge of the modules. All coupons were returned (packaging and transportation methods are provided in subsection 4.3 of this thesis) to the solar laboratory at the University of Exeter at the expiration of their exposure period and subject to optical transmittance measurement by employing Perkin Elmer Lambda 1050 UV/VIS/NIR spectrophotometer. A clean, low iron glass coupon was initially subjected to this measurement, followed by the exposed coupons. This is to re-establish the optimal light transmittance level of a low iron glass and to be able to determine the percentage optical losses of the soiled coupons that were exposed. Since the various PV modules exposed response in various wavelength ranges, a coupon was subjected to measurement from 200 nm to 1200 nm to accommodate UV (ultraviolet), VIS (Visible), and NIR (Near Infra-Red) transmittance. Data were analysed using PerkinElmer UV WinLab software and the UV WinLab data

processor and viewer, then further saved in an excel worksheet. Equation (5.9) below was used to validate the data obtained from optical scanning, where T (λ) is the spectral transmission, Δλ is the change in wavelength and S (λ) is the relative spectral distribution of solar radiation.

$$\boldsymbol{\tau_{solar}} = \frac{\sum_{\lambda=200nm}^{1200nm} \boldsymbol{S(\lambda)T(\lambda)\Delta\lambda}}{\sum_{\lambda=200nm}^{1200nm} \boldsymbol{S(\lambda)\Delta\lambda}} \quad (5.9)$$

Furthermore, the degradation of coupons was calculated using Equation (5.10), where Δ is the change, τ_x is transmittance data of a coupon positioned at an angle relative to a horizontal surface, τ_{clean} is the transmittance data of a clean coupon.

A percentage difference was obtained by comparing the optical data of each soiled coupon and a clean coupon. These values are used as the estimated possible soiling occurring for each month in the studies' site. A transmittance graph against wavelength presents the results in the subsequent section.

$$\Delta\tau_x = \frac{(\tau_{clean} - \tau_x)}{\tau_{clean}}(\%) \quad (5.10)$$

5.2.5 Mass of accumulated dust

The soiled coupons were weighed to determine the Mass of accumulated dust using the Mettler Toledo ME204 sensitive scale. The exposed coupons were initially weighed, and the record was documented; then, every coupon was washed with liquid soap and hot water, dipped into a beaker filled with acetone and dried with a hand dryer and weighed again. The transmittance of each coupon was rechecked after the second measurement to ensure particles were removed entirely. The values of the Mass obtained during the first and the second weighing were used in determining the weight of accumulated dust on every coupon using Equation (5.11), where ρ_d is the deposited dust density, $\rho A \rho d C$ is the area density of a soiled coupon, ρAC is the area density of a coupon after cleaning (clean coupon), and 10^6 is the conversion factor g/mm^2 to g/m^2 since the coupon area is 50 x 50 mm.

$$\rho_d(g/m^2) = \rho A \rho d C_{(g/mm^2)} \times 10^6 - \rho A_{(g/mm^2)} \times 10^6 \quad (5.11)$$

5.2.6 Particle characterisation

Particle characterisation was conducted on a soiled coupon, where the coupon was initially carbon coated by employing Emi-Tech K950 carbon coating machine to ensure that a fine conductive metal layer is placed on the samples. This layer inhibits charges, improves the required signal of secondary electrons, and reduces any possible thermal damage; overall, it usually enhances the sample imaging. The coupon is then subjected to the imaging scan using SEM (Scanning Electronic Microscope) Quantal FEG 650 equipped with an EDX (Energy Dispersive X-ray). The EDX graphs provided elements that make a mineral, and the data were analysed using online databases (webmineral.com, mindat.org and minerals.net) to identify the type of minerals and their characteristics. This study focused and investigated only the diaphaneity of the identified elements as its main characteristic that could influence light transmittance.

5.2.6.1 Site AQI

The air quality index of the experiment site was obtained from the Air Plum lab and employed to validate the monthly and seasonal optical losses recorded on the coupons, the dust accumulation on the PV surfaces and the minerals observed during the SEM/EDX analysis. Tanesab et al. (2017) demonstrated that the concentration of airborne particulate matter and weather conditions are directly related to dust deposition, adhesion, and its removal process. Table 5.2 below illustrates the primary pollutant and their concentrations in Kano, Nigeria, considering seasonal variation.

Table 5.2: Seasonal variation of the maximum rate of airborne pollutant in Kano.

Main Pollutants	AQI		µg/m³	
	Dry Season	Wet Season	Dry Season	Wet Season
PM2.5	251	17	201	9
PM10	251	19	321	18
NO2	27	4	49	8
O3	5	17	13	43

5.2.7 Weather data collection

Mekhilef et al. (2012) stated that wind velocity, humidity, and dust operate together to influence soiling, and none of them should ever be missed or isolated when investigating dust accumulation on PV. Therefore, a Maplin professional weather station was installed at the experiment site with the capacity to record temperature, humidity, wind speed and direction, pressure, rain, solar radiation, and UV. The weather station is installed beside the PV modules and communicates using the wireless signal at a frequency of 433 MHz to the monitoring console, installed in a room that is about 50m away. The display console is powered by a battery, installed with charge control, and the energy comes from the grid source; this method was used due to security advice for the safekeeping of the monitoring console. Figure 5.2 shows the weather station installation and the monitoring console set-up.

The weather station provided a large amount of data, but for this research, the main weather variables required were temperature, humidity, wind speed and direction, rain and solar radiation. Monthly averages of these data were illustrated in Figure 5.4 for analysis of weather influence on dust accumulation on PV modules. As mentioned in the literature review, weather conditions such as wind and rain were reported to influence dust accumulation negatively and are further discussed in the subsequent section.

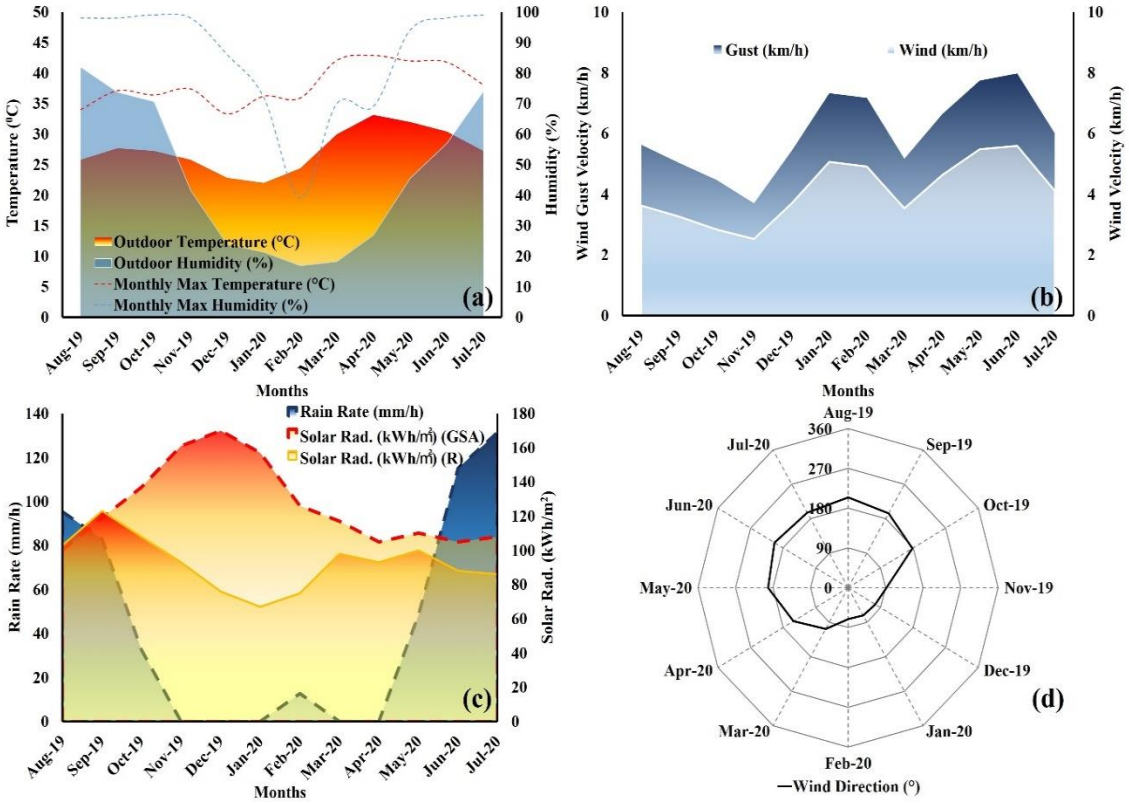

Figure 5.4: Critical measured weather parameters illustrating average monthly variation from August 2019 to July 2020 (a) temperature and humidity, (b) wind velocity, (c) rain rate and solar irradiance (comparing DNI obtained from GSA and on-site measured DNI), and (d) wind direction.

5.3 Results

5.3.1 PV output performance

This section presents the experimental results of the various research assessments of PV performance from the initial on-site test for the monthly measurement during outdoor exposure. The optical loss results are illustrated to validate the PV performance reduction and further highlight the mass of accumulated dust on each coupon. It further outlines the mineral particle deposited on the coupon during the exposure. The results are depicted in diagrams (Figure 5.6, Figure 5.7, Figure 5.8, and Figure 5.9) and tables (Table 5.3, Table 5.4, Table 5.5, and Table 5.6) below, highlighting some significant outcomes.

5.3.2 Initial on-site measurement

The initial on-site measurement is to re-establish the performance of the modules after transportation. It is to find out if the device has any invisible issues such as

cracks. The measurement results in Figure 5.5 show that I_{SC} at different irradiance are good, and the solar cells respond accordingly compared to the laboratory measurement shown in Figure 5.3. However, the V_{OC} results recorded slightly decreased values due to the higher temperature being more significant than the 25° used for standard condition testing. The pc-Si module yielded the expected output shows an FF (fill factor) of about 74 at sunrise. However, it produced the maximum output at 1300 (LT) when the irradiance is about 931 W/m^2, and the temperature is about 32°C, where P_{max} is about 74 W, I_{SC} is 8.19 A, I_{mpp} is 7.55, V_{OC} is 13.8 V, and V_{mpp} is 9.8 V. The lowest output recorded on the device was at 1800 (LT) when the irradiance is reading about 0 W/m^2, and ambient temperature is about 30.5°C, where Pmax is about 2 W, I_{SC} is 0.28 A, I_{mpp} is 0.21, V_{OC} is 12.3 V, and V_{mpp} is 10.3 V.

The mc-Si module yielded standard output, which shows an FF of about 78 at sunrise. However, it produced the maximum output at 1300 (LT) when the irradiance is about 937 W/m^{2,} and the temperature is about 32°C, where P_{max} is about 88 W, I_{SC} is 8.71 A, I_{mpp} is 8.22, V_{OC} is 14.2 V, and V_{mpp} is 10.8 V. The lowest output recorded on the device was at 1800 (LT) when the irradiance is reading about 0 W/m^{2,} and ambient temperature is about 30.5°C, where Pmax is about 2 W, I_{SC} is 0.27 A, I_{mpp} is 0.21, V_{OC} is 12.9 V, and V_{mpp} is 11.3 V.

The CdTe module yielded anticipated output, which shows an FF of about 69 at sunrise. However, it produced the maximum output at 1300 (LT) when the irradiance is about 923W/m^{2,} and the temperature is about 32°C, where P_{max} is about 65W, I_{SC} is 1.02 (A), I_{mpp} is 0.83, V_{OC} is 100.5 (V), and V_{mpp} is 77.4 (V). The lowest output recorded on the device was at 1800 (LT) when the irradiance is reading 0W/m^2 and ambient temperature is about 30.5°C, where Pmax is about 2W, I_{SC} is 0.33 (A), I_{mpp} is 0.03, V_{OC} is 86.8 (V), and V_{mpp} is 70.7 (V).

The a-Si module yielded the expected output at shows an FF of about 68 at sunrise. However, it produced the most excellent output at 1300 (LT) when the irradiance is about 969 W/m^{2,} and the temperature is about 32°C, where P_{max} is about 131 W, I_{SC} is 2.40 A, I_{mpp} is 2.08, V_{OC} is 82.0 V, and V_{mpp} 63.2 V. The lowest output recorded on the device was at 1800 (LT) when the irradiance is reading

0W/m^2 and ambient temperature is about 30.5°C, where P_{max} is about 2 W, I_{SC} is 0.05 A, I_{mpp} is 0.04, V_{OC} is 86.5 V, and V_{mpp} is 50.9 V.

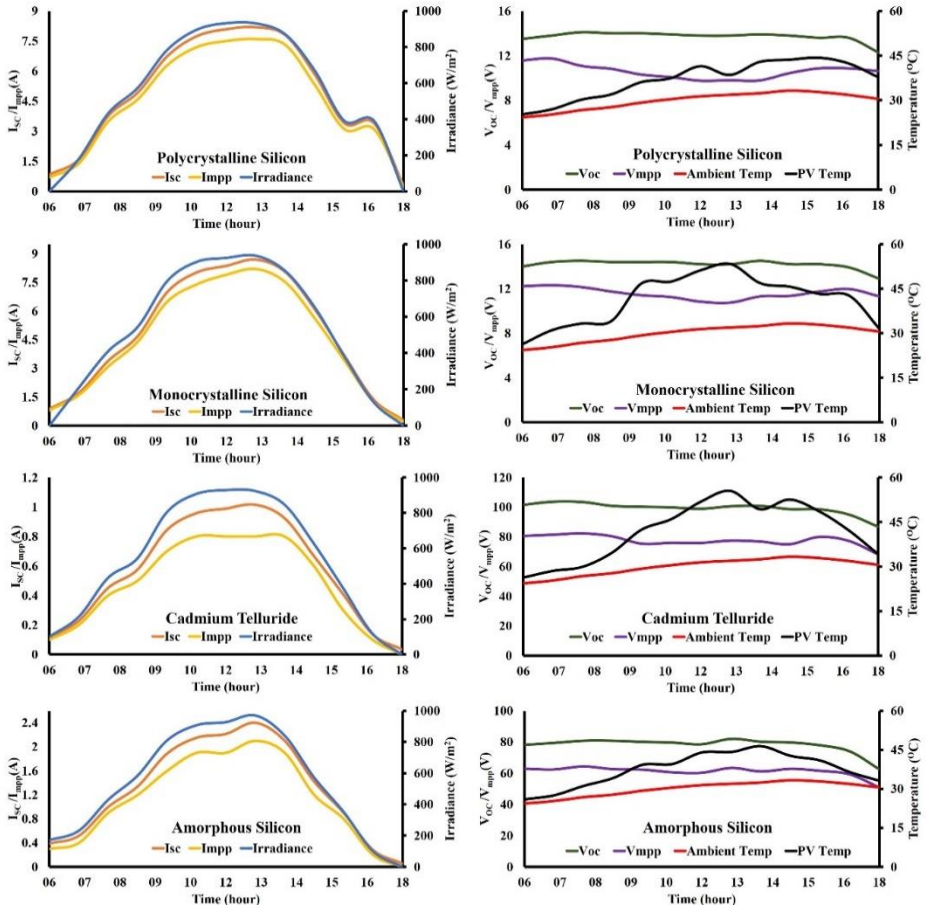

Figure 5.5: Hourly variation of PV performance for the four exposed modules.

5.3.2.1 Monthly measurement

The monthly PV output result demonstrates several factors influencing the performance of the devices. However, this research is focused on the effect of soiling on PV performance. The findings show how PV performance degraded within a short time after installation. PV output performances are presented in the diagrams below, where measured IV curves and IV curves converted to the standard conditions are illustrated. Figure 5.6 shows that the pc-Si module's performance was very high at the beginning of exposure (August-2019). The measured P_{mpp} output value at 1,250 W/m^2 is about 102 W. The P_{mpp} value is generated under standard conditions (83 W) and compared with the nominal value where the output shows a difference of about 17.5%, as shown in Figure 5.6. The same illustration shows a difference between the measured $I_{SC,}$ which is 10.78 A, the STC I_{SC} is 8.73 A and the NOM I_{SC}, which is 8.95 A. Similarly, it

shows the difference between the measured $I_{mpp,}$ 9.87 A, STC I_{mpp}, 8.06 A and NOM I_{mpp}, 8.32 A. The most significant degradation is recorded in January 2021, where the measured P_{mpp} value at 871 W/m^2 is about 26 W. The P_{mpp} value is generated under standard conditions (30 W) and compared with the nominal value (101 W) obtained during the indoor measurement, where the output shows a variance of about 70.2%, as demonstrated in Figure 5.11(a). The lowest degradation was recorded in December 2019 when the module was clean to start a one-year reading without cleaning. Hence this is not assumed to be the lowest degradation. The lowest degradation is recorded in January 2020, where the measured P_{mpp} value at 853 W/m^2 is about 72 W. The P_{mpp} value is generated under standard conditions (85 W) and compared with the nominal value obtained during the indoor measurement, where the output shows a discrepancy of about 15.8%, as illustrated in Figure 5.11(a).

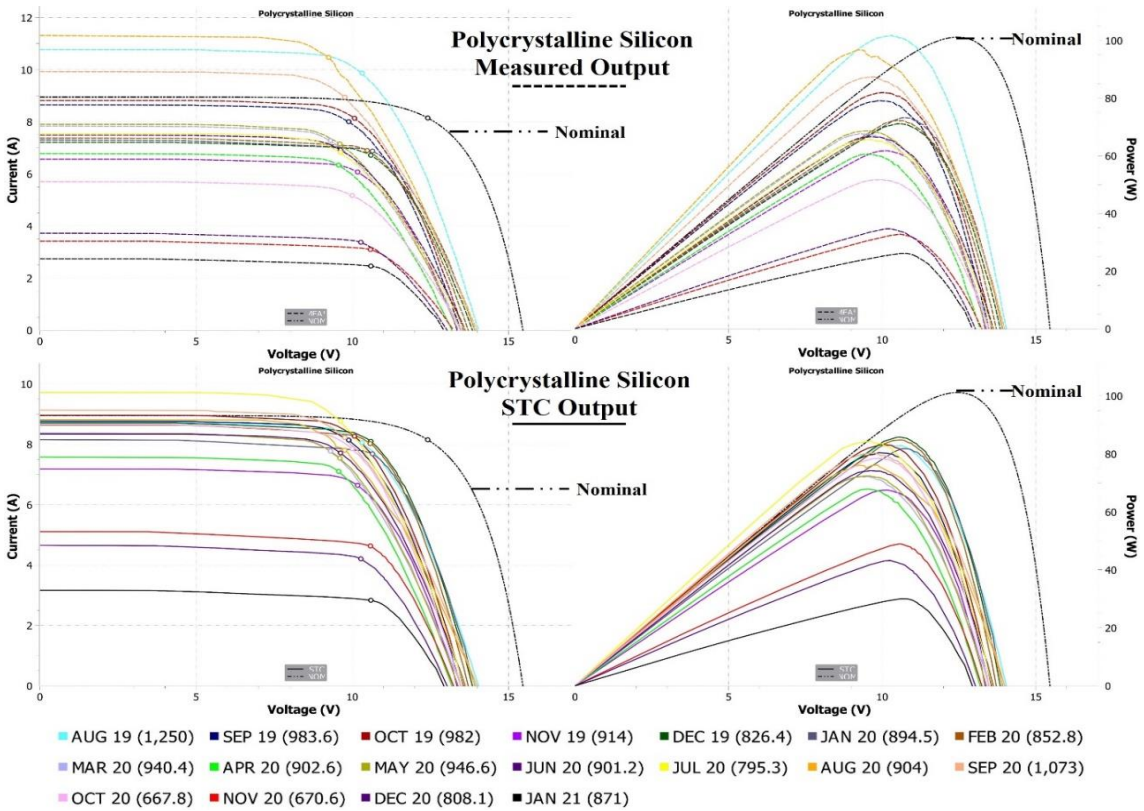

Figure 5.6: Monthly measured and converted STC performance variation of the pc-Si module at a different irradiance for 17 months in relation to nominal outputs.

Table 5.3: pc-Si monthly electrical output parameter variation including I_{SC}, V_{OC}, FF, P_{max}, V_{mpp}, I_{mpp}, solar irradiance, and ambient temperature when considering the maximum irradiance.

Polycrystalline Silicon Module								
Month	**P_{max}**	**V_{OC} (V)**	**I_{SC} (A)**	**FF**	**V_{mpp} (V)**	**I_{mpp}(A)**	**Irr (W/m2)**	**A T (^{O}C)**
Aug-19	101.539	14	10.78	67.28	10.31	9.9	1250	37.62
Sep-19	79.32275	13.5	8.651	67.92	9.886	8	983.6	38.49
Oct-19	82.17247	13.6	8.818	68.52	10.07	8.1	982	37.62
Nov-19	61.97492	13.4	6.564	70.46	10.17	6.1	914	39.27
Dec-19	70.93178	13.8	7.213	71.26	10.59	6.7	826.4	30.28
Jan-20	73.109	13.9	7.301	72.04	10.64	6.9	894.5	31.24
Feb-20	72.19001	13.7	7.379	71.41	10.48	6.9	852.8	33.9
Mar-20	67.78574	13.5	7.837	64.07	9.303	7.3	940.4	39.36
Apr-20	60.63355	13.2	6.778	67.77	9.564	6.3	902.6	42.55
May-20	68.71484	13.4	7.905	64.87	9.601	7.2	946.6	43.32
Jun-20	66.54905	13.6	7.489	65.34	9.624	6.9	901.2	39.03
Jul-20	65.77325	13.6	7.539	64.15	9.623	6.8	795.3	37.72
Aug-20	96.55777	13.9	11.31	61.42	9.245	10.5	904	37.04
Sep-20	87.39955	14	9.925	62.9	9.76	8.9	1073	33.71
Oct-20	51.84891	13.5	5.7	67.38	9.996	5.2	667.8	38.39
Nov-20	32.69507	13.2	3.415	72.53	10.58	3.1	670.6	38.15
Dec-20	34.58224	13	3.72	71.51	10.27	3.4	808.1	35.45
Jan-21	26.01708	12.9	2.741	73.58	10.59	2.5	871	38.49

Figure 5.7 demonstrates that the mc-Si module's output was relatively high at the beginning of exposure (August-2019). The measured P_{mpp} value at 1,026 W/m^2 irradiance is about 97 W. The P_{mpp} values generated under standard conditions (96W) compared with a nominal value (109W) where the output shows a difference of about 12.2%, as demonstrated in Figure 5.11(a). Figure 5.7 shows the discrepancies between the measured I_{SC} as 9.29 A, the STC I_{SC} 9.16 A and the NOM I_{SC} is 9.20 A. Similarly, it shows the variance between the measured $I_{mpp,}$ 8.63 A, STC I_{mpp}, 8.54 A and NOM I_{mpp}, 8.63 A. The most significant performance degradation of the mc-Si modules was recorded in January 2021, where the P_{mpp} measured value at 904 W/m^2 irradiance is about 30 W, I_{SC} is about 2.89 A, and the I_{mpp} is about 2.66 A. The P_{mpp} value under standard conditions (34 W) is generated and compared with the nominal (109 W) value obtained during the indoor measurement, where the output shows a variance of about 68.6%, as provided in Figure 5.11(a). The actual lowest degradation was recorded in August 2020; all the parameters are highlighted at the beginning of this paragraph.

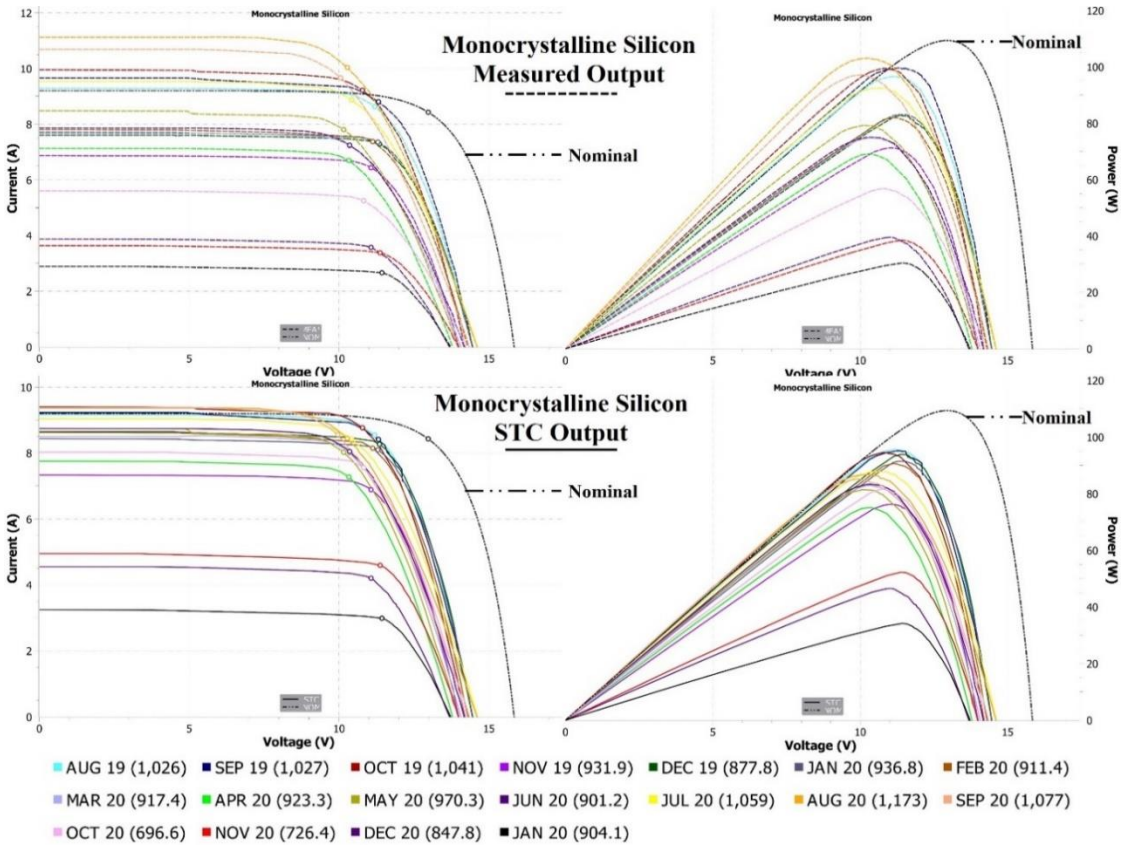

Figure 5.7: Monthly measured and converted STC performance variation of the mc-Si module at a different irradiance for 17 months in relation to nominal outputs.

Table 5.4: mc-Si monthly electrical output parameter variation including I_{SC}, V_{OC}, FF, P_{max}, V_{mpp}, I_{mpp}, solar irradiance, and ambient temperature when considering the maximum irradiance.

Monocrystalline Silicon Module								
Month	**P_{max}**	**V_{OC} (V)**	**I_{SC} (A)**	**FF**	**Irr (W/m2)**	**Ta (^{O}C)**	**V_{mpp} (V)**	**I_{mpp}(A)**
Aug-19	96.86	14.5	9.289	71.91	1026	35.83	11.19	8.6
Sep-19	99.98	14.5	9.661	71.37	1027	36.61	11.31	8.8
Oct-19	99.49	14.2	9.952	70.4	1041	36.51	10.78	9.2
Nov-19	71.27	14	6.869	74.11	931.9	38.49	11.07	6.4
Dec-19	83.02	14.5	7.602	75.32	877.8	30.71	11.35	7.3
Jan-20	83.29	14.5	7.707	74.53	936.8	31.97	11.3	7.4
Feb-20	81.99	14.3	7.801	73.5	911.4	33.9	11.12	7.4
Mar-20	75.02	14.1	7.652	69.53	917.4	38.93	10.36	7.2
Apr-20	69.25	13.8	7.133	70.35	923.3	45.55	10.33	6.7
May-20	79.34	14	8.481	66.82	970.3		10.15	7.8
Jun-20	75.16	14.2	7.86	67.34	901.2	39.51	10.35	7.2
Jul-20	92.36	14.6	9.536	66.34	1059	35.69	10.42	8.9
Aug-20	103.13	14.6	11.12	63.52	1173	34.77	10.27	10
Sep-20	96.93	14.3	10.69	63.41	1077	35.88	10.05	9.7
Oct-20	56.79	14.2	5.605	71.35	696.6		10.82	5.3
Nov-20	38.49	14	3.636	75.61	726.4	36.85	11.37	3.4
Dec-20	39.59	13.7	3.87	74.68	847.8	37.19	11.07	3.6
Jan-21	30.38	13.7	2.89	76.74	904.1	38.69	11.43	2.7

Figure 5.8 shows that the CdTe module's performance was very high at the beginning of exposure (August-2019), and it is the month when the lowest degradation was recorded. The measured P_{mpp} at 1,148 W/m^2 is about 88 W. The P_{mpp} value is generated under standard test conditions (71W) and compared with the nominal value where the output shows a difference of about 11.3%, as illustrated in Figure 5.11(a). Furthermore, the results show variance between the measured $I_{SC,}$ which is 1.35 A, the STC I_{SC} is 1.09 A, and the NOM I_{SC} is 1.02 A. Similarly, it shows the difference between the measured I_{mpp}, 1.11A, STC I_{mpp}, 0.89 A and NOM I_{mpp}, which is 0.88 A. The most significant performance degradation is recorded in January 2021, where the measured P_{mpp} value at 887 W/m^2 is about 16W. The P_{mpp} value is generated under standard conditions (18 W) and compared with the nominal value (80 W) obtained during the indoor measurement, where the output shows a variance of about 77%, as demonstrated in Figure 5.11(a).

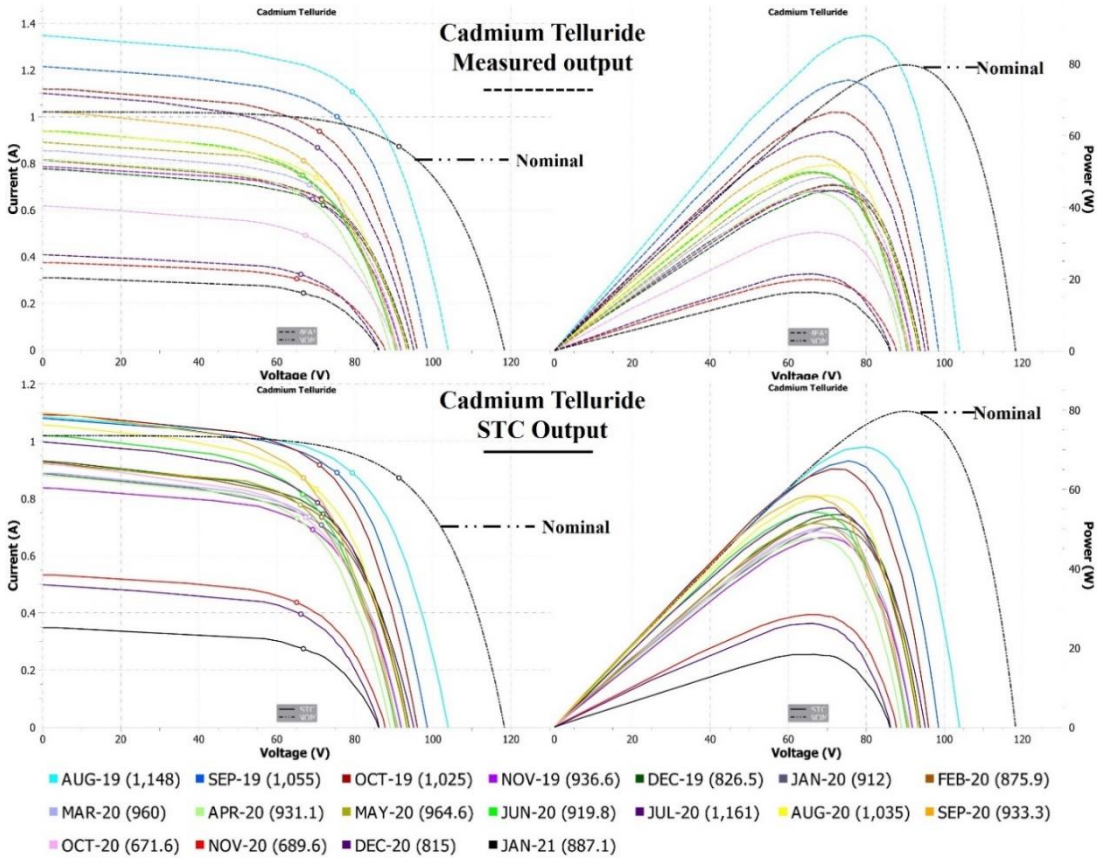

Figure 5.8: Monthly measured and converted STC performance variation of CdTe module at a different irradiance for 17 months in relation to nominal outputs.

Table 5.5: CdTe monthly electrical output parameter variation including I_{SC}, V_{OC}, FF, P_{max}, V_{mpp}, I_{mpp}, solar irradiance, and ambient temperature when considering the maximum irradiance.

Cadmium Telluride								
Month	**P_{max}**	**V_{OC} (V)**	**I_{SC} (A)**	**FF**	**V_{mpp} (V)**	**I_{mp}p(A)**	**Irr (W/m2)**	**A T (^{O}C)**
Aug-19	87.86	103.9	1.348	62.73	79.35	1.1	1148	32.26
Sep-19	75.42	98.5	1.215	63.02	75.43	1	1055	37.82
Oct-19	66.51	96	1.119	61.91	70.95	0.9	1025	35.88
Nov-19	44.75	91.8	0.785	62.1	69.19	0.6	936.6	38.78
Dec-19	44.63	93.8	0.776	61.31	71.89	0.6	826.5	31.2
Jan-20	46.34	93.9	0.816	60.48	71.4	0.6	912	32.21
Feb-20	46.08	93.3	0.814	60.68	71.49	0.6	875.9	33.52
Mar-20	48.34	92	0.853	61.6	68.36	0.7	960	39.61
Apr-20	44.09	89	0.814	60.86	67.29	0.7	931.1	46.27
May-20	49.55	90.4	0.891	61.52	66.04	0.8	964.6	44.34
Jun-20	49.89	90.5	0.937	58.83	66.63	0.7	919.8	39.75
Jul-20	61.12	95.1	1.101	58.37	70.44	0.9	1161	37.57
Aug-20	51.79	93.5	0.937	59.12	70.1	0.7	1035	37.86
Sep-20	54.29	91	1.023	58.32	66.84	0.8	933.3	38.59
Oct-20	33.11	90.7	0.618	59.07	67.33	0.5	671.6	
Nov-20	19.92	87.7	0.375	60.57	65.09	0.3	689.6	36.46
Dec-20	21.44	86.2	0.408	60.95	66.16	0.3	815	
Jan-21	16.27	86	0.309	61.22	66.8	0.2	887.1	38.49

Figure 5.9 indicates that the yield of the a-Si module was substantially higher at the beginning of exposure (August-2019), and it is the month when the lowest performance reduction was recorded. The measured P_{mpp} value at 1,169 W/m^2 is about 152 W. The P_{mpp} values are generated under standard test conditions (135W) and compared with a nominal value (136 W) where the output shows a difference of about 1%, as shown in Figure 5.11(a). Figure 5.9 shows a difference between the measured $I_{SC,}$ 2.81 A, the STC I_{SC} 2.45 A and the NOM, which is 2.28 A. Equally, it shows the variance between the measured $I_{mpp,}$ 2.39 A, STC, 2.12 A and NOM, which is 1.98 A. The most severe degradation is recorded in January 2021, where the measured P_{mpp} value at 907 W/m^2 is about 27 W. The P_{mpp} value is generated under standard conditions (30 W) and compared with the nominal value (136 W) obtained during the indoor measurement, where the output demonstrates a dissimilarity of about 78.3%, as illustrated in Figure 5.11(a).

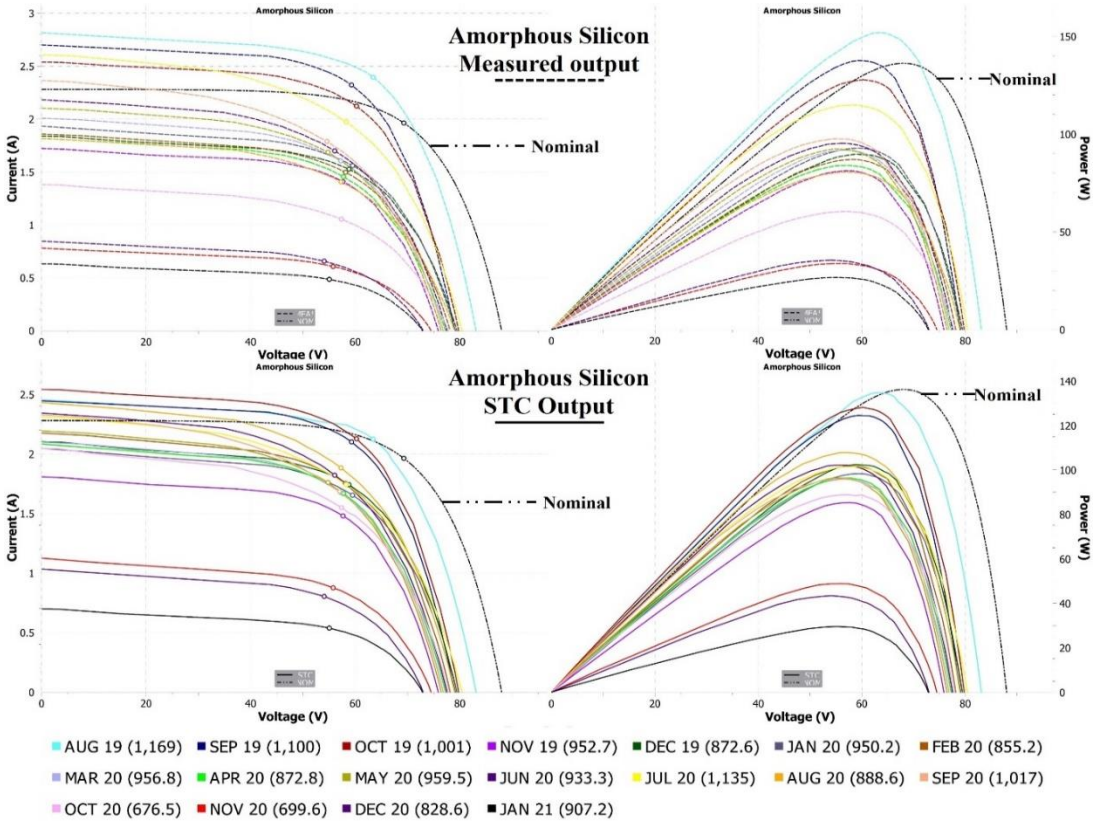

Figure 5.9: Monthly measured and converted STC performance variation of a-Si module at different irradiance for 17 months in relation to its nominal output.

Table 5.6: a-Si monthly electrical output parameter variation, including I_{SC}, V_{OC}, FF, P_{max}, V_{mpp}, I_{mpp}, solar irradiance, and ambient temperature when considering the maximum irradiance.

Amorphous Silicon Module								
Month	**P_{max}**	**V_{OC} (V)**	**I_{SC} (A)**	**FF**	**V_{mpp} (V)**	**I_{mpp}(A)**	**Irr (W/m²)**	**A T (°C)**
43678	151.8956	83.1	2.816	64.91	63.43	2.4	1169	32.16
43709	137.6935	79	2.701	64.53	59.29	2.3	1100	39.22
43739	127.8784	79.8	2.54	63.09	60.24	2.1	1001	35.88
43770	81.22194	75.9	1.721	62.18	57.66	1.4	952.7	38.73
43800	89.73678	79.4	1.838	61.49	58.8	1.5	872.6	30.81
43831	92.7319	79.1	1.932	60.68	59.49	1.6	950.2	
43862	87.09018	78.2	1.858	59.94	58.14	1.5	855.2	34.19
43891	91.87704	76.9	2.008	59.5	57.23	1.6	956.8	38.69
43922	84.05588	77.3	1.819	59.78	57.75	1.5	872.8	
43952	92.43299	76.4	2.103	57.53	54.8	1.7	959.5	
43983	95.17939	77.5	2.181	56.31	56.07	1.7	933.3	38.93
44013	114.8414	80.4	2.607	54.79	58.28	2	1135	38.93
44044	80.55504	79	1.816	56.15	55.82	1.4	888.6	36.8
44075	97.64039	76.8	2.364	53.78	54.6	1.8	1017	38.64
44105	60.42359	77.8	1.379	56.32	57.36	1.1	676.5	
44136	33.79097	74.5	0.78	58.15	55.76	0.6	699.6	35.69
44166	35.49972	73	0.845	57.55	54.06	0.7	828.6	37.91
44197	26.63956	72.8	0.632	57.9	55.04	0.5	907.2	38.25

Figure 5.10 presents the significant impact of soiling on the PV performance, where I_{SC} and I_{mpp} drastically degraded towards the end of the study as more accumulation is recorded. It is observed that wider gaps were recorded on both pc-Si and mc-Si I_{SC} and I_{mpp} and less gap on CdTe and a-Si modules during the last four months of the study. The less influence of the soiling is related to the spectral response wavelength where the CdTe and a-Si operate with the range of UV and VIS range, but the others operate in UV, VIS, and NIR ranges. This makes it easy for accumulated particles to absorb, attenuate, scatter easily, or reflect incoming light, thereby reducing the potential photon from reaching the solar cells.

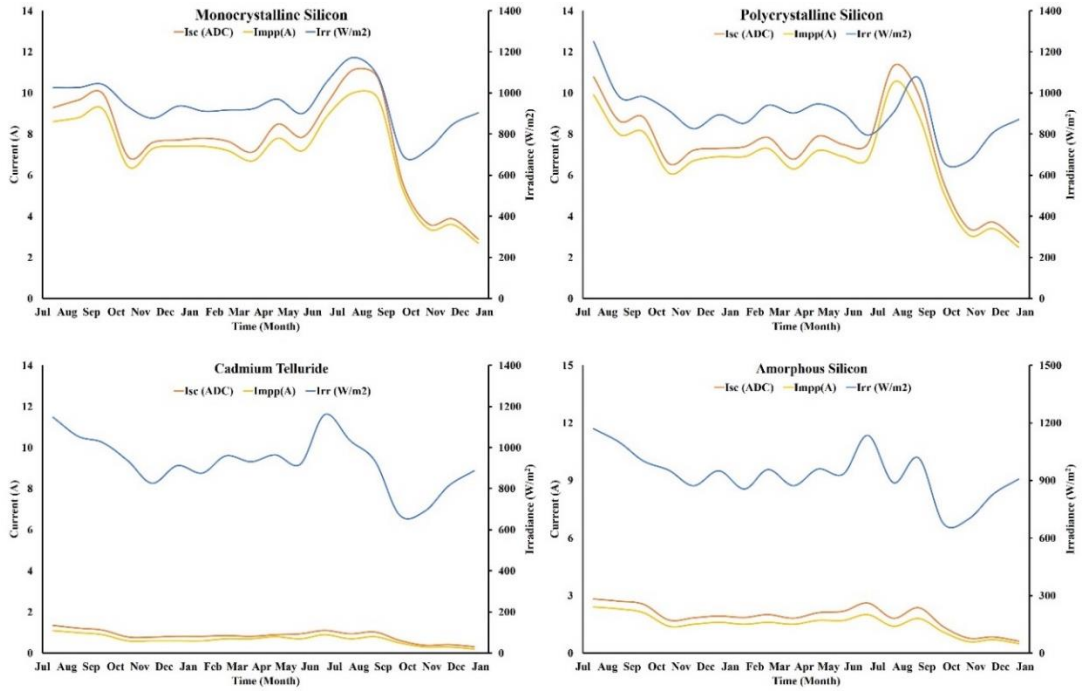

Figure 5.10: Monthly variation of short circuit current and current at maximum power point from August 2019 to January 2021.

A comparison chart illustrating the changes between the PV output in STC and NOM shows a similar variation to the chart illustrating the efficiency change shown in Figures(a) and (b). The month with the lowest efficiency change for a pc-Si module is February-2020, where about 18% loss was recorded. However, another low-efficiency change was recorded in December 2019 (17%) due to cleaning to restart the measurement at the end of the year, but it would not count as the lowest since it was intentionally cleaned. The month with the lowest efficiency change for mc-Si was recorded in September-2019 with about 15%

loss. The lowest efficiency change for CdTe and a-Si occurs at the beginning of the exposure (August-2019), with a 3% reduction for both modules. Even though the modules were cleaned in December, the efficiency was not fully regained. On the other hand, substantial losses were recorded on all modules towards the end of the experiment, with 71% efficiency reduction on the pc-Si, 71% for an mc-Si, 77% for the CdTe, and 78% for a-Si modules.

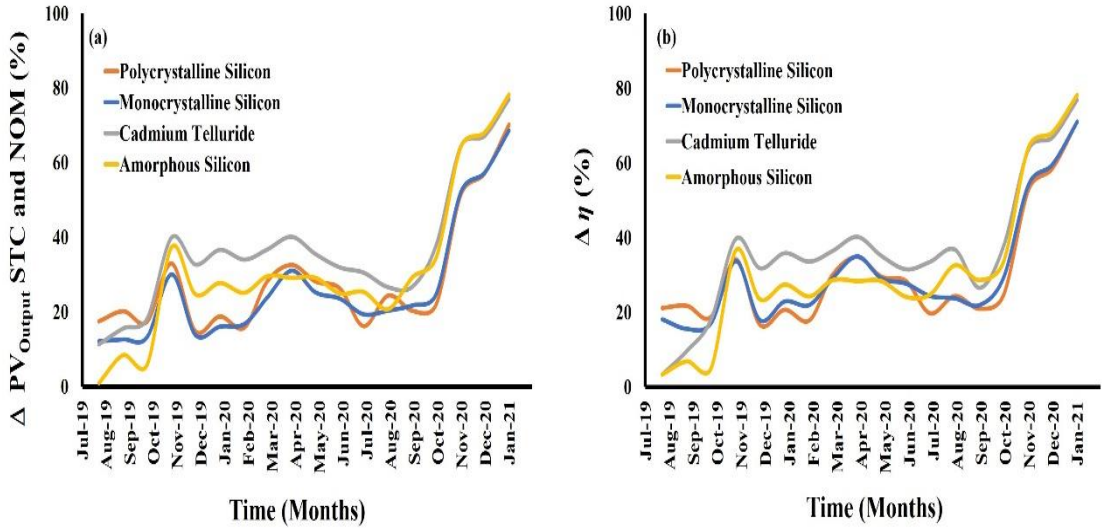

Figure 5.11: (a) Monthly variation of the change between PV outputs converted to STC and PV output under Nominal condition, and (b) monthly variation of the change in PVs efficiencies.

5.3.3 Optical losses

5.3.3.1 Monthly

The optical assessment result shows significant losses, where the various coupons have individual soiling rates. The results are clustered into monthly, seasonal (dry and Wet), and annual (ANN). The monthly result in Figure 5.12 shows losses of coupons from all months compared to a clean coupon's optical characteristic. The most significant loss for monthly coupons was recorded from January, where about 50% reduction was observed, and the least was recorded from the August coupon with about 2% loss.

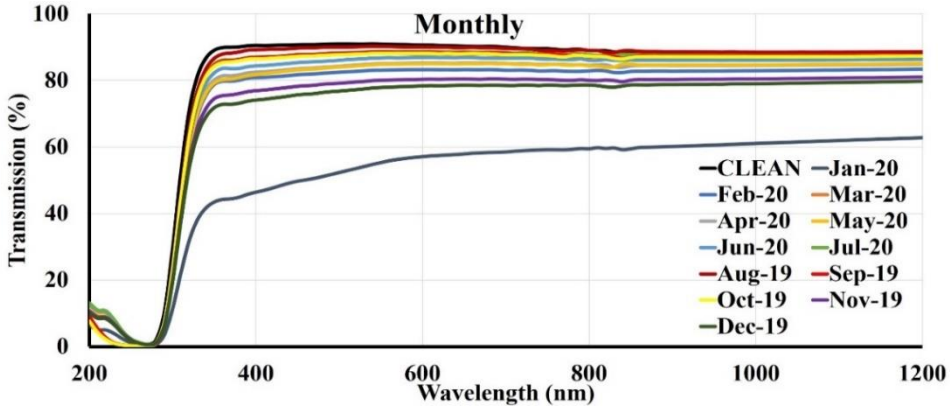

Figure 5.12: Monthly variation of optical losses of soiled coupons compared with a clean one.

5.3.3.2 Seasonal

Seasonal optical loss results are illustrated in Figure 5.13, where the losses of coupons exposed during the two major seasons (dry and wet) are depicted. It shows losses of coupons from both seasons compared with the optical characteristics of a clean coupon. The results illustrate the high soiling losses during the dry season with about 43% optical loss, while only 7.21% optical loss was recorded on the wet season coupon.

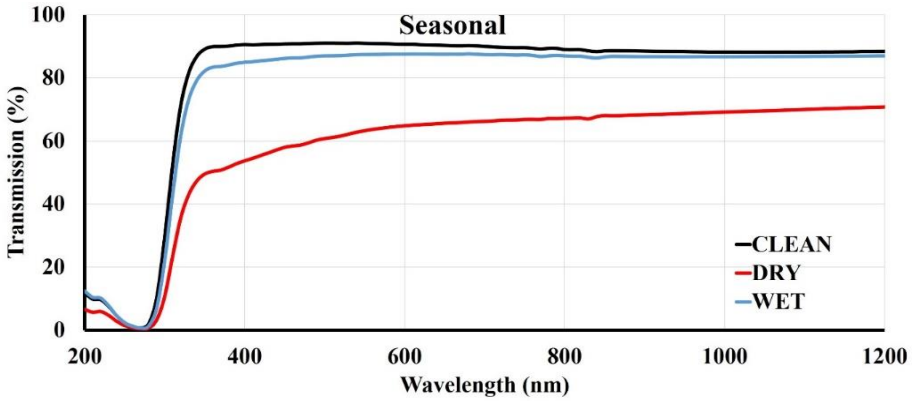

Figure 5.13: Seasonal optical losses variation of soiled coupons compared with a clean one.

5.3.3.3 Annual

The annual optical loss result is illustrated in Figure 5.14, where the losses of coupon exposed for about 17 months is depicted. It shows optical losses of the annual coupon compared with the optical characteristic of a clean coupon. The

results illustrate the high soiling losses where about 68% optical loss was recorded.

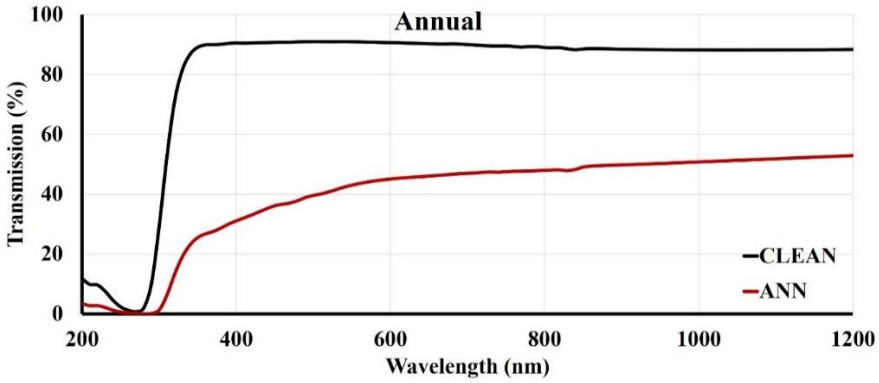

Figure 5.14: Annual (ANN) optical losses of soiled coupons compared with a clean one.

5.3.4 Mass of accumulated dust

The masses of accumulated dust on various coupons were examined through a systematic approach. The finding shows that January appears to have the most significant Mass with about 5.92 g/m^2 deposited on the coupon while the least is August with 0.40 g/m^2 when considering monthly deposition, as illustrated in Figure 5.15. Furthermore, optical losses were plotted as a function of dust density, where a linear line is observed showing that the higher the Mass of accumulated dust, the more optical losses to be recorded.

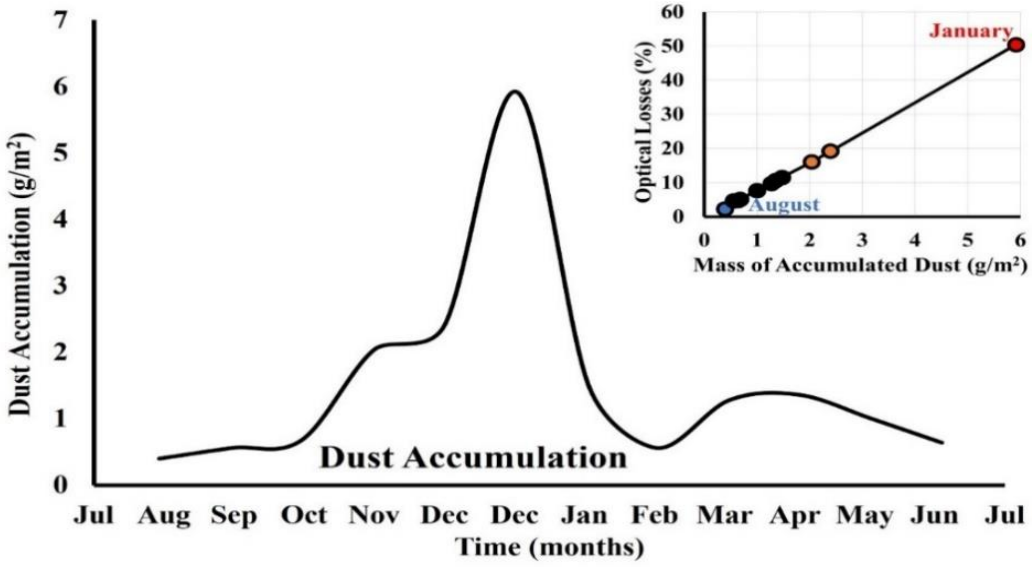

Figure 5.15: Monthly variation of accumulated dust as a function of time and an illustration of accumulated dust mass as a function of the optical losses.

5.3.5 Particle characterisation

The SEM images in Figure 5.16(b) shows how dust particles are naturally deposited over the coupons with less wide gaps, yet on a closer view showing in Figure 5.16(a) with a scale of 50 µm, it shows that a large amount of light would not reach the solar cell since some particles with a broader diameter greater than 100µm are occupying space, and others are even wider. The exposed modules' spectral responses are all within UV, VIS and NIR wavelength, from 0.2 µm to about 1.2 µm.

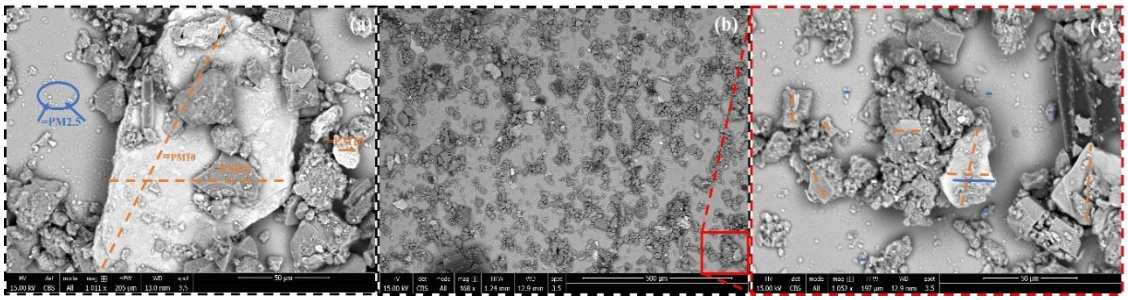

Figure 5.16: SEM images illustrating the presence of massive PM_{10} and $PM_{2.5}$ particles on a coupon exposed in Kano, Nigeria.

EDX results provided graphs shown in Figure 5.17, highlighting element composition employed in identifying the minerals. All graphs were repeatedly recorded from different positions on the coupon. Findings show minerals such as Stilpnomelane that has opaque optical characteristics and Illite that possess translucent optical characteristics. However, results show that some minerals such as Anxite, Beryl, and Quartz tend to have transparent optical characteristics. All the EDX results and their optical characteristics are highlighted in Table 5.7.

Table 5.7: Minerals and their diaphaneity.

s/n	Mineral	Diaphaneity
1.	Axinite	Translucent to transparent
2.	Beryl	Transparent to sub-translucent
3.	Chloride (Chamosite)	Translucent to sub-translucent
4.	Garnet (Andradite)	Transparent to translucent
5.	Illite	Translucent

6.	Melilte	Translucent
7.	Stilpnomelane	Sub-translucent to opaque
8.	Quartz	Transparent to Translucent

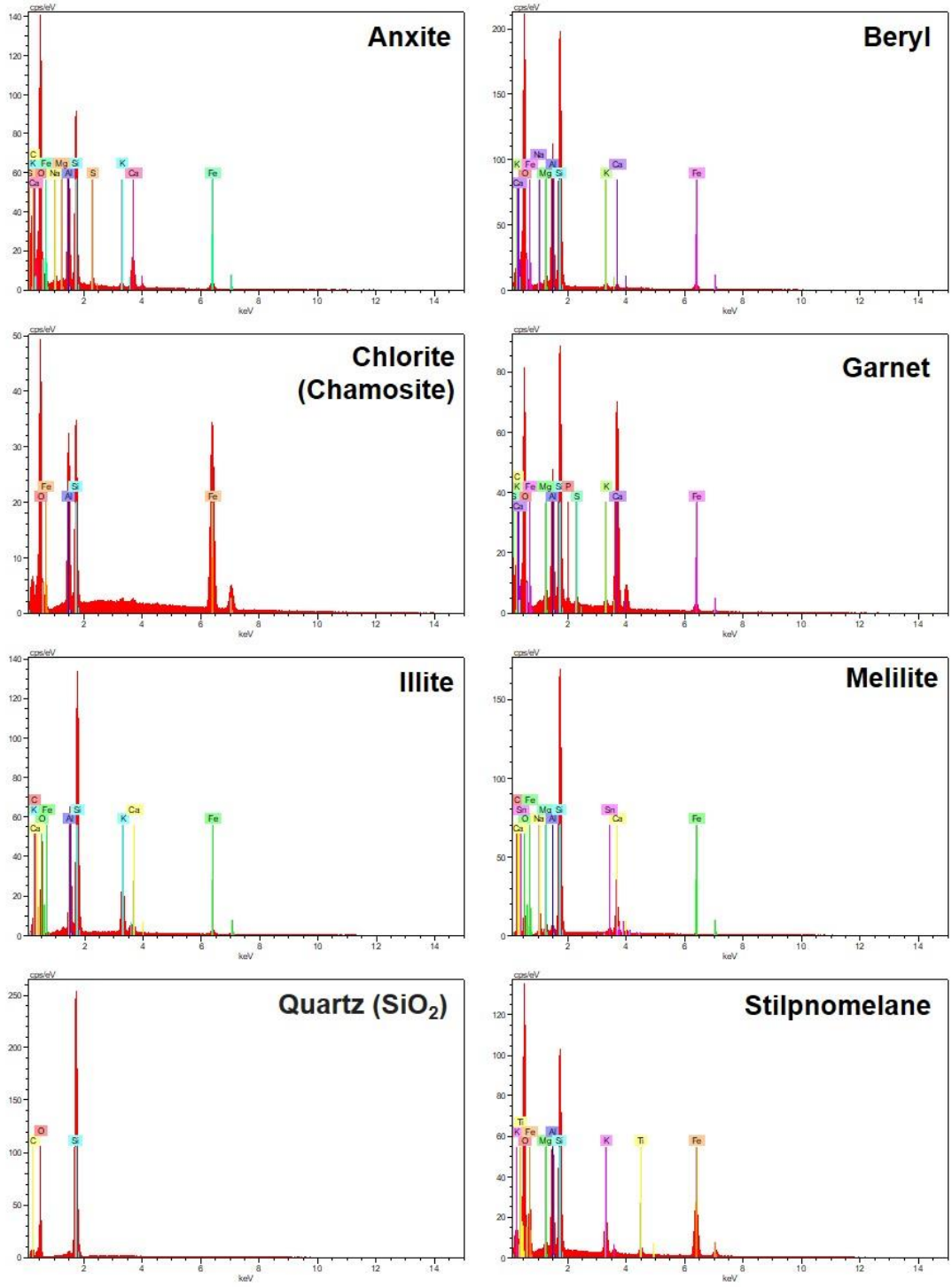

Figure 5.17: EDX graphs highlighting mineral elements that could have a deteriorating impact on light transmittance.

5.4 Discussion

This section presents the analysis of the experiments undertaken to characterise the PV modules' performance under Nigeria's extreme conditions. The initial laboratory results were used as a baseline to determine the percentage difference of I_{SC}, I_{mpp}, P_{mpp}, and efficiency losses when soiling occurs on PV surfaces. Optical loss results were analysed to determine the losses and accumulated particle mass for a particular period. Furthermore, weather conditions during significant losses were examined to know when and how they influence soiling on PV. Accumulated particles on coupons surface were analysed to determine the types of minerals and why they negatively influence light transmittance. For a better understanding of the kind of accumulation recorded, a digital image showing all the four modules is provided in Figure 5.18.

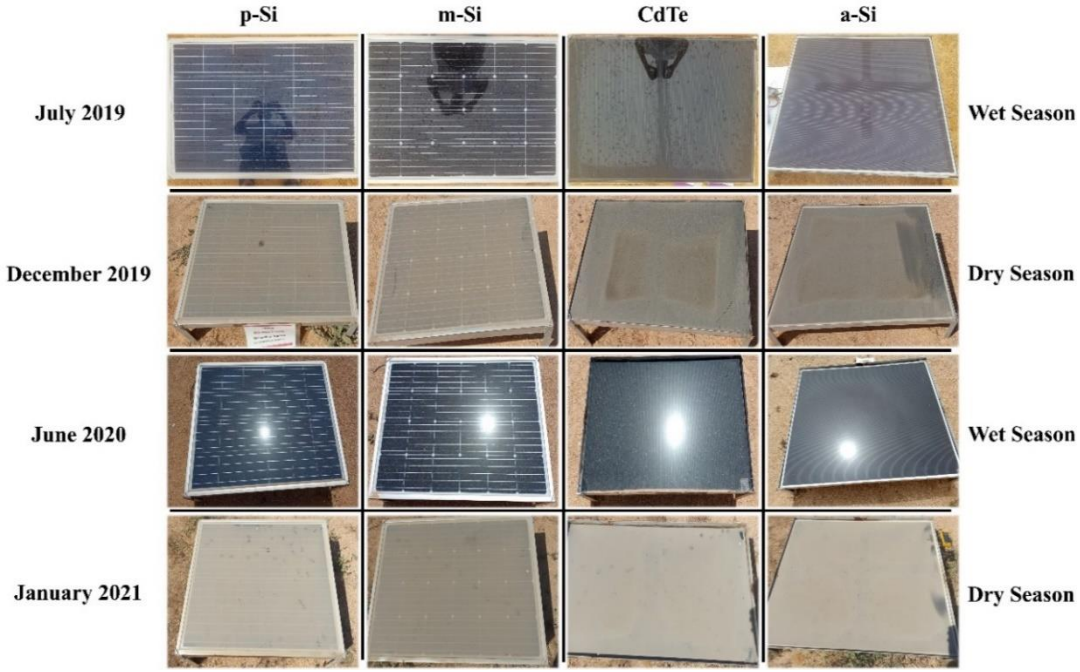

Figure 5.18: Digital images highlighting variations between clean modules and soiled modules during exposure.

The initial in-situ performance assessment results confirmed that all the modules are in perfect condition after transportation. It also confirmed that the laboratory performance characterisation results are correct, and the insulation resistance of all the modules is with factory acceptance level >200 MOhm. The FF measured at sunrise shows the expected value ranging from 0.68 for a-Si, 0.69 for CdTe, 0.74 for pc-Si, and 0.78 mc-Si. All these values were recorded at a PV

temperature greater than 25°C. Kalogirou (2009) stated that any solar cell with an FF greater than 0.7; is working correctly, and the FF would decrease as the temperature increases. When the results at the peak of irradiance are converted to STC, it appears to have I_{SC} greater than the NOM value for all modules, except for the pc-Si module, where a majority of the time, the I_{SC} is less than the NOM value, but when the temperature drops, it becomes the same. Simultaneously, the V_{OC} under STC remains lower than NOM at all times, which is due to temperature. The findings reveal a slight degradation of a minor degradation at sunrise on the a-Si and CdTe module due to the devices' characteristics. It has been reported that a-Si and CdTe could suffer degradation of efficiency when first exposed and tends to stabilise within a short period (Guerra et al., 2017).

The monthly performance results show a significant loss in some months, with the greatest towards the end of the study. The findings were compared against the initial laboratory measurement and the initial in-situ measurement. The significant losses recorded from various months are related to the soiling and temperature. However, the research focused on the soiling aspect where photons are attenuated, absorbed and scattered by mineral particles accumulated on the modules' surface. Within one year without cleaning and seventeen months of exposure, enormous losses of the I_{SC} and the I_{mpp} were recorded, with the pc-Si module having 65% I_{SC} and 66% I_{mpp} reductions. At the same time, the mc-Si module shows 65% of I_{SC} and 66% of I_{mpp}. Higher degradations were recorded on thin-film modules with 66% of I_{SC} and 69% of I_{mpp} reduction for the CdTe module, whereas the a-Si module has a 69% of I_{SC} and 73% of I_{mpp} degradation. I_{SC} and I_{mpp} are both directly dependant on the intensity of the incident light, which leads to overall performance degradation. Kalogirou (2009) stated that the relationship between solar radiation and I_{SC} is linear since the increase in solar radiance leads to an increase in I_{SC} and similarly decreases in light penetration of solar cells, leading to a decrease in I_{SC}. Reductions recorded on crystalline modules appear to be similar. However, more significant losses were recorded on the thin-film modules, with a-Si having greater losses than CdTe. Significant efficiency degradation was recorded from all modules, as illustrated in Figure 5.11(b). A closer examination of the findings reveals that factors such as temperature stimulate higher-efficiency degradation. However, these reductions

are mainly related to soiling on the PV devices, demonstrating the harmful impact dust accumulation could cause in the region over a short period.

The variation between the I_{SC}/I_{mpp} reductions and the efficiency reduction is relatively small. Unsurprisingly, findings show an alarming performance loss from all the modules, which is directly related to soiling as this causes the I_{SC} decrease reported earlier with the most significant total power loss of about 78.3% for a-Si, 77% for CdTe, 70% for pc-Si, and 68.6% for the mc-Si module. Likewise, PV efficiency results also presented a high degradation with about 78% degradation for a-Si, 77% for CdTe, and 71% for the mc-Si and pc-Si modules.

Weather conditions play a vital role in influencing dust accumulation on the surface and sometimes play the mitigating role, cleans the surface and reduce PV temperature. The average weather illustrated in Figure 5.4(b) shows that the most significant wind velocity was about 6 km/h in Jun 2020. It also shows the heaviest rainfall in July 2020 (about 131 mm/h), followed by June 2020 (about 115 mm/h). The average wind direction during these months is mainly south-south, according to Figure 5.4(d), showing it is coming from the Atlantic region. These two parameters serve as a natural cleaning for the modules, and that is why the high performance was recorded during those two months and the following August. Said et al. (2018) reported that high wind speed with an inward direction could reduce the temperature by dissipating convective heat from the PV device to sustain conversion efficiency as long as the wind direction blows towards the system.

On the other hand, lower wind velocity was recorded around November, December, and early January at about 3 km/h wind speed (shown in Figure 5.4(b)), mainly from the North East were recorded. The wind speed improves and becomes very active in January, triggering the Harmattan season characterised by dry and dusty particles reported to be generated from the Saharan desert (Meindinyo et al., 2017). It is hard to see any form of rainfall or high humidity rate in the region during this season, and the weather station recorded zero rainfall, as shown in Figure 5.4(c).

Humidity tends to be high at the beginning of the Harmattan season due to the transition from wet to dry season, and it then drastically drops within a couple of days, causing massive dust accumulation on surfaces at the beginning of the season (November). This is the main reason why high PV losses are recorded at the beginning of the dry season. High humidity is recorded during the wet season, as shown in Figure 5.4(a), which corresponds to the rainfall rate shown in Figure 5.4(c). Humidity tends to influence capillary adhesion significantly. On the first morning of *in-situ* data collection, it was observed that dew has settled on the surfaces of the module, which is a recipe for disaster. When water droplets with dust particles settled on a surface due to condensation and are later heated, the particles will dry and re-solidify, causing the particles' cementation (Isaifan et al., 2019; Figgis et al., 2018; Ilse et al. 2016; Ghazi and Ip 2014). It is reported that cemented particles are tough to remove from surfaces and sometimes impossible (Hachicha et al., 2019). Modules were cleaned using a similar technique (brush) used in the same solar farm during December 2019 to regain optimum performance and efficiency, but it was discovered that cementation occurred in some parts of a-Si and CdTe, requiring more thorough cleaning. Emziane and Al Ali (2015) used a brush in restoring PV modules that do not provide the desired outcome. The temperature in this region is always higher than 25°C during the day when the peak of irradiance is expected, and the thin-film module tends to have a heat tolerance to a certain extent, but a-Si tend to take longer to cool off after exposure. Temperature plays a vital role in PV performance; it also plays a significant role in influencing particles' retention on PV surfaces. The temperature increases with an intensity of irradiance over a short period; similarly, the PV temperature also increases with the ambient temperature increase. Soiling on the PV surface causes a decrease in PV temperature as the ambient temperature increases since the particles provide both optical and thermal resistance and shield to the incident irradiance. Xu et al. (2017) supported this claim and stated that the PV temperature of a module covered with dust has a lower temperature than a clean PV module.

The optical results demonstrate significant losses, with the highest coupon exposed in January and the lowest coupon in August. This finding corresponds to the initial statement highlighting that January happens to be the peak of the dry season, whereas August is the peak of the rainy season. The optical results

for the season confirm this, where it shows that higher losses are recorded during the dry season compared with the wet season. The moisture content in the air around PV decreases with ambient temperature, making the PV local surrounding area dry. Therefore, low-level wind can easily cause soil erosion by lifting particles from the surface and move them to a different location (Mekhilef et al., 2012). Kazem et al. (2017) reported that the PM_{10} level in the atmosphere is a factor causing the increase in surface uncleanliness, mainly when the wind velocity is less and humidity is low. Optical losses were exacerbated on the annual coupon, which was removed during the dry season. Findings reveal that the most significant loss is recorded in January, and the relationship between the optical losses and Mass accumulated is directly proportional. The higher the dust mass and the higher the optical losses recorded. It clearly shows that dust density is not linearly dependent on the length of exposure but rather on climatic conditions. However, accumulation will increase with time. This is also in line with Said et al. (2018) that stated that dust density does not increase linearly with time. Dust formation on the various coupons surfaces that caused all the optical losses illustrated in Figure 5.12, Figure 5.13 and Figure 5.14 could lower the amount of light reaching the solar cell, leading to a reduced number of electron-hole pairs.

The SEM reveals the sizes of mineral particles which are large and dispersedly distributed on the coupon. Some particle diameter was observed to be wider than 100 µm and spectral wavelength on which all the PV modules are ≤ 1.2 µm. It shows that mineral particles could absorb, attenuate, scatter or reflect the photon flux. The EDX reveals minerals with opaque, translucent and sub translucent optical characteristics, which confirms the reason for light absorption, reflection, attenuation, and scatter, leading to photons' reduction, hence decreasing the number of possible electron-hole pairs that could be generated and lessen the potential current (A). Air Plum Lab (2021) provided data of the primary pollutant suspended in the atmosphere across the region, which show a high concentration of PM_{10} suspended in the atmosphere with the most significant concentration recorded during the dry season, causing a high reduction of irradiance reaching the solar cell. The data are consistent with the findings of SEM presented in Figure 5.16.

The accumulation during the dry season is not influenced by precipitation since Figure 5.4(c) clearly illustrates zero precipitation. Deposition occurs when wind acts as the transport agent through Brownian and turbulent diffusion, interception, sedimentation, electrical migration, diffusiophoresis and thermophoresis (Zaihidee et al., 2017). In comparison, deposition during the dry season in the region can occur with the influence of dew, humidity and wind, whereas all the above mentioned with the addition of precipitation occurs during the wet season. The main adhesion force assumed to be causing particle retention on surfaces are capillary force, electrostatic force, and Van der Waal forces. Van der Waal force and electrostatic force are expected to be highly active during the dry season, whereas all forces (capillary force, Van der Waal forces, and electrostatic force) were expected to be active during the wet season. However, the availability of the high rainfall rate and high wind speed promotes particles detachment and removal during the wet season, and the wind is blowing from the opposite direction of the primary source of dust that injects particles into the atmosphere. The capillary force created bridges that cement particle surfaces are assumed to be very active at the beginning and the end of the wet season where light rainfall was recorded. The Van der Waal force and electrostatic force are less dominant, with the first acting between particles and then between particles and surface within a short range (Ilse et al., 2018). The second acts between particles and surface, and its strength mainly depend on the electric field. It can act positively by repulsing the dust particle or in a negative way of attracting the particles.

In contrast, the findings are compared with losses recorded on the solar farm, which is the research site of this study shows significant power losses at the peak time of solar irradiance with about only a couple of weeks without cleaning during the transition from wet to dry season. The solar farm performance, reduces to about 88%, with a total power output of about 117 kW/MW, was recorded on a Sunday, 01/09/2019. The irradiance at the time this loss was recorded indicated 1028 W/m^2 for the East orientation sensor and 1094 W/m^2 for the West orientation sensor. The calculated performance ratio was about 0.22054. This massive reduction is due to the cleaning staff being on a break based on the assumption that rainfall will clean the modules and maintenance. However, a certain percentage of performance was regained after a thorough cleaning was conducted with brushes. The solar farm never operated at its optimum

performance, even during the inauguration. The analysed power data collected from the farm show that the maximum performance ratio was recorded during the inauguration, which is about 1.51 PR (3:2), 67% of the installed capacity. This fact was validated with a published report from Nigeria Electricity Hub (2018), which stated that it generates around 600 kW at the project's launching. Despite a weekly manual cleaning with brushes, further degradations to about 55% record during the dry season (03/03/2020) with a total power output of about 548.96 kW/MW and lower degradation 65% was recorded during the wet season. It is observed that cleaning with brushes improves performance but not to the required standard. Caution should be observed in generalising the solar farm's findings as some parameters such as temperature effect, cable losses, and inverter losses were not considered. However, the findings show similar trends of >50% losses on solar farm installation and the four exposed modules.

The finding demonstrated a significant performance degradation triggered by soiling on all the PV modules exposed with wide seasonal and monthly variation. Similarly, significant losses of solar farm yield were observed with a seasonal and monthly variation. Findings reveal that mitigation technique (manual cleaning with brushes) used in the solar farm does not significantly improve the performance; thus, a more appropriate one should be determined. It provides realistic data and methodology that could be used for further research across the PV soiling community and scientists at large.

There is no standard soiling rate that could be globally applied as the results presented validated literature that shows extreme soiling in the region compared with what was earlier reported in the region. These findings would add to the growing knowledge in the field of PV soiling. Gupta et al. (2019) recommended increasing a suitable number of PV modules to compensate for losses caused by environmental factors. This study opposed the recommendation since an increasing number of modules would not solve the problem; instead, it would increase the level of financial commitment that cannot yield the required profit. Identifying the leading causes of soiling and its rate over seasonal and periodic variation should be a prerequisite for developing solar in a region with high airborne dust particles. The determining soiling losses of a site with high potential could play a decisive predictive role of optimum PV performance over a period. It

is vital to identify a cost-effective yet appropriate mitigation technique to restore and sustain the solar farm's optimum performance. Findings can be employed to ensure the optimum yield of a 7.1 MW solar farm, and another ongoing solar farm project larger with a capacity of greater than 100 MW in the same city is maintained using the reported soiling rate and periods with deposition. Sustaining this development is highly significant to the penetration of PV technology in the region, reducing the energy deficit and scaling up clean energy to attain SDG-7.

5.5 Summary and conclusion

In summary, this section of the thesis illustrated the impact of soiling on PV performance in both standard test conditions and extreme outdoor weather conditions (considering wind, humidity, rain, temperature and dust particles as influencing factors) in Nigeria. The findings reveal a massive performance decrease due to soiling on all exposed modules, with the most significant I_{SC} reduction recorded about 73% on a-Si and least of about 65% of the Si modules in one year without cleaning and seventeen months of exposure. The outcome shows egregious performances and efficiency losses of all exposed modules, a yield loss of 78.3% for a-Si, 77% for CdTe, 70% for polycrystalline and 68.6% for the monocrystalline Si module Whereas, approximately efficiency loss of 78% for a-Si, 77% for CdTe and 71% for both mono and multi-crystalline Si modules were recorded. A wide variation was recorded between months and seasons, with January 2021 and dry presenting the higher rates. The Results of optical losses validated the above performance losses with a similar trend. The particle characterisation reveals that mineral particles >PM_{10} size with opaque and translucent morphology were the primary constituent dust formation on the examined coupons. Various experimentations conclude that the region's prevailing soiling rate is exceptionally high and required immediate attention to prevent further PV performance losses and possible future system degradation within a short period for all the installations.

6 Chapter Six - Soiling mapping through optical losses for Nigeria

6.1 Introduction

The amount of soiling loss varies with location, human activities in the region, and climate (Cano et al., 2014; Ghazi et al., 2014). The reported soiling losses range from as low as 0.5% soiling rate reduction of PV output in a day (Sulaiman et al., 2015), 63% in a month (Alnaser et al., 2018) to about 50% reduction of PV yield in 6 months (Adinoyi and Said, 2013) without cleaning. A clean low iron glass has 91% transparency (Chanchangi et al., 2020), reducing the amount of irradiance reaching the solar cells and preventing it from generating the optimum yield. Since the most commonly used and one of the best PV covering materials available in the market already possesses some transmission limitations, there is a need to prevent or reduce any further optical losses to ensure maximum irradiance reaches the solar cell to harvest a higher yield. As stated earlier, the soiling losses rates cannot be constant for different regions since it varies with location and human activities in the location and climate.

Employing a constant value as a soiling rate cannot be accepted as it would illustrate an unrealistic PV potential of a region. Standards such as the AS4509.2 (3.4.3.6) using ±5% (Standards Australia, 2002), SAND2014-19199 using 3% and 2% (Patrick and Bruce, 2014), and Enphase Energy (2014) using 3% as a soiling de-rating factor is grossly inappropriate for some regions. Tanesab et al. (2018) recommended reviewing rates and considering regions with high potential and extreme weather conditions. The GSA (2020) used constant soiling values for installation categories such as; 3.5% for 1kWp, 4.5% for small residential, 4% for medium commercial, 3.5% for large scale, and 6% for floating large scale. However, GSA (2020) clearly stated that the PV yield they provide is an estimation and not an actual value as some important factors (such as soiling) is not adequately calculated. These values grossly underestimate the magnitude of PV yield degradation that soiling losses could cause in some regions across the world, especially the Middle East and North Africa (MENA), Saharan, sub-Saharan Africa, and regions with high levels of atmospheric dust.

This chapter of the thesis investigated the effect of soiling on PV performance, focusing on environmental variability as a factor. It aims to develop a low-cost soiling station and collected optical losses data to develop a soiling map that can be used for PV installation planning and maintenance cost optimisation. The soiling map is compared with a map published on the GSA website, and variations were presented. The study's secondary objectives are to examine the accumulated dust samples and identify their minerals, including each mineral's diaphaneity. Also, the weather and the air quality index (AQI) were employed for analysis purposes to determine the cause of accumulation on coupons.

This novel approach is motivated by GSA's recent progress in providing solar energy information, which could be improved by adopting the method used in this study since it offered a low-cost soiling station that could be used to determine the actual regional soiling rates. The approach could stimulate further soiling research across the globe. This section of the thesis contributes to the body of knowledge with the unique, low-cost approach used to determine the soiling losses value, which policymakers can use, PV companies, researchers, and potential PV investors. This sub-section of the thesis's findings may lead to a better understanding of soiling problems since the work highlights the significance of the effect of soiling, considering environmental differences as an influencing factor. The findings provided a more accurate and realistic soiling information rate for better PV installation and maintenance planning to achieve higher yields. The detailed procedures and methods are provided in the following sub-section of this thesis. Sub-section 6.3 illustrates results obtained from this study, while sub-section 6.4 provides a detailed analysis and discussion of the results.

6.2 Method

Soiling in Nigeria was investigated using low iron glass coupons across geopolitical zones in the country. An in-house low-cost research jig was designed using solid works and fabricated with a 3D printer (Stratasys uPrint SE 3D printer) using an ABS (Acrylonitrile Butadiene Styrene) P430XL material. This research jig was selected after an initial comparative test using ABS, wooden and a metallic material. Results obtained show a high chance of particles moving onto the surfaces of coupons from wood and rusted metal during extreme weather conditions. The ABS material has excellent thermal characteristics and remains

stable at a temperature between -20° to 80°C. About 315 pieces 50 mm X 50 mm X 4 mm coupons of low iron glasses were distributed in the six geopolitical zones (North-Central, North East, Northwest, South East, South-South and South-West) and main base of data collection (Kaduna State). Each station has three holders (one for monthly, one for seasonal and one for annual coupons), and each holder has three slots (one for vertical, one for tilt and one for horizontal) for exposing coupons to outdoor weather conditions. A flowchart illustrating the various steps through the research methodology of this subsection of the thesis is provided in Appendix B – Figure 0.6.

Table 6.1 shows the distribution of coupons in various locations across the country, while Figure 6.1 shows typical samples of soiled coupons after exposure and further illustrates how each soiling station is being installed. All exposed coupons were sealed in special crates fabricated using the above-mentioned 3D printer and transported back to the solar laboratory at the University of Exeter for detailed characterisation. Monthly coupons were exposed on the first day of the month, and then the coupon will be removed and replaced with a new clean coupon on the first day of the following month. Seasonal coupons were installed at the beginning of September when the research started to assume the wet season is coming to an end and marks the beginning of the dry season. Seasonal coupons were removed and replaced according to specific locations' seasons. Annual coupons were exposed at the end of the year and allowed to last for 12 calendar months before they were removed.

Table 6.1: Coupons dimensions and distribution.

Coupons (Low Iron Glass)		
Length	50 mm	
Height	50 mm	
Thickness	4 mm	
Monthly	**3** coupons X **7** sites X **12** months	**252**
Seasonal	**3** coupons X **7** sites X **2** seasons	**42**
Annually	**3** coupons X **7** sites X **1** year	**21**
	TOTAL	**315**
Coupons: 3 (Vertical, Horizontal and Tilt) Seasons: 2 (Dry and Raining) Sites: 6 Geo-Political Zones and main base of operation		

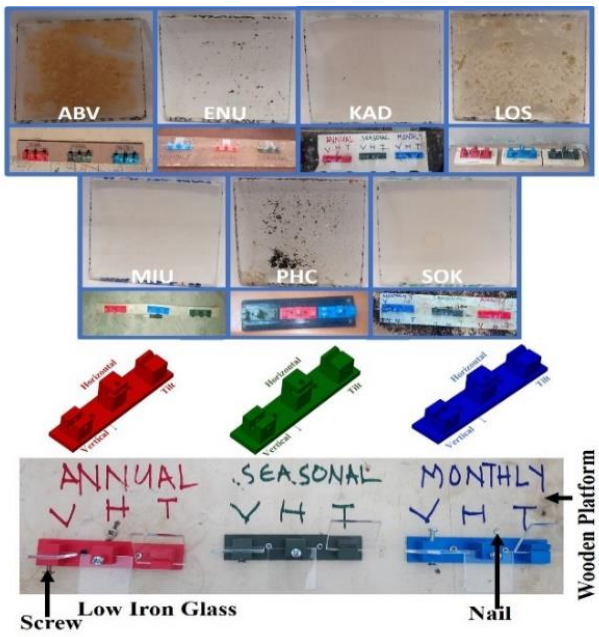

Figure 6.1: Digital image of soiled coupons for each region and a digital image of the soiling station set-up illustrating coupons' positioning.

6.2.1 Site

As earlier stated, coupons were deployed in seven locations (soiling stations) across the country; all the soiling stations and their specific coordinates are illustrated below.

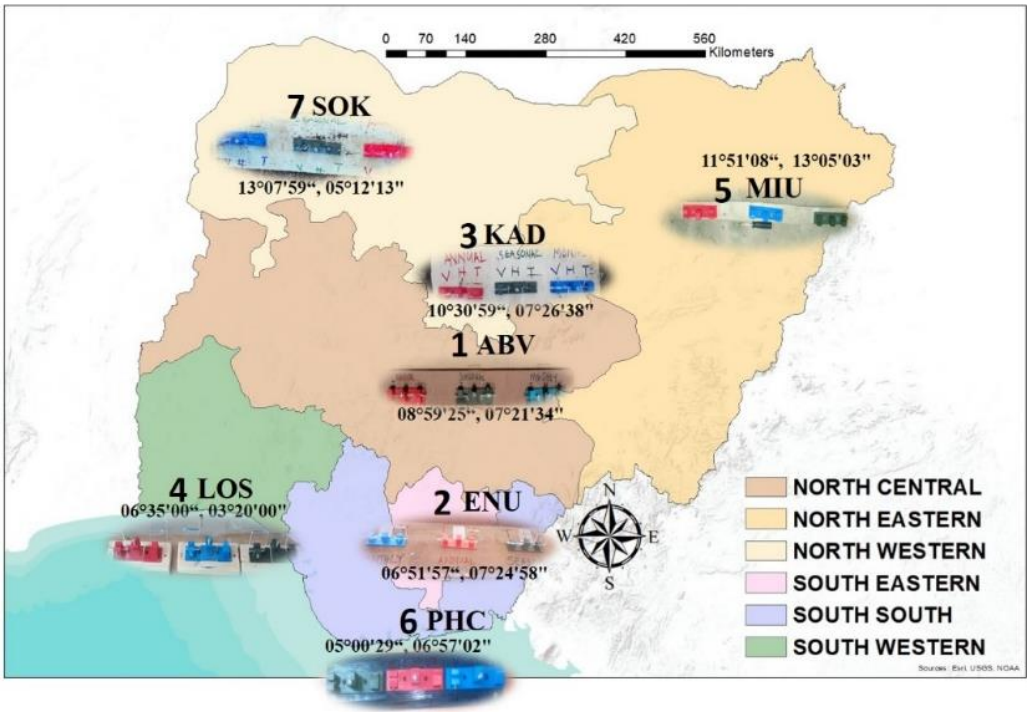

Figure 6.2: Map of Nigeria showing the geopolitical zone and their soiling stations.

Javed et al. (2017) reported that wind speed and humidity are the two most interactive variables that determine the rate at which airborne dust particles settle on a platform. Monthly average weather data (precipitation, sunny days, cloud, humidity, and wind) of the soiling stations sites are also provided in Figure 6.3, used for analysis purposes. The weather data showed periods when the dry, dusty weather condition occurred and periods when precipitation (mainly rainfall) happened, which can sometimes help remove or reduce the accumulated dust.

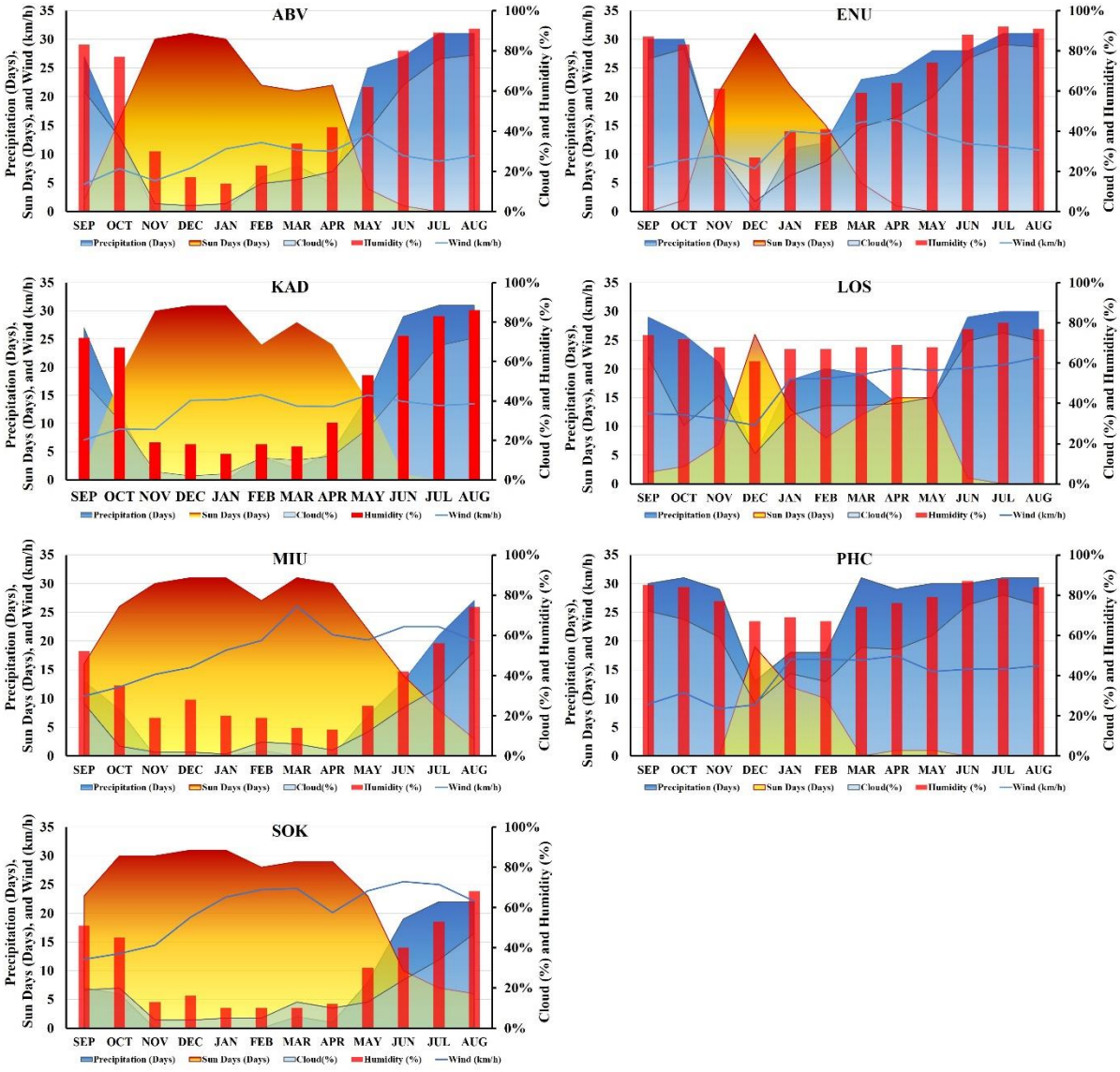

Figure 6.3: Monthly weather information variation for soiling stations sites (data obtained from World Weather Online, 2019).

6.2.2 Optical characterisation

The spectral characterisation was conducted to define the accumulated dust particles' transparency level on the various coupons. This experiment was

conducted when samples were brought back to the University of Exeter laboratory. Perkin Elmer Lambda 1050 UV/VIS/NIR spectrophotometer was employed to examine each exposed coupon. A clean coupon was usually examined at the beginning of every test to set a benchmark of the optimum transmittance level that could be achieved. Afterwards, each sample was then subjected to a transmittance measurement. NIR (Near Infra-Red), VIS (Visual) and UV (Ultraviolet) transmittance levels of each coupon are examined, ranging from 250 nm to 2500 nm wavelength. This wavelength range is considered to accommodate all the different PV technologies (solar cells) available in the market as they respond only within this spectrum. Results obtained in this experiment was validated using Equation (6.1) below, where S (λ) is the relative solar radiation wavelength distribution, Δλ is the change in wavelength, and T (λ) is the spectral transmission.

$$\boldsymbol{\tau_{solar}} = \frac{\sum_{\lambda=250nm}^{2500nm} \boldsymbol{S(\lambda)T(\lambda)\Delta\lambda}}{\sum_{\lambda=250nm}^{2500nm} \boldsymbol{S(\lambda)\Delta\lambda}} \tag{6.1}$$

Transmission losses were calculated using Equation (6.2) below, and the extreme optical losses results were used instead of average to accommodate a possible worst-case scenario. The results are presented in percentage reduction, where τ_{clean} is the transmittance data of clean coupon and τ_x is the transmittance data of an exposed coupon on a certain angle.

$$\Delta\tau_x = \frac{(\boldsymbol{\tau_{clean}} - \boldsymbol{\tau_x})}{\boldsymbol{\tau_{clean}}}(\%) \tag{6.2}$$

6.2.3 Particle characterisation

The sample particle characterisation was conducted to determine the chemical composition of dust particles in various soiling stations. One coupon with a high soiling rate for each of the various soiling stations was carefully selected and exposed to imaging characterisation. Each sample was initially prepared with carbon coating using an Emi-Tech K950 device before being subjected to microscopic scanning. The SEM (S) Quanta FEG 650 was employed to generate the secondary electron (SE) image and backscattered electrons (BSE) image that was used for further mineral data acquisition using the EDX (Energy Dispersive X-ray). The EDX generated graphs highlighting mineral samples elements and

their content level, which helped identify the various minerals' chemical composition. Minerals and their morphological characteristics such as diaphaneity were identified using online minerals databases such as minerals.net, mindat.org and webminerals.com.

Additional information regarding the air quality of various regions in Nigeria was obtained from the Air Plume lab. The data were required for in-depth analysis of suspended particles in the atmosphere across the various regions. Air quality data highlights aerosol particles' categories used to analyse and validate the SEM/EDX imaging and analysis minerals. Table 6.2 illustrates the Air Quality Index (AQI) of various regions and the primary pollutants.

6.2.4 Soiling mapping

This is a new approach for presenting PV soiling data. The coupon's transmittance data was collected from optical characterisation. PV output and direct normal irradiance data were collected from Global Solar Atlas, considering the small residential capacity of 1kWp. This data was used in calculating soiling losses, and the results were presented innovatively for easy understanding and further application. Linear interpolation was employed to determine the optical transmittance degradation of each soiling site's optimum PV tilt angle since coupons were not positioned at that angle. This interpolation technique was considered since it could establish data points whenever there are established discrete data points. Equation (6.3) below was employed to achieve this interpolation, where $\Delta_{\tau_{(Optimum)}}$ is the calculated change of transmittance of a coupon at an optimum angle, $\beta_{(x)}$ is the optimum tilt angle of a particular station, $\beta_{(45)}$ is the tilt angle described in this research where coupons are positioned as tilt which is 45°, $\beta_{(0)}$ is the horizontal angle which a coupon is positioned on the research jig in soiling stations, $\Delta_{\tau_{(0)}}$ is the optical loss recorded on a coupon positioned on a horizontal plane, and $\Delta_{\tau_{(45)}}$ is the optical loss recorded on the coupon positioned on the tilt angle plane (45°).

$$\Delta_{\tau_{(Optimum)}} = \frac{(\beta_{(x)} - \beta_{(45)})\,(\Delta_{\tau_{(0)}} - \Delta_{\tau_{(45)}})}{(\beta_{(0)} - \beta_{(45)})} + \Delta_{\tau_{(45)}} \tag{6.3}$$

ArcMap 10.6.1 from ArcGIS was employed to design the soiling map using the PV output and soiling losses data. ArcMap from ArcGIS is a software that provides the platform to present geographic information in layers and could be used to perform a wide range of GIS-related tasks, including compilation, organization, and modification of GIS datasets, use of geoprocessing for analytical and visual purposes (ArcGIS, 2018). The application is mainly used by government administrative established compared with MapBox, leaflet, and Google and has the highest market share in the mapping application industry (Enlyft, 2021). This application was employed in this study because it provides flexibility to create and edit datasets. The application is secured and requires a license for online access that allows users to load required real-world geographical information data (GIS-Geography, 2021). Three software's (ArcGIS, MapBox, and Tableau) were employed to develop the mapping, but the result was better achieved using the ArcGIS because of the advanced inbuild tools that support modification of datasets.

Kriging interpolation technique is an advanced geostatistical approach that generates an estimated surface from a given scattered set of points with z-values (Desktop.ArcGIS, 2016). This technique uses an interactive investigation of the spatial behaviour of the inputted data to select an excellent estimation for output generation. Desktop.ArcGIS (2016) provided a multistep process in achieving kriging interpolation, including exploratory statistical data analysis, variogram spatial structural modelling, creating the surface, and exploring surface variation. The main dissimilarity with other spatial interpolation techniques in ArcGIS, such as the inverse distance weighted (IDW) and Spline interpolation, is that it is not a deterministic approach based on surrounding values but a geostatistical approach that is based on a statistical model which includes autocorrelation, where it could produce a significant measure of accuracy during predictions (Desktop.ArcGIS, 2016). Krishnan and Ganguli (2021) reported that the Kriging interpolation model could provide high accuracy and lower computational cost for predicting distribution spatial frequencies compared to other deterministic techniques. Zhang et al. (2021) reported that kriging model fitting accuracy could reach up to 0.980. Fischer et al. (2021) supported this claim by examining three interpolation techniques (inverse distance weighted, ordinary Kriging, and

Empirical Bayesian Kriging), and the ordinary kriging consistently yielded more accurate results compared to others. The technique assumes the distance of sample points reflects spatial correlation to explain surface variance. It uses all points provided to generate output in a specified radius using a mathematical function of unbiasedness (Desktop.ArcGIS, 2016). Based on this literature and a comparative assessment using GSA map and its data (direct normal irradiance and PV performance with 4.5% soiling rate), the accuracy of IDW and kriging were investigated, and our finding shows that Kriging interpolation provides better map output that is more similar to the GSA map. As such, the technique was employed for generating soiling maps. An interpolation technique was employed, based on Equation (6.4) below provided by Venkatramanan et al. (2019). The Kriging interpolation is a geostatistical method that provides smooth estimates to determine an unknown spatial value of a location. Venkatramanan et al. (2019) defined Kriging interpolation as the best technique for unbiased linear estimation of unknown spatial values and temporal variables, where Z_K^* is the smooth estimate produced by Kriging interpolation, $\succ_i$ is the weight for Zi, which is to ensure unbiasedness of the estimation, and Zi is the variable.

$$Z_K^* = \sum_{i=1}^{n} \succ_i Zi \tag{6.4}$$

Equation (6.5) provided by Venkatramanan et al. (2019) represents the unbiased condition of Kriging interpolation, where Z_V is the actual value and the Z_K^* is the calculated estimated value, which is:

$$E\{Z_V - Z_K^*\} = 0 \tag{6.5}$$

Equation (6.6) provided by Venkatramanan et al. (2019) shows the summation of the weight $(\succ_i)$ which is:

$$\sum_{i=1}^{n} \succ_i = 1.0 \tag{6.6}$$

Equation (6.7) provided by Venkatramanan et al. (2019) shows the estimation variance of Kriging interpolation, where $\bar{C}(V, V)$ is the covariance between the

variables of the samples, μ is the Lagrange parameter, $\bar{C}(v_i, V)$ is the covariance between the estimations and the variables of the samples, which is:

$$\sigma_K^2 = E\left\{\left[Z_V - Z_K^*\right]^2\right\} = \bar{C}(V, V) + \mu - \sum_{i=1}^{n} \lambda_i \bar{C}(v_i, V)^{(4.4)} \quad (6.7)$$

6.3 Results

The spectrophotometer was employed to determine the transmittance losses on coupons, SEM/EDX were used to determine the soiled particle chemical composition, and ArcGIS (ArcMap 10.6.1) was employed to develop a soiling losses map. All the results are illustrated in this section.

6.3.1 Optical transmittance losses

The optical losses results are grouped in a period of exposure, and each group is further divided into subgroups based on their positioning angles. This is to illustrate transmittance losses of various locations at a glance for better understanding.

Figure 6.4 illustrates the annual transmittance losses results where the most significant loss of about 59% was recorded on the ABV coupon that was positioned on a horizontal plane, while the lowest loss was about 3% and was recorded on the MIU coupon that was positioned at a vertical angle.

The seasonal results are illustrated in two groups (the dry season and the wet season). Figure 6.4 illustrates the dry season transmittance losses results where the most significant loss of about 88% loss was recorded from the horizontally placed ABV coupon, while the lowest loss is about 4% from the vertically placed ENU coupon. On the other hand, Figure 6.4 illustrates wet season transmittance losses, and the most significant losses were recorded from LOS and PHC coupons positioned on horizontal planes, with the first having about 55% reduction and the latter having about 45%. The lowest transmittance losses for the wet season were recorded from KAD and MIU coupons, with both having about a 3% reduction when coupons were positioned vertically.

The monthly optical transmittance losses are presented based on the month of exposure and are further sub-divided into groups according to their positioning. Figure 6.5 shows optical losses during January, where the most significant loss of about 30% reduction was recorded from the LOS coupon when exposed horizontally. The lowest loss was about a 2% decrease and was recorded from both SOK and MIU's coupons when they were positioned vertically. The optical transmission results of coupons for February present the most significant optical losses when considering a monthly reduction. Figure 6.5 shows optical losses during February, where the most significant loss of about 38% reduction was recorded from the ABV coupon when positioned on a horizontal plane, and the lowest loss was about a 2% decrease from the LOS coupon when positioned vertically.

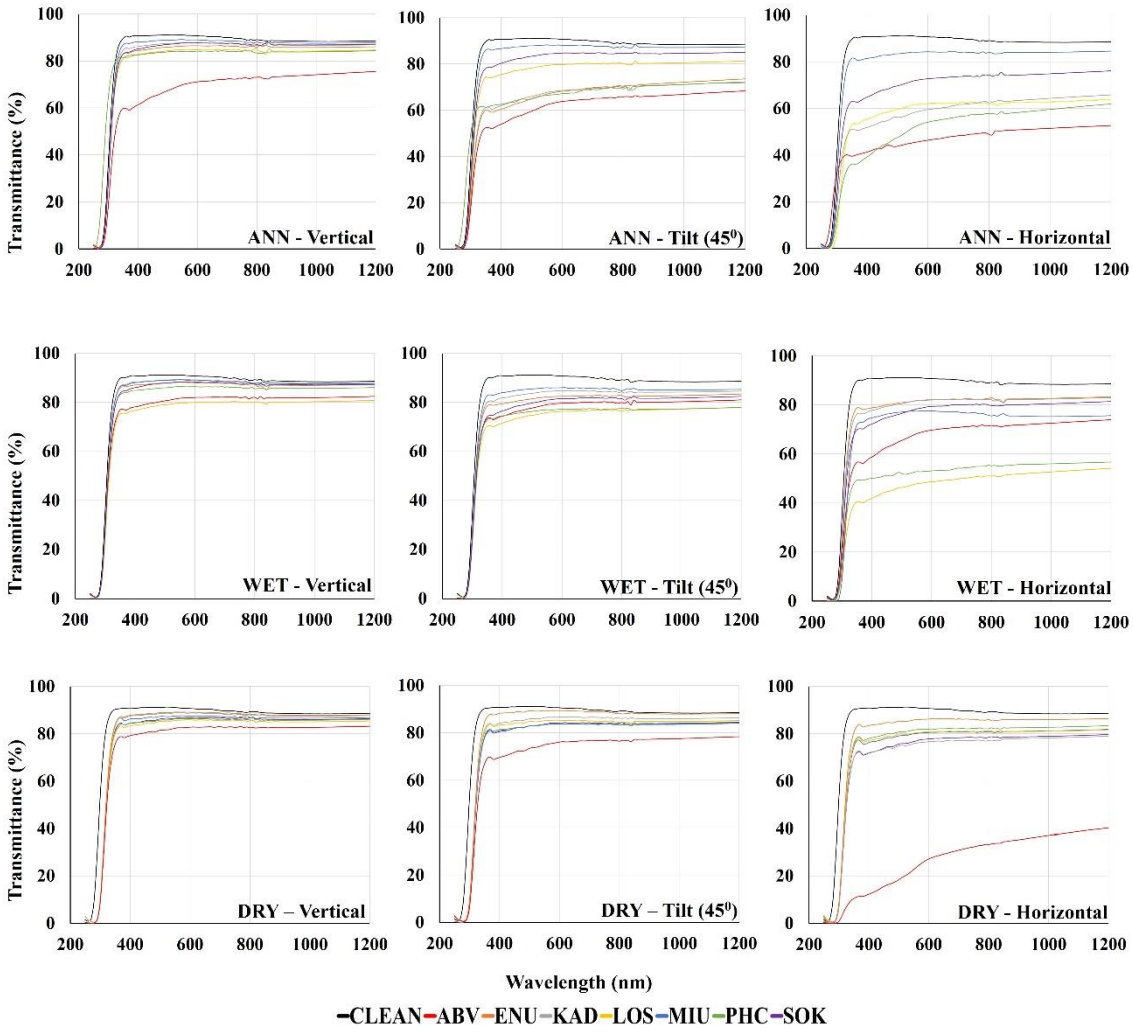

Figure 6.4: Annual (ANN) and seasonal (Dry and Wet) optical transmission losses variation of vertical, 45° tilt, and horizontal positioning orientation for regions in Nigeria.

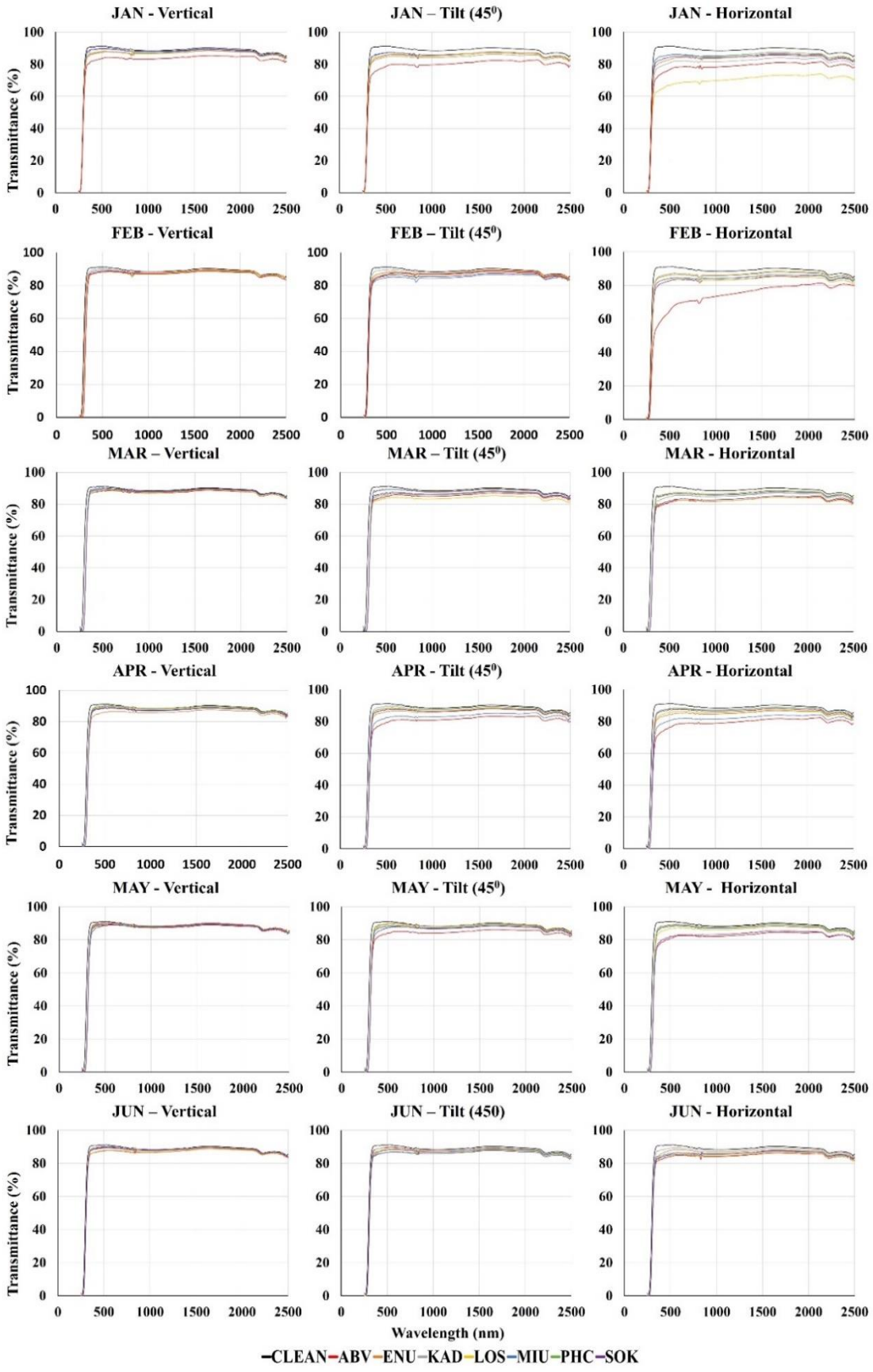

Figure 6.5: Monthly optical transmission losses from January to June of vertical, 45^{o} tilt and horizontal orientation for Nigeria.

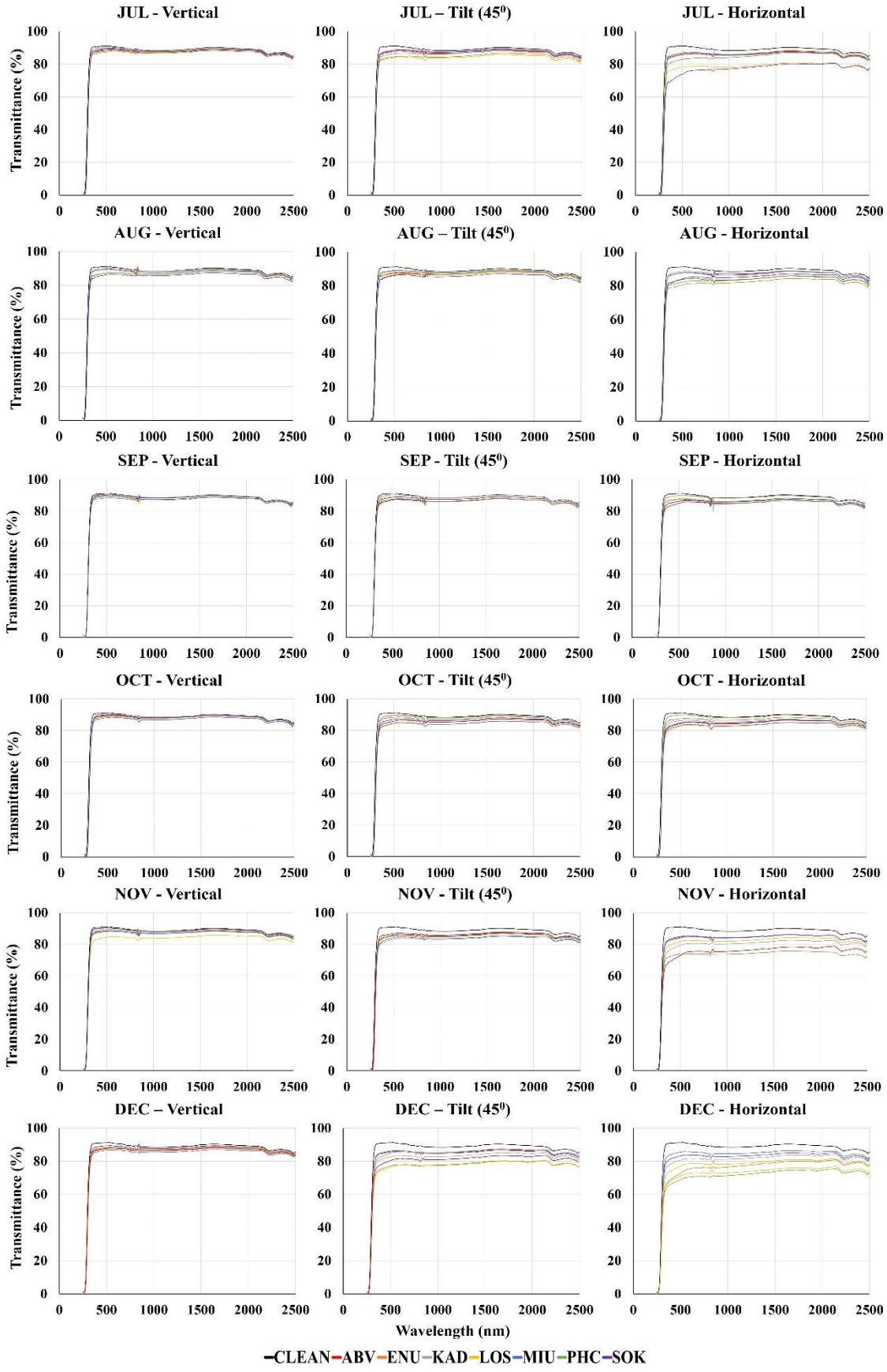

Figure 6.5: Monthly optical transmission losses from July to December of vertical, 45º tilt and horizontal orientation for Nigeria.

The optical results of coupons from March present significant optical losses. Figure 6.5 shows optical losses during March, with about 14% from the ABV coupon, 13% for SOK when both coupons were positioned on a horizontal plane. The lowest optical loss was about 2% and was recorded from the MIU coupon positioned vertically.

The optical transmission results of coupons for April present significant optical losses when considering a monthly reduction. Figure 6.5 shows optical losses during April, where the most significant loss of about 21% reduction was recorded from the ABV coupon when it was positioned on a horizontal plane. The lowest optical loss was about 2% less, and it was recorded from the KAD coupon when it was positioned vertically.

The optical transmission results of the coupons for May show significant optical losses when considering a monthly reduction. Figure 6.5 shows optical losses during May, where the most significant loss of about 21% was recorded on the ABV coupon when positioned on a horizontal plane. The lowest optical loss was about 2% less, and it was recorded from the KAD coupon when it was positioned vertically.

Figure 6.5 shows optical losses during June, where the maximum reduction of about 10% was recorded from the ABV coupon when it was positioned on a horizontal plane. The lowest optical loss was about 2% and was recorded from ABV and KAD's coupon when positioned vertically.

The optical transmission results of coupons for July present significant optical losses. Figure 6.5 shows optical losses during July, where the highest loss of about 24% was recorded from the SOK coupon when it was positioned on a horizontal plane. In July, the lowest transmittance loss was recorded from KAD's coupon, with a 3% reduction when the coupon was positioned at a vertical angle.

The optical transmission results of coupons for August present significant optical losses. Figure 6.5 shows optical losses during August, where the highest loss of about 13% was recorded on the ENU coupon when it was positioned on a

horizontal plane. In August, the lowest transmittance losses were recorded from the KAD's and LOS's coupons, with about a 2% reduction when the coupons were positioned at a vertical angle.

The optical transmission results of coupons for September present the overall lowest optical losses when considering a monthly reduction. Figure 6.5 shows optical losses during September, where the most significant loss of about 9% reduction was recorded on the ABV coupon when it was positioned on a horizontal plane. In September, the lowest transmittance losses were recorded from the ABV, ENU, and LOS coupons, with about 1% only when the coupons were positioned at a vertical angle.

The optical transmittance results for October coupons present significant losses. Figure 6.5 shows optical losses during October, where the most significant loss of about 12% was recorded on the LOS coupon when it was positioned on a horizontal plane. In October, the lowest transmittance losses were recorded from the ENU and KAD coupons, with about a 1% reduction only when the coupons were positioned at a vertical angle.

Figure 6.5 shows the optical losses during November, where the most significant loss of about 24% was recorded on the ABV coupon when it was positioned on a horizontal plane. In November, the lowest transmittance losses were recorded from the ENU and SOK coupons, with about a 1% reduction only when the coupons were positioned at a vertical angle.

Figure 6.5 shows optical losses during December, where a tremendous loss of about 28% reduction was recorded on the PHC coupon when positioned at the horizontal plane. In December, the lowest transmittance loss was recorded from the SOK coupon, with about a 3% reduction when positioned at a vertical angle.

6.3.2 Particle characterisation

This section presents the results of the SEM/EDX scanning. Figure 6.6 shows SEM images of particle samples with their various locations, highlighting their sizes and spaces occupied on the coupons. However, the backscattered electron images (BSE) were employed for in-depth analysis to determine the mineral

composition using EDX. Data obtained from the EDX analysis were employed to identify the essential mineral and their characteristics using the online mineral data databases such as minerals.net, mindat.org and webminerals.com.

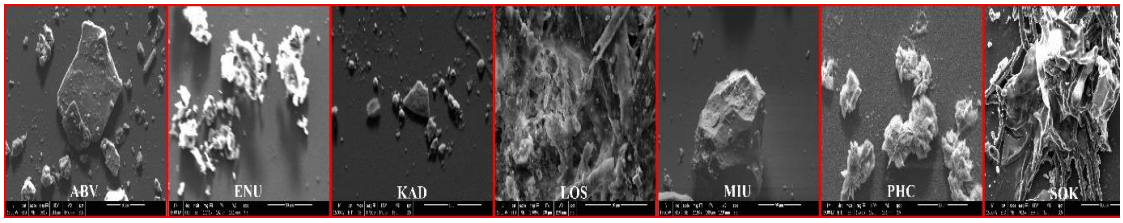

Figure 6.6: SEM imaging of accumulated particles on exposed and soiled coupon surfaces for all research sites.

A critical property (diaphaneity) of each identified mineral was investigated, and some of the minerals possess a characteristic that would have a negative implication on light transmittance. Table 6.2 highlights some minerals that were repeatedly identified during the particle characterisation. The Northern region results show the diaphaneity property of some minerals appear to be translucent and opaque for coupons from North-East and North-Central possess. In contrast, the coupons from North-West appears to have minerals with both transparent and translucent properties. In the Southern region, the result from Table 6.2 shows that the coupon from the South-East possesses minerals that appear to be transparent, translucent, and some are opaque. The South-South particles recorded on the coupon have minerals with opaque properties, while the minerals identified on the South-West coupon possess translucent and opaque transparency properties.

Table 6.2: Mineral and transparency characteristics.

S/N	Location Region Latitude/Longitude	Minerals	Diaphaneity	Annual Average Best day Worst day	Main Pollutant	
					AQI	µg/m³
1	**ABV (Abuja)** North Central **08°59'25" 07°21'34"**	Chlorite (Chamosite) Montmorillonite Pyroxene (Spodumene)	Translucent to sub-translucent Translucent to Opaque Transparent to Translucent	75 AQI Best – 17 AQI Worst – 330 AQI	PM_{10} – 343.701 $PM_{2.5}$ – 399.8376 SO_2 – 6.585912 CO – 9.989174 O_3 – 111.584 NO_2 – 19.28564	PM_{10} – 469.9216 $PM_{2.5}$ – 349.8376 SO_2 – 6.585912 CO – 1997.835 O_3 – 178.5344 NO_2 – 38.57129
2	**ENU (Enugu)** South East **06°51'57" / 07°24'58"**	Tourmaline (Dravite) Analcite Pectolite	Transparent to translucent to opaque Translucent Transparent to Translucent	75 AQI Best – 16 AQI Worst – 399 AQI	PM_{10} – 450.6894 $PM_{2.5}$ – 524.9337 SO_2 – 21.14407 CO – 22.21146 O_3 – 111.551 NO_2 – 46.64713	PM_{10} – 641.1031 $PM_{2.5}$ – 474.9337 SO_2 – 24.00424 CO – 4398.062 O_3 – 178.4817 NO_2 – 75.5295
3	**KAD (Kaduna)** North West Main Base **10°30'59" / 07°26'38"**	Tourmaline Chlorite (chamosite) Garnet (almandine)	Translucent to opaque Translucent to sub-translucent Transparent to Translucent	96 AQI Best – 22 AQI Worst – 388 AQI	PM_{10} – 415.8191 $PM_{2.5}$ – 394.7018 SO_2 – 32.1398 CO – 15.90905 O_3 – 94.59928 NO_2 – 26.87789	PM_{10} – 585.3105 $PM_{2.5}$ – 344.7018 SO_2 – 62.4893 CO – 3181.81 O_3 – 153.5191 NO_2 – 49.17053
4	**LOS (Lagos)** South West **06°35'00" / 03°20'00"**	Stilpnomelane Beryl Amphibole	Subtranslucent to opaque Transparent to subtranslucent Translucent to Subopaque	65 AQI Best – 14 AQI Worst – 392 AQI	PM_{10} – 322.2883 $PM_{2.5}$ – 336.3448 SO_2 – 51.97719 CO – 72.08806 O_3 – 170.9607 NO_2 –73.71526	PM_{10} – 435.6612 $PM_{2.5}$ – 286.3448 SO_2 – 133.8973 CO – 8278.764 O_3 – 273.5371 NO_2 – 136.9166
5	**MIU (Maiduguri)** North East 11°51'08" / 13°05'03"	Zeolite (Clinoptilite) Ilmenite Illite	Transparent Opaque Translucent	117 AQI Best – 21 AQI Worst – 562 AQI	PM_{10} – 362.8626 $PM_{2.5}$ – 455.5584 SO_2 – 12.57944 CO – 8.919709 O_3 – 90.81521 NO_2 – 19.40652	PM_{10} – 500.5801 $PM_{2.5}$ – 405.5584 SO_2 – 12.57944 CO – 1783.942 O_3 – 148.9783 NO_2 – 38.81303
6	**PHC (Port Harcourt)** South-South **05°00'29" / 06°57'02"**	Felspar (albite) Schorlomite Scapolite	Transparent, Translucent Opaque Translucent to Opaque	62 AQI Best – 13 AQI Worst – 321 AQI	PM_{10} – 322.2219 $PM_{2.5}$ – 366.4977 SO_2 – 32.53361 CO – 17.73402 O_3 – 122.8129 NO_2 – 41.3967	PM_{10} – 435.555 $PM_{2.5}$ – 316.4977 SO_2 – 63.86763 CO – 3546.805 O_3 – 196.5006 NO_2 – 68.52894
7	**SOK (Sokoto)** North West **13°07'59" / 05°12'13"**	Chlorite (Chamosite) Montmorillonite Feldspar (labradorite)	Translucent to subtranslucent Translucent to Opaque Translucent to transparent	95 AQI Best – 20 AQI Worst – 418 AQI	PM_{10} – 557.227 $PM_{2.5}$ – 369.7053 SO_2 – 14.13457 CO – 12.26496 O_3 – 128.1533 NO_2 – 41.19882	PM_{10} – 811.5631 $PM_{2.5}$ – 319.7053 SO_2 – 14.13457 CO – 2452.992 O_3 – 205.0454 NO_2 – 68.2651

6.3.3 Soiling mapping

This is the cartography of presenting regional PV performance data and highlighting soiling losses for enhanced illustration. In combination with PV Output data obtained from the Global Solar Atlas, the transmission losses were used to develop a new soiling losses map for Nigeria. Since the PV output collected from Global solar was based on each location's optimum angle, a linear interpolation was employed to obtain optical transmission losses data at the optimum angle, which is comprehensively explained in the methodology section of this chapter of the thesis.

The soiling maps are grouped based on the period of exposure (monthly, seasonally, and yearly), as highlighted in Table 6.1. Each group includes a direct normal irradiance (GSA, 2020), PV output without soiling, and PV output with soiling based on the transmission losses data presented above, and the PV output with a constant 4.5% soiling value provided by GSA (2020). This is employed to illustrate solar energy potential and the variation between this study's result and the Global Solar Atlas website's information. This approach is more illustrative and descriptive such that a reader can visualise the losses disparity at a glance for a better understanding.

The annual soiling mapping shows significant soiling losses in the South-East, South-West, South-South, and North-Central. Figure 6.7 (a) illustrates the country's annual solar energy potential, while Figure 6.7 (b) shows the annual PV output potential with no soiling. Figure 6.7 (c) illustrates the annual soiling losses determined through optical losses, which show the most significant soiling loss was recorded in North-Central where the initial PV output degraded from about 1505.76 kWh/kWp to 691.3 kWh/kWp and the lowest loss was recorded in the North-East region where initial PV output decreased from 1705.76 kWh/kWp to about 1554.52 kWh/kWp. Figure 6.7 (d) shows the annual PV output reduction due to constant soiling losses value (4.5%) where the greatest was observed to be in the North-East region with PV yield degradation from 1705.76 kWh/kWp to about 1629 kWh/kWp, and the lowest reduction was in the South-West where the reduction was from 1299.48 kWh/kWp to about 1241 kWh/kWp.

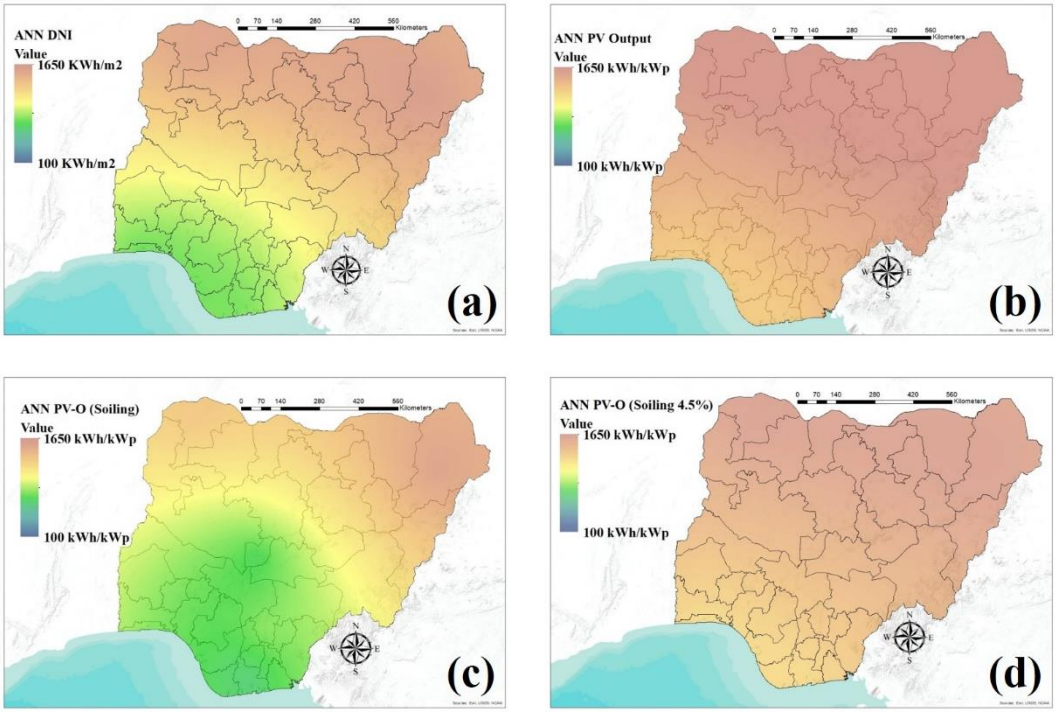

Figure 6.7: Annual mapping illustrating a regional variation of DNI potential and PV output for Nigeria highlighting soiling losses disparity – (a) DNI (b) PV Output (c) PV Output with soiling (d) PV Output with 4.5% soiling.

The seasonal soiling mapping results show a significant variation in soiling losses during the two seasons across regions. Figure 6.8 (a) illustrates solar energy potential for the country's dry season, while Figure 6.8 (b) shows the dry season's PV output potential without soiling. Figure 6.8 (c) illustrates the soiling losses, which show the most significant soiling loss determined using optical losses data that was recorded in North-Central where the PV output decrease from about 818.53 kWh/kWp to 245.56 kWh/kWp and the lowest loss was recorded in the South-South region where PV output reduced from 240.6 kWh/kWp to about 204.5 kWh/kWp. Figure 6.8 (d) shows PV output reduction due to soiling losses where the most significant reduction was observed in the North-East region from 1064.1 kWh/kWp to about 1016.2 kWh/kWp, and the lowest reduction was from South-South where the reduction was from 240.6 kWh/kWp to about 229.8 kWh/kWp.

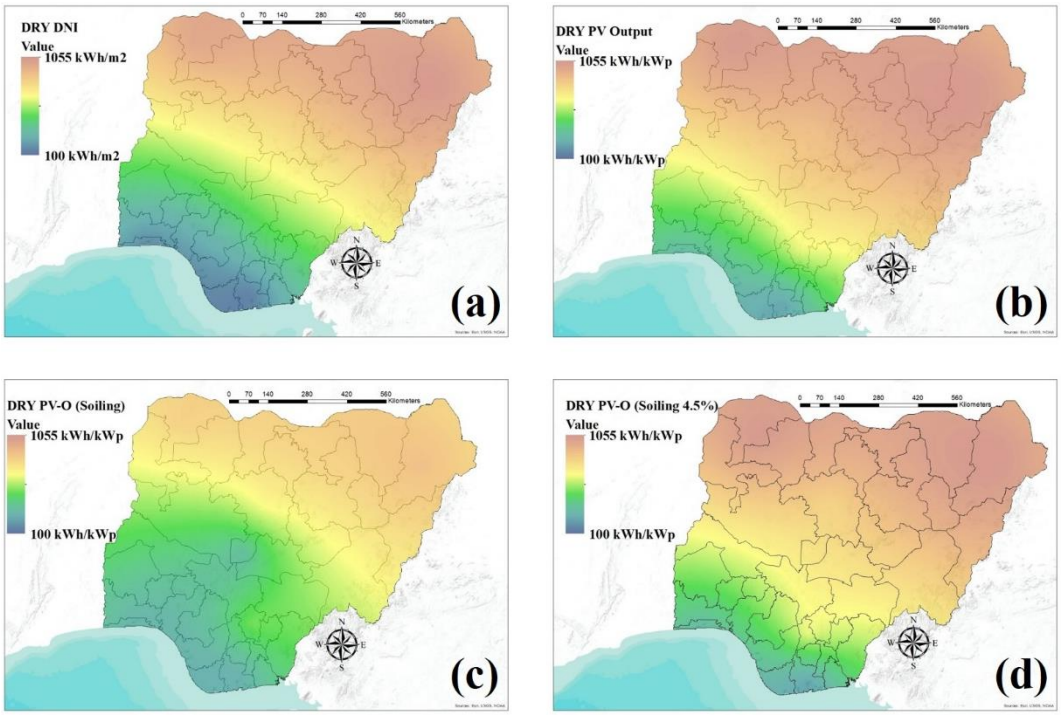

Figure 6.8: Dry seasonal mapping illustrating a regional variation of DNI potential and PV output for Nigerian highlighting soiling losses disparity – (a) DNI (b) PV Output (c) PV Output with soiling (d) PV Output with 4.5% soiling.

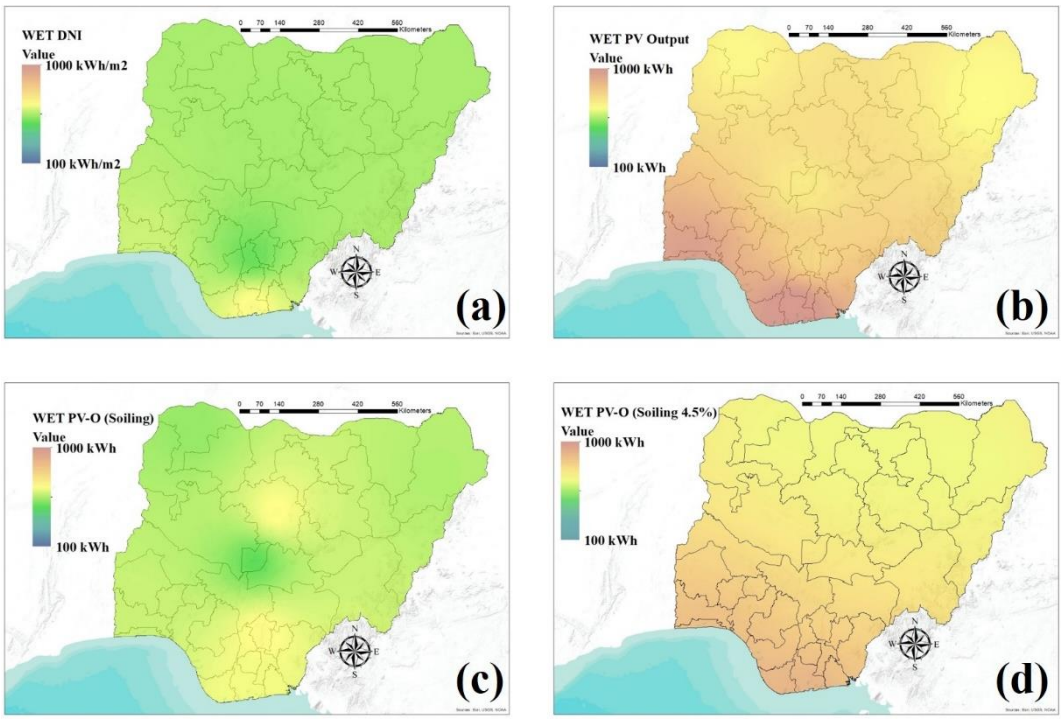

Figure 6.9: Wet seasonal mapping illustrating a regional variation of DNI potential and PV output for Nigeria highlighting soiling losses disparity – (a) DNI (b) PV Output (c) PV Output with soiling (d) PV Output with 4.5% soiling.

On the other hand, Figure 6.9 (a) illustrates solar energy potential for the wet season in the country, while Figure 6.9 (b) shows PV output potential for the wet season without soiling. Figure 6.9 (c) illustrates the PV yield with soiling losses for the wet season. It shows the most significant soiling loss determined using optical loss data were recorded in South-South, where the PV output decreased from about 1063.4 kWh/kWp to about 627.4 kWh/kWp, and the lowest loss was recorded in the North-East region where PV output reduced from 641.3 kWh/kWp to about 551.5 kWh/kWp. Figure 6.9 (d) shows the wet season PV output with constant soiling losses rate (4.5%), where the most significant reduction was recorded in the South-South region from 1063.4 kWh/kWp to about 1015.5 kWh/kWp, and the lowest reduction was from the North-East where the reduction was from 641.3 kWh/kWp to about 612.4 kWh/kWp.

The monthly results show different rates of soiling losses for each month. Consequently, the results are shown in month-based maps. Figure 6.10 (a) illustrates the January solar energy potential of the country, while Figure 6.10 (b) shows the January PV output potential without soiling. Figure 6.10 (c) illustrates the January soiling losses determined using optical losses, which show the most significant soiling loss was recorded in the South-West where the initial PV output degraded from about 112.4 kWh/kWp to 82.49 kWh/kWp and the lowest loss was recorded in the South-South region where initial PV output decreased from 116.4 kWh/kWp to about 108.29 kWh/kWp. Figure 6.10 (d) shows the January PV output with constant soiling losses rate (4.5%) where the greatest was observed in the North-East region from 160.5 kWh/kWp to about 153.3 kWh/kWp, and the lowest reduction was in the South-West where the reduction was from 112.4 kWh/kWp to about 107.3 kWh/kWp.

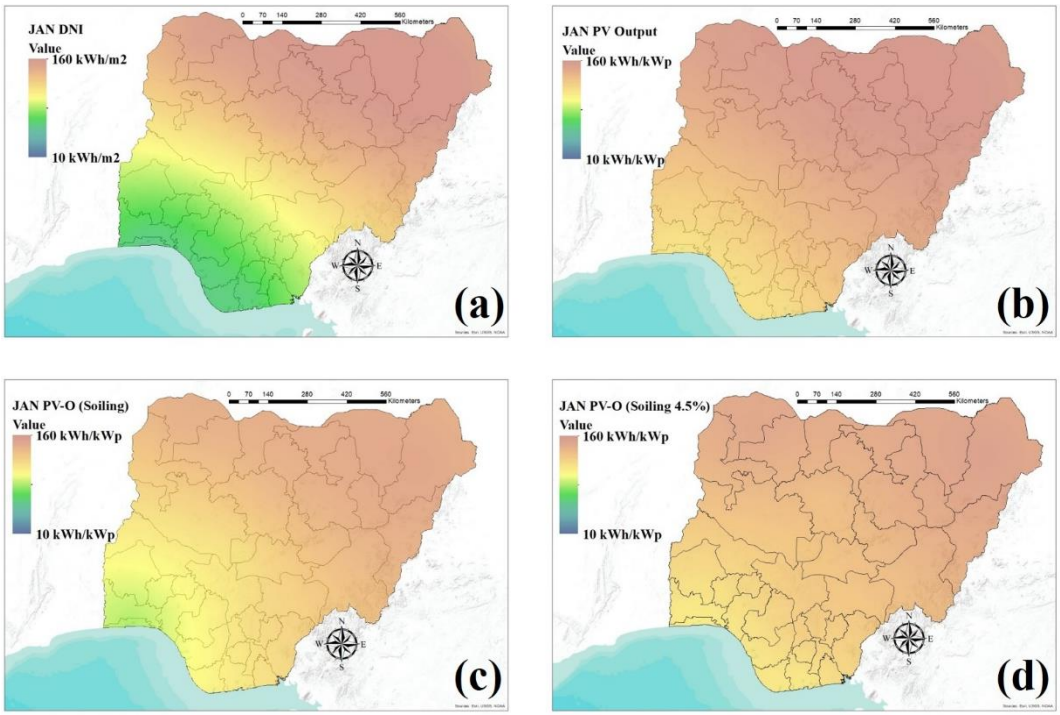

Figure 6.10: January mapping illustrating a regional variation of DNI potential and PV output for Nigeria highlighting soiling losses disparity – (a) DNI (b) PV Output (c) PV Output with soiling (d) PV Output with 4.5% soiling.

Figure 6.11 (a) illustrates the February solar energy potential of the country, while Figure 6.11 (b) shows the February PV output potential without soiling losses. Figure 6.11 (c) illustrates the February PV output with soiling losses determined using optical losses data. It shows the most significant soiling loss was recorded in North-Central where the initial PV output degraded from about 125.0 kWh/kWp to 88.35 kWh/kWp, and the lowest loss was recorded in the South-South region where initial PV output decreased from 104.5 kWh/kWp to about 97.33 kWh/kWp. Figure 6.11 (d) shows the February PV output with a constant soiling losses value (4.5%) where the greatest was observed in the North-East region from 143.4 kWh/kWp to about 136.9 kWh/kWp, and the lowest reduction was in the South-South where the reduction was from 104.5 kWh/kWp to about 99.8 kWh/kWp.

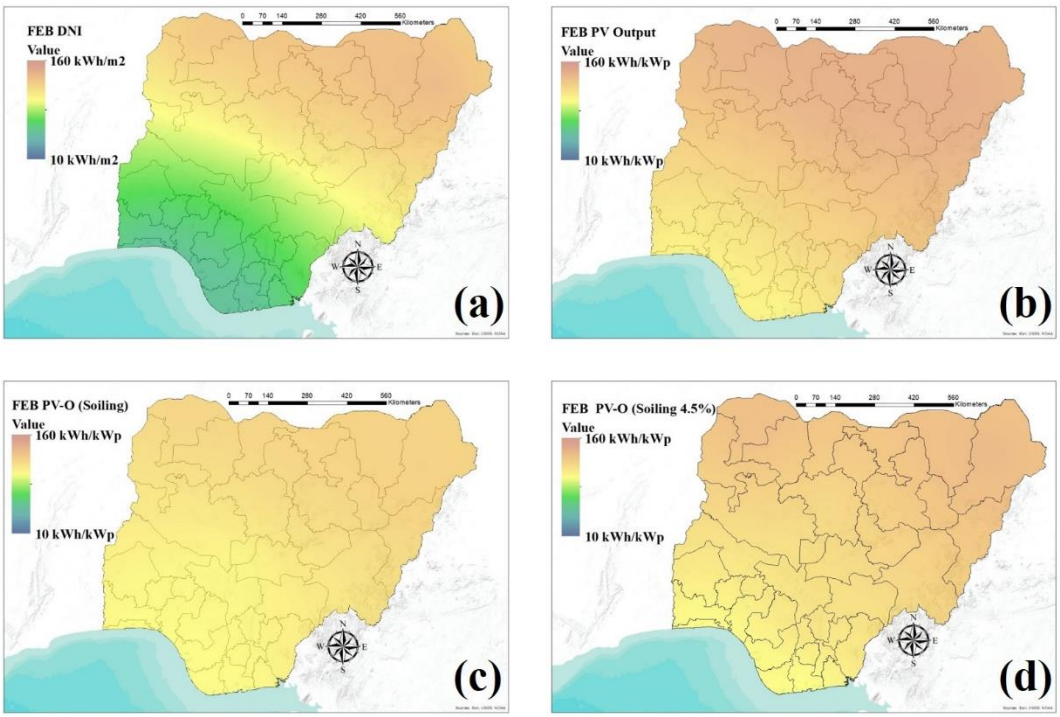

Figure 6.11: February mapping illustrating a regional variation of DNI potential and PV output for Nigeria highlighting soiling losses disparity – (a) DNI (b) PV Output (c) PV Output with soiling (d) PV Output with 4.5% soiling.

Figure 6.12 (a) illustrates the March solar energy potential of the country, while Figure 6.12 (b) shows the March PV output potential without soiling losses. Figure 6.12 (c) illustrates the March soiling losses determined using optical losses data, which show that the most significant soiling loss was recorded in North-Central where the PV output degraded from about 133.1 kWh/kWp to 116.06 kWh/kWp and the lowest loss was recorded in the South-East region where PV output decreased from 121.0 kWh/kWp to about 113.98 kWh/kWp. Figure 6.12 (d) shows the March PV output with a constant soiling losses value (4.5%), where the most significant PV yield reduction was observed in the North-East region from 150.0 kWh/kWp to about 143.5 kWh/kWp, and the lowest reduction was in the South-South where the reduction was from 108.9 kWh/kWp to about 104.2 kWh/kWp.

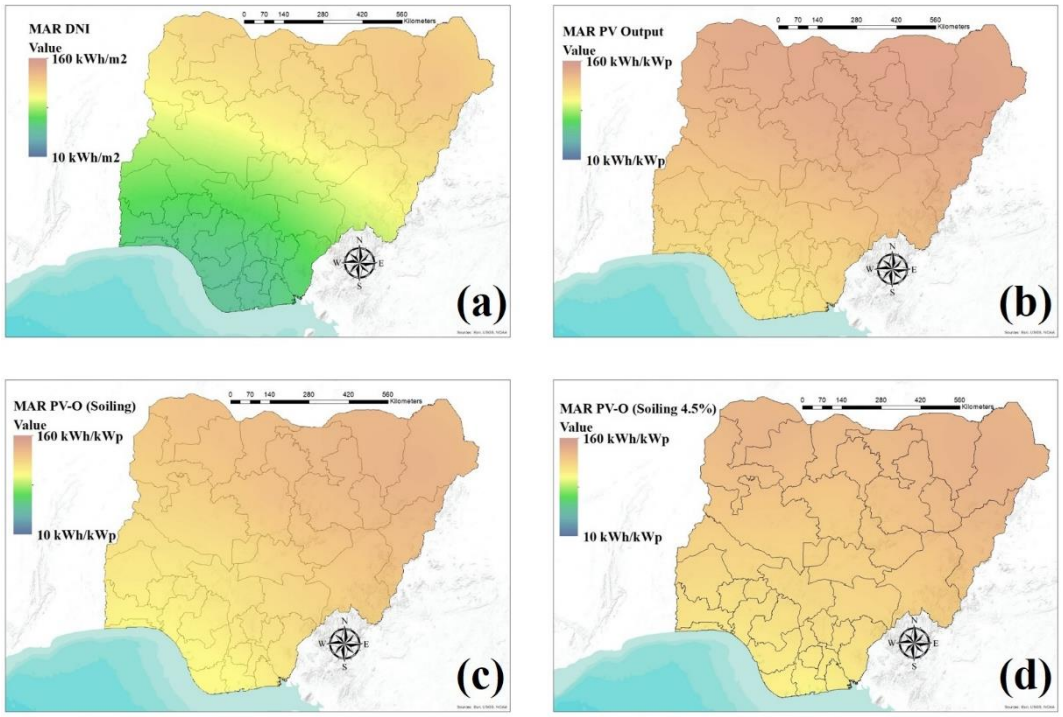

Figure 6.12: March mapping illustrating a regional variation of DNI potential and PV output for Nigeria highlighting soiling losses disparity – (a) DNI (b) PV Output (c) PV Output with soiling (d) PV Output with 4.5% soiling.

Figure 6.13 (a) illustrates the April solar energy potential of the country, while Figure 6.13 (b) shows the April PV output potential without soiling. Figure 6.13 (c) illustrates the April soiling losses determined using optical losses, which show the most significant soiling loss was recorded in North-Central where the initial PV output degraded from about 123.1 kWh/kWp to 98.5 kWh/kWp and the lowest loss was recorded in the North-West (KAD) region where initial PV output decreased from 134.0 kWh/kWp to about 128.7 kWh/kWp. Figure 6.13 (d) shows the April PV output reduction due to constant soiling losses value (4.5%) where the greatest was observed in the far North-West region (SOK) from 137.0 kWh/kWp to about 130.8 kWh/kWp, and the lowest reduction was in the South-South where the reduction was from 113.5 kWh/kWp to about 108.4 kWh/kWp.

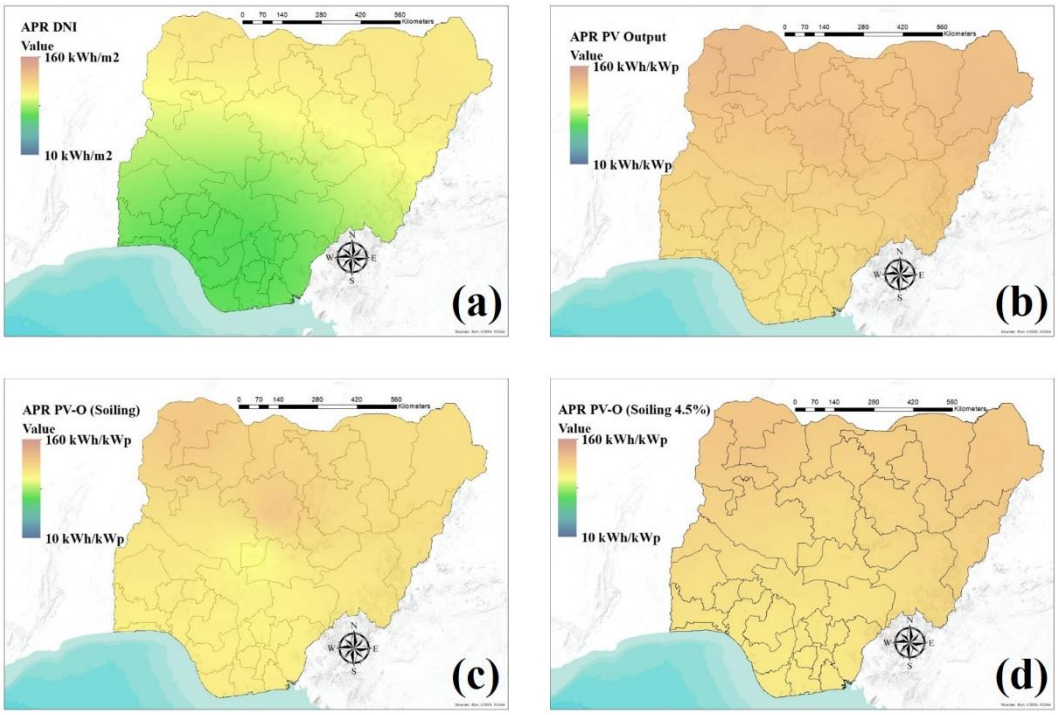

Figure 6.13: April mapping illustrating a regional variation of DNI potential and PV output for Nigeria highlighting soiling losses disparity – (a) DNI (b) PV Output (c) PV Output with soiling (d) PV Output with 4.5% soiling.

Figure 6.14 (a) illustrates the month of May solar energy potential of the country, while Figure 6.14 (b) shows the month of May PV output potential without soiling losses. Figure 6.14 (c) illustrates the month of May PV yield with soiling losses determined using optical losses data, which show the most significant soiling loss was recorded in North-Central where the PV output degraded from about 123.1 kWh/kWp to 104.7 kWh/kWp and the lowest loss was recorded in the South-East region where PV output decreased from 115.7 kWh/kWp to about 112.4 kWh/kWp. Figure 6.14 (d) shows the month of May PV output with a constant soiling losses value (4.5%) where the greatest was observed in the North-West region (KAD) from 134.0 kWh/kWp to about 124.8 kWh/kWp, and the lowest reduction was in the South-South where the reduction was from 113.5 kWh/kWp to about 108.7 kWh/kWp.

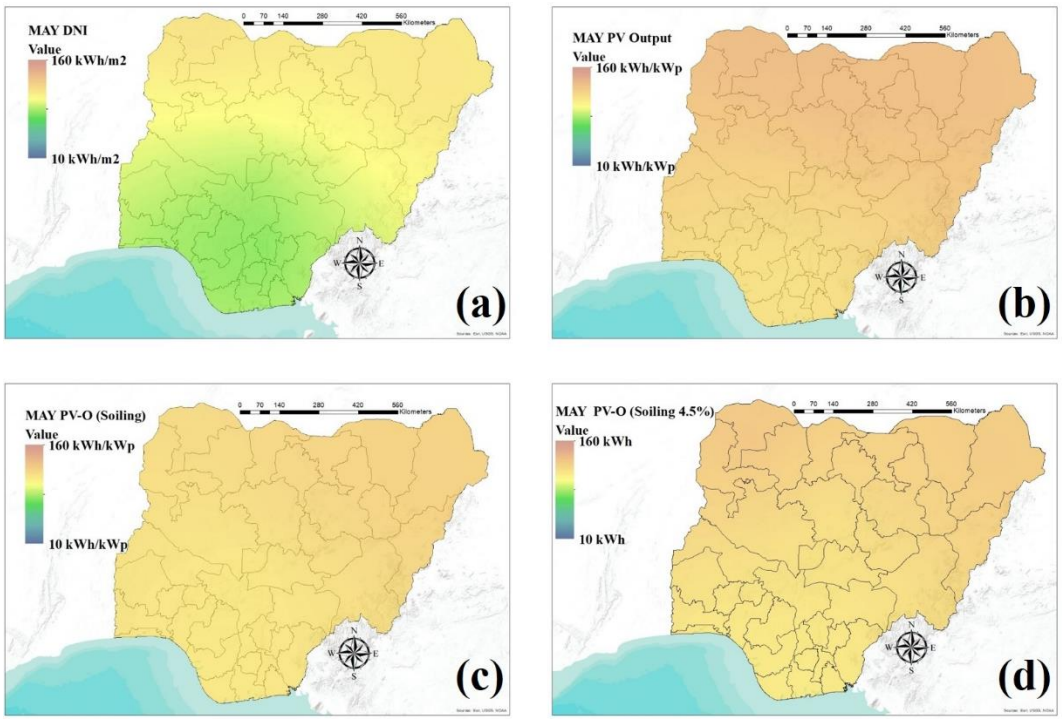

Figure 6.14: May mapping illustrating a regional variation of DNI potential and PV output for Nigeria highlighting soiling losses disparity – (a) DNI (b) PV Output (c) PV Output with soiling (d) PV Output with 4.5% soiling.

Figure 6.15 (a) illustrates the month of June solar energy potential of the country, while Figure 6.15 (b) shows the PV output potential without soiling for June. Figure 6.15 (c) illustrates the PV output with soiling losses determined using optical losses for June, which show that the most significant soiling loss was recorded in the far North-West (SOK), where the PV output degraded from about 127.4 kWh/kWp to 117.2 kWh/kWp. The lowest loss was recorded in the North West region (KAD), where PV output decreased from 117.3 kWh/kWp to about 112.6 kWh/kWp. Figure 6.15 (d) shows the PV output with a constant soiling losses value (4.5%) for June, where the greatest was observed in the far North-West region (SOK) from 127.4 kWh/kWp to about 121.7 kWh/kWp, and the lowest reduction was in the South-West where the reduction was from 97.0 kWh/kWp to about 92.6 kWh/kWp.

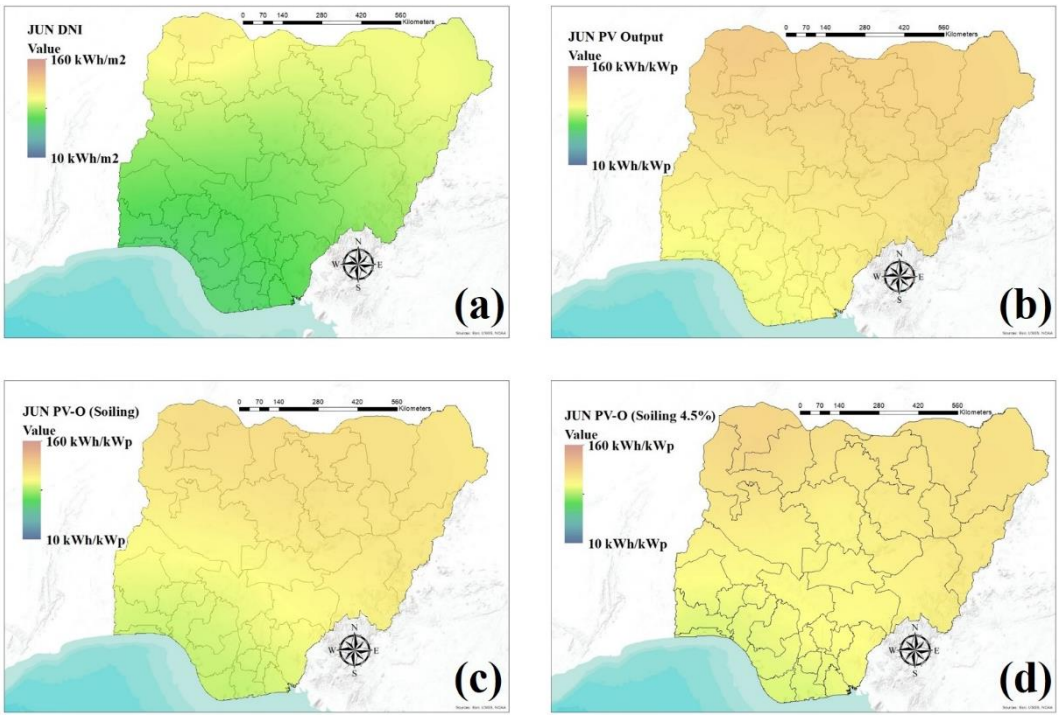

Figure 6.15: June mapping illustrating a regional variation of DNI potential and PV output for Nigeria highlighting soiling losses disparity – (a) DNI (b) PV Output (c) PV Output with soiling (d) PV Output with 4.5% soiling.

Figure 6.16 (a) illustrates the month of July solar energy potential of the country, while Figure 6.16 (b) shows the July PV output potential without soiling losses. Figure 6.16 (c) illustrates the July soiling losses determined using optical loss data, which show that the most significant soiling loss was recorded in the far North-West (SOK), where the PV output degraded from 129.84 kWh/kWp to 107.77 kWh/kWp. The lowest loss was recorded in the North-Central region, where PV output decreased from 104.61 kWh/kWp to about 98.33 kWh/kWp. Figure 6.16 (d) shows the July PV output with a constant soiling losses value (4.5%), where the most significant PV degradation was observed in the far North-West region (SOK) from 129.84 kWh/kWp to about 107.77 kWh/kWp, and the lowest reduction was in the North-Central where the reduction was from 104.61 kWh/kWp to about 99.9 kWh/kWp.

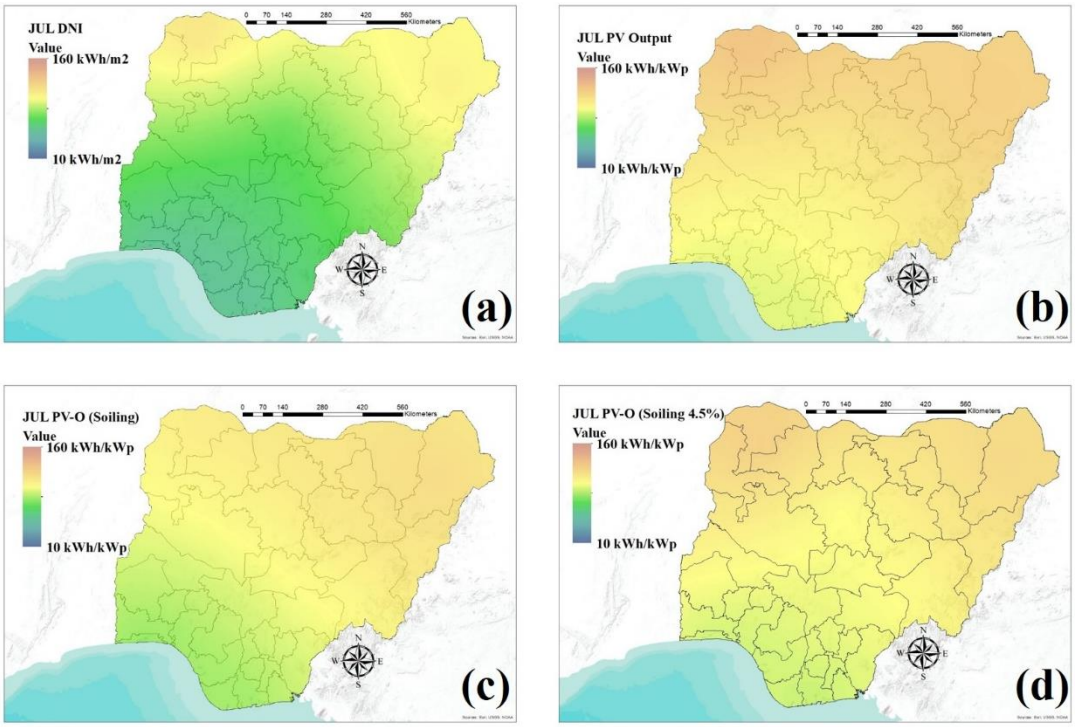

Figure 6.16: July mapping illustrating a regional variation of DNI potential and PV output for Nigeria highlighting soiling losses disparity – (a) DNI (b) PV Output (c) PV Output with soiling (d) PV Output with 4.5% soiling.

Figure 6.17 (a) illustrates the August solar energy potential of the country, while Figure 6.17 (b) shows the August PV output potential without soiling losses. Figure 6.17 (c) illustrates the August PV output with soiling losses determined using optical losses data. The map shows the most significant soiling loss was recorded in the far North-West (SOK), where the PV output degraded from about 126.2 kWh/kWp to 113.6 kWh/kWp. The lowest loss was recorded in the North-West (KAD) region, which decreased from 107.3 kWh/kWp to about 103.04 kWh/kWp. Figure 6.17 (d) shows the August PV output with a constant soiling losses value (4.5%) where the most significant PV yield degradation was observed in the far North-West region (SOK) from 126.2 kWh/kWp to about 120.5 kWh/kWp, and the lowest reduction was in the South-East where the reduction was from 94.9 kWh/kWp to about 90.6 kWh/kWp.

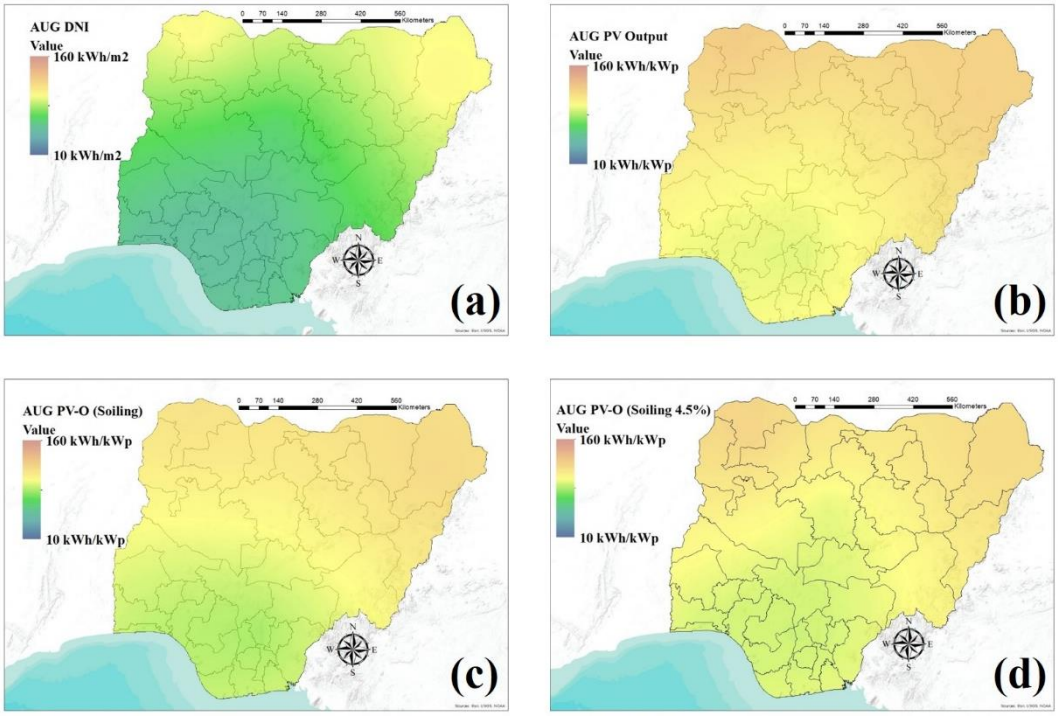

Figure 6.17: August mapping illustrating a regional variation of DNI potential and PV output for Nigeria highlighting soiling losses disparity – (a) DNI (b) PV Output (c) PV Output with soiling (d) PV Output with 4.5% soiling.

Figure 6.18 (a) illustrates the September solar energy potential of the country, while Figure 6.18 (b) shows the September PV output potential without soiling losses. Figure 6.18 (c) illustrates the September PV output with soiling losses determined using optical losses data, which show that the most significant soiling loss was recorded in North-Central where the PV output degraded from about 115.3 kWh/kWp to 105.91 kWh/kWp and the lowest loss was recorded in the South-West region where PV output decreased from 100.0 kWh/kWp to about 98.00 kWh/kWp. Figure 6.18 (d) shows the September PV output with a constant soiling losses value (4.5%) where the most significant PV degradation was observed in the far North-West region (SOK) from 141.4 kWh/kWp to about 135 kWh/kWp, and the lowest reduction was in the South-West region, where the reduction was from 100.0 kWh/kWp to about 95.5 kWh/kWp.

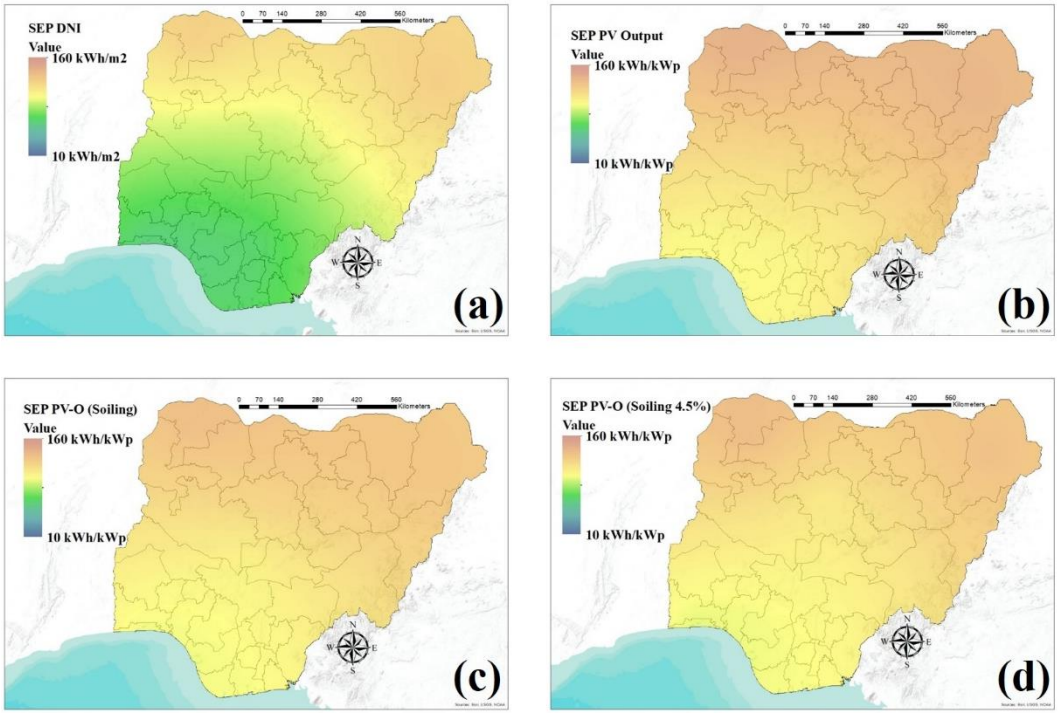

Figure 6.18: September mapping illustrating a regional variation of DNI potential and PV output for Nigeria highlighting soiling losses disparity – (a) DNI (b) PV Output (c) PV Output with soiling (d) PV Output with 4.5% soiling.

Figure 6.19 (a) illustrates the October solar energy potential of the country, while Figure 6.19 (b) shows the October PV output potential without soiling losses. Figure 6.19 (c) illustrates the October PV output with soiling losses determined using optical losses data, which show that the most significant soiling loss was recorded in North-East where the PV output degraded from about 155.0 kWh/kWp to 139.48 kWh/kWp. Furthermore, the lowest loss was recorded in the South-East region, where PV output decreased from 118.3 kWh/kWp to about 114.77 kWh/kWp. Figure 6.19 (d) shows the October PV output reduction with a constant soiling losses value (4.5%) where the greatest was observed in the North-East region from 155.0 kWh/kWp to about 148.0 kWh/kWp, and the lowest reduction was in the South-East where the reduction was from 118.3 kWh/kWp to about 113 kWh/kWp.

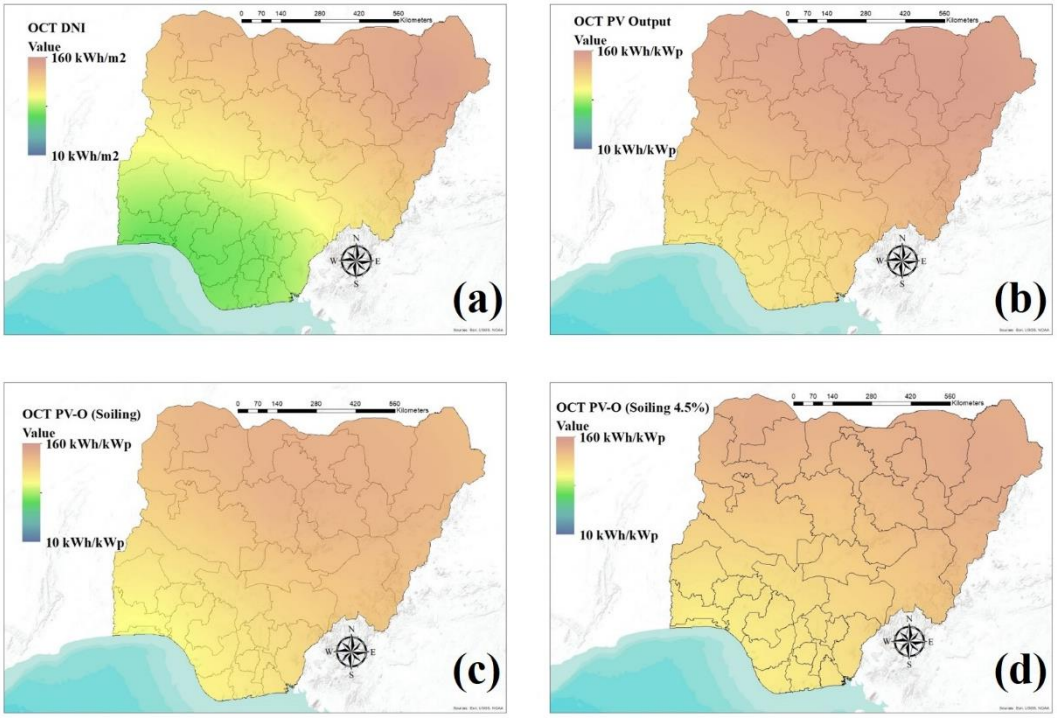

Figure 6.19: October mapping illustrating a regional variation of DNI potential and PV output for Nigeria highlighting soiling losses disparity – (a) DNI (b) PV Output (c) PV Output with soiling (d) PV Output with 4.5% soiling.

Figure 6.20 (a) illustrates the November solar energy potential of the country, while Figure 6.20 (b) shows the November PV output potential without soiling losses. Figure 6.20 (c) illustrates the November PV output with soiling losses determined using optical losses, which show that the most significant soiling loss was recorded in North-Central, where the PV output degraded from about 149.7 kWh/kWp to 121.15 kWh/kWp. Furthermore, the lowest loss was recorded in the far North-West (SOK) region, where the PV output decreased from 151.3 kWh/kWp to about 139.4 kWh/kWp. Figure 6.20 (d) shows the November PV output with a constant soiling losses value (4.5%) where the greatest was observed in the North-West (KAD) region from 156.9 kWh/kWp to about 149.8 kWh/kWp, and the lowest reduction was in the South-West where the reduction was from 112.3 kWh/kWp to about 107.2 kWh/kWp.

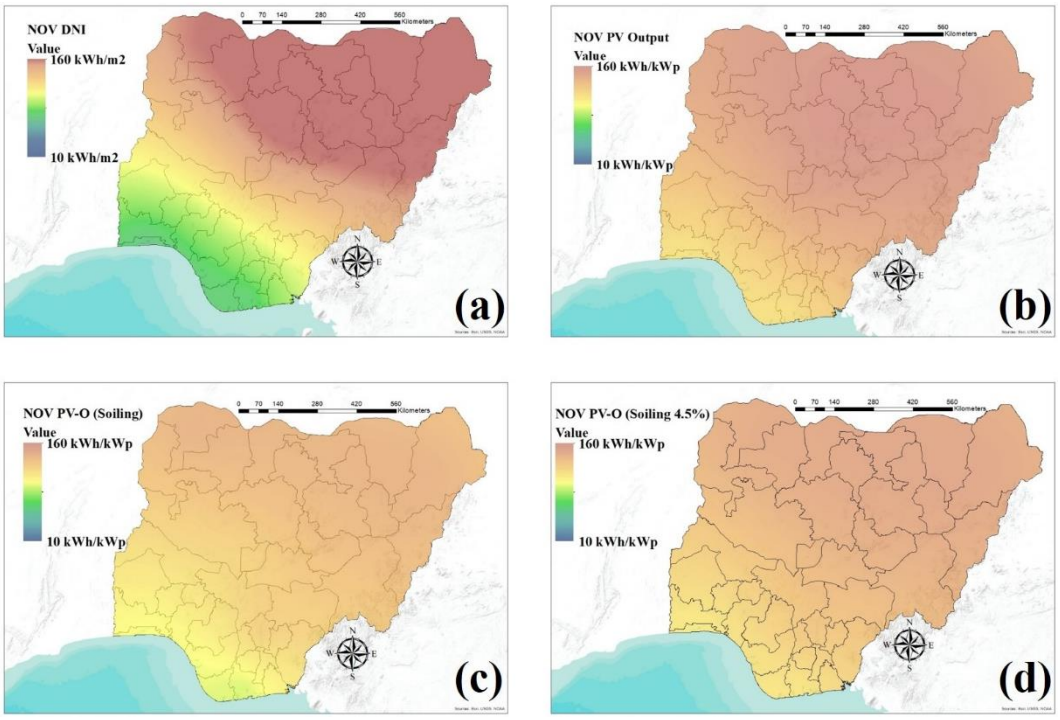

Figure 6.20: November mapping illustrating a regional variation of DNI potential and PV output for Nigeria highlighting soiling losses disparity – (a) DNI (b) PV Output (c) PV Output with soiling (d) PV Output with 4.5% soiling.

Figure 6.21c (a) illustrates the December solar energy potential of the country, while Figure 6.21 (b) shows the December PV output potential without soiling losses. Figure 6.21 (c) illustrates the December PV output with soiling losses determined using optical losses data, which show that the most significant soiling loss was recorded in South-South where the PV output degraded from about 124.2 kWh/kWp to 91.07 kWh/kWp. Furthermore, the lowest loss was recorded in the North-East region, where PV output decreased from 159.7 kWh/kWp to about 146.9 kWh/kWp. Figure 6.21 (d) shows the December PV output with a constant soiling losses value (4.5%) where the greatest was observed in the North-East region from 159.7 kWh/kWp to about 152.5 kWh/kWp, and the lowest reduction was in the South-West region where the reduction was from 119.2 kWh/kWp to about 113.8 kWh/kWp.

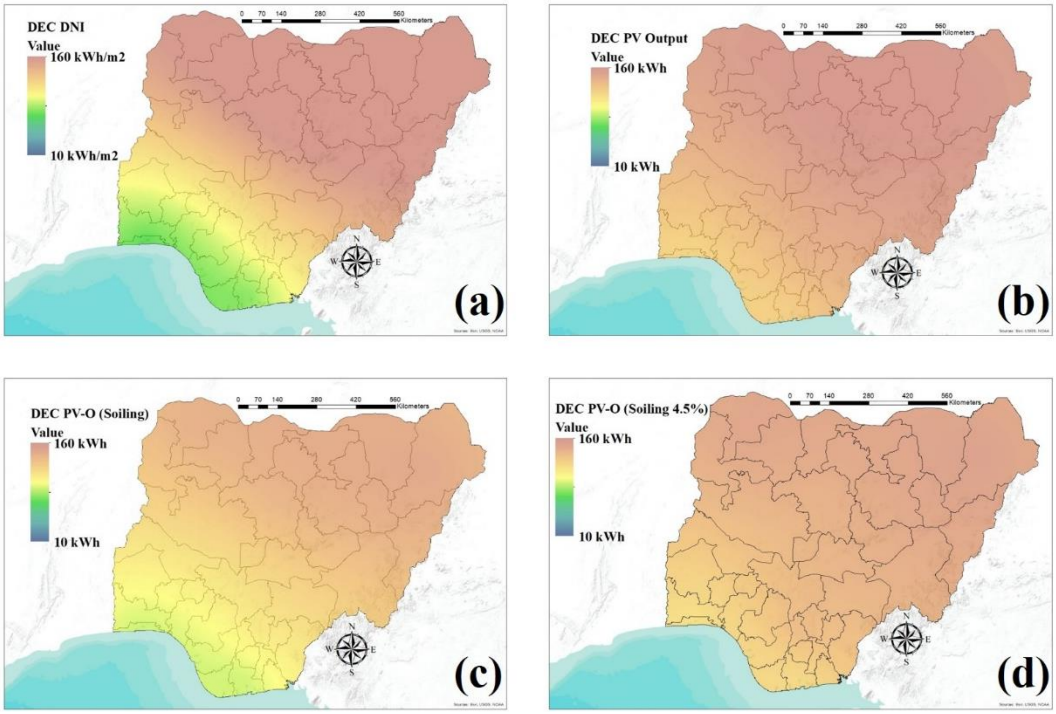

Figure 6.21: December mapping illustrating a regional variation of DNI potential and PV output for Nigeria highlighting soiling losses disparity – (a) DNI (b) PV Output (c) PV Output with soiling (d) PV Output with 4.5% soiling.

6.4 Discussion

All the optical loss results presented in the previous section are percentage reductions from a cleaned, low iron glass coupon. This section summarises and discusses the key findings based on critical observation and evaluation of results considering additional parameters such as weather, atmospheric particles, and AQI presented in the methods section.

The transmission losses values obtained from the previous section's results highlighted a significant variation between a cleaned coupon and coupons exposed to outdoor weather conditions. The most intriguing finding considering the optical transmission results is high losses identified in coupons position on the horizontal plane across all the soiling stations. The greatest soiling among the annual coupon was recorded in ABV, the weather condition throughout the year as shown in Figure 6.3, where the dry season is longer than the wet season, and the AQI appears to be very high as shown in Table 6.2 and Figure 7. However, it has been observed that the primary pollutants are not extremely

dangerous based on the information provided in Figure 8, but most of them have a very devastating effect on light transmittance.

The seasonal optical transmission losses results are additional information necessary to understand better the consequences of soiling on PV. The result shows wide variation between the dry season and the wet season, with the dry season showing the most significant losses in the Northern region due to Saharan dust (during Harmattan season) and while the wet season is presenting more losses in the Southern part. A most significant optical loss was recorded during the dry season in ABV, which is related to massive construction activities going on the federal capital territory (including road, rail, and building constructions) (CCE News Team, 2020). On the other hand, the most significant optical loss recorded during the wet season was in PHC, which is related to the region's massive oil exploration activities (Chanchangi et al., 2020). The high optical losses rate in the South part of the country during the wet season is due to the longer duration of the wet season, which comes with light rain that lasted for about nine months, as shown in Figure 6.3 to the Atlantic Ocean. Figure 6.3 shows the wind speed in ABV is lowest, and the humidity is highest considering the Northern region and similarly for PHC considering the Southern region, which highlighted why more accumulation was recorded in ABV during the dry season and PHC during the wet season. More detailed information on the region's seasonal variation, causing soiling, is presented in Chanchangi et al. (2020).

The optical loss results, considering the months as an exposure period, provide vital information that breakdown the soiling formation data into a period that can be employed in many applications such as research, installation planning and maintenance planning. The results illustrated different optical losses each month, and the greatest was recorded on the ABV coupon installed on a horizontal plane from February. Other months such as November, December, January, and April also presented highly significant losses. According to weather data provided in Figure 6.3, all the above months tends to fall within the dry season that occurs with an influx of the Saharan desert that sweep the country. The atmospheric particles are blown away by the low-level jet (North-

easterly) winds from the North (Northeast and Northwest) to the Northcentral and then the Southern part of the country, causing high formation on surfaces in the Northcentral since the wind speed tends to drop around the region. AQI tends to be very high during these dry months across the country, but the cumulative annual average would be meagre. The AQI and the primary pollutant AQI might tend to be very high in some regions, and the soiling level would be shallow; this is because the high wind does not allow settlement on platforms.

SEM/EDX analysis helped validate the optical losses by highlighting minerals that can absorb, attenuate, or scatter light. Table 6.2 presents SEM/EDX results showing that some of the particles on ABV's coupon are translucent and opaque, reducing light penetration. A significant amount of dust accumulated on the coupon because of the wet weather condition (light rain in February) that created cementation and lower wind velocity. A mineral particle such as Montmorillonite was found on the coupon, opaque and came from clay and predominantly used as a building material in the region. Chamosite transparency is translucent to sub-translucent and is a mineral found in the environment with low iron deposition. As Chanchangi et al. (2020) reported, this mineral can be found in laterite and sometimes loamy soil, and these are also used as building materials in the region. Spodumene is obtained when minerals are ignited, and this could be due removal or breaking of rocks for road construction, quarry activity or mining. These minerals identified from the ABV coupon show that the region's high soiling rate is directly related to construction activity and weather activity. To further validate the minerals recorded, the primary pollutant and AQI from Table 6.2 were analysed, which shows that PM_{10} and $PM_{2.5}$ are very high value; this supports the claim that particles recorded on the coupons are from construction sites landfills and windblown dust.

Particles recorded from ENU shows minerals with transparent, translucent and opaque optical characteristics. Table 6.2 shows some of the minerals (Tourmaline and Analcites) with the property that could reduce the optical transparency of the covering surface of PV devices as it could absorb, attenuate, scatter or reflect light. Table 6.2 shows that the PM_{10} and $PM_{2.5}$ have very high values; sometimes, in the years, this is related to coal exploration

activities and usage in the state. The CO is also high due to the burning of fossil fuels from vehicles or machinery.

Particles recorded from KAD shows minerals that appear to be translucent and opaque. These particles could have a negative impact on light transmittance. Table 6.2 shows a high presence of PM_{10}, $PM_{2.5}$ and SO_2 in the atmosphere. The PM_{10} and $PM_{2.5}$ are related to construction, agriculture and windblown dust coming from far Northern regions. The SO_2 in the region is related to the industrial activities and oil refining in the region.

Particles recorded from the LOS coupon shows translucent and opaque minerals, which could have a detrimental effect on light transmittance. A significant amount of particles was observed on the surface due to the high humidity that promotes adhesion force. Table 6.2 shows a high amount of all primary pollutants (PM_{10}, $PM_{2.5}$, SO_2, CO, and O_3) present in the atmosphere. This region is densely populated and has many ongoing industrial and construction activities, and since it is near the coastline, it also has sea salt dust. The high presence of SO_2 is directly related to the burning of fossil fuels and coal.

Particles recorded from the MIU coupon shows minerals that are transparent, translucent and opaque. The two latter ones could affect the light from reaching the solar cells. The minerals and their diaphaneity are shown in Table 6.2. A less amount of particles could settle on the coupon due to strong wind and dry weather conditions, reducing the various adhesion forces. Table 6.2 shows that PM_{10} and $PM_{2.5}$ have the most outstanding value among the primary pollutants, and the AQI highlights that the dust particles are windblown particles from the nearby Saharan desert. It has been presented in Chanchangi et al. (2020) that atmospheric dust around the MIU region is windblown dust from the Saharan desert.

Particles such as Albite, Schorlomite and Scapolite recorded from PHC have an optical characteristic (translucent and opaque) that could reflect, scatter or attenuate the light. Considering the primary pollutant and AQI from Table 6.2, it

was observed that PHC has a high amount of $SO_{2,}$ which is related to oil exploration activities and burning large amounts of fossil fuel. Similarly, CO concentration in the atmosphere was observed to be very high in the region. However, the annual average of the AQI is lower than in other regions since the region has a long wet season.

The particle recorded from SOK's coupon shows minerals similar to those recorded from ABV (Chamosite and Montmorillonite). All these minerals possess translucent and opaque characteristics, but due to the weather condition, which is mostly dry and heavy wind, as shown in Figure 6.3, the particles did not settle on the coupons. The PM_{10} and $PM_{2.5}$ shown in Table 6.2 have the most significant values of the leading pollutant and AQI in the region, and this supports the kind of minerals recorded since particles are windblown dust from the nearby Saharan desert.

Findings show optical losses on all coupons, although a few are minor. However, causes of accumulation required additional information, as included in some paragraphs above. The analysis shows that particles in the atmosphere or the AQI cannot be used as the only source for determining the accumulation rate as wind speed, humidity, and precipitation could play a vital role in promoting particle settlement on surfaces.

The soiling mapping results presented in the previous sub-section highlighted a significant variation between this study's results and information presented by the GSA, with higher soiling rates determined during this study. The variation observed from the annual mapping is significantly broad. The maximum variation was observed from ABV, where a 746.69 kWh/kWp difference was recorded between the PV output using soiling data from this study and the PV yield based on 4.5% soiling. All the annual soiling data from the other various sites in this study presented higher soiling rates than the GSA constant value, shown in Figure 6.22.

Each season presented a massive variation between the PV yield (with soiling data obtained from this study) and GSA PV yield (a constant soiling rate of

4.5%). The maps show that the most significant disparity recorded in the Northern region during the dry season was from ABV with about 536.14 kWh/kWp difference, while the most significant disparity recorded during the wet season was from PHC with about 388.12 kWh/kWp. This regional soiling disparity directly related to seasons is due to the inter-tropical displacement caused by the Coriolis force. During the dry season, the PV yield is higher in the Northern region, and the most significant soiling loss was recorded in the North-central. While during the wet season, the Southern region tends to have a high PV yield due to the longer duration of the season in the region and the most significant soiling loss was recorded in the South-South region. As earlier mentioned, during the dry season, the dust movement is influenced by north-easterly low-level jet winds from the Saharan desert. During the wet season, the dust movement is influenced by south-westerly winds from the Gulf of Guineas and the Niger-Delta region, where oil exploration activities are ongoing. By observing the weather information pattern provided in Figure 6.3, it is easy to know that the Northern and the Southern region have a climatic pattern that substantially influences dust settlement and accumulation on an exposed surface. The maps in Figure 6.8 and Figure 6.9 illustrated higher PV yield degradation due to soiling rates in both seasons compared to GSA values, and these seasonal variation data can be found in Figure 6.22.

It is necessary to understand the monthly PV yield, considering the effect of soiling. There are individual monthly differences between PV yield employing soiling data from this study and PV yield with a 4.5% constant soiling rate. A closer examination of results reveals that some months (mainly during the dry season), such as November, December, January, February, March and April, have a higher PV yield degradation variation rate. The most significant variation was observed in February, where about 31.05 kWh/kWp disparity was recorded in ABV, followed by December with 27.53 kWh/kWp in PHC, January with 24.81 kWh/kWp in LOS, November with 21.85 kWh/kWp in ABV. The few negative figures shown in Figure 6.22 are present when the percentage of the GSA soiling rates become higher than the optical losses recorded from this study. Variations are less during the months that fall within the wet season. Some months have PV yield with soiling values that turns out to be lower than GSA

values because the soiling rates are lower than 4.5% (GSA soiling value). The map for May illustrated that PV yield (with soiling determined from this study) in three regions (ENU, LOS, and PHC) all from the Southern part of the country are less than 4.5% (GSA soiling value); the June map shows only one region (KAD); the August map shows two regions (KAD and MIU); the September map shows three regions (ENU, KAD, and LOS); while the October map shows only one region (ENU). Variation data for each month is shown in Figure 6.22 below.

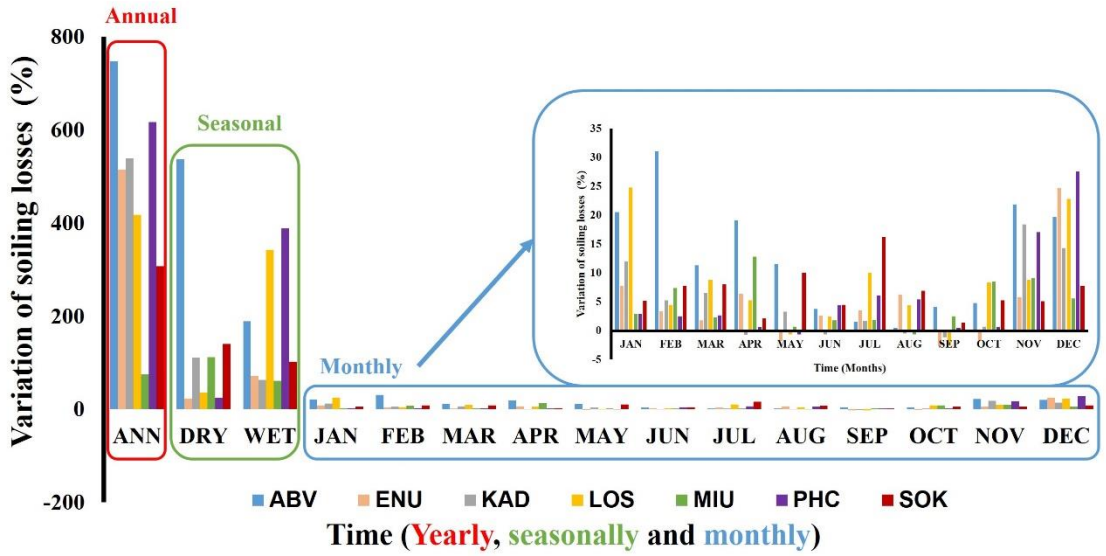

Figure 6.22: Variation of soiling losses between GSA and result from this study. The Monthly illustrates the variation of each region in every calendar month. The Annual (ANN) highlights the annual variation, Dry and Wet show the seasonal variation, highlighting dry seasonal variations and the latter showing wet seasonal variations for the seven regions. Soiling stations are highlighted using various colours in the chart.

As earlier stated, the PV yield presented in the Global solar atlas was clearly emphasised that it does not adequately account for several important factors that potentially impact the PV output. However, soiling data cannot be constant, and caution should be taken when generalising such information since it can significantly impact the PV yield and mislead the potential users of the information. This study's finding demonstrated more realistic soiling, as shown in Figure 6.22, where the soiling site's disparity values were illustrated,

comparing PV yield with soiling data from this study and PV yield with constant 4.5% soiling considering the exposure period.

There are significant benefits from this study's output since the previous information is misleading due to less accuracy of the soiling information, which might be causing wrong installing and maintenance planning which could lead to less yield or system failure at the extremity. The findings provided more accurate and realistic information for better PV installation and maintenance planning to achieve increased yield. The result could assist in optimising the maintenance procedure to generate more output at a lower maintenance cost. The low-cost novel approach employed in this study has potential advantages; it could guide researchers to examine the appropriate mitigating techniques required for a particular region in the country and prompt a significant step toward finding a lasting solution to the PV soiling problem.

This method could be further refined by considering increasing the number of soiling stations and narrowing down the distance. It is recommended that Global solar atlas should install a soiling station in some regions to acquire *in-situ* soiling data that would reduce the variation gap discovered in this study and provide researchers, policymakers, potential PV investors, and commercial PV companies with more realistic PV yield potential. Finally, the information presented in this study should be used for determining appropriate cleaning procedure and optimising it to improve the penetration and scale-up of the solar energy technologies in regions with high energy demand and low penetration to achieve the sustainable development target goal 7 *("Ensure access to affordable, reliable, sustainable and modern energy for all"*).

6.5 Summary and conclusion

This section of the thesis demonstrated the concept of employing optical losses data to illustrate potential PV performance reductions using a mapping approach. It presented an investigation of optical losses in seven locations across Nigeria using a low-cost in-house soiling station. The results show that coupons position on horizontal planes accumulates more dust than the tilt angle

(45°) and vertical plane. The study reveals ABV as the region with the most significant soiling rate in the country and February as the month when the most significant soiling rate occurs. The outcome shows that the Northern region has a higher soiling rate during the dry season, with ABV having the most significant rate. While during the wet season, the Southern region shows a higher accumulation rate, with LOS and PHC been on top of the list. SEM/EDX analysis confirmed that minerals collected on coupon surfaces negatively affect light transmittance, causing the recorded optical losses. The AQI and pollutant data validate the type of particles recorded. The weather condition shows why high accumulation rates are recorded from each region and during a specific season. The study demonstrated a unique technique that illustrated a wide variation of soiling losses rate between this study and under-reported and grossly underestimated soiling by previous studies (Mithhu et al., 2021; Li et al., 2020; Micheli et al., 2019; Cordero et al., 2018) and also by GSA (2020), which might be due to overlooking of regional variability and the seasonal difference that plays a vital role in increasing or decreasing the losses.

7 Chapter Seven - In-Situ assessment of low-cost mitigation techniques in Northern Nigeria

7.1 Introduction

Dust and impurities accumulation on PV system surfaces presents a significant problem to the output performance of the PV technology, causing substantial yield losses due to scattering and absorption of incident irradiance on PV cells as presented in the previous chapters of this thesis. Mitigating the problem is vital for the penetration and sustenance of renewable energy in the developing world. Therefore, the scientist has put a massive effort to develop a mechanism that can prevent soiling losses or restore optimum PV output performance, and several techniques were reported by Chanchangi et al. (2020), Gupta et al. (2019), and Jamil et al. (2017). The techniques have the individual capacity to reduce dust. Still, no flawless approach has been recommended for the region in focus. Each technique presents a different level of performance concerning the environmental condition of the location it has been deployed and the type of PV cover surface it is cleaning. However, some techniques have a long list of drawbacks, such as cost and uncontrolled water requirement supply, known as the primary concerns for the region in focus (Sayyah et al., 2017; Quan and Zhang, 2017). This section of the thesis briefly highlights the main soiling mitigation approaches in the subsequent paragraph.

Renewable energy sees rapid investment coming its way in developing and developed countries due to climate change and energy security (Sarver et al., 2013). Nigeria has recently commissioned three solar farms (3.5 MWp of solar PV, 8.1 MWh energy storage system and 2.4 MW of backup generators) and the largest off-grid in sub-Saharan Africa (Energy Storage, 2019) in huge investment towards developing its renewable energy sector in the arid northern region of the country. However, in a recently completed study, it has been observed that soiling could cause an output loss of about 68% to 78% when the installation is left unclean for 12 months in the same city that homes two large operational solar farms. Chesnutt et al. (2017) stated a need to prevent energy losses by providing a cost-effective soiling mitigation technique that is relatively neglected. Piliougine

et al. (2013) recommended evaluating PV cleaning cost and the economic impact of output losses caused by soiling for large PV plants. However, the literature provides the economic impact (Ilse et al., 2019; Micheli et al., 2021; Zeedan et al., 2021). Ilse et al. (2019) and Ghosh (2020) stated, in 2018, the electricity generation from PV was reduced by 3% - 4%, resulting in revenue losses of around €3 - €5 billion, and this is related to soiling losses which further projected to reach €4 - €7 billion by 2023.

Despite the extensive work and progress made in resolving soiling problems using both restorative and preventive approaches provided in the literature, significant studies are limited to examining a single technique, and others focused on reviewing publications reported from different regions. There is an insufficient investigation, comparative analysis and extensive performance studies of the techniques under the outdoor condition in the same site, considering variables (seasonal variation, PV surface covering material, and weather parameters). Therefore, this study comparatively investigated the performance of various mitigation techniques on two PV surface covering materials (acrylic plastic and low iron glass), considering seasonal variations in the arid region of Northern Nigeria, which is relatively neglected. Thus, neither cost analysis nor economic implication was presented. However, the approach used in this chapter of the thesis could provide guidance to be adopted and applied in other regions since cost analysis varies with location (based on the economic capacity), as later described in the methodology. The solution might probably lie in considering more variables, as each technique has advantages/disadvantages and their effectiveness are dependent on the variable mentioned above. This chapter of the thesis has two-fold contribution: first, developing and examining different PV soiling mitigation approaches in the outdoor condition in a region with massive investment in solar PV. Secondly, investigating the system performance using a multivariable method. The finding could prevent future unnecessary PV output losses due to soiling in the region. The thesis chapter demonstrated a relatively low-cost approach based on findings reported in the literature (Sarver et al., 2013; Deb and Brahmbhatt, 2017; Jamil et al., 2017; Ilse et al., 2019) to investigate the most suitable techniques for a region and stimulate more research across the PV soiling community and scientists. It could serve as a foundation to estimate the

possible frequency and financial commitment for PV farm maintenance in the region that could entice prospective investors and governments.

7.2 Method

The research examines five low-cost PV soiling mitigation techniques (hydrophobic self-cleaning; mechanised cleaning; natural cleaning, manual cleaning with a brush; and manual cleaning with squeegee and water) to solve a persisting soiling problem that adversely affects PV performance. These techniques were selected based on their simplicity of implementation. Bayero University Kano 1 MW solar farm (11°59'02.1"N, 8°28'52.5"E) is where coupons were exposed to examine dust level accumulation. It was carefully selected since it is the most polluted country (IQ Air, 2021) with an operational solar farm. Ten 50 mm x 50 mm x 4 mm low iron glasses and acrylic plastics with five were exposed for thirty-one days during the dry season (January 2020). Another set of ten was exposed for the same duration during the wet season (August 2020). Coupons were exposed on various platforms according to cleaning methods. The prior knowledge of weather activity in the region helped determine incoming wind direction during the two-season for coupon's surface orientation during exposures. It was reported by Kazem and Chaichan (2019) that incoming wind has a more significant influence in removing particles from the surface. A flowchart illustrating the various steps through the research methodology of this subsection of the thesis is provided in Appendix B – Figure 0.7.

7.2.1 Cleaning techniques

7.2.1.1 Hydrophobic self-cleaning coating

Hydrophobic coatings have low mechanical stability due to their high surface roughness. Silicon oxide-titanium dioxide (SiO_2-TiO_2) composite layer can help retain the coating's stability for several cycles. Rosales and Esquivel (2020) reported that TiO_2 offers photocatalytic property, chemical stability, low toxicity, highly available and optical properties since it possesses high scattering, resulting from a high refractive index and large bandgap. While, SiO_2 exhibit thermal stability, hydrophobic and hydrophilicity properties (Rosales and Esquivel (2020). Composite SiO_2-TiO_2 has been reported to enhance hydrophobicity when

deposited on marble (Kapridaki and Maravelaki-Kalaitzaki, 2013), improves the contact angle, anti-reflection and lower 1.4 nm roughness of glass (Mazur et al. 2016). Wu et al. (2007) examined the properties of composite SiO_2-TiO_2 and reported that SiO_2 support hydrophilicity and stability of nanoporous TiO_2. The presence of TiO_2 in composite decrease the contact angle (Rosales and Esquivel, 2020), but Ye et al. (2013) reported a design with a triple layer of SiO_2, TiO_2 and SiO_2–TiO_2 using tetrabutyl orthotitanate (TBOT) and Tetraethyl-orthosilicate (TEOS) as precursors and Hexamethyldisilazane (HDMS) for anti-reflective surface modification. Their approach increases average transmittance in the visible region and improves the contact angle, proving that hydrophobicity can be improved by employing HDMS. This study adopted Ye et al. (2013) in developing a self-cleaning to sustain the coating's transmittance and stability.

The hydrophobic coating development was carried out using a solution-processed silica-titania composite. The overall fabrication is schematically represented in Figure 7.1. The details of the fabrication protocol have been described as follows. It was prepared using the following procedure:

Solution A was prepared using 2.1 ml of Tetraethyl-orthosilicate (TEOS) deposited in a beaker and mixed with 30 ml of ethanol. This solution was stirred for about 30 minutes at room temperature. After that, 2.0 ml of Hexamethyldisilazane (HMDS) was added and further stirred for 15 minutes at room temperature. Finally, 3ml of deionised) water (DI) was added to the solution and was stirred for an additional 3 hours to make it a transparent solution.

Another solution (Solution B) was prepared using A 5 g of SiO_2 (Silicon dioxide) nanoparticles mixed with 25 ml of butyl acetate. The solution was stirred for 4 hours at room temperature.

Solution A and solution B were mixed in a beaker at a 1:1 ratio to form solution C, and it was stirred for an hour at room temperature. Afterwards, solution C was kept ageing for ten days.

On the fifth day, solution D was prepared by mixing 0.12 (M) of TTiP [Titanium (IV) isopropoxide] in 100 ml of 2-propanol and DI water (1:1) mixture. It was stirred for twenty minutes at room temperature. Coupons (low iron glass and acrylic plastic) were dipped in solution C1 for five minutes and allowed to dry, dip into solution D for five minutes and allowed to dry, and dip again in solution C for five minutes and allowed to dry. These dipping procedures were repeated three times before the coupons are placed on a hot plate at 200°C for thirty minutes. Solution C1 was drop cast on another set of coupons employed about 7 ml of the solution on one side of the coupons using a similar pattern as used when dipping. Dropping solution C on coupons and allowed to dry, then solution D allowed to dry and finally, dropping solution C and allowed to dry. On the tenth day, another solution D was prepared using the same quantity and materials mentioned above. Solution C and solution D were deposited using the dropping and dipping techniques on various coupons (low iron glass and acrylic plastic).

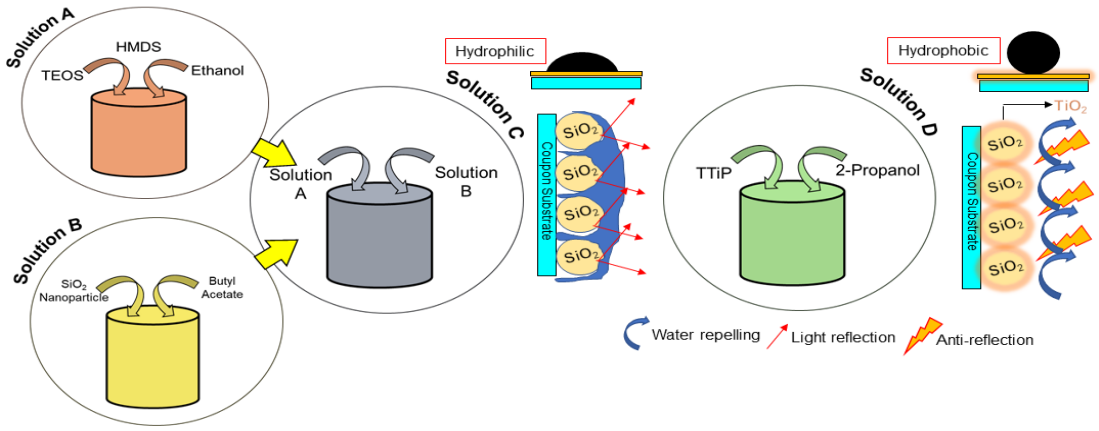

Figure 7.1: Schematic representation of SiO_2-TiO_2 composite for self-cleaning coating development.

The intention of doing the solution C-solution D, and again solution C repeatedly is to secure the film's homogeneity. Besides, only SiO_2 coating is not enough to protect water, and also, sometimes it cannot show an anti-reflective property, and resulting dust accumulation can easily be there (Rosales and Esquivel, 2020). The use of SiO_2 nanoparticles in powder form decreased the glasses' transparency. On the other hand, TiO_2 exhibits anti-reflection properties (reflected light at air/coating and coating/substrate interfaces), adequate transparency, and more light to the layer. Besides, the potent oxidising agents (O_2^- and OH●) on the

coating surface generated by the charge carriers of TiO_2 during the absorption of high-energy photos can decompose absorbed organic molecules. SiO_2 further acts as inert support of the TiO_2 layer and accelerates the self-cleaning properties for the water and dust, and prevents oily dirt or organic matter. Hybrid SiO_2-amorphous TiO_2 also exhibited excellent stability under UV-light irradiation. SiO_2 imparts an efficient UV scattering because of the extensive refractive index of SiO_2 (Isaifan et al., 2017; Tetteh et al., 2020; Fathi et al., 2017).

Dipping inside the TTiP solution forms an amorphous layer of TiO_2. It is essential to from such an amorphous layer, as amorphous TiO_2 contains a higher bandgap (~310 nm) than crystalline TiO_2 (~400 nm) (Fonseca-Cervantes et al., 2020); therefore, it is a promising candidate to performance the UV-shielding ability. Thus, the sequential composition of SiO_2-TiO_2 is essential to improve the coupon substrate's mitigation property. These systems are easy to produce on a large scale at a low cost and exhibit high mechanical and chemical durability. Thus, these materials are suitable for bi-functional anti-reflective and self-cleaning coatings for large substrates for the solar module.

7.2.1.1.1 Coating surface wettability study

Ossila contact angle goniometer was employed to measure each coupon's average water contact angle value, which defines the coating's hydrophobicity. Equation (7.1), known as Young's equation provided by Kung et al. (2019) and Good (1992), was employed to validate the coating's hydrophobicity. Uncoated coupons (low iron glass and acrylic plastic) were initially measured, then subsequently, coated coupons were examined. Coated coupons were also subjected to optical transmittance checks to select the best coupon with a high hydrophobic rate and a high transmittance level, where θ is the contact angle between the liquid and the coupon surface, γ^{sl} is the interfacial free energy of the solid or liquid, γ^{sv} is the coupon surface free energy, and γ^{lv} liquid surface free energy. This Equation (7.1) is further illustrated in Figure 7.2 for a better understanding.

$$\gamma^{sl} = \gamma^{sv} + \gamma^{lv} \cos\theta \tag{7.1}$$

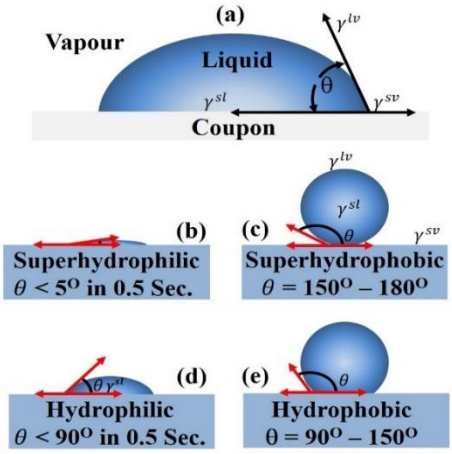

Figure 7.2: Illustrative variation of hydrophobicity and hydrophilicity levels.

Findings illustrating water contact angle variation of coated (with hydrophobic layer) and uncoated coupon is provided in Table 7.1. It is compared with Figure 7.2 to determine the wettability status of various coupons.

Table 7.1: Captured images of hydrophobicity levels of coupons with their various levels of contact angles.

Coating Sample	**Average Water Contact Angle**	**Captured Image**
Bare Glass	35°	
Bare Plastic	77.5°	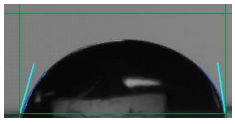
Coated Plastic CDC-10-Dipping	110°	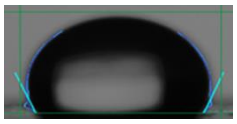
Coated Glass CDC-10-Dropping	126°	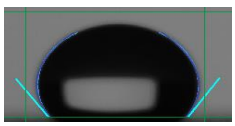

7.2.1.2 Mechanised cleaning

An in-house, low-cost mechanised cleaning platform was developed to examine how effectively mechanised cleaning performs in dry, dusty regions. The platform was developed using acrylic plastic with a 12 V Bosch motor wiper and its blade powered by a 12 V 4.5 Ah battery and a 15 A toggle switch non-illuminating. The battery is removable as alligators insulated clips were used to connect to terminals. The platform was designed using SolidWorks, and the file was exported as DFX to Boxford BGL 690 80W Laser Cutter machine, where all the parts were cut into shapes. It was designed to allow placement of coupons at a 12° tilt angle, reported at the site's optimum tilt angle as earlier mentioned. The top platform has four slots to accommodate 50 mm x 50 mm coupons with 4 mm thickness (two low iron glass coupons and two acrylic plastic coupons). No abrasion will occur at the intersection point during the blade's movement. Figure 7.3 illustrates the schematic diagram of the design with two digital images. Like other techniques, this cleaning approach was operated on once a week. The design could be improved using a sensor and an Arduino for automation.

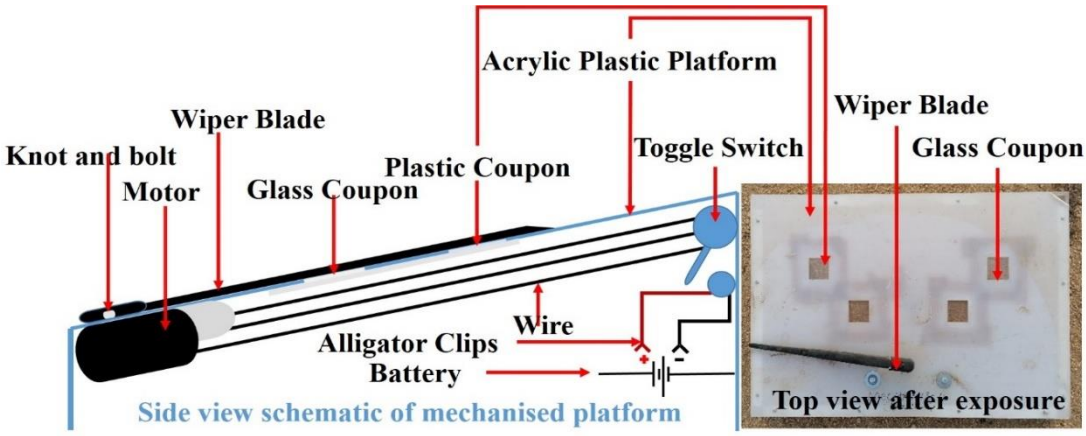

Figure 7.3: Schematic diagram illustrating various mechanised cleaning platform components with two digital images before and after exposure.

7.2.1.3 Manual cleaning

The manual cleaning was device into two categories: water and the other without water. Manual cleaning with water was conducted by pouring water on the exposed coupon's surface and employing squeegee to wipe off the surface. This procedure is performed once a week. On the other hand, manual cleaning with a

brush, which is the cleaning technique used in the solar farm (site of the experiment), was conducted using a dry brush to scrub the exposed coupons' surfaces. Similar to other techniques, cleaning is performed once a week.

Coupons that undergo manual cleaning, no cleaning and self-cleaning were exposed using an in-house developed platform that positioned coupons at an optimum tilt angle of the site (12°). Figure 7.4 shows a digital image illustrating coupons exposure.

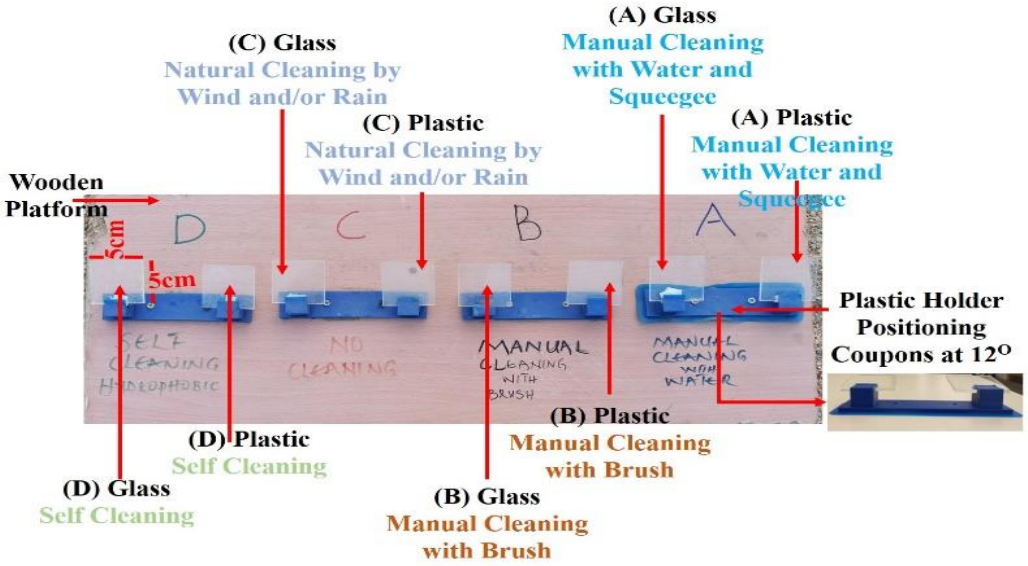

Figure 7.4: Digital image of coupons placed on various holders.

7.2.2 Optical losses characterisation

All coupons were subjected to optical transmittance characterisation to determine the level of deterioration. Coupons are examined using a clean coupon (glass or plastic) as a baseline except for the self-cleaning, which were examined using the transparency of a coated before exposure as a benchmark to determine optical losses. The Perkin Elmer Lambda 1050 UV/VIS/NIR spectrophotometer was employed to conduct spectral transmittance measurement from UV (Ultra Violet), VIS (Visible) and NIR (Near Infra-Red) wavelength levels. It is to determine which deposition technique provides the highest transmittance and establish a point of reference for comparison and Equation (7.2) provided by Ghosh et al. (2018) was used for validation, where $\tau(\lambda)$ is the spectral transmission, $\Delta\lambda$ is the change in wavelength and $S(\lambda)$ is the relative spectral distribution of solar radiation.

$$\tau = \frac{\sum_{\lambda=250nm}^{1250nm} S(\lambda)\tau(\lambda)\Delta\lambda}{\sum_{\lambda=250nm}^{1250nm} S(\lambda)\Delta\lambda} \quad (7.2)$$

Equation (7.3) was used to determine the percentage difference between a soiled coupon and a clean coupon for manual cleaning technique, mechanised technique, and no cleaning. Still, for self-cleaning, the transmittance level was measured after coating was used as the baseline, where Δ is the change, τ_x is transmittance data of a coupon positioned at an angle relative to a horizontal surface, $\tau_{Unexposed}$ is the transmittance data of a clean coupon or a coated coupon before exposure.

$$\Delta\tau_x = \frac{(\tau_{Unexposed} - \tau_x)}{\tau_{Unexposed}}(100) \quad (7.3)$$

7.2.3 Weather condition

Weather data such as wind speed and rain was collected to see the possible effect of natural cleaning from both. A Maplin professional weather station was installed on-site to capture the weather during coupons' exposure. Figure 7.5 (a) and (b) provides wind velocity and rain rate. It is worth mentioning that coupons were exposed during the peak of both seasons where high wind velocity is expected in both seasons, and increased rainfall rate is expected during the wet season, which significantly influences the high performance of natural cleaning technique used as a benchmark for all others.

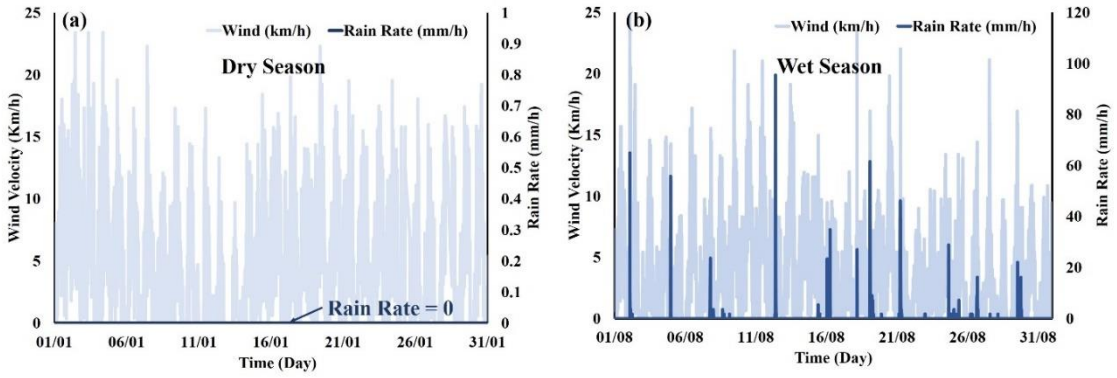

Figure 7.5: Weather charts illustrating wind velocity and rainfall rate during (a) dry season and (b) wet season.

7.2.4 Technique's performance assessment

The performances of the soiling mitigation techniques were evaluated using five parameters: Initial cost, which is determined from the cost of the required materials for fabrication and hour of labour; a monthly operational cost which is determined from calculated, the ongoing cost of operation such as monthly wages for the operator, parts for maintenance over a particular duration, and contingency plan for parts failure; effectiveness of the technique which is determined from optical losses on both coupons; reliability which is determined from five factors (operation, engineering and automation, maintenance, reliable, safety); and limitation which determine from disadvantages reported in Jamil et al.(2017); Deb and Brahmbhatt (2017); Gupta et al. (2019); and observation from this study as shown in Table 2, Table 3, Table 4, Table 5, and Table 6.

A summation variable for each factor determined the value of a parameter presented in the result section. For example, hours of labour are determined using UK minimum wage (£8.72/hours) (Gov. UK, 2021), and cost of labour is calculated using Nigeria minimum wage (£0.3125/hours) (My wage.NG, 2021) since the maintenance operation is conducted in Nigeria. The UK minimum wage was used to calculate labour time during design and development since both the hydrophobic coating and mechanised platform were fabricated in the UK and transported to Nigeria. In contrast, the Nigerian minimum wage was used to calculate the continuous labour cost and equipment maintenance over time, considering the equipment's lifecycle time in question since human labour will be locals at the installation site.

The initial cost for mechanised and self-cleaning approaches was determined by summing the materials cost and the labour cost for fabrication considering estimated hours spent. Thus, the initial cost for manual cleaning is related to cleaning materials and PPE, and the zero initial cost was allocated to natural cleaning. Using Equation (7.4), mathematical modelling was employed to calculate the initial cost of materials and wages for the techniques by substituting the appropriate value for each variable where applicable; otherwise, 0 is used for unrelated parameters accordingly.

$$C_i = \sum p_{(PPE)} + p_{(tool)} + \sum p_{(mat)} + W^{flex} + \sum p(comp^1) + w\ (\%) \quad (7.4)$$

where $\sum p_{(PPE)}$ is the total price of all the PPEs required, $p_{(tools)}$ represents the price of tools, $\sum p_{(mat)}$ signifies the summation price of coating materials, $\sum p(comp^1)$ denotes the summation price of all components used in fabricating the mechanised platform, w is the wages for coating the hydrophobic layer on the coupons.

The monthly cost was determined relative to each approach as follows: the Natural cleaning have zero monthly maintenance cost; the manual cleaning with squeegee and water comes with the monthly cost of water, the monthly cost of labour, the monthly cost of buying safety PPE (personal protective equipment) (cost are divided into months to spread the cost changing the PPE on an annual basis); the monthly cost for manual cleaning with a brush was determined by calculating the labour cost, tools and PPE; the self-cleaning monthly cost was calculated by splitting the initial cost of coating substances and fabrication labour/re-installing the covering materials into months since the coating is expected to be ineffective after four years as presented in the literature: the mechanised platform requires replacement of the battery, the cost of labour for maintenance operation. Mathematical modelling using Equation (7.5) was employed to calculate the monthly cost implication of sustaining the performance of each technique by substituting the appropriate value for each variable where applicable; otherwise, 0 is used for unrelated parameters.

$$C_m = cyc_{(L_{(w\times l)}+Q_{H_2O})} + \left(\frac{p_{(PPE)}}{t_1}\right) + \left(\frac{p_{(tool)} \times o_{(tool)}}{t_1}\right) + \left(\frac{\sum p_{(mat)} + W^{flex}}{t_2}\right) + \left(\frac{\sum p(com)}{t_1}\right)(\%) \quad (7.5)$$

where cyc is the number of cycles required in a month, L is the labour which is derived from w workers' wages multiply by l number of workers, $Q_{H_2O}$is the quantity of water, p represents price, $p_{(PPE)}$ is the price of *PPE*, t_1 is time (signifying 12 months maintenance cycle), $o_{(tools)}$ is the number of tools, $\sum p_{(mat)}$ represents the cost of hydrophobic coating materials, W^{flex} is the wages for re-

coating, t_2 is the time coating is expected to degrade and requires re-coating, and $\sum p(com)$ is the summation of prices of all the components (example: wiper lade and battery) required to be changed after one year of operation.

The change of transmittance reduction in percentage reduction for each coupon is used as the effectiveness value, which is determined by comparing a clean coupon and soiled coupon after exposure for all coupons except for coupons with a hydrophobic coating. Its effectiveness is determined by calculating the change in transmittance reduction in the coated coupon percentage before and after exposure. This used the value obtained from Equation (7.6) below.

$$\text{Effectiveness } (\eta) = 100 - \frac{(\tau_{Unexposed\ coupon} - \tau_{exposed\ coupon})}{\tau_{Unexposed\ coupon}} \times 100 \quad (7.6)$$

The five reliability factors were allocated percentage for each variable and were summed up to determine how the system's reliability can operate. In this study, reliability is considered the likelihood of a product's safe and required performance over the stipulated time in a specific environment. A reliability model was adopted from Signoret and Leroy (2021), where they presented five reliability components (probability of success, durability, dependability, quality over time, availability to perform a function). These components were modified and into five components stated in Equation (7.7), where each component is graded with 20%, and the summation was added to determine the system's reliability.

$$R_{Si}(\%) = O_{(O+P)} + E_{(D+Q)} + M_{(O+M)} + R_{(I)} + S_{(H+S)} \quad (7.7)$$

where operation ($O_{(O+P)}$) represent the availability to perform a function the success probability is high, engineering design ($E_{(D+Q)}$) standing for system design and quality of the system over its stipulated operational time, maintenance ($M_{(O\&M)}$) signifies the durability of the system in adverse conditions, reliability ($R_{(I)}$) denotes the dependability of the system to work alone, safety ($S_{(H\&S)}$) is representing health and safety, how safe the system could be operated. Values are allocated to each component considering the reported literature concerning the process conducted in developing the approach.

Limitation constraint presented in the literature and observed during this study is allocated a percentage rating (20% each for a limitation) and was summed up. The difference from 100% was used as a percentage level. This is a rough estimate to illustrate the limitation and show how each approach has more than one.

7.3 Results

This section illustrates the findings where results are categorised into sub-sections: the optical losses section and the soiling mitigation technique's performance assessment. Both are further subdivided into their specific technique.

7.3.1 Optical losses and quantitative performance assessment

7.3.1.1 Manual cleaning with squeegee and water

The period of exposure plays a significant role in determining the optical losses. Despite the effort of weekly manual cleaning using water and squeegee, substantial optical losses were recorded of about 9% transmittance reduction on the exposed acrylic plastic during the dry season and 6% during the wet season. On the other hand, minor optical losses were recorded on low iron glass coupons with about a 4% reduction during the dry season and 3% during the wet season. Optical losses on the low iron glass during both exposure times are less than 50% compared to acrylic plastic. Figure 7.6 illustrates both coupons' optical losses during the different exposure periods.

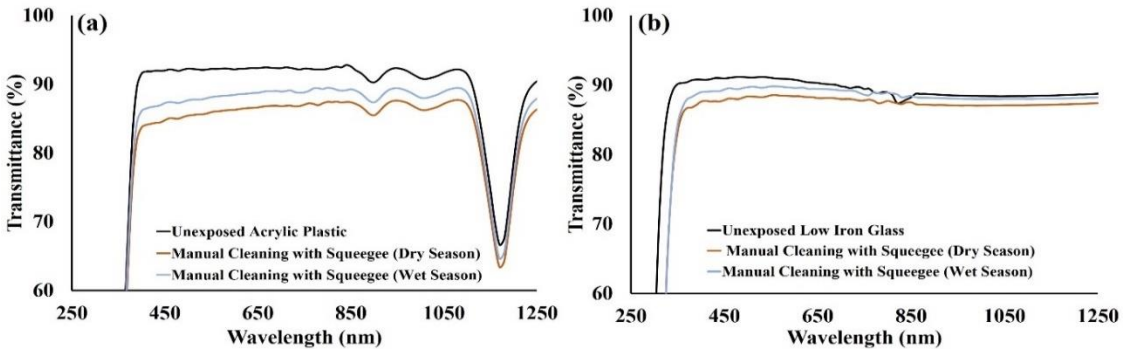

Figure 7.6: Optical transmission losses variation of a soiled coupon with a clean one exposed under manual cleaning with squeegee/water (a) acrylic plastic (b) low iron glass coupon.

Performance evaluation was conducted using a multivariable approach. The finding for manual cleaning with a squeegee and water, as shown in Figure 7.7, illustrated that the technique has a low initial cost for equipment required to accomplish the task, the reliability of this technique is average, and the monthly maintenance cost is average in developing nation with meagre minimum wage and it highly effective on both coupons. Based on the findings presented in Figure 7.7, this mitigation approach is rated as an average technique. However, the method is rated high in limitation.

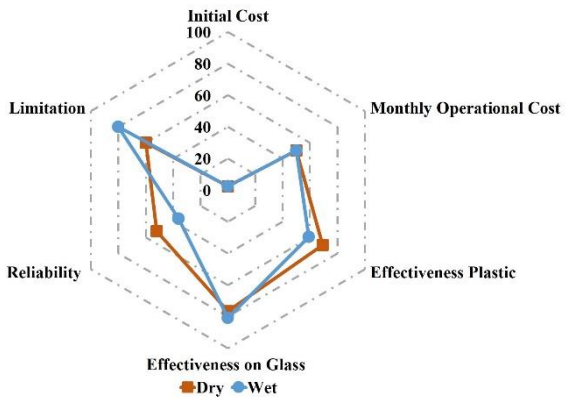

Figure 7.7: Performance assessment of manual cleaning with squeegee/water illustrating cost variation, limitation, effectiveness on coupon cleaning, and reliability.

7.3.1.2 Manual cleaning with a brush

Higher optical losses were recorded when coupons, despite weekly manual cleaning using a brush with a considerable seasonal variation. The result demonstrates the common phenomenon where a significant loss of 17% was recorded on the acrylic plastic during the dry season and 14% during the wet season, as illustrated in Figure 7.8. On the other hand, considerably lower optical losses were recorded from the low iron glass with about a 5% reduction in coupons exposed during dry and wet seasons.

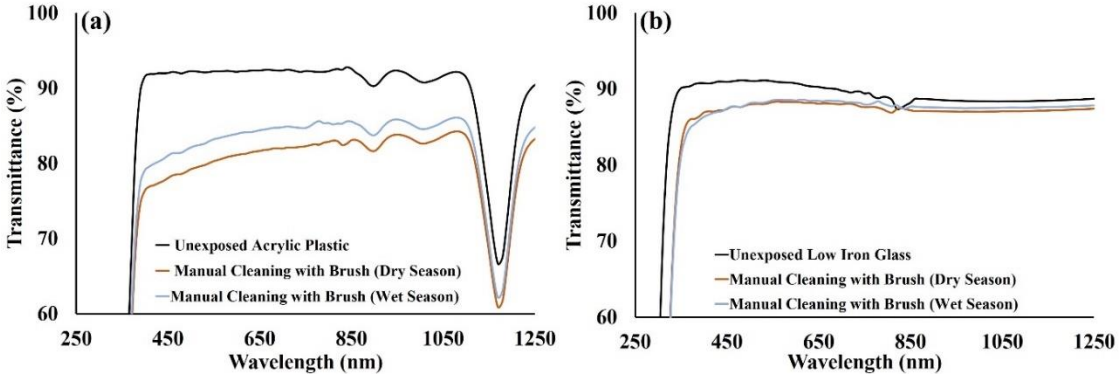

Figure 7.8: Optical transmission losses variation considering the seasonal disparity of a soiled coupon with a clean one exposed under manual cleaning with brush (a) acrylic plastic, (b) low iron glass coupon.

The findings from Figure 7.9 shows that this technique presented a low initial cost, high effectiveness on low iron glass, but average on acrylic plastic; the monthly cost is average in a developing country where the minimum wage is meagre. However, the technique presented a high rating in limitation and appeared to have a very low-reliability rating. Overall, based on the results demonstrated in Figure 7.9, the technique is grossly inefficient as its performance is below average during the two seasons.

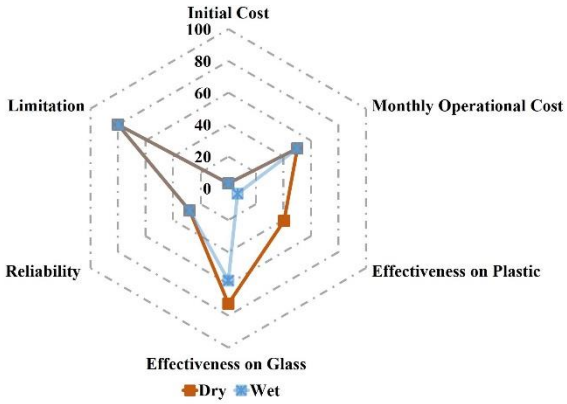

Figure 7.9: Performance assessment of manual cleaning with brush illustrating cost variation, limitation, effectiveness on coupon cleaning, and reliability.

7.3.1.3 Natural cleaning by wind and rain

As expected, a significant increment in optical losses is observed when natural cleaning by wind and rain were expected to act as a soiling cleaning technique. The results illustrated the most substantial losses in Figure 7.10 shows that about

28% optical loss reduction was recorded on acrylic plastic when exposed during the dry season and about 15% during the wet season. Similarly, considerably higher optical losses were recorded on the low iron glass, with about a 15% reduction on a coupon exposed during the dry season and a 14% reduction during the wet season. There was a wide variation (10%) of optical losses between acrylic plastic coupons and low iron glass coupons exposed during the dry season. Still, a relatively small difference was observed during the wet season.

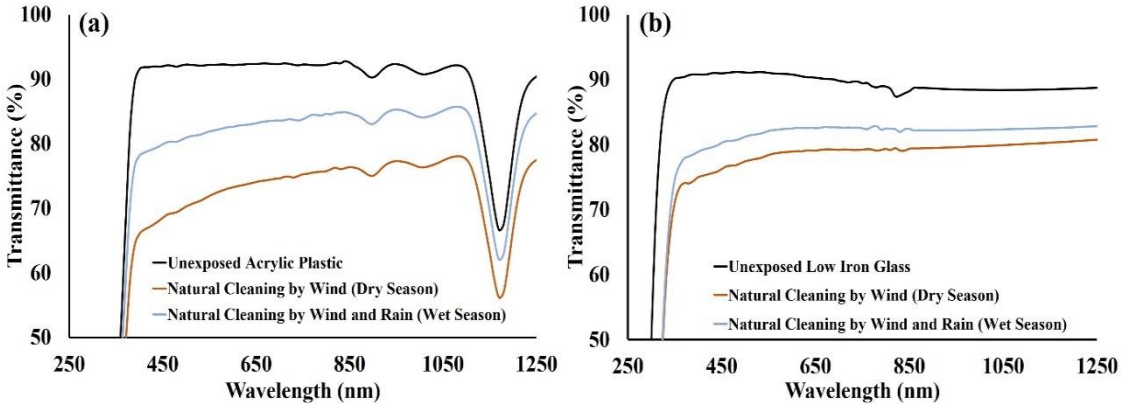

Figure 7.10: Optical transmission losses variation considering the seasonal disparity of a soiled coupon with a clean one exposed under natural cleaning by wind and rainfall (a) acrylic plastic (b) low iron glass coupon.

The natural cleaning technique's assessment findings are presented in Figure 7.11. It shows zero initial cost, zero monthly cost, and effective on both coupons during both seasons. This technique's overall performance during both seasons is below average, making it an unreliable approach. Conversely, the technique has a high rating in limitation and extremely low reliability during the dry season but average during the wet season.

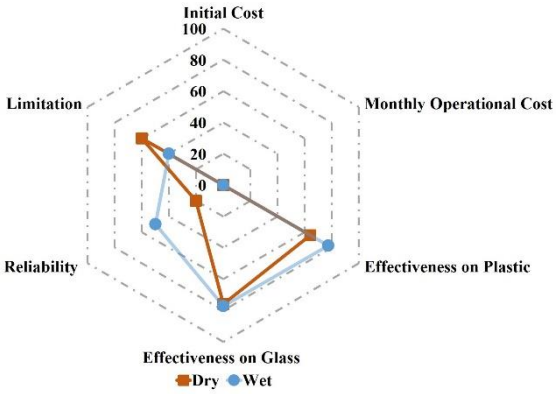

Figure 7.11: Performance assessment of natural cleaning with wind and rainfall illustrating cost variation, limitation, effectiveness on coupon cleaning, and reliability.

7.3.1.4 Self-cleaning

The optical losses of exposed coated coupons were determined using an unexposed coated coupon's optical transmittance as the benchmark instead of a clean coupon. However, Figure 7.12 (a) and Figure 7.12 (b) presented the optical transmittance characterisation of a clean coupon, followed by the unexposed coated coupon and then the exposed coupons. The result from self-cleaning techniques illustrated in Figure 7.12 (a) showed an optical loss of about 8% reduction when a coated acrylic plastic was exposed during the dry season and 3% on a similar coupon exposed during the wet season. On the other hand, findings illustrated in Figure 7.12 (b) show that a 5% reduction was recorded on a coated low iron glass coupon exposed during the dry season and only about 1% reduction was recorded on a coupon exposed during the wet season, which is the lowest losses recorded on all the exposed coupon from various mitigation techniques.

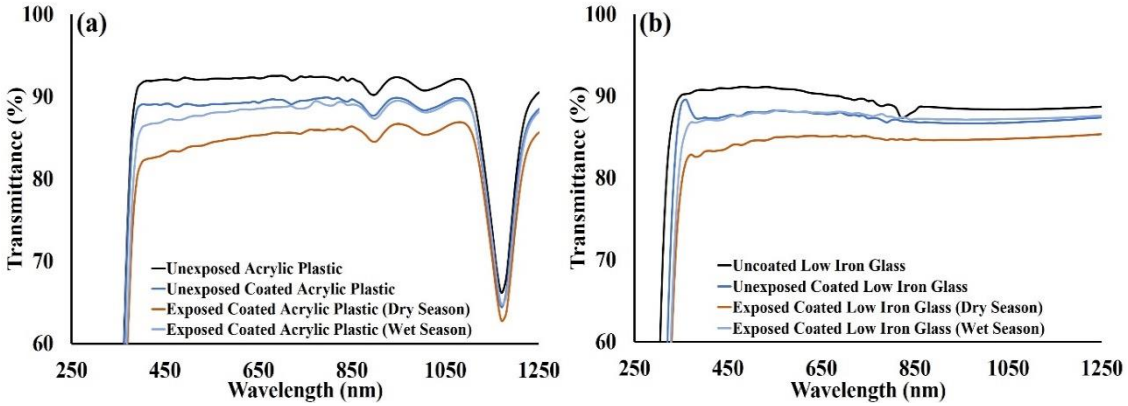

Figure 7.12: Optical transmission losses variation considering the seasonal disparity of a soiled coupon with a clean one exposed under self-cleaning by hydrophobic coating (a) acrylic plastic, (b) low iron glass coupon.

This is the only technique where results are presented in two radar charts to illustrate the variation of the cost implication between tiny coupons (50 mm x 50 mm) and a 320 W solar panel (1956 mm x 992 mm). The result illustrated in Figure 7.13 (a) shows that the technique has a low initial cost, meagre monthly maintenance cost, appears to be effective on both coupons with a better performance during the wet season, and reliability rating is high coupons. However, a high limitation rating is presented during the dry season, and an average limitation is presented during the wet season. The overall performance rating for self-cleaning on a coupon offered an average rating for a dry season but an above-average rating during the wet season. On the other hand, Figure 7.13 (b) presented a sizeable solar module estimation that shows a low maintenance cost, high effectiveness on coupons, and a high-reliability rate. However, it comes with a high initial cost and a high rating of limitation on both coupons. The overall performance based on the estimation result shows the high-performance rating on both coupons during both seasons.

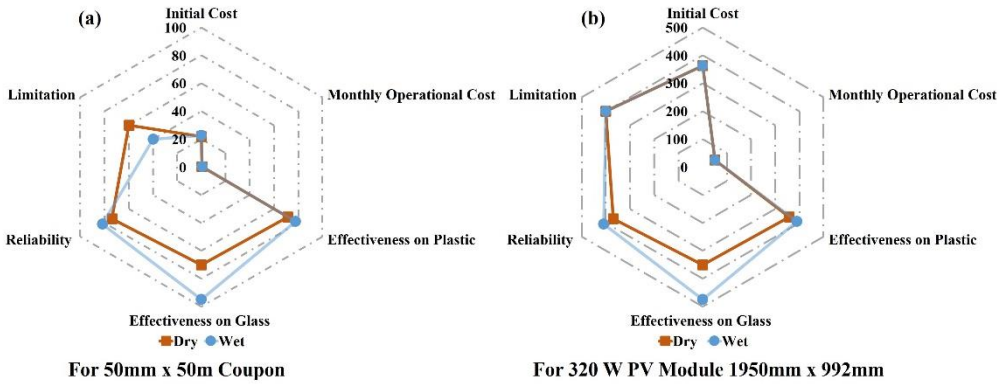

Figure 7.13: Performance assessment of hydrophobic self-cleaning illustrating cost variation, limitation, effectiveness on coupon cleaning, and reliability for (a) coating on 50 mm x 50 mm coupon, (b) estimation of coating 1956 mm x 992 mm PV module.

7.3.1.5 Mechanised cleaning

The mechanised cleaning technique's impact shows quite surprising findings where high optical losses were recorded. Figure 7.14 (a) shows that ~9% reduction was recorded on acrylic plastic coupons exposed during the dry season and 10% during the wet season. On the other hand, the result illustrated in Figure 7.14 (b) shows relative low optical losses on the exposed low iron glass coupon that were cleaned using a mechanised technique with about 5% reduction during the dry season and about 6% decrease during the wet season.

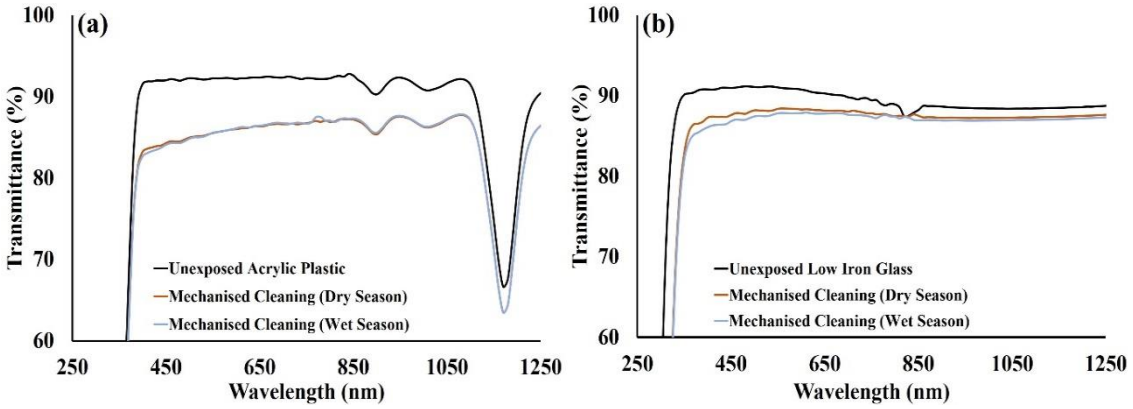

Figure 7.14: Optical transmission losses variation considering the seasonal disparity of a soiled coupon with a clean one exposed under mechanised cleaning with wiper (a) acrylic plastic, (b) low iron glass coupon.

The finding for the mechanised cleaning technique shown in Figure 7.15 illustrated that the technique has a low/near average initial cost of equipment required for installation. The monthly operational and maintenance cost is average in developing nations with meagre minimum wage, the system reliability during the dry season is above average. However, it is below average during the wet season; it is highly effective on both coupons during the dry season. The effectiveness appears to be above average on the low iron glass during the dry season and below average on acrylic plastic during the wet season for both coupons. However, the technique is rated high in limitation. Based on the findings presented in Figure 7.15, this mitigation approach is rated as an average technique.

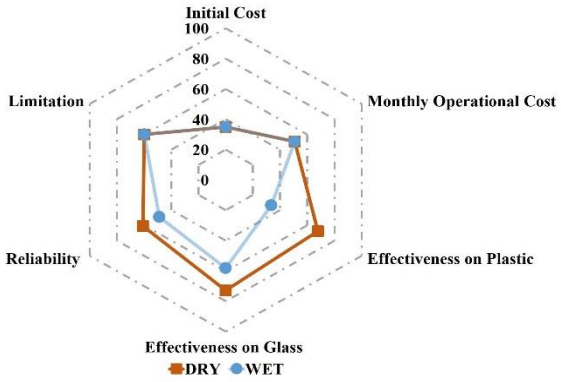

Figure 7.15: Performance assessment of mechanised cleaning approach illustrating cost variation, limitation, effectiveness on coupon cleaning, and reliability.

The findings are not constant, and the two variables (coupon and season of exposure) presented a considerable variety. These disparities may be understated; however, they could lead to system performance failure over an increased length of exposure and make mitigation techniques redundant and useless. This section demonstrated optical losses and performance variations in various techniques considering time stamps and covering materials. It highlighted different performance parameters considered, and its grading is for the techniques.

A variation was observed across all-optical transmittance results around the region of 350 – 850 nm wavelength, where more losses were recorded as the wavelength gets lower towards the UV range. It assumed that tiny particles could efficiently attenuate or absorb the influx of photons with smaller wavelengths. When the photon's wavelength is larger, falling in the VIS and NIR range category, more in wavelength is assumed to escape attenuation and absorption by the tiny particles when they are not evenly distributed on a surface.

7.4 Discussion

The negative impact of soiling seems to be of particular importance, and various mitigation techniques were examined to identify the most suitable one for the region. There is no doubt that there might be a stringent criterion used to improve this approach. However, the knowledge of the optical losses is essential in determining each soiling mitigation technique's performance, and it is vital to evaluate each technique's performance since it is location dependent.

The results presented in the previous section shows substantial performance variation among the various mitigation techniques. Findings show that the most significant optical losses were recorded on the coupons under the natural cleaning technique during the dry season with about 28% reduction in acrylic plastic and 15% for low iron glass. The lowest optical loss was recorded on a glass coupon under self-cleaning during the wet season with about a 1% reduction. The technique that yielded the most favourable performance for both dry and wet seasons was the self-cleaning technique on a coupon; however, manual cleaning with squeegee and water also presented a high performance during the dry season. The self-cleaning method presented high performance during the dry season because of reducing the adhesion force provided by the composite material used in the coating, which reduces the accumulation rate. On the other hand, the technique that offered the lowest performance during the dry season was cleaning with a brush and mechanised cleaning for the wet season. Although natural cleaning happens to deliver a high loss during the dry season, it can be observed that it is not the most ineffective during the wet season. Sarver

et al. (2013) supported this claim by stating that natural cleaning can sometimes be the most effective approach with zero cost.

The computational performance analysis shows that seasonal variation influences the performance disparity of the various techniques; besides, coupon type is a critical factor strongly linked to the particular technique. The analysis shows that the self-cleaning approach offers high performance on both coupons during the wet season and glass during the dry season. Manual cleaning with squeegee/water and self-cleaning have almost the same performance rating on acrylic plastic during the dry season. The self-cleaning coating can suspend particles and protect the covering material, and when the water comes, it can roll it off the panel surface.

Quan et al. (2017) stated that anti-soiling coating could reduce dust adhesion on a coated surface. The statement justifies the low accumulation on the coupon's surface, particularly during the wet season. Figure 7.5 (a) shows high wind velocity during averages of > 4 m/s for both seasons, and in addition to that heavy rainfall, was presented during the wet season, as illustrated in Figure 7.5 (b). Gholam et al. (2017) stated that wind velocity above 4 m/s could play a critical role in determining the accumulation rate on surfaces. It is compatible with the claim that high wind velocity plays a vital role in removing particles. It is assumed that this wind also reduces the amount of accumulated dust on coupons, so the uncleaned coupons were referred to as natural cleaning coupons. A higher rating of about 50% was recorded on a low iron glass exposed in the same solar farm in the same month but different surface orientation. The only disparity is that coupons used in this research were positioned in the North-East direction facing the incoming wind during dry season exposure (January 2020), while the other coupon was exposed to the region's optimum surface orientation (0°/180°). Hee et al. (2012) illustrated how an inward wind reduces accumulation on a facing coupon and more reduction in rainfall.

The findings also show techniques that did not yield the expected performance, with the worst recorded on the manual cleaning using a brush for both coupons during the wet season and on plastic during the dry season. Mechanised

techniques appear to present the worst performance on glass coupons exposed during the dry season. This lesson is directly related to cleaning the coupon with a dirty brush and a dusty wiper brush. Both the brush and the wiper were cleaned at the beginning of the study but were intentional, never washed to determine if they can contribute to additional losses. Figure 7.3 illustrated the mechanised platform's image before and after exposure, and it was observed that the platform and wiper blade, in particular, accumulated a significant amount of dust.

The main reason for employing glass and plastic over PV cells' surfaces is to protect them from harsh environmental conditions. The findings highlighted that acrylic plastic has higher transmittance levels (92%) before exposure than low iron glass (91%). However, more significant optical losses were recorded on acrylic plastic coupons under all the mitigation techniques attributed to its adhesion characteristic and prone to scratches. It indicates why low iron glass remains the better option since it has less attractive forces and is less prone to scratches. Sarver et al. (2013) stated that, so far, glass has been demonstrated to be the long-lasting serving PV covering material that is durable for the system's lifetime. The optical loss findings of a manual technique demonstrated a significant transmittance reduction during the dry season. The loss from cleaning with a brush on acrylic plastic triples the low iron glass loss. The acrylic plastic possesses three negative factors (prone to degradation due to UV, easily scratched and high adhesion force), making it a less preferable material for the arid and semi-arid region (Chanchangi et al., 2020a; Midtdal and Jelle, 2013).

All the soiling mitigation approaches investigated have few limitations, with some related to exposure location. Some presented manageable limits, while others presented an insurmountable limitation impediment. The manual cleaning with squeegee and water presented such as; requiring personnel which needs to be provided with adequate training, untrained personnel can easily break a panel or cause other damages, and maintenance staff are prone to electrocution. The manual cleaning with the brush provided limitations such as; requiring personnel which need to be provided with adequate training, abrasion could occur in acrylic, plastic, untrained personnel can easily break a panel or cause other damages, maintenance staff are prone to electrocution during the wet season if not using

proper personal protective equipment (PPE). The natural cleaning technique possesses limitations such as; uncertainty, seasonal variation, particular PV orientation for optimum cleaning, might require monitoring, and might cause negative impact such as cementation when light rainfall occurs after a sandstorm. The self-cleaning mitigation possesses its limitation: seasonal dependency, high maintenance cost for large scale, the coating could only last for only two to three years (Jamil et al., 2017). Some limitations were also identified for the mechanised mitigation approach: the high cost of installation and extensive maintenance, reliability issues might arise when automated to operate with a sensor, blade requires cleaning during the dry season; otherwise, high level of abrasion might occur.

Some comprehensive reviews of the various soiling technique's efficiency and performance provided insufficient procedures and performance data. Therefore, according to the application technique, a comparative summary of performance variations is presented in Table 7.2 to Table 7.5 below.

Table 7.2: Summary of performance variation illustrating a comparison between this study and published review studies for Natural cleaning.

Technique	Research	Requirement	Advantages	Disadvantages	Efficiency			Improvement
Natural Cleaning	Gupta et al. (2019)	• Rainfall • Wind • Snow • Gravity • PV Tilt angle	• Zero Cost	• Weather dependent • Location dependent • Ineffective on small dust particle	• Not Available			• Not Available
	Jamil et al. (2017)	• PV Tilt Angle • Rain	• No Cost	• Dependent on-site condition • Dependent on weather • Only deal with large dust particles, more than 10 µm rather than smaller ones (2–10 µm)	• Unpredictable • It could be less effective			• Superhydrophobic or hydrophobic coating to enhance performance with rain
	Deb and Brahmbhatt (2017)	• PV tilted to 23-25 • Rain	• Zero cost	• Weather and location-dependent; • Only large particles	• Unpredictable • surface property can be improvised			• Not Available
	This study	• High wind Velocity • Heavy rainfall • PV orientation • PV tilt angle	• Zero Cost • It can be integrated to work with other technologies to reduce costs. • Highly effective in regions with heavy rain.	• Weather dependent • Site dependent • Unreliable	**Coupon**	**Season**		• An optimal performance can be integrated with other techniques to reduce maintenance costs. • Required monitoring to achieve high performance.
						Dry	**Wet**	
					Plastic	72%	88%	
					Glass	85%	86%	

Table 7.3: Summary of performance variation illustrating a comparison between this study and published review studies for manual cleaning.

Technique	Research	Requirement	Advantages	Disadvantages	Efficiency			Improvement
Manual cleaning	Gupta et al. (2019)	• Human resources • Water • Brushes • Cloths • Detergent • Ladder	• Effective in recovering PV Performance • Performed whenever required	• High labour cost • Water limitation in arid regions • Scratches may be developed with time	• 100%			Not Available
	Jamil et al. (2017)	• Workforces • Water • Detergent/Chemical • Brush/Cloth • Equipment	• Highly efficient in restoring the PV performance	• High cleaning cost • Abrasion could be produced	• Effective in any condition			• Resource for cheap labour to reduce the cleaning cost • The use of soft material could replace brushes
	Deb and Brahmbhatt (2017)	• Labour • Water • Cleansing agents • Equipment	• Considerably efficient in reinstating PV cleanliness	• High cost • It could be abrasive to the PV surface	• Effective at all times			• Cheap labour is required
	This Study	• Personnel • Water • Squeegee	• Reliable and effective • Cheap labour in a developing country • On-demand • Job opportunity • Reduce PV temperature for better performance	• Expensive in the developed world • Tendency of abrasion • Prone to electric shock	**Coupon**	**Season**		• PPE should be used at all times to avoid electric shock • Personnel should be provided with adequate PV maintenance training
						Dry	**Wet**	
					Plastic	91%	94%	
					Glass	96%	97%	
		• Personnel • Brush	• On-demand • Job opportunity	• Unreliable • Very difficult to regain high PV performance • Very expensive in developed countries	**Coupon**	**Season**		• Cleaning should be conducted with water during the dry season • Wind direction should be determined before cleaning to avoid dust transfer from one module to another.
						Dry	**Wet**	
					Plastic	83%	86%	
					Glass	95%	95%	

Table 7.4: Summary of performance variation illustrating a comparison between this study and published review studies for hydrophobic self-cleaning.

Technique	Research	Requirement	Advantages	Disadvantages	Efficiency			Improvement
Self-cleaning Super-hydrophobic Surface	Gupta et al. (2019)	• Forming hydrophobic • Chemical coating • Water	• Requires zero power • Improve the natural cleaning	• Limited lifetime • Reduced the optical performance	• 71.80%			Not Available
	Jamil et al. (2017)	• Fabricated hydrophobic layer • Chemical coating Water	• Passive and power are not required.	• Uncertain durability of plastic due to UV • Acid rain and salty air might cause layer degradation • Dust accumulation increases with time • Dependent on rainfall • High initial cost whenever applied to large scale PV system	• Moderately performance efficiency in the presence of rain			• The use of high polymer, glass or coating could increase durability • Require cleaning during the dry season.
	Deb and Brahmbhatt (2017)	• Hydrophobic layer • Chemical coating or screen layer • water	• Passive method • Power not required	• Degradation of the plastic screen due to UV • Dust accumulation with time • Cleaning requires water	• Medium efficiency in the rain			• Requires weatherproof surface to improve performance • Require regular cleaning
	This study	• Chemicals for Coating • Determining transparency and hydrophobicity. • Water	• Does not require human support during the wet season. • Passive approach • Highly reliable during the wet season.	• Uncertain durability of plastic. • Water dependent. • Performance reduces during the dry season. • Lifetime is very minimal • Reduces transmittance	**Coupon**	**Season**		• PV manufacturing companies or glass companies should accept changing covering surfaces for recycling a couple of times during the life cycle. • These techniques required integrating additional techniques to support it during extreme dry, dusty weather such as Harmattan.
						Dry	**Wet**	
					Plastic	92%	97%	
					Glass	95%	99%	

Table 7.5: Summary of performance variation illustrating a comparison between this study and published review studies for mechanised cleaning.

Technique	Research	Requirement	Advantages	Disadvantages	Efficiency			Improvement
Mechanised Cleaning	Gupta et al. (2019)	• Wipers • Blower • Brushes • Motors • Gears • Chains • Sensors	• Reduces labour cost • Automation • Both cleaning & scrubbing	• Maintenance requirement • Energy consumption • High capital cost	• 95%			Not Available
	Jamil et al. (2017)	• Brush/Wiper Mechanical prime Mover components (motor, gears, and chains) • Robotic (optional)	• Dropping system temperature with water • Automatic activation of cleaning with sensors and controls • Bird scaring • Decreases labour cost and increases system independency	• Abrasion due to contact with PV panel's surface. • Cleaner quickly get dirty (brush and wiper) • The system requires its maintenance • Energy consumption • High initial cost	• Useful in an uncertain time			• Cleaning schedule to be arranged when the system is not operating to avoid shock • Soft material should replace brushes and wipers • The automated motorised part could save the energy
	Deb and Brahmbhatt (2017)	• Motor • Brush • Wiper • Robot (if any)	• Reduces temperature with water • Automated operation by sensors and controller • Scares birds • Less labour cost • The system can be independent	• The surface is abrasive due to direct contact with PV • Dust accumulation on cleaning material • Increase in energy consumption • Higher capital cost; • Higher maintenance cost	• Uncertainty inefficiency			• Cleaning frequency should be reduced to minimise abrasion • A High-efficiency motor could reduce the energy required for operation • The system required periodic maintenance
	This study	• Wiper/Blade • Electric Motor • Battery • Operational personnel or Arduino for automation	• Reduces labour cost • Can operate independently • Energy can be used obtained from the system when excess energy is available • Scares birds, rodents and reptiles	• System initial and maintenance cost is high • Required continues maintenance • Accumulated dust on the brush could cause surface abrasion.	**Coupon**	**Season**		• Water injection through blades could improve cleaning efficiency during the dry season. • Blade or brush should periodically be cleaned to avoid accumulation. • Appropriate maintenance should be provided before sunrise.
						Dry	**Wet**	
					Plastic	91%	90%	
					Glass	95%	94%	

It should be noted that literature used in comparison Table 7.2 Table 7.3 Table 7.4 Table 7.5 are obtained from review articles and not actual research were as data presented from this study are actual findings obtained through experiments. Table 7.2 compared the findings from examining the effectiveness of the Natural cleaning technique and other reported findings. It shows that PV orientation is a factor necessary for influencing the natural cleaning of a region. It assists when wind direction and heavy rain flows towards the module. Two vital points were provided as additional advantages observed from this study: heavy rain could be highly effective. The technique could be integrated with others to improve their performance in regions with high rain rates. The advantages appear to be almost the same, highlighting the unreliability of the technique, weather dependent, and location. The study provided optical efficiency degradation based on transmittance reduction for two seasons and considering PV surface covering material.

Comparison of the manual cleaning result obtained from this study and the reported findings in Table 7.3 show variations and inadequate consideration of some regions concerning labour. The literature shows that the technique is costly, related to the cost implication of labour that varies between developed countries and underdeveloped. In developed countries it labour is costly while it is cheap in underdeveloped countries. This technique serves as a source creating job opportunities for the community and promoting local acceptance in under development. The efficiency of this technique has not been reported, but it is widely employed. This study provided performance levels considering seasonal variation and types of coupons.

Manual cleaning with squeegee and water is a widely used technique in regions with the availability of water. It improves the performance in two ways; improving transmittance and reducing temperature. These two factors could allow the generation of optimal yield. The literature is relatively silent on the impact of temperature reduction, but this study highlighted it in Table 7.3. The similarity observed in the performance comments where all studies presented show the technique is efficient in recovering from soiling losses. However, Gupta et al. [4]

were the only ones among the literature that provided value that is not specific on the seasonal disparity and type of coupon variation. Self-cleaning provides a preventive and restoration approach, and the literature shows it requires water and performance is generally reported to moderate. However, this study shows that it is highly reliable during wet seasonal. The findings show better performance of the technique on the low iron glass compared to acrylic plastic. The disparity was observed in the performance comments, where the literature presented in Table 7.4 shows the technique's performance is low. However, Gupta et al. [4] were the only ones in the literature that provided a higher value that is not closer to this study.

The comparison table of mechanised technique (Table 7.5) provided similar information between literature and this study, except in performance where only Gupta et al. [4] and this study provided a similar numerical value on low iron glass coupon exposed during a dry season. Literature provided studies that proposed some improvement on the various technique. This comparative information highlighted the variation from these studies and others and illustrated the novelty of the research work.

The outcome of various experiments shows that the self-cleaning technique is the approach that exhibited the highest performance during both the wet season and dry season. The manual cleaning with squeegee and water also revealed high performance during the dry season. Although this is only a limited study, the full potential of approaches could be further investigated. However, PV modules need cleaning to sustain or restore output performance, and thus far, this study is the only outdoor research in the region. Therefore, the study recommends using a hybrid cleaning technique during the dry season where self-cleaning (hydrophobic or superhydrophobic coating) and manual cleaning with water and only self-cleaning (hydroponic or superhydrophobic coating) cleaning during the wet season for the region. Using water can improve the cleaning rate during the dry season without rainfall; it will also help reduce the temperature for better performance. This study recommends using low iron glass in arid or semi-arid regions with high solar irradiance, temperature and UV. The low iron glass

coupon appears to be the most suitable PV covering material since it has fewer adhesion forces and is less affected by UV light. Additional research is recommended to investigate the use of various mitigation techniques on an exposed working solar module in the arid or semi-arid region to determine their effectiveness and stability over a longer duration and a periodic frequency cycle.

7.5 Summary and conclusion

Chapter seven of the thesis investigated the effectiveness of low-cost mitigation techniques that could solve all the problems (impact of dust, considering influencing factors) highlighted from chapter three to chapter six of the thesis. The findings show a variance of performance among different soiling mitigation techniques. The hydrophobic self-cleaning provides about 99% transmittance recovery during the wet season, manual cleaning and self-cleaning restoring about 95% transmittance during the dry season. The result further demonstrated that low iron glass is more durable and practical than acrylic plastic when exposed to harsh conditions. In conclusion, the study demonstrated that self-cleaning coating could be employed as the region's primary cleaning strategy during the wet season and a hybrid approach, including self-cleaning and manual cleaning with water during the dry season. This could sustain the performance PV at an optimal level year-round and reduce unnecessary soiling losses, which would portray a positive image of the technology and improve its penetration in the region.

The outcome of various experiments shows that the self-cleaning technique is the approach that exhibited the highest performance during both the wet season and dry season. The manual cleaning with squeegee and water also revealed high performance during the dry season. Although this is only a limited study, and the full potential of approaches could be further investigated. However, PV modules need cleaning to sustain or restore output performance, and thus far, this study is the only outdoor research in the region. Therefore, the study recommends using a hybrid cleaning technique during the dry season where self-cleaning (hydrophobic or superhydrophobic coating) and manual cleaning with water and only self-cleaning (hydrophobic or superhydrophobic coating) cleaning

during the wet season for the region. The use of water will improve the cleaning rate during the dry season in the absence of rainfall; it will also help reduce the temperature for better performance. The low iron glass coupon appears to be the most suitable PV covering material since it has fewer adhesion forces and is less affected by UV light.

8 Chapter Eight - Conclusion and recommendations

8.1 Conclusion

The rapid growth of Nigeria's population has created a wide gap between the demand and supply of electricity, and the overdependence on fossil fuel has severe adverse socio-economic, environmental and health effects. The country is suffering from an unstable, unreliable, and inadequate supply of electricity. Energy poverty is very high, yet the enormous abundant renewable energy in the country is still relatively untapped. The economic and environmental benefits of the PV technology have made the system the most sustainable clean energy solution to enable developing countries to achieve SDG-7. This has led them to invest in solar energy to increase the penetration of renewable energy in their supply mix and reduce global warming. However, besides the low efficiency of the technology, which is undergoing massive research globally, dust accumulation adversely affects its performance. It has a detrimental effect on PV performance, and this area has been drastically underestimated and understudied in regions with massive solar energy potential, low PV penetration and a high energy deficit in some regions such as Nigeria.

To improve solar PV technology penetration and reduce GHG emission in Nigeria, the impact of dust accumulation on PV performance has been investigated, considering seven influencing factors to determine the most suitable approach to mitigate the problem. This study reviewed Nigeria's energy crisis and renewable energy focusing on solar energy potential and penetration. Several challenges were identified, and the study was narrowed and focused on resolving a particular technical issue (the effect of soiling on PV performance). Chapter three of this thesis presented a detailed indoor experiment on the impact of 13 dust samples on PV performance, considering two different PV surface covering materials using two deposition conditions. Several outdoor studies investigated the impact of dust, considering weather conditions, environmental variation, PV positioning, and PV surface covering materials. Several mitigation techniques were investigated on-site to determine the most suitable approach for the region.

The outcome confirms that Nigeria has enormous solar energy potential because of its proximity to the Sun Belt. Solar energy technologies were identified and recommended as the most viable solution to Nigeria's energy crisis; thus, this thesis emphasises that the federal government must vigorously pursue integrating these technologies into its supply mix.

The findings from the indoor study reveal the following: charcoal powder has the most significant effect on light transmittance, affecting short circuit current and causing the most significant degradation in PV yield performance (98% power reduction), while salt was found to be the lowest (7% power output reduction). A number of dust particles (such as salt, coarse, carpet dust and cement) appear to possess good optical characteristics, but the negative attributes outweigh these due to the accumulation in layers. The research identified acrylic plastic as the material that accumulates a higher quantity of dust than low iron glass. The wet deposition of dust particles (representing dew or light rain) promotes the retention of more particles on a surface than dry deposition since the capillary force can create bridges between particles and the surface.

The result of angular dependencies of soiling loss reveals some exciting points/results. Horizontal positioning of a coupon could influence significant dust accumulation causing transmission reduction from 5% to 38% over a month; the tilt (45°) positioning resulted in about 3% to 17%, while the vertical position decreased 1% to 10%. About 88% transmission reduction for a coupon exposed on a horizontal plane during the dry season was recorded, 37% during the wet season. For the 45° tilt position, 4% was recorded during the dry season and 19% for the wet season. For the vertical position, 14% was recorded during the dry season and 15% for the wet season. The annual optical losses presented a similar trend showing transmission reduction of about 59%, 42%, and 34% for horizontal, tilt (45°) and vertical positions. These reductions of light transmittance resulted in a corresponding degradation of power performance output.

The outcome of PV yield losses correlation presented an alarming performance decrease due to soiling on all exposed modules. The most significant I_{SC}

reduction recorded was on a-Si with a 73% decrease, and the lowest was about a 65% decrease for the Si modules in one year without cleaning and seventeen months of exposure. Egregious performances and efficiency losses were recorded on exposed modules, presenting a yield loss of 78.3% for a-Si, 77% for CdTe, 70% for pc-Si, and 68.6% for the mc-Si module. Simultaneously, efficiency losses of 78% for a-Si, 77% for CdTe, and 71% for both mc-Si and pc-Si modules were recorded. A wide variation was recorded between months and seasons, January 2021 and dry presenting the most effective rates. Results of optical losses validated the above performance losses with a similar trend. The particle characterisation reveals that mineral particles >PM_{10} size with opaque and translucent morphology were the primary constituent dust formation on the examined coupons.

The PV soiling mapping results through optical losses demonstrated high optical losses in a region with enormous solar energy potential but shallow PV penetration. Coupons positioned on horizontal planes accumulate more dust than the tilt angle (45°) vertical plane. ABV was the region with the most significant soiling rate in the country, and February was the month with the highest level. The northern region has a higher soiling rate during the dry season, with ABV having the most effective rate, while during the wet season, the Southern region shows a higher accumulation rate, with LOS and PHC topping the list. SEM/EDX analysis confirmed that minerals collected on coupon surfaces negatively affect light transmittance, causing the recorded optical losses. The AQI and air pollutant data validate the type of particles recorded. The weather condition shows why high accumulation rates are recorded from each region and during a specific season.

The findings from the outdoor experimental investigation on the effectiveness of soiling mitigation approaches. A variance of performance among different soiling mitigation techniques, with the self-cleaning (hydrophobic coating) providing 99% transmittance recovery during the wet season and manual cleaning and self-cleaning restoring 95% transmittance during the dry season. The most significant loss was recorded on an acrylic plastic coupon exposed under natural cleaning

strategy during the dry season with a 28 % transmittance reduction. It was observed that high wind velocity has a more negligible cleaning effect when compared with heavy rainfall. The low iron glass was more durable and effective than acrylic plastic when exposed to harsh environmental conditions.

In summary, the study illustrated a range of dust particles with different properties posing different levels of light transmittance disturbance to PV cells. The study developed a low-cost approach to investigating soiling. Soiling is related to PV angular positioning (tilt angle), with the horizontal position accumulating more, and the density slowly decreases as the angle becomes inclined towards the vertical direction. The angular positioning influences dust accumulation density with a higher mass recorded on a coupon exposed to an extreme condition in a horizontal position compared to tilt (45°) and vertically. However, other parameters such as weather conditions, particles characteristics, PV covering materials, location, and exposure period could significantly influence the accumulation, and some might be more sensitive than angular orientation. This thesis demonstrated a unique technique that illustrated optical losses by employing a radical approach and showing a wide variation of soiling losses under-reported by previous studies and grossly underestimated by GSA (2020). This might be due to overlooking regional variation and the seasonal difference that plays a vital role in increasing or decreasing the losses rate. The study offers a successful low-cost approach that could be employed to determine global PV soiling rates. It has established that a self-cleaning coating could be employed as Nigeria's primary cleaning strategy during wet and a hybrid approach, including self-cleaning and manual cleaning with water during the dry season. The approach could maintain the PV performance at an optimal level year-round and reduce unnecessary soiling losses, which would present a positive image of the technology to potential investors and improve its penetration in the region.

The asperity of all the yield losses observed cannot be overlooked. The research work concludes that the region's prevailing soiling is exceptionally high and requires immediate attention since a sizeable financial commitment has been made. Besides, to prevent further performance losses and possible future system degradation within a short period for all the installations, protecting or restoring

the PV performance from soiling could amplify penetration of the technology so that sustainable development goal 7 ("Ensure access to affordable, reliable, sustainable and modern energy for all") target can be realistically achieved.

8.2 Recommendations for future work

Based on the findings and observations from various studies conducted throughout this research, the following are provided:

The Nigerian government must pursue the documented policy (NREEEP) of incorporating renewable energy in the supply mix, diversifying and increasing the supply. The government should also try making an effort to implement the policy and its recommendations.

Solar energy remains the most viable option to solve the persisting energy crisis in Nigeria as it can supply electricity from off-grid and remote areas. It can reduce both the pressure mounted on fossil fuel and has a limited negative impact on our ecosystem and its inhabitants and, as such, should be urgently exploited.

The angular solar PV positioning at a horizontal plane should be avoided where possible as long as PV performance is not compromised.

The findings provided soiling periods for various regions in Nigeria. The data could be used in forecasting soiling events in the region and for planning cost-effective maintenance. In this way, optimal scheduling for the prevention and restoration of PV performance could be achieved to accelerate its penetration and minimise emissions.

The low-cost soiling study should be adopted to investigate the effect of dust accumulation on PV in all geographical regions worldwide to acquire data that can be used for more efficient and effective planning of any future solar PV installation.

Finally, this research strongly recommends further study on each technique's performance and cost analysis on a full pledge PV panel over a longer duration in different regions. Developing a cost-effective approach to producing a bi-functional coating on a solar cell cover should be considered one of several urgent needs by the solar cell industry.

Bibliography

Abdallah, A., Martinez, D., Figgis, B., and El Daif, O. (2016). Performance of Silicon Heterojunction Photovoltaic modules in Qatar climatic conditions. *Renewable Energy,* ***97*** (2016), 860-865. DOI: https://doi.org/10.1016/j.renene.2016.06.044.

Abderrezek, M., and Fathi, M. (2017). Experimental study of the dust effect on photovoltaic panels' energy yield. *Solar Energy,* ***142*** (2017), 308-320. DOI: http://dx.doi.org/10.1016/j.solener.2016.12.040.

Abdolzadeh, A., and Nikkhah, R. (2019). Experimental study of dust deposition settled over tilted PV modules fixed in different directions in the southeast of Iran. *Environmental Science and Pollution Research,* ***26*** (2019), 31478–31490.

Adaramola, M. S. (2014). Viability of grid-connected solar PV energy system in Jos, Nigeria. *International Journal of Electrical Power & Energy Systems,* ***61*** (10), 64-69. DOI: 10.1016/j.ijepes.2014.03.015.

Adaramola, M. S., Paul, S. S. and Oyewola, O. M. (2014). Assessment of decentralised hybrid PV solar-diesel power system for applications in the Northern part of Nigeria. *Energy for Sustainable Development,* ***19*** (2014), 72-82.

Adıgüzel, E., Özer, E., Akgündoğdu, A., and Yılmaz, A. E. (2019). Prediction of dust particle size effect on the efficiency of photovoltaic modules with ANFIS: An experimental study in the Aegean region, Turkey. *Solar Energy,* ***177*** (2019), 690-702. DOI: https://doi.org/10.1016/j.solener.2018.12.012.

Adinoyi, M. J., and Said, S. A. M. (2013). Effect of dust accumulation on the power outputs of solar photovoltaic modules. *Renewable Energy,* ***60*** (2013), 633-636. DOI: http://dx.doi.org/10.1016/j.renene.2013.06.014.

Adom, P. K., and Adams, S. (2017). Energy savings in Nigeria. Is there a way of escape from energy inefficiency? *Renewable and Sustainable Energy Reviews,* ***81*** (2018), 2421-2430.

AfDB. (2017). African Economic Outlook, 2017: Entrepreneurship and Industrialisation.

Air-Plume-Labs (2020). "Air Quality in Abuja." Retrieved 15/07/2020, 2020, from https://air.plumelabs.com/air-quality-in-abuja-9S42.

Air-Plume-Labs. (2020). Air Quality Index. Retrieved from https://air.plumelabs.com/en/.

Aïssa, B., Isaifan, R. J., Madhavan, V. E., and Abdallah, A. A. (2016). Structural and physical properties of the dust particles in Qatar and their influence on the PV panel performance. Scientific Reports.

Ajayi, O. O., and Ajayi, O. O. (2013). Nigeria's energy policy: Inferences, analysis and legal ethics toward RE development. *Energy Policy, **60*** (2013), 61-67.

Ajayi, O. O., Ohijeagbon, O. D., Mercy, O., and Ameh, A. (2016). Potential and econometric analysis of standalone RE facility for rural community utilisation and embedded generation in North-East Nigeria. *Sustainable Cities and Society, **21*** (2016), 66-77.

Akimbami, J. K. (2001). Renewable Energy Resources and Technologies in Nigeria: Present Situation, Future Prospects and Policy Framework. *Mitigation and Adaptation Strategies for Global Change, **6*** (2001), 155-181.

Akinboro, F. G., Adejumobi, L. A., and Makinde, V. (2012) Solar energy installation in Nigeria: Observations, prospect, problems and solution. *Transnational Journal of Science and Technology, **2*** (4), 73-84.

Akinyele D.O., Rayudu., R. K., and Nair, N. K. C. (2015). Global progress in photovoltaic technologies and the scenario of development of solar panel plant and module performance estimation: Application in Nigeria. *Renewable and Sustainable Energy Reviews, **48*** (2015), 112-139.

Akinyele, D. O., Rayudu, R. K., and Nair, N. K. C. (2017). Life cycle impact assessment of photovoltaic power generation from crystalline silicon-based solar modules in Nigeria. *Renewable Energy, **101*** (2017), 537-549.

Akuru, U. B., Onukwubeb, E. I., Okoroc, I. O., and Obe, E. S. (2017). Towards 100% renewable energy in Nigeria. *Renewable and Sustainable Energy Reviews, **71*** (2017), 943-953.

Al Naser, N. W., Al Othman, M. J., Dakhel, A. A., Batarseh, I., Leed, J.K., Najmaii, S., Alothman, A., Al Shawaikh, H., and Alnaser, W. E. (2018). Comparison between the performance of man-made and naturally cleaned PV panels in the middle of a desert. *Renewable and Sustainable Energy Reviews, **82*** (2018), 1048-1055. DOI: http://dx.doi.org/10.1016/j.rser.2017.09.058.

Al Shabaan, G., Shehab, W. A., and Abu-Al-Aish, A. (2016). Effects of Dust Grain Size and Density on the Monocrystalline PV Output Power. *International Journal of Applied Science and Technology,* ***6*** (1), 81-86.

Al Shehri, A., Parrott, B., Carrasco, P., Al Saiari, H., and Taie, I. (2016). Impact of dust deposition and brush-based dry cleaning on glass transmittance for PV modules applications. *Solar Energy,* ***135*** (2016), 317-324. DOI: http://dx.doi.org/10.1016/j.solener.2016.06.005.

Al-Ammri, A., Ghazi, A., and Mustafa, F. (2013). *Dust effects on the performance of PV street light in Baghdad city*. Paper presented at the 2013 International Renewable and Sustainable Energy Conference (IRSEC), Ouarzazate, Morocco. https://ieeexplore.ieee.org/stamp/stamp.jsp?tp=&arnumber=6529687.

Al-Hasan, A. Y. (1998). A new correlation for direct beam solar radiation received by a photovoltaic panel with sand dust accumulated on its surface. *Solar Energy,* ***63*** (5), 323-333.

Aliyu, A. K., Modu, B., and Tan, C. W. (2017). A review of renewable energy development in Africa: A focus in South Africa, Egypt and Nigeria. *Renewable and Sustainable Energy Reviews,* ***81*** (2018), 2502-2518.

Aliyu, A. S., Dada, J. O., and Adam, I. K. (2015). Current status and prospects of renewable energy in Nigeria. *Renewable and Sustainable Energy Reviews,* ***48*** (2015), 336-346.

Alnasser, M. A. T., Mahdy, A. M. J., Abass, K. I., Chaichan, M. T., and Kazem, H. A. (2020). Impact of dust ingredient on photovoltaic performance: An experimental study. *Solar Energy,* ***195*** (2020), 651-659. DOI: https://doi.org/10.1016/j.solener.2019.12.008.

Al-Showany, E. F. A. (2016). The Impact of the Environmental Condition on the Performance of the Photovoltaic Cell. *American Journal of Energy Engineering, 4* (1), 1-7. DOI: 10.11648/j.ajee.20160401.11.

Anumaka, M. C. (2012). The scenario of Electricity in Nigeria. *International Journal of Engineering and Innovative Technology (IJEIT),* ***1*** (6), 2277-3754.

Appels, R., Lefevre, B., Herteleer, B., Goverde, H., Beerten, A., Paesen, R., Medts, K., Driesen, J., and Poortmans, J. (2013). Effect of soiling on

photovoltaic modules. *Solar Energy,* ***96*** (2013), 283-291. DOI: http://dx.doi.org/10.1016/j.solener.2013.07.017.

Argungu, G. M., More, A. U., Dabai, K. A., Abdulazeez, S., and Ahmad, S. K. (2019). Algorithm for the Performance Evaluation of Three Selected Wind Energy Conversion Systems (WECS) for Electricity Generation in Minna, Nigeria *Science Journal of Energy Engineering,* ***7*** (2), 29-31. DOI: 10.11648/j.sjee.20190702.12.

Asl-Soleimani, E., Farhangi, S., and Zabihi, M. S. (2001). The effect of tilt angle, air pollution on the performance of photovoltaic systems in Tehran. *Renewable Energy,* ***24*** (2001), 459–468.

Australian-Standard (2002). AS 4509.2-2002 Standalone power systems - System design guidelines. 3.4.3.6 De-rating Factor. Sydney, Australia, Standards Australia International Ltd. **3.4.3.6.**

Ayodele, T. R., and Ogunjuyigbe, A. S. O. (2015). Increasing household solar energy penetration through load partitioning based on the quality of life: The case study of Nigeria. *Sustainable Cities and Society,* ***18*** (2015), 21-31.

Azouzoute, A., El Ydrissi, M., Zitouni, H., Hajjaj, C., and Garoum, M. (2021). Dust Accumulation and Photovoltaic Performance in Semi-Arid Climate: Experimental Investigation and Design of Cleaning Robot. In S. Motahhir & A. M. Eltamaly (Eds.), *Advanced Technologies for Solar Photovoltaics Energy Systems* (pp. 47-74). Cham: Springer International Publishing.

Bassey-Etuk, E. and Ifeanyi-Nwaoha, C. ((2017)). How Generation Works: The Process, Nigeria's Energy Mix and Future Plans. *EmPower Nigeria,* ***1*** (6), 1.

Baurzhan, S., and Jenkins, G. P. (2016). Off-grid solar P.V.: Is it an affordable or appropriate solution for rural electrification in Sub-Saharan African countries? *Renewable and Sustainable Energy Reviews,* ***8*** (60), 1405-1141.

Beattie, N. S., Moir, R. S., Chacko, C., Buffoni, G., Roberts, S. H., and Pearsall, N. M. (2012). Understanding the effects of sand and dust accumulation on photovoltaic modules. *Renewable Energy,* ***48*** (2012), 448 - 452. DOI: http://dx.doi.org/10.1016/j.renene.2012.06.007.

Becher, R., Øvrevik, J., Schwarze, P. E., Nilsen, S., Hongslo, J. K., and Bakke, J. V. (2018). Do Carpets Impair Indoor Air Quality and Cause Adverse Health Outcomes: A Review. *Int. J. Environ. Res. Public Health,* ***15*** (184), 1-14.

Bernard, O. (2016). The effect of settling harmattan dust on photovoltaic modules in Walewale, Northern Ghana. (Master). Kwame Nkrumah University of Science and Technology.

Boyle, L., Flinchpaugh, H. and Hannigan, M. (2016). Assessment of PM dry deposition on solar energy harvesting systems: Measurement–model comparison. *Aerosol Science and Technology,* ***50*** (4), 380-391. DOI: http://dx.doi.org/10.1080/02786826.2016.1153797.

BP. (2017). bp Statistical Review of World Energy June 2017. In 66th (Ed.), *BP Statistical Review of World Energy* (66 ed.). London: BP PLC.

Brenneman, R. (2016). Air. From https://richardbrenneman.files.wordpress.com/2016/11/blog-air.jpg.

Bugaje, I. M. (1999). Remote Area power supply in Nigeria: the prospect of solar energy. *Renewable Energy,* ***18*** (1999), 491-500.

Bunyan, H., Ali, W. and Alnaser, M. (2016). Enhancing the Performance of Photovoltaic Panel by Proper Washing Periods in Kuwait. *Smart Grid and Renewable Energy,* ***7*** (2016), 190-196. DOI: http://dx.doi.org/10.4236/sgre.2016.76015.

Cano, J., John, J. J., Tatapudil, S., and TamizhManil, G. (2014). Effect of Tilt Angle on Soiling of Photovoltaic Modules. Paper presented at the 2014 IEEE 40th Photovoltaic Specialist Conference (PVSC), Denver, CO USA. https://ieeexplore.ieee.org/document/6925610.

Chanchangi, Y. N., Ghosh, A., Sundaram, S., and Mallick, T. K. (2020). An analytical indoor experimental study on the effect of soiling on PV, focusing on dust properties and PV surface material. *Solar Energy,* ***203*** (2020), 46–68. DOI: https://doi.org/10.1016/j.solener.2020.03.089.

Chanchangi, Y. N., Ghosh, A., Sundaram, S., and Mallick, T. K. (2020). Dust and PV Performance in Nigeria: A review. *Renewable and Sustainable Energy Reviews,* ***121*** (2020), 1-14. DOI: https://doi.org/10.1016/j.rser.2020.109704.

Chesnutt, J. K. W., Ashkanani, H., Guoc, B. and Wua, C. (2017). Simulation of microscale particle interactions for optimising an electrodynamic dust shield to clean desert dust from the solar panels. *Solar Energy, **155*** (2017), 1197-1207. DOI: http://dx.doi.org/10.1016/j.solener.2017.07.064.

CIA. (2018). The World Factbook. Retrieved 07/01/2018, 2018, from https://www.cia.gov/library/publications/resources/the-world-factbook/geos/ni.html.

Conceiç~ao, R., Silva, H. G., Fialho, L., Lopes, F. M. and Collares-Pereira, M. (2019). PV system design with the effect of soiling on the optimum tilt angle. *Renewable Energy, **133*** (2019): 787-796.

Cordero, R. R., Damiani, A., Laroze, D., MacDonell, S., Jorquera, J., Sepúlveda, E., Feron, S., Llanillo, P., Labbe, F., Carrasco,J., Ferrer, J., and Torres, G. (2018). Efects of soiling on photovoltaic (PV) modules in the Atacama Desert. *Scientific Reports, **8*** (13943), 1-14. doi:DOI:10.1038/s41598-018-32291-8.

Costa, S. C. S., Diniz, S A. A. C., and Kazmerski, L. L. (2016). Dust and soiling issues and impacts relating to solar energy systems: Literature review update for 2012–2015. *Renewable and Sustainable Energy Reviews, **63*** (2016), 33-61. DOI: http://dx.doi.org/10.1016/j.rser.2016.04.059.

Costa, S. C. S., Sonia, A., Diniza, A. C. and Kazmerskia, L. L. (2018). Solar energy dust and soiling R&D progress: Literature review update for 2016. *Renewable and Sustainable Energy Reviews, **82*** (2018), 2504-2536. DOI: http://dx.doi.org/10.1016/j.rser.2017.09.015.

Dajuma, A., Yahaya, S., Touré, S., Diedhiou, A., Adamou, R., Konaré, A., Sido, M., and Golba, M. (2016). The sensitivity of Solar Photovoltaic Panel Efficiency to Weather and Dust over West Africa: Comparative Experimental Study between Niamey (Niger) and Abidjan (Côte d'Ivoire). *Computational Water, Energy, and Environmental Engineering, **5*** (4), 123-147. DOI: 10.4236/cweee.2016.54012.

Darwish, Z. A., Kazem, H. A., Sopian, K., Al-Goul, M. A., and Alawadhi, H. (2015). Effect of dust pollutant type on photovoltaic performance*. Renewable and Sustainable Energy Reviews, **41*** (2015), 735-744. DOI: http://dx.doi.org/10.1016/j.rser.2014.08.068.

Deb, D., and Brahmbhatt N. L. (2017). Review of yield increase of solar panels through soiling prevention and a proposed water-free automated cleaning solution. *Renewable and Sustainable Energy Reviews,* ***82*** (3), 3306-3313. DOI: http://dx.doi.org/10.1016/j.rser.2017.10.014.

Doherty, O. M., Riemer, N., and Hameed, S. (2014). Role of the convergence zone over West Africa in controlling Saharan mineral dust load and transport in the boreal summer. *Tellus B: Chemical and Physical Meteorology,* ***66*** (2014), 1-17. DOI: https://doi.org/10.3402/tellusb.v66.2319.

Efurumibe, E. L. (2013). Barriers to the development of renewable energy in Nigeria. *Scholarly Journals of Biotechnology,* ***2*** (1), 11-13.

El-Minir, H. K., Ghitas, A. E., Hamid, R. H., El-Hussainy, F., Beheary, M. M., and Abdel-Moneima, K. M. (2006). Effect of dust on the transparent cover of solar collectors. *Energy Conversion and Management,* ***47*** (2006), 3192-3203. DOI: https://doi.org/10.1016/j.enconman.2006.02.014.

El-Nashar, A. M. (1994). The Effect of Dust Accumulation on the Performance of Evacuated Tube Collectors. *Solar Energy,* ***53*** (1), 105-115.

EL-Shobokshy, M. S., and Hussein, F. M. (1993). Effect of Dust with Different Physical Properties on the Performance of Photovoltaic Cells. *Solar Energy,* ***5*** (6), 505-511.

Emetere M. E., Okoro, U., Etete, B., and Okunbor, G. (2016). Free energy option and its relevance to improving domestic energy demands in southern Nigeria. *Energy Reports,* ***2*** (2016), 229-236.

Emodi, N. V., Emodi, C. C., Murthyc, G. P., and Emodi, A. S. A. (2017). Energy policy for low carbon development in Nigeria: A LEAP model application. *Renewable and Sustainable Energy Reviews,* ***68*** (2017), 247-261.

Emziane, M., and Al Ali, M. (2015). Performance assessment of rooftop PV systems in Abu Dhabi. *Energy and Buildings*, ***108*** (1 December 2015), 101-105. doi:http://dx.doi.org/10.1016/j.enbuild.2015.08.057

Energy_Storage (2019). Africa's largest off-grid solar hybrid goes online at Nigerian University BUK. Retrieved from https://www.energy-storage.news/news/africas-largest-off-grid-solar-hybrid-goes-online-at-nigerian-university-buk.

Enphase-Energy (2014). Guide to PV Watts De-rate Factors for Enphase Systems When Using PV System Design Tools. Online, Enphase Energy.

Evwind. (2017). Agreements signed for two solar power plants in Nigeria. Retrieved from https://www.evwind.es/2017/04/27/agreements-signed-for-two-solar-power-plants-in-nigeria/59605.

Ezeokoli, O. N., and Ifeanyi-Nwaoha, C. (2018). Distribution Infrastructure Demands. *EmPower Nigeria,* ***26*** (1), 1.

Fathi, M., Abderrezek, M., and Friedrich, M. (2017). Reducing dust effects on photovoltaic panels by hydrophobic coating. *Clean Techn Environ Policy,* ***19*** (2017), 577-585. DOI:10.1007/s10098-016-1233-9.

Figgis, B., Ennaouia, A. Ahzia, S., and Rémond, Y. (2017). Review of PV soiling particle mechanics in desert environments. *Renewable and Sustainable Energy Reviews,* ***76*** (2017), 872-881. DOI: http://dx.doi.org/10.1016/j.rser.2017.03.100.

Figgis, B., Goossens, D., Guod, B., and Ilse, K. (2019). "Effect of tilt angle on soiling in the perpendicular wind." *Solar Energy,* ***194*** (2019), 294–301.

Figgis, B., Nouviairec, A., Wubulikasimud, Y., Javedd, W., Guod, B., Ait-Mokhtarc, A., Belarbic, R., Ahzia, S., Rémond, Y., and Ennaouie, A. (2018). Investigation of factors affecting condensation on soiled PV modules. *Solar Energy,* ***159*** (2018), 488-500. DOI: https://doi.org/10.1016/j.solener.2017.10.089.

FOA. (2018). NGA. from http://www.fao.org/countryprofiles/index/en/?iso3=NGA.

Fonseca-Cervantes, O. R., Pérez-Larios, A., Arellano, V. H. R., Sulbaran-Range, B., and González, C. A. G. (2020). Effects in Band Gap for Photo catalysis in TiO_2 Support by Adding Gold and Ruthenium. *Processes,* ***8*** (9), 1032. DOI: https://doi.org/10.3390/pr8091032.

Fouad, M. M., Shihatab, L. A., and Morgana, E. I. (2017). An integrated review of factors influencing the performance of photovoltaic panels. *Renewable and Sustainable Energy Reviews,* ***80*** (2017), 1499-1511. DOI: https://doi.org/10.1016/j.rser.2017.05.141.

G.I.S., S. (2017). Global Horizontal Radiation. Retrieved 20/12/2017, from https://solargis.com/assets/graphic/free-map/GHI/Solargis-Nigeria-GHI-solar-resource-map-en.png.

Ghazi, S., and Ip, K. (2014). The effect of weather conditions on the efficiency of PV panels in the southeast of the UK. *Renewable Energy, **69*** (2014), 50-59. DOI: http://dx.doi.org/10.1016/j.renene.2014.03.018.

Ghazi, S., Ip. K., and Sayigh A. (2013). Preliminary study of environmental particles on solar flat surfaces in the UK. *Energy Procedia, **42*** (2013), 765-774. DOI: 10.1016/j.egypro.2013.11.080.

Ghazi, S., Sayigh, A. and Ip, K. (2014). Dust effect on flat surfaces – A review paper. *Renewable and Sustainable Energy Reviews, **33*** (2014), 742-751. DOI: http://dx.doi.org/10.1016/j.rser.2014.02.016.

Gholami, A., Khazaee, I., Eslami, S., Zandi, M., and Akrami, E. (2018). Experimental Investigation of dust deposition effects on photovoltaic output performance. *Solar Energy, **159*** (1 January 2018), 346-352. DOI: https://doi.org/10.1016/j.solener.2017.11.010.

Gholami, A., Saboonchi, A., and Alemrajabi, A. A. (2017). The experimental study of factors affecting dust accumulation and their effects on the transmission coefficient of glass for solar applications. *Renewable Energy, **112*** (2017), 466-473. DOI: http://dx.doi.org/10.1016/j.renene.2017.05.050.

Ghosh, A. (2020) "Potential of building integrated and attached/applied photovoltaic (BIPV/BAPV) for adaptive less energy-hungry building's skin: A comprehensive review", *Journal of Cleaner Production, **276*** (2020), 123343.

Ghosh, A. (2020a). Possibilities and Challenges for the Inclusion of the Electric Vehicle (EV) to Reduce the Carbon Footprint in the Transport Sector: A Review. *Energies, **13*** (2020), 2602.

Ghosh, A., Sundaram, S., and Mallick, T. K. (2018). Investigation of thermal and electrical performances of a combined semitransparent PV-vacuum glazing. *Applied Energy, **228*** (15), 1591-1600. DOI: https://doi.org/10.1016/j.apenergy.2018.07.040.

Giwa, A., Alabi, A., Yusuf, A., and Olukan, T. (2017). A comprehensive review on biomass and solar energy for sustainable energy generation in Nigeria. *Renewable and Sustainable Energy Reviews, **69*** (2017), 620-641.

Good, R. J. (1992). Contact angle, wetting, and adhesion: a critical review. *Journal of Adhesion Science and Technology, **6*** (12), 1269-1302. DOI: 10.1163/156856192X00629.

Goossens, D., and Van Kerschaever, E. (1999). Aeolian Dust Deposition on Photovoltaic Solar Cells: The Effects of Wind Velocity and Airborne Dust Concentration on Cell Performance. *Solar Energy,* ***66*** (4), 277-289.

GOV.UK. (2021). National minimum wage rates. Retrieved from https://www.gov.uk/national-minimum-wage-rates.

Green-Rhino-Energy. (2016). C.S.T. System. from http://www.greenrhinoenergy.com/solar/technologies/cst_systems.php

GSA (2020). "Abuja Municipal." Retrieved 15/07/2020, 2020, from https://globalsolaratlas.info/detail?s=9.008417,7.274639&m=bookmark&pv=small,180,13,1.

GSA. (2020). Map. Retrieved from https://globalsolaratlas.info/map

GSA. (2021). Site. Retrieved from https://globalsolaratlas.info/map?c=11.894839,8.536414,11&s=11.894839,8.536414&m=site

Guan, Y., Zhang, H., Xiao, B., Zhou, Z., and Yan, X. (2017). In-situ Investigation of the effect of dust deposition on the performance of polycrystalline silicon photovoltaic modules. *Renewable Energy,* ***101*** (2017), 1273-1284. DOI: http://dx.doi.org/10.1016/j.renene.2016.10.009

Guo, B., Figgis, B., and Javed, W. (2019). Measurement of electrodynamic dust shields efficiency in field conditions. *Journal of Electrostatics,* ***97*** (January 2019), 26-30. DOI: https://doi.org/10.1016/j.elstat.2018.11.007.

Gupta, V., Sharma, M., Pachauri, R. K., and Babu, K. N. D. (2019). A comprehensive review on the effect of dust on the solar photovoltaic system and mitigation techniques. *Solar Energy,* ***191*** (2019), 596-622. DOI: https://doi.org/10.1016/j.solener.2019.08.079.

Hachicha, A. A., Al-Sawafta, I., and Said, Z. (2019). Impact of dust on the performance of solar photovoltaic (PV) systems under United Arab Emirates weather conditions. *Renewable Energy,* ***141*** (2019), 287-297.

Hammad, B., Al–Abed, M., Al–Ghandoor, A., Al–Sardeahe, A, and Al–Bashir, A. (2018). Modelling and analysing dust and temperature effects on photovoltaic systems' performance and optimal cleaning frequency: Jordan case study. *Renewable and Sustainable Energy Reviews,* ***82*** (2018), 2218-2234. DOI: http://dx.doi.org/10.1016/j.rser.2017.08.070.

Hasan, A., and Sayigh, A. A. M. (1992). The effect of sand dust accumulation on the light transmittance, reflection, and absorbance of the PV glazing." Renewable Energy, Technology and Environment. Pergamon Press, Oxford: 461-466.

Hassan, G., Yilbas, B.S., Said, S.A.M., and Matin, A. (2016). Chemo-mechanical characteristics of mud formed from environmental dust particles in humid ambient air. (22 July 2016 ed., Vol. 6). Natural Research: Scientific Reports.

Hee, J. Y., Kumar, L. B., Danner, A. J., Yang, H., and Bhatia, C. S. . (2012). *The Effect of Dust on Transmission and Self-cleaning Property of Solar Panels.* Paper presented at the International Conference on Materials for Advanced Technologies 2011, Symposium O.

Hegazy, A. A. (2001). Effect of dust accumulation on solar transmittance through glass covers of plate-type collectors. *Renewable Energy, **22*** (2001): 525-540.

Heydarabadi, H., Abdolzadeh, M., and Lari, K. (2017). Simulation of airflow and particle deposition settled over a tilted Photovoltaic module. *Energy **139*** (2017), 1016-1029.

IEA. (2017). Total primary energy supply Nigeria. Retrieved 06/12/2017, 2017, from:https://www.iea.org/statistics/statisticssearch/report/?year=2015&country=Nigeria%20&product=RenewablesandWaste.

IEA. (2018). Retrieved 20/01/2018, 2018, from https://www.iea.org/topics/renewables/solar/

IEA. (2019). Nigeria Energy Outlook. Retrieved from: https://www.iea.org/articles/nigeria-energy-outlook

IEA. (2021). Nigeria_Energy_Outlook: Analysis from Africa Energy Outlook 2019. Retrieved from https://www.iea.org/articles/nigeria-energy-outlook

Ikem, I. A., Nyong, O. E., Takim, S. A., and Osim-Asu, D. (2016). Integration of Renewable Energy Sources to the Nigerian National Grid - Way out of Power Crisis. *International Journal of Engineering Research, **5*** (8), 694-700.

Ilenikhena, P. A., and Ezemonye, L. I. N. (2010) Solar Energy Application in Nigeria, in W.E.C. Montreal 2010. 2010. p. 1-13.

Ilse, K. K., Figgis, B. W., Naumann, V., Hagendorf, C., and Bagdahn, J. (2018). Fundamentals of soiling processes on photovoltaic modules. *Renewable and Sustainable Energy Reviews,* ***98*** (2018), 239-254. DOI: 10.1016/j.rser.2018.09.015.

IQ-Air. (2021). Nigeria. Retrieved from https://www.iqair.com/us/nigeria.

IRENA. (2018). Solar. Retrieved 01/05/2018, 2018, from http://www.irena.org/solar.

Isaifan, R. J., Johnson, D., Ackermann, L., Figgis, B., and Ayoub, M. (2019) Evaluation of the adhesion forces between dust particles and photovoltaic module surfaces. *Solar Energy Materials and Solar Cells,* ***191*** (2019), 413-421.

Isaifan, R. J., Samara, A., Suwaileh, W., Johnson, D., Yiming, W., Abdallah, A. A., and Aïssa, B. (2017). Improved Self-cleaning Properties of an Efficient and Easy to Scale-up TiO2 Thin Films Prepared by Adsorptive Self-Assembly. *Scientific Reports,* ***7*** (2017). DOI: https://doi.org/10.1038/s41598-017-07826-0.

Islam, M. A., Hassanuzzaman, M., Rahim, A. Nahar, A. and Hoseinuzzaman, M. (2014). Global Renewable Energy-Based electricity generation and smart grid system for electricity security. *The World Science Journal,* ***1*** **(**2014), 13.

Jamil, W. J., Abdul Rahman, H., Shaari, S., and Salam, Z. (2017). Performance degradation of the photovoltaic power system: Review of mitigation methods. *Renewable and Sustainable Energy Reviews,* ***67*** (2017), 876-891. DOI: http://dx.doi.org/10.1016/j.rser.2016.09.072.

Javed, W., Guo, B., and Figgis, B. (2017). Modelling of photovoltaic soiling loss as a function of environmental variables. *Solar Energy,* ***157*** (2017), 397-407. DOI: http://dx.doi.org/10.1016/j.solener.2017.08.046.

Jiang, Y, Lu, L, Ferro, A, R., and Ahmadi, G. (2018). Analysing wind-cleaning process on the accumulated dust on solar photovoltaic (PV) modules on flat surfaces. *Solar Energy* ***159*****,** (2018), 1031–1036. DOI: https://doi.org/10.1016/j.solener.2017.08.083.

Jiang, Y., and Lu, L. (2015). A study of dust accumulating process on solar photovoltaic modules with different surface temperatures. Paper

presented at The 7th International Conference on Applied Energy – ICAE2015, Abu Dhabi, United Arab Emirates.

Jiang, Y., Lu, L., and Sun, K. (2011). Experimental Investigation of the impact of airborne dust deposition on the performance of solar photovoltaic (PV) modules. *Atmospheric Environment,* ***45*** (2011), 4299-4304. DOI: doi:10.1016/j.atmosenv.2011.04.084.

Jickells, T. D., Baker, A. R., & Chance, R. (2016). Atmospheric transport of trace elements and nutrients to the oceans. *Philosophical Transactions of the Royal Society A: Mathematical, Physical and Engineering Sciences,* ***374*** (2081), 20150286. DOI:10.1098/rsta.2015.0286

John, J. J., Warade, S., Tamizhmani, G., and Kottantharayil, A. (2016). Study of Soiling Loss on Photovoltaic Modules With Artificially Deposited Dust of Different Gravimetric Densities and Compositions Collected From Different Locations in India. *IEEE Journal of Photovoltaics,* ***6*** (1), 236-243. DOI: 10.1109/JPHOTOV.2015.2495208.

Kalashnikov, O. V., and Sokolik, I. N. (2004). Modelling the radiative properties of non-spherical soil-derived mineral aerosols. *Journal of Quantitative Spectroscopy & Radiative Transfer,* ***87*** (2004), 137-166. DOI: 10.1016/j.jqsrt.2003.12.026.

Kaldellis, J. K., and Kapsali, M. (2011). Simulating the dust effect on the energy performance of photovoltaic generators based on experimental measurements. *Energy,* ***36*** (2011), 5154-5161. DOI: 10.1016/j.energy.2011.06.018.

Kaldellis, J. K., Fragos, P., and Kapsali, M. (2011). Systematic experimental study of the pollution deposition impact on the energy yield of photovoltaic installations. *Renewable Energy,* ***36*** (2011), 2717 - 2724. DOI: 10.1016/j.renene.2011.03.004.

Kalogirou, S. A. (2009). *Solar Energy Engineering: Processes and Systems,* London, Academic Press, Elsevier.

Kalogirou, S. A. (2014). *Solar Engineering Processes and Systems*. Oxford: Elsevier.

Kalogirou, S. A., Agathokleous, R., and Panayiotou, G. (2013). On-site PV characterisation and the effect of soiling on their performance. *Energy,* ***51*** (2013), 439-460.

Kapridaki, C., and Maravelaki-Kalaitzaki, P. (2013). TiO2-SiO2–PDMS nano-composite hydrophobic coating with self-cleaning properties for marble protection. *Progress in Organic Coatings,* ***2013*** (76), 400–410. DOI: https://doi.org/10.1016/j.porgcoat.2012.10.006.

Kazem, A. A., Chaichan, M. T., and Kazem, H. A. (2014). Dust effect on photovoltaic utilisation in Iraq: A review article. *Renewable and Sustainable Energy Reviews,* ***37*** (2014), 734-749. DOI: http://dx.doi.org/10.1016/j.rser.2014.05.073.

Kazem, H. A., and Chaichan, M. T. (2019). The effect of dust accumulation and cleaning methods on PV panels' outcomes based on an experimental study of six locations in Northern Oman. *Solar Energy.* ***187*** (2019), 30–38. DOI: https://doi.org/10.1016/j.solener.2019.05.036.

Kazem, H. A., and Chaichan, M. T. (2016). Experimental analysis of the effect of dust's physical properties on photovoltaic modules in Northern Oman. *Solar Energy,* ***139*** (2016), 68-80. DOI: http://dx.doi.org/10.1016/j.solener.2016.09.019.

Kazem, H. A., Khatib, T., Sopian, K., Buttinger, F., Elmenreich, W., and Albusaidi, A. S. (2013). Effect of Dust Deposition on the Performance of Multi-Crystalline Photovoltaic Modules Based on Experimental Measurements. *International Journal of Renewable Energy Research,* ***3*** (4), 850-853.

Kazmerski, L. L., Diniz, A. S., Maia, C. B., Viana, M. M. Costa, S. C., Brito, P. P., Campus, C. D., Neto, V. L. M., Hanriot, S., and Oliveira Cruz, L. R. (2016). Fundamental Studies of Adhesion of Dust to PV Module Surfaces: Chemical and Physical Relationships at the Microscale. *IEEE Journal of Photovoltaics,* ***6*** (3), 719-729. DOI: 10.1109/JPHOTOV.2016.2528409.

Khanum, K. K., Rao, A., Balaji, N. C. Mani, M. and Ramamurthy, P. C. (2016). Performance evaluation for PV systems to synergistic influences of dust, wind and panel temperatures: spectral insight. IEEE, 1715-1718.

Kimber, A., Mitchell, L., Nogradi, S., and Wenger, H. (2006). The Effect of Soiling on Large Grid-Connected Photovoltaic Systems in California and the Southwest Region of the United States. IEEE, 2391-2395.

Klugmann-Radziemska, E. (2015). Degradation of the electrical performance of a crystalline photovoltaic module due to dust deposition in northern

Poland. *Renewable Energy,* ***78*** (2015), 418-426. DOI: http://dx.doi.org/10.1016/j.renene.2015.01.018.

Kumar, S. S., and Nagarajan, C. (2016). Performance-Economic and Energy Loss Analysis of 80 KWp Grid Connected Roof Top Transformerless Photovoltaic Power Plant. *Circuits and Systems,* ***7*** (2016), 662-679. DOI: http://dx.doi.org/10.4236/cs.2016.76056.

Kung, C. H., Sow, P. K., Zahiri, B., and Mérida, W. (2019). Assessment and Interpretation of Surface Wettability Based on Sessile Droplet Contact Angle Measurement: Challenges and Opportunities. *Advanced Material Interfaces,* ***6*** (18), 1-27. DOI: https://doi.org/10.1002/admi.201900839.

Lay-Ekuakille, L., Ciaccioli, A., Griffo, G., Visconti, P. and Andria, G. (2018). Effects of dust on photovoltaic measurements: A comparative study. *Measurement,* ***113*** (2018), 181-188. DOI: http://dx.doi.org/10.1016/j.measurement.2017.06.025

Leggett, J. (2009). *The Solar Century: The Past, Present and World-Changing Future of Solar Energy.* London: Green Profile.

Leonardo, M., Fernández, E. F., Smestad, G. P., Alrashidi, H., Sarmah, N., Sellami, N., Hassan, I. A. I., Kasry, A., Nofuentes, G., Sood, N., Pesala, B., Sunduram, S., Almonacid, F., Reddy, K. S., Muller, M., and Mallick, T. P. (2017,). A unified global investigation on the spectral effects of soiling losses of PV glass substrates: preliminary results. *IEEE 44th Photovoltaic Specialist Conference (PVSC) 25-30 June 2017,* Washington, DC.

Li, C., Kattawara, G. W., and Yang, P. (2004). Effects of surface roughness on light scattering by small particles. *Journal of Quantitative Spectroscopy & Radiative Transfer,* ***89*** (2004), 123-131. DOI: 10.1016/j.jqsrt.2004.05.016.

Li, X., Mauzerall, D. L., and Bergin, M. H. (2020). Global reduction of solar power generation efficiency due to aerosols and panel soiling. *Nature Sustainability,* ***3*** (2020), 720–727. doi:https://doi.org/10.1038/s41893-020-0553-2

Liqun, L., Zhiqi, L., Zhiyi, S., and Chunxia, L. (2012). Degraded output characteristic at the atmospheric air pollution and economy analysis of PV power system: A case study Electrical Review, 281-284. Retrieved from http://pe.org.pl/articles/2012/9a/61.pdf.

Longueville, F., Hountondji, Y., Henry, S., and Ozer, P. (2010). What do we know about the effects of desert dust on air quality and human health in West Africa compared to other regions? *Science of the Total Environment,* ***409*** (2010), 1-8. DOI: 10.1016/j.scitotenv.2010.09.025.

Lu, H., Lu, L., and Wang, Y. (2016). Numerical Investigation of dust pollution on a solar photovoltaic (PV) system mounted on an isolated building. *Applied Energy,* ***180*** (2016), 27-36. DOI: http://dx.doi.org/10.1016/j.apenergy.2016.07.030.

Maghami, M. R., Hizam, H., Gomea, C., Radzi, M. A., Rezadad, M. I., and Hajighorbani, S. (2016). Power loss due to soiling on the solar panel: A review. *Renewable and Sustainable Energy Reviews,* ***59*** (2016), 1307-1316. DOI: http://dx.doi.org/10.1016/j.rser.2016.01.044.

Makmee, T., and Pengwang, E. (2021). *Design and Experiment of Four-side Stretch Slingbased Solar Cleaning Robot*. Paper presented at the 7th International Conference on Engineering, Applied Sciences and Technology (ICEAST), Pattaya, Thailand.

Mani, F., Pulipaka, S., and Kumar, R. (2016). Characterisation of power losses of a soiled PV panel in the Shekhawati region of India. *Solar Energy,* ***131*** (2016), 96-106. DOI: http://dx.doi.org/10.1016/j.solener.2016.02.033.

Mani, M., and Pillai, R. (2010). Impact of dust on solar photovoltaic (PV) performance: Research status, challenges and recommendations. *Renewable and Sustainable Energy Reviews,* ***14*** (2010), 3124-3131. DOI:0.1016/j.rser.2010.07.065.

Martin, N., and. Ruiz, J. M. (2001). "Calculation of the PV modules angular losses under field conditions by means of an analytical model." Solar Energy Materials & Solar Cells, **70** (2001): 25-38.

Mas'uda, A. A., Wirbab, A. V., Muhammad-Sukkic, F., Mas'ude, I. B., Munirf, A,. and Yunus, N. M. (2015). An assessment of renewable energy readiness in Africa: a Case study of Nigeria and Cameroon. *Renewable and Sustainable Energy Reviews,* ***51*** (2015), 775-784.

Mazumder, M., Horenstein, M. N., Stark, J. W., Girouard, P., Sumner, R., Henderson, B., Sadder, O., Hidetaka, I., Biris, A. S., and Sharma, R. (2013). Characterisation of Electrodynamic Screen Performance for Dust Removal from Solar Panels and Solar Hydrogen Generators. *IEEE*

Transactions on Industry Applications, ***49*** (4), 1793 - 1800. DOI:10.1109/TIA.2013.2258391.

Mazur, M., Wojcieszak, D., Kaczmarek, D., Domaradzki, J., Song, S., Gibson, D., Placido, F., Mazur, P., Kalisz, M., and Poniedzialek, A. (2016). Functional photocatalytically active and scratch-resistant anti-reflective coating based on TiO2 and SiO2. *Applied Surface Science,* ***380*** (1): 165-171. DOI: https://doi.org/10.1016/j.apsusc.2016.01.226.

Meindinyo, R. K. O., Misra, M. C., and Orji, R. C. (2017) Impact of Harmattan Sun and Dust of the Eye in a Nigeria City. *IOSR Journal of Research & Method in Education (IOSR-JRME),* ***7*** (3), 36-41. DOI: 10.9790/7388-0703013641.

Mejia, F. A., and Kleissl, J. (2013). Soiling losses for solar photovoltaic systems in California. *Solar Energy,* ***95*** (September 2013), 357-363. Retrieved from https://doi.org/10.1016/j.solener.2013.06.028.

Mekhilef, S., Saidur, R., and Kamalisarvestani, M. (2012). Effect of dust, humidity and air velocity on the efficiency of photovoltaic cells. *Renewable and Sustainable Energy Reviews,* ***16*** (2012), 2920-2925. DOI: 10.1016/j.rser.2012.02.012.

Micheli, L., Deceglie, M. G., and Muller, M. (2019). Mapping Photovoltaic Soiling Using Spatial Interpolation Techniques. *IEEE Journal of Photovoltaics,* ***9*** (1), 272-277. doi:10.1109/JPHOTOV.2018.2872548

Micheli, L., Fernández, E. F., Aguilera, J. T., & Almonacid, F. (2021). Economics of seasonal photovoltaic soiling and cleaning optimization scenarios. *Energy,* ***215***, 119018. doi:https://doi.org/10.1016/j.energy.2020.119018

Micheli, L., and Muller, M. (2017). An investigation of the key parameters for predicting PV soiling losses. *Prog. Photovolt: Res. Appl. ,* ***25*** (2017), 291–307. DOI: 10.1002/pip.2860

Middleton, N. J. (2017). Desert dust hazards: A global review. *Aeolian Research,* ***24*** (2017), 53-63. DOI: http://dx.doi.org/10.1016/j.aeolia.2016.12.001.

Mindat. (2019). Albite. Retrieved on 25/02/2019 from https://www.mindat.org/min-96.html.

Minerals.net. (2019). Minerals. Retrieved from https://www.minerals.net/mineral/albite.aspx.

Mishra, S. K., Agnihotri, R., Yadav, P. K., Singh, S., Prasad, M. V. S. N., Praveen, P. S., Tawale, J. S., Rashmi, Mishra, N. D., Arya, B. C., and Sharm, C. (2015). Morphology of Atmospheric Particles over Semi-Arid Region (Jaipur, Rajasthan) of India: Implications for Optical Properties. *Aerosol and Air Quality Research,* ***15*** (2015), 974-984.

Mitdal, K., and Jelle, B. P. (2013). Self-cleaning glazing products: A state-of-the-art review and future research pathways. *Solar Energy Materials & Solar Cells,* ***109*** (2013), 126–141. DOI: http://dx.doi.org/10.1016/j.solmat.2012.09.034.

Mohamed, A. O., and Hasan, A. (2012). Effect of Dust Accumulation on Performance of Photovoltaic Solar Modules in Sahara Environment. *J. Basic. Appl. Sci. Res,* ***2*** (11), 11030-11036.

Mohammed, Y. S. Mustafa, M. W., Bashir, N., and Mokhtar, A. S. (2013). Renewable energy resources for distributed power generation in Nigeria: A review of the potential. *Renewable and Sustainable Energy Reviews,* ***22*** (2013), 257-268.

Mohammed, Y. S., Mustafa, M. W., Bashir, N., and Ibrahem, I. S. (2017). Existing and recommended renewable and sustainable energy development in Nigeria based on autonomous energy and microgrid technologies. *Renewable and Sustainable Energy Reviews,* ***75*** (2017), 820-838.

Monyei, C. G., Adewumia, A. O., Obolo, M. O., and Sajou, B. (2017). Nigeria's energy poverty: Insights and implications for smart policies and framework towards a smart Nigeria electricity network. *Renewable and Sustainable Energy Reviews,* ***81*** (2018), 1582-1601.

Mshelia, H. I. (n.d.) Energy Access for All: The role of clean energy in alleviating energy poverty. *Clean Energy for All.* Retrieved 29/11/217, 2017, from https://ng.boell.org/sites/default/files/uploads/2013/10/clean_energy_-_green_deal_nigeria_study.pdf.

Mywage.ng. (2021). Minimum-wage. Retrieved from https://mywage.ng/salary/minimum-wage-1

Nahar, N. M., and Gupta, J. P. (1990). Effect of dust on the transmittance of glazing materials for solar collectors under arid zone conditions of India. *Solar & Wind Technology,* ***7*** (2–3), 237–243. DOI:https://doi.org/10.1016/0741-983X(90)90092-G.

NBET (2017). Hydro map of Nigeria. Retrieved 06/12/2017, 2017, from https://nbet.com.ng/our-customers/generation/hydro-map-of-nigeria/.

NBS. (2017). Power Generation Statistics Q1 2017 *Q1 2017* (Vol. Q1 2017, pp. 1-18). NBS Abuja: NBS/ Nigerian Electricity Regulatory Commission.

NEENigeria. (2013). Wind- Nigeria. from http://www.neenigeria.com/html/wind_energy.html

Nelson, V., and Starcher, K. (2016) *Introduction to Renewable Energy* Florida: C.R.C. Press.

NERC. (2017). Renewable Energy. Retrieved 31/12/2017, 2017, from http://www.nercng.org/index.php/home/operators/renewable-energy.

NERC. (2020). Industry statistics. Retrieved from https://nerc.gov.ng/index.php/library/industry-statistics/397-peak#data.

NERC. (2021a). Industrial statistics. Energy Sent Out. Retrieved from https://nerc.gov.ng/index.php/library/industry-statistics/374-energy-sent#data.

Nigeria-Electricity-Hub. (2018). BUK Establishes first-megawatt scale solar project in Nigerian University. Retrieved from https://www.nigeriaelectricityhub.com/2018/10/05/buk-establishes-first-megawatt-scale-solar-project-in-nigerian-university/

Nirmal, A., Kyaw, A. K. K., Sun, X. W., and Demir, H. V. (2014). Microstructured porous ZnO thin film for increased light scattering and improved efficiency in inverted organic photovoltaics. *Optics Express, **22*** (S6), A1412-A1421. DOI: https://doi.org/10.1364/OE.22.0A1412.

Nnaji CE, Uzoma, C.C. and Chukwu, J.O. (2010) The role of renewable energy resources in poverty alleviation and sustainable development in Nigeria. *Continental J Social Sciences **1*** (2010), 31 – 7.

NREEEP. (2015). *National Renewable Energy and Energy Efficiency Policy*. Abuja.

Nundy, S., Ghosh, A., and Mallick, T. K. (2020). Hydrophilic and Superhydrophilic Self-Cleaning Coatings by Morphologically Varying ZnO Microstructures for Photovoltaic and Glazing Applications. American Chemical Society (ACS) *Omega, **2020*** (5), 1033−1039. DOI: 10.1021/acsomega.9b02758

Nwokocha, C. O., Okoro, U. K., and Usoh, C. I. (2017). Photovoltaics in Nigeria e Awareness, attitude and the expected benefit based on a qualitative survey across regions. *Renewable Energy, **116*** (2018), 176-182.

Ochei, M. C., and Adenola, E. Variability of Harmattan Dust Haze Over Northern Nigeria. *Journal of Pollution, **1*** (2), 1-8.

Off_Grid_Nigeria. (2017). 1-2 MW lower Usuma dam solar plant completed feed excess capacity grid. Retrieved from https://www.offgridnigeria.com/1-2mw-lower-usuma-dam-solar-plant-completed-feed-excess-capacity-grid/.

Ogbaje, S. (2017). Dust haze weather to prevail on Tuesday – NiMet. Retrieved 01/06/2018, from https://www.environewsnigeria.com/dust-haze-weather-prevail-tuesday-nimet/.

Ohunakin, O. S., Adaramola, M. S., Oyewola, O. M., and Fagbenle, R. O. (2014). Solar energy applications and development in Nigeria: Drivers and barriers. *Renewable and Sustainable Energy Reviews, **32*** (2014), 294-301.

Ohunakin, S. O. (2010). Energy Utilisation and renewable energy sources in Nigeria. *Journal for engineering and applied science, **5*** (2), 171-177.

Oji, J. O., Idusuyi, N., Aliu, T. O., Petinrin, M. O., Odejobi, O. A., and Adetunji, A. R. (2012). The utilisation of Solar Energy for Power Generation in Nigeria. *International Journal of Energy Engineering, **2*** (2), 54-59.

Okoye, C. O., Taylan, O., and Baker, D. K. (2016). Solar energy potentials in strategically located cities in Nigeria: Review, resource assessment and PV system design. *Renewable and Sustainable Energy Reviews, **55*** (2016), 550-566.

Olivares, D., Ferreda, P., Matos, C., Marzo, A., Cabrera, E., Porttilo, C., and Llanos, J. (2018). Characterisation of soiling on PV modules in the Atacama Desert. Paper presented at the 7th *International Conference on Silicon Photovoltaics, Silicon PV 2017*, Lausanne, Switzerland.

Olujimi, O. O., Oputu, O., Fatoki, O., Aroyewun, O., Ester, O., Ali, O., and Baruani, J. (2015). Heavy Metals Speciation and Human Health Risk Assessment at an Illegal Gold Mining Site in Igun, Osun State, Nigeria. *J Health Pollution, **5*** (8), 19-32.

Onohaebi, S. O., and Eseosa, O. (2014). Smart Grid and Energy Management in Nigeria Integrated Power System. *International Journal of Engineering Innovation & Research,* ***3*** (6), 732-736.

OPEC. (2016). OPEC: Annual Statistical Bulletin. In 2016 (Ed.), *Organization of the Petroleum Exporting Countries*. Vienna, Austria: Organization of the Petroleum Exporting Countries.

OPEC. (2017). Nigeria facts and figures. Retrieved 06/12/2017, 2017, from http://www.opec.org/opec_web/en/about_us/167.htm

Oseni, M. O. (2011). An analysis of the power sector performance in Nigeria. *Renewable and Sustainable Energy Reviews,* ***15*** (2011), 4765- 4774.

Oseni, M. O. (2012). Households' access to electricity and energy consumption pattern in Nigeria. *Renewable and Sustainable Energy Reviews,* ***16*** (2012), 990– 995.

Oseni, M. O. (2016). Get rid of it: To what extent might improve reliability reduce self-generation in Nigeria? *Energy Policy,* ***93*** (2016), 246-254.

Oyedepo, S. O. (2012). Energy and Sustainability development in Nigeria: The way forward. *Energy, Sustainability and Society 2012, 2:15,* ***2*** (15), 1-17.

Oyedepo, S. O. (2012a). On energy for sustainable development in Nigeria. *Renewable and Sustainable Energy Reviews,* ***16*** (2012), 2583- 2598.

Ozoegwu, C. G., Mgbemene, C. A., and Ozor, P. A. (2017). The status of solar energy integration and policy in Nigeria. *Renewable and Sustainable Energy Reviews,* ***70*** (2017), 457-471.

Patrick, D. B., and Bruce, H. K. (2014). A Handbook on Artificial Soils for Indoor Photovoltaic Soiling Tests. SAND2014-19199. Albuquerque, Sandia National Laboratories, Sandia Corporation.

Paudyal, B. R., and Shakya, S. R. (2016). Dust accumulation effects on the efficiency of solar PV modules for off-grid purpose: A case study of Kathmandu. *Solar Energy,* ***135*** (2016), 103-110. DOI: http://dx.doi.org/10.1016/j.solener.2016.05.046.

Pavan, A. M., Mellit, A., and De Pieri, D. (2011). The effect of soiling on energy production for large-scale photovoltaic plants. *Solar Energy,* ***85*** (5), 1128-1136. DOI: https://doi.org/10.1016/j.solener.2011.03.006.

Pedersen, H., Strauss, J., and Selj, J. (2016). Effect of soiling on photovoltaic modules in Norway. *6th International Conference on Silicon Photovoltaics, Silicon PV* 2016, Chambéry, France.

Picotti, G., Borghesani, P., Cholette, M. E. and Manzolini, G. (2018). Soiling of solar collectors – Modelling approaches for airborne dust and its interactions with surfaces. *Renewable and Sustainable Energy Reviews, **81*** (2018), 2343-2357. DOI: http://dx.doi.org/10.1016/j.rser.2017.06.043.

Piliougine, M., Cañete, C., Morenoa, R., Carretero, J., Hirose, J. Ogawab, S., and Sidrach-de-Cardona, M. (2013). Comparative analysis of energy produced by photovoltaic modules with the anti-soiling coated surface in arid climates. *Applied Energy, **112*** (2013), 626-634. DOI: http://dx.doi.org/10.1016/j.apenergy.2013.01.048.

Potenza, M. A. C., Albani, S., Delmonte, B., Villa, S., Sanvito, T., Paroli, B., Pullia, A., Baccolo, G., Mahowald, N., and Maggi, V. (2016). Shape and size constraints on dust optical properties from the Dome CICE core, Antarctica (16 June 2016 ed., Vol. 6:28162): *Scientific Report, **6*** (2016).

Qasem, H., Betts, T. R., Mullejans, H., AlBusairi, H., and Gottschalg, R. (2011). *Effect of dust shading on photovoltaic modules.* Paper presented at the Proceedings of the 26th European photovoltaic solar energy conference and exhibition (26th EUPVSEC) Hamburg, Germany.

Qasem, H., Betts, T. R., Mullejans, H., AlBusairi, H., and Gottschalg, R. (2019). Effect of dust shading on photovoltaic modules. Proceedings of the 26th European photovoltaic solar energy conference and exhibition (26th EUPVSEC) Hamburg, Germany, WIP.

Quan, Y., and Zhang, L. (2017). Experimental Investigation of the anti-dust effect of transparent hydrophobic coatings applied for solar cell covering glass. *Solar Energy Materials & Solar Cells, **160*** (2017), 382–389. DOI: http://dx.doi.org/10.1016/j.solmat.2016.10.043.

Quora. (2016). Where are the strongest winds and nastiest dust in the world? Retrieved 01/06/2018, 2018, from https://www.quora.com/Where-are-the-strongest-winds-and-nastiest-dust-in-the-world.

Rafindadi, A. A. (2016). Does the need for economic growth influence energy consumption and CO2 emissions in Nigeria? Evidence from the

innovation. Accounting test. *Renewable and Sustainable Energy Reviews, **62*** (2016), 1209-1225.

Rahman, M. M., Islam. M. A., Karim, A. H. M. Z., and Ronee, A. H. (2012). Effects of Natural Dust on the Performance of PV Panels in Bangladesh. *I.J.Modern Education and Computer Science, **10*** (2012), 26-32. DOI: 10.5815/ijmecs.2012.10.04.

Ramli, M. A. M., Prasetyono, E., Wicaksana, R. W., Windarko, N. A., Sedraoui, K., and Al-Turki, Y. A. (2016). On the Investigation of photovoltaic output power reduction due to dust accumulation and weather conditions. *Renewable Energy, **99*** (2016), 836-844. DOI: http://dx.doi.org/10.1016/j.renene.2016.07.063.

Reddy P., Gupta M.S., Nundy S., Karthick A., Ghosh A., (2020) Status of BIPV and BAPV system for a less energy-hungry building in India - A review, *Applied Sci, **10*** (7) 2337. DOI: https://doi.org/10.3390/app10072337.

REN21 (2019). Renewables, 2020 Global Status Report. Retrieved 22/07/2020, from https://www.ren21.net/gsr-2020/.

REN21. (2017). Renewables, 2017 Global Status Report. Paris: REN21 Secretariat.

REN21. (2018). Global Status Report. Retrieved 07/05/2018, 2018, from http://www.ren21.net/status-of-renewables/global-status-report/.

REN21. (2020). Renewables 2020: Global Status Report (GSR, 2020). Retrieved from Paris: REN21 Secretariat: https://www.ren21.net/wp-content/uploads/2019/05/gsr_2020_full_report_en.pdf.

Roche, M. Y. a. I.-N., C. (2017). Cost of Generating Power. *EmPower Nigeria, **10*** (1), 1.

Rosales, A., and Esquivel, K. (2020). SiO2@TiO2 Composite Synthesis and Its Hydrophobic Applications: A Review. *Catalysts, **10*** (2). DOI: https://doi.org/10.3390/catal10020171.

Said, S. A. M., and Walwil, H. M. (2014). Fundamental studies on dust fouling effects on PV module performance. *Solar Energy, **107*** (2014), 328-337. DOI: http://dx.doi.org/10.1016/j.solener.2014.05.048.

Said, S. A. M., Hassana, G., Walwila, H. M., and Al-Aqeelia, N. (2018). The effect of environmental factors and dust accumulation on photovoltaic modules and dust-accumulation mitigation strategies. *Renewable and Sustainable*

Energy Reviews, ***82*** (2018), 743-760. DOI: http://dx.doi.org/10.1016/j.rser.2017.09.042.

Salim, A. Huraib, F., and Eugenio, N. (1988). PV power-study of system options and optimisation: *Proceedings of the 8th European PV Solar Energy Conference.*

Sambo, A. (2009). Strategic Developments in Renewable Energy in Nigeria. *Research Gate*, 15-19.

Sambo, A. S., and Bala, E. J. (2012). *Penetration of Solar Photovoltaic into Nigeria's Energy Supply Mix*. Paper presented at the ASES/WREF 2012, Denver, Colorado. https://ases.conference-services.net/resources/252/2859/pdf/SOLAR2012_0906_full%20paper.pdf.

Sambo, A. S., Zarma, I. H., Ugwuoke, P. E., Dioha, I. J., and Ganda, Y. M. (2014). Implementation of Standard Solar P.V. Projects in Nigeria. *Journal of Energy Technologies and Policy,* ***4*** (9), 22-28.

Sanusi, Y. A., and Owoyele, G. S. (2016). Energy poverty and its spatial differences in Nigeria: reversing the trend. *Energy Procedia,* ***93*** (2016), 53 - 60.

Sanusi, Y. K. (2012). The Performance of Amorphous Silicon PV System under Harmattan Dust Conditions in a Tropical Area. *The Pacific Journal of Science and Technology,* ***13*** (1), 168-175.

Sarver, T., Al-Qaraghuli, A., and Kazmerski, L. L. (2013). A comprehensive review of the impact of dust on the use of solar energy: History, investigations, results, literature, and mitigation approaches. *Renewable and Sustainable Energy Reviews* ***22*** (2013), 698-733.

Sayyah, A., Crowell, D. R., Raychowdhury, A., Horenstein, M. N., and Mazumder, M. K. (2017). An experimental study on the characterisation of electric charge in electrostatic dust removal. *Journal of Electrostatics* ***87*** (2017), 173-179. DOI: http://dx.doi.org/10.1016/j.elstat.2017.04.001.

Sayyah, A., Eriksen, R. S., Horenstein, M. N. and Mazumder, M. K. (2017). Performance Analysis of Electrodynamic Screens Based on Residual Particle Size Distribution. *IEEE Journal of photovoltaic,* ***7*** (1), 221-229. DOI:10.1109/JPHOTOV.2016.2617088.

Sayyah, A., Horenstein, M. N., and Mazumder, M. K. (2014). Energy yield loss caused by dust deposition on photovoltaic panels. *Solar Energy, **107*** (2014), 576-604. DOI: http://dx.doi.org/10.1016/j.solener.2014.05.030.

Semaoui, S., Arab, A. H., Boudjelthia, E. K., Bacha, S., and Zeraia, H. (2015). Dust effect on optical transmittance of photovoltaic module glazing in a desert region*. Energy Procedia **74*** (2015), 1347-1357.

Shaaban, M., and Petinrin, J. O. (2014). Renewable energy potentials in Nigeria: Meeting rural energy needs. *Renewable and Sustainable Energy Reviews, **29*** (2014), 72-84.

Shaik, S., Bhardwaj, M., Agarwal, S., Yendaluru, R. S., Hasanuzzaman, M. D., and Sharma, K. V. (2021). Evaluation of Optical Transmissivity of Transparent Materials on the Performance of Solar Flat Plate Collectors. *Journal of Solar Energy Engineering, **143*** (5). doi:10.1115/1.4050214

Signoret, J., and Leroy, A. (2021). *Reliability Assessment of Safety and Production Systems: Analysis, Modelling, Calculations and Case Studies*. Springer Nature Switzerland AG 2021: Springer, Cham.

Sisodia, A. K., and Mathur R. M. (2019). Impact of bird dropping deposition on solar photovoltaic module performance: a systematic study in Western Rajasthan. *Environmental Science and Pollution Research**, 26*** (30), 31119-31132. DOI: https://doi.org/10.1007/s11356-019-06100-2.

Solar GIS (2017). Global Horizontal Radiation. Retrieved 20/12/2017, from https://solargis.com/assets/graphic/free-map/GHI/Solargis-Nigeria-GHI-solar-resource-map-en.png.

Son, J., Kundu, S., Verma, L. K., Sakhuja, M., Danner, A. J., Bhatia, C. S., and Yang, H. (2012). A practical super hydrophilic self-cleaning and anti-reflective surface for outdoor photovoltaic applications. *Solar Energy Materials & Solar Cells **98*** (2012), 46–51. DOI: doi:10.1016/j.solmat.2011.10.011.

Steer A, S. R., Bond J, Watson R, Georgieva K, and Raczynski, A. (2000.). *Fuel for thought – an environmental strategy for the energy sector.* The World Bank; Washington, DC: World Bank.

Sulaiman, S. A., Guangul, F. M., Hidayat-Mat., M. N., and Mohammed Bou-Rabee, A. (2015). *Real-Time Study on the Effect of Dust Accumulation on Performance of Solar PV Panels in Malaysia* Paper presented at the 1 st

International Conference on Electrical and Information Technologies ICEIT'2015, March 25-27, 2015 Marrakech, Morocco. https://ieeexplore.ieee.org/stamp/stamp.jsp?tp=&arnumber=7162938

Sulaiman, S. A., Hussain, H. H., Nik Leh, N. H., and Razali, M. S. I. (2011). Effects of Dust on the Performance of PV Panels. *International Journal of Mechanical and Mechatronics Engineering,* ***5*** (10), 2028-2033. DOI: scholar.waset.org/1307-6892/10305.

Sundaram, S., Benson, D., and Mallick, T. P. (2016). *Solar Photovoltaic Technology Production: Potential Environmental Impacts and Implications for Governance*. London: Elsevier.

SunWindSolar. (2013). Solar Radiation Spectrum. 01/01/2018, from https://sunwindsolar.com/solar-radiation-spectrum/.

Tanaka, T. Y., and Chiba, C. (2006). A numerical study of the contributions of dust source regions to the global dust budget. *Global and Planetary Change,* ***52*** (2006), 88-104.

Tanesab, J., Parlevliet, D., Whale, J., and Urmee, T. (2019). The effect of dust with different morphologies on the performance degradation of photovoltaic modules. *Sustainable Energy Technologies and Assessments,* ***31*** (2019), 347-354. DOI: https://doi.org/10.1016/j.seta.2018.12.024.

Tanesab, J., Parlevliet, D., Whale, J., and Urmee, T. (2016). Dust effect and its economic analysis on PV modules deployed in a temperate climate zone. *3rd International Conference on Power and Energy Systems Engineering, CPESE 2016*, Kitakyushu, Japan.

Tanesab, J., Parlevliet, D., Whale, J., and Urmee, T. (2018). "Energy and economic losses caused by dust on residential photovoltaic (PV) systems deployed in different climate areas." *Renewable Energy* ***120*** (2018): 401-412. DOI: https://doi.org/10.1016/j.renene.2017.12.076.

Tanesab, J., Parlevliet, D., Whale, J., Urmee, T., and Pryor, T. (2015). The contribution of dust to performance degradation of PV modules in a temperate climate zone. *Sol. Energy,* ***120*** (2015), 147-157. DOI: http://dx.doi.org/10.1016/j.solener.2015.06.052.

Taylor, H. F. W. (1992). *Cement Chemistry*. London: Academic Press, Inc.

Tetteh, E. K., Rathilal, S., and Naidoo, D. B. (2020). Photocatalytic degradation of oily waste and phenol from a local South Africa oil refinery wastewater using response methodology. *Scientific Reports* ***10*** (2020). DOI: https://doi.org/10.1038/s41598-020-65480-5.

Touati, F., Al-Hitmi, M. A., Chowdhury, N. A., Hamad, J. A., and Gonzales, A. J. S. P. (2015). Investigation of solar PV performance under Doha weather using a customised measurement and monitoring system. *Renewable Energy,* ***89*** (2016), 564-577. DOI: http://dx.doi.org/10.1016/j.renene.2015.12.046.

Touati, F., Chowdhury, N. A., Benhmed, K., Gonzales, A. J, R. S. P., Al-Hitmi, M. A., Benammar, M., Gastli, A., and Ben-Brahim, L. (2017). Long-term performance analysis and power prediction of PV technology in the State of Qatar. *Renewable Energy,* ***113*** (2017), 952-965. DOI:http://dx.doi.org/10.1016/j.renene.2017.06.078

TSP. (2017). Breakdown of Electricity Generation by Energy Source. Retrieved 14/06/2017, 2017, from http://www.tsp-data-portal.org/Breakdown-of-Electricity-Generation-by-Energy-Source#tspQvChart

TSP. (2017a). Historical Electricity Generation Statistics Retrieved 14/06/2017, 2017, from http://www.tsp-data-portal.org/Historical-Electricity-Generation-Statistics#tspQvChart

Ullah, A., Imran, H., Maqsood, Z., and Butt, N. Z. (2019). "Investigation of optimal tilt angles and effects of soiling on PV energy production in Pakistan." *Renewable Energy,* ***139*** (2019), 830-843.

UN. (2017). World Statistics Pocketbook 2017 edition (Vol. **41**). New York: UN.

Urrejola, E., Antonanzas, J., Ayala, P., Salgado., M., Ramírez-Sagner, G., Cortés, C., Pino, A., and Escobar, R. (2016). Effect of soiling and sunlight exposure on the performance ratio of photovoltaic technologies in Santiago, Chile. *Energy Conversion and Management,* ***114*** (2016), 338-347. DOI: http://dx.doi.org/10.1016/j.enconman.2016.02.016.

Usman, Z. G., Abbasoglu, S., Ersoy, N. T., and Fahrioglu, M. (2015). Transforming the Nigerian power sector for sustainable development. *Energy Policy,* ***87*** (2015), 429-437.

Venkatramanan, S., Chung, S. Y., and Prasanna, M. V. (2019). GIS and Geostatistical Techniques for Groundwater Science. Amsterdam, Netherlands: Elsevier.

Vincent, E. N., and. Yusuf., S. D. (2014). Integrating Renewable Energy and Smart Grid Technology into the Nigerian Electricity Grid System. *Smart Grid and Renewable Energy, **5*** (2014), 220-238.

Wakim, F. (1981) Introduction of PV power generation to Kuwait," Kuwait. Institute for Scientific Researchers, Kuwait City.

Wang, H., Meng, X., and Chen, J. (2020). Effect of air quality and dust deposition on power generation performance of the photovoltaic module on the building roof. *Building Service, Engineering, Research and Technology, **41*** (1), 73–85. DOI: 10.1177/0143624419868806.

Wang, P., Kong, M., Du, W., Wang, L., and Ni, L. (2020a). The effect of pollutants on leakage current and power degradation of photovoltaic modules. *Renewable Energy, **146*** (2020), 2668-2675. DOI: https://doi.org/10.1016/j.renene.2019.08.055.

Web mineral. (n.d.). Schorl. Retrieved from: http://webmineral.com/data/Schorl.shtml#.XHPZ2KL7SUk.

Weber, B., Quiñones, A., Almanza, R., and Duran, M. D. (2014). Performance Reduction of PV Systems by Dust Deposition. *Energy Procedia, **57*** (2014), 99-108. doi: 10.1016/j.egypro.2014.10.013.

WEC. (2020). World Energy: Issues Monitor 2017 *Exposing the New Energy Realities* (2017 ed., pp. 1-157). London: World Energy Council.

WHO. (2017). Population using solid fuels (estimates). Retrieved 08/12/2017, 2017, from http://apps.who.int/gho/data/node.main.135?lang=en.

Wijeratne, D., Jaswal, T., Pasemann, J., and Sircar, S. (2016). Powering Nigeria for the Future. *The Power Sector in Nigeria, **1*** (July 2016), 1-34.

Williams, R. B., Tanimoto, R., Simonyan, A., and Fuerstenau, S. (2007). *Vibration characterisation of self-cleaning solar panels with piezoceramic actuation.* Paper presented at the Collection of Technical Papers-48th AIAA/ASME/ASCE/AHS/ASC Structures, Structural Dynamics and Materials Conference, Honolulu, Hawaii.

World-Bank. (2021). Indicator. Retrieved from https://data.worldbank.org/indicator/SP.POP.TOTL?locations=NG

WorldBank. (2017). Electric power transmission and distribution losses (% of output). Retrieved 06/12/2017, 2017, from https://data.worldbank.org/indicator/EG.ELC.LOSS.ZS?end=2014&locations=NG-SS-GB-NE&name_desc=true&start=1960&view=chart&year=1990.

WorldBank. (2017). Electricity production from renewable sources, excluding hydroelectric (kWh). Retrieved 06/12/2017, 2017, from https://data.worldbank.org/indicator/EG.ELC.RNWX.KH?end=2014&locations=NG-GB-NE-DE-ZA-GH&name_desc=true&start=1960&view=chart&year=1990.

WorldBank. (2017). Methane emissions in the energy sector (thousand metric tons of CO_2 equivalent). Retrieved 06/12/2017, 2017, from https://data.worldbank.org/indicator/EN.ATM.METH.EG.KT.CE?end=2008&locations=NG-GB-ZA-IN-AE&start=1969.

WorldBank. (2017). Population, total. Retrieved 06/12/2017, 2017, from https://data.worldbank.org/indicator/SP.POP.TOTL?locations=NG.

World-Bank-Group (2020). "Access to electricity (% of the population) - Nigeria." Retrieved 15/07/2020, 2020, from https://data.worldbank.org/indicator/EG.ELC.ACCS.ZS?locations=NG&view=chart.

World-Bank-Group. (2016). GLOBAL SOLAR ATLAS: Nigeria. Retrieved 02/02/2019, 2019, from https://globalsolaratlas.info/downloads/nigeria.

World Weather Online. (2019). Weather. Retrieved from: https://www.worldweatheronline.com/.

World Weather Online (2020). Abuja Monthly Climate Averages. from https://www.worldweatheronline.com/abuja-weather-averages/federal-capital-territory/ng.aspx.

Wu, Z., Lee, D., Rubner, M. F., and Cohen, R. E. (2007). Structural Color in Porous, Superhydrophilic, and Self-Cleaning SiO2/TiO2 Bragg Stacks. *Nano-Micro Small,* ***3*** (8), 1445-1451. DOI: https://doi.org/10.1002/smll.200700084.

Xu, R., Ni, K., Hu, Y., Si, J., Wend, H., and Yu, D. (2017). "Analysis of the optimum tilt angle for a soiled PV panel." *Energy Conversion and Management* ***148*** (2017): 100–109.

Yakubu, A. and Ifeanyi-Nwaoha, C. (2017). Power to the People: Solving the 100 Million People Problem. *EmPower Nigeria,* ***16*** (1), 1.

Ye, L., Zhang, Y., Zhang, X., Hu, T., Ji, R., Ding, B., and Jiang, B. (2013). Sol-gel preparation of $SiO_2/TiO_2/SiO_2$-TiO_2 broadband anti-reflective coating for solar cell cover glass. *Sol. Energy Mater. Sol. Cells,* ***111*** (2013), 160–164. DOI: https://doi.org/10.1016/j.solmat.2012.12.037.

Yusuf, I. A. (2014). Nigeria: Overrun by electric power generators. Retrieved 19/01/2018, 2018, from http://thenationonlineng.net/nigeria-overrun-by-electric-power-generators/

Zaihidee, F. M., Mekhilef, S. Seyedmahmoudian, M., and Horan, B. (2016). Dust as an unalterable deteriorative factor affecting PV panel's efficiency: Why and how. *Renewable and Sustainable Energy Reviews,* ***65*** (2016), 1267-1278. DOI:http://dx.doi.org/10.1016/j.rser.2016.06.068.

Zhang, Y., Sakhuja, M., Lim, F. J., Tay, S., Tan, C., Bieri, M., Krishnamurthy, V. A., Wang, D., Krishnakumar, P. K., Ha, J., Zhao, L., and Reindl, T. (2017). The PV System Doctor – Comprehensive diagnosis of PV System Installation. Paper presented at the SNEC 11th International Photovoltaic Power Generation Conference & Exhibition, SNEC 2017 Scientific Conference, Shanghai, China.

Zorn, E., and Walter, T. R. (2016). Influence of volcanic tephra on photovoltaic (PV) -modules: an experimental study with application to the 2010 Eyjafjallajökull eruption, Iceland. *Journal of Applied Volcanology,* ***5*** (2), 1-14. DOI: 10.1186/s13617-015-0041-y.

Zorrilla-Casanova, J., Piliougine, M., Carretero, J., Bernaola-Galván, P., Carpena, P., Mora-López, L. and Sidrach-de-Cardona, M. (2013). Losses produced by soiling in the incoming radiation to photovoltaic modules. Prog. *Photovolt: Res. Appl.,* ***21*** (2013), 790-796. DOI:10.1002/pip.1258.

Zeedan, A., Barakeh, A., Al-Fakhroo, K., Touati, F., and Gonzales, A. S. P. (2021). Quantification of PV Power and Economic Losses Due to Soiling in Qatar. *Sustainability,* ***13*** (6), 3364. Retrieved from https://www.mdpi.com/2071-1050/13/6/3364

Appendices

Appendix A - Nigeria's Key statistics and energy outlook

Overview of key statistical indicators

Nigeria is a sub-Saharan country located in West Africa on the Gulf of Guinea. The Niger Republic borders it to the north, Cameroun to the east, the Benin Republic to the west and the Atlantic Ocean to the South. The country has a total surface area of 923 768. 00 km^2 comprised of about 1.4% water area (13,000 km^2) and about 98.6% land area (910,768 km^2) (UN, 2017; Ajayi et al., 2016; Akinyele et al., 2017). The country lies between latitudes 4.321°N and 14.1°N of the equator and longitude 2.721°E and 14.641°E to the Greenwich meridian (Ajayi et al., 2016; Akinyele et al., 2015). It has varied terrain, including elevated areas, mountains, rivers, lakes, forests and plains scattered and varies from semi-desert and savannah in the north to tropical forest and coastal swamp in the southern part (Anumaka, 2012; Shaaban and Petinrin, 2014). The country has 78% of agricultural land that comprises 37.3% of arable land, 7.4% of permanent crops and 33.3% of permanent pastures. It also has a forest land area of 9.5% and others 12.5 %. The country's irrigated land area is about 2,930 sq km (CIA, 2018).

Nigeria is the 7th most populous nation globally, with an estimated population of 200.96 million in 2019 (World Bank, 2021). The average population growth was rated at about 2.7% per annum. The urban population was estimated at 47.8% of the total population, and 52.2% was the estimated rural population. According to Nwokocha et al. (2018), the country has over 500 ethnic groups with diverse cultures.

Nigeria is divided into 36 states and FCT (Federal Capital Territory). The states are grouped into six geopolitical zones, including NE (North-East), NC (North-Central), NW (North-West), SE (South-East), SS (South-South) and SW (South-West) (Shaaban and Petinrin, 2014; Giwa et al., 2017).

The nation's economy is highly dependent on crude oil, with about 90% of Nigeria's income related to oil activity. The country's GDP stands at

approximately USD 448.2 Billion with an annual growth of 2.208 in 2019; GDP per capita growth is USD -0.38 (World Bank, 2021). About 14.7% of the employed population are in the industry, while 57.4% are employed in public services. The country's estimated CO_2 emission is 96.3 million tons / 0.6 tons per capita. The estimated energy supply per capita is 32 Gigajoules (UN, 2017).

Meteorologically, the country enjoys two tropical climatic conditions, the wet and dry seasons. These seasonal durations differ by region: the southern part experiences a more extended wet season that lasts from March to December with a maximum of 2600 mm/yr, and December to March is the dry season. The southern part is usually humid and hot. On the other hand, the Northern region is typically dry and hot, with an average temperature range between 32°C to 42°C. The rainy season in northern Nigeria commences around April and lasts till October with about 110 mm/yr, and the dry season is from October to April and is accompanied by dry, dusty wind (harmattan) (Shaaban and Petinrin, 2014; Giwa et al., 2017; and Oji et al., 2012).

Nigeria's oil and gas

Nigeria is a country that has abundant natural resources such as fossil fuels (oil and gas). Based on these resources, population and other factors, the country is commonly called the giant of Africa. The country relies on the oil and gas industry as its primary revenue source (Adom and Adams, 2017). Unfortunately, these resources have not been used effectively to resolve the persisting socio-economic problems and other challenges, including the country's energy crisis for more than two decades.

Nigeria is a member of the OPEC (Organisation of the Petroleum Exporting Country). The country's crude oil reserve and Libya's, when combined, account for 2/3 (two-thirds) of the African oil reserve. In Nigeria, oil was first discovered in a town called Oloibiri, in Bayelsa State, in the Niger Delta, South-South region, in 1956, just before independence. The country has continued to witness a steady increase in exploration activities over the decades. This exploration, growth arises from a funding scheme that is related to production-sharing arrangements. The exploration activities are both onshore and offshore (in the Atlantic Ocean).

In 2015, the country had about 29 active oil rigs, a pipeline network of 5001km around the country, with about 22 (twenty-two) oil depots (Anumaka, 2012; OPEC, 2016). According to OPEC (2016), Nigeria has four functioning oil and gas refineries (Port Harcourt Refining Company (PHRC) in Port Harcourt, Warri Refining and Petrochemical Company (WRPC) in Warri, Kaduna Refining and Petrochemical Company (KRPC) Kaduna and PHRC Old Port Harcourt) with a total production capacity of 445.0 (1,000 b/cd) but produces only 24.1 (1000 b/d), while the country's oil demand is about 407.8 (1000 b/d) (OPEC, 2016). These clearly show the low performance of local refining capacity, as crude oil is exported for refining purposes and then imported back for local consumption. This low performance results from poor maintenance, inadequately trained staff, underfunding, corruption and vandalism.

Oil

Despite the oil resources, its populace is frequently suffering from shortages of oil products, based on the above facts relating to insufficient refining capacity. The country's crude oil export reached about 2,132.0 (1000 b/d), and the import level of petroleum products stands at about 441.0 (1000 b/d). The country has a proven crude oil reserve of 37,453 million barrels, equivalent to approximately 5.0 billion tonnes. In 2015, Nigeria produced about 2329 barrels/day. While in 2016, the country produced about 2053 barrels per day, a decrease of about -11.9%. Its refining capacity is approximately 446.0 (1,000 b/d), and the output of the refined petroleum products is about 53.5 (1,000 b/d), while the country's oil demand is about 393.1 (1,000 b/d) (OPEC, 2017; BP, 2017). In 1999, It was documented that the country had a proven reserve of 25 billion barrels. In 2004, it increased to about 34 billion barrels in 2017, and it would continue to increase to about 37 billion barrels, and by 2030 it is projected to reach 68 billion barrels (Anumaka, 2012) potentially. In 2015, Nigerian OPEC production percentages were reduced to 5.8% compared to 7%, which had a devastating effect on the country's economy because of the overdependence on the oil and gas sector (Wijeratne et al., 2016).

Natural Gas

Nigeria is ranked second globally in the natural gas reserves after Algeria (Anumaka, 2012). The reserves are proven to be extremely large at 3 (three) times the amount of oil in the country. In 2017, Nigeria had a proven natural gas reserve of about 5.4 trillion m^3 (cubic meter), equivalent to 190.7 trillion ft^3 (cubic feet). In 2007, the country produced 50.1 billion $m^{3,}$ which is 45.1 tonnes of oil equivalent of natural gas, while in 2016, it produced 44.9 billion m^3 and 40.4 million tonnes of oil equivalent of natural gas (OPEC, 2017; BP, 2017). About 25.2 billion m^3 of natural gas was exported (OPEC, 2017). Nigeria had been wasting its gas through gas flaring in the Niger Delta until 1990 when the Nigerian National Petroleum Corporation (NNPC) concluded the agreements with Chevron/Shell and established Nigeria LNG (Liquefied Natural Gas) 2 (two) years later, and commenced production in 1999 (Anumaka, 2012). According to Shaaban and Petinrin (2014), about 45.8 Billion kWh of heat is discharged into the South-South region of Nigeria from gas flaring of about 1.8 billion ft^3 of gas daily, which led to the country being rated among one of the highest CO_2 (Carbon dioxide) and GHG (Green House Gas) producers in the world. According to Anumaka (2012); Shaaban and Petinrin (2014), Nigeria is assumed to be one of the world's highest gas flaring nations. Anumaka (2012) further stated that the country is losing vast quantities in this way, with an estimated loss of USD 18.2 million every day. These immense resources could be used in generating electricity and other developmental and infrastructural projects.

Coal

Coal is the oldest natural resource discovered and exploited in Nigeria. It was discovered in 1909, and mining began years later, having a recorded production output of 24.500 tons in 1916 (Anumaka, 2012). Unlike oil and gas, about 95% of the production was consumed locally for transportation (railways), industrial activities (cement production) and electricity production. The country has a proven reserve of about 639 million tonnes of coal, and the inferred reserves are estimated at 2.75 billion tonnes (Anumaka, 2012). The utilisation of coal drastically dropped just after the discovery of crude oil. The diesel-powered trains and various sources of electricity generation were also introduced in the country. The available potential can still be utilised in production activities and power

generation, but its by-products have a severe negative effect on human health and the environment.

Brief historical background of electricity in Nigeria

Historically, electricity generation in Nigeria can be traced to 1896 in Lagos state, 15 (fifteen) years after it was first produced in England (Anumaka, 2012; and Oseni, 2011). In 1929 Nigeria Electricity Supply Company (NESCO) commenced its construction operations of a hydropower plant in Jos, Plateaus state in the northern part of the country (Monyei et al., 2017; Kumar et al., 2016). In 1951, the colonial legislative council established the Electricity Corporation of Nigeria (ECN) through parliament. The body was established to manage electricity supply and development (Anumaka, 2012; Monyei et al., 2017; Vincent and Yusuf; 2014). In 1962, expansion led to the Niger Dam Authority (NDA) development through the Nigerian parliament's act to construct and maintain dams for electricity generation, water supply, agriculture and irrigation activities (Anumaka, 2012). The agreement at that time was that all energy produced by NDA would be sold to ECN.

In 1972, Nigerian Electricity Power Authority (NEPA) was established, ECN and NDA were merged to form NEPA, and the Authority was mandated to control and manage the entire activities of the power sector (Anumaka, 2012). NEPA monopolised the sector for over 3 (three) decades (1972-2005). It managed both the generation, transmission and distribution of electricity in the country. With the rapid increase of population, the demand continued to increase, and it reached a stage where the demand superseded the supply. Coupled with dilapidated infrastructure and unqualified workforce, NEPA was encountering difficulties in managing the sector. Therefore, in 1979, the Energy Commission of Nigeria (ECN) was established through parliament with the statutory mandate to strategically plan and coordinate national energy policy (Anumaka, 2012).

In 2001, National Electric Power Policy (NEPP) was introduced, which led to the power sector revolution. This policy developed an Electric Power Sector Reform (EPSR) documented in the same year, but the document was not signed until 2005 (Vincent and Yusuf, 2014). After this process, NEPA was transformed and

renamed Power Holding Company of Nigeria (PHCN). In the same year, the president signed the Power Sector Reform Bill law and established the Nigerian Electricity Regulatory Commission (NERC) to regulate energy sector activities, issue licenses to stakeholders, determine and regulate tariffs, and enforce standards. The commission enabled the unbundling of the sector and involvement of the private sectors in both generation and distribution, but this privatisation process was delayed by union agitation and protests until 2006 (Anumaka, 2012).

In 2005, NERC also established Niger Delta Power Holding Company Limited (NDPHC) as a limited liability entity to manage the National Integrated power projects (NIPP) in the Niger Delta region (Usman et al., 2015).

In 2010, Nigeria Bulk Electricity Trading (NBET) Plc was established through an act of parliament with a mandate to serve as a broker between distribution companies and Independent power producers (IPP) (Usman et al., 2015). The federal government also established the Nigerian Electricity Liability Management Company (NELMCO) to oversee the assets and liabilities of the PHCN, and in the same year, another reform called the Power Sector Roadmap was initiated (Monyei et al., 2017). Finally, privatisation of energy generation and distribution was completed in 2014 and companies were handed over to respective purchasers accordingly (Usman et al., 2015).

In 2015, the federal government approved National Renewable Energy and Energy Efficiency Policy (NREEEP). This policy intends to integrate renewable energy into the national supply mix to increase electricity access to the population (Yakubu and Ifeanyi-Nwaoha, 2017).

The history of electricity generation and supply for over 2 (two) decades has remained inadequate. The presidency has spent billions of dollars, but the lack of comprehensive policies and corruption has severely limited the sector's rate of progress and compels the sector to slow performance progression. Appendix A - Figure 0.1 below depicts the history of energy generation in Nigeria for three decades.

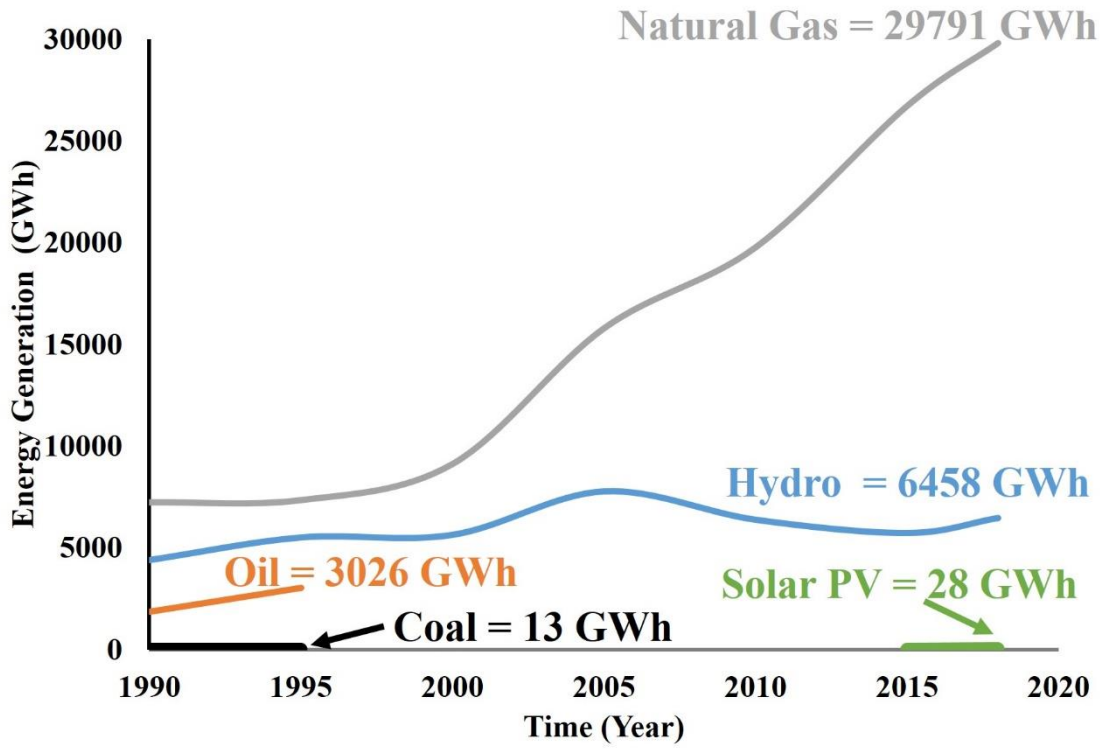

Appendix A - Figure 0.1: Variation of energy generation and their sources over three decades (IEA, 2020).

Nigeria's electricity infrastructure

Nigeria is a country that has access to abundant non-renewable and renewable resources capable of harvesting electricity. However, electricity generation to meet the demand has been one of the country's significant challenges. According to Akinyele et al. (2017), Nigeria's electricity infrastructure's low status has led to increased use of fossil fuel in powering generators by a large number of Nigerians to meet their daily needs. This problem has left many Nigerians without an option other than to adopt self-energy generation using fossil fuel-powered generators and traditional biomass. According to Anumaka (2012), Nigeria's electricity grid generation has been dominated by gas and other oil, hydroelectric, and coal sources. In 2014, Nigeria produced around 30 TWh of electricity distributed in the following manner: Oil 6 TWh, Hydroelectricity 6 TWh, Gas 18 TWh, solar energy 28 GWh (IEA, 2020). This distribution is shown in Appendix B - Figure 0.2.

Sub Sectors

Nigeria's electricity system is divided into three sub-sectors, namely: generation, transmission and distribution. These sectors currently have 23 (twenty-three) grid-connected energy generation plants (Hydro and thermal) controlled by the government and private sectors. The industry has a transmission company with an extensive network connection around the country and is managed by the government alone. The distribution sector has 11 (eleven) companies that manage distribution to consumers owned and operated by private companies. These sub-sectors are described in detail in the subsequent section and summarised in Appendix B - Figure 0.2.

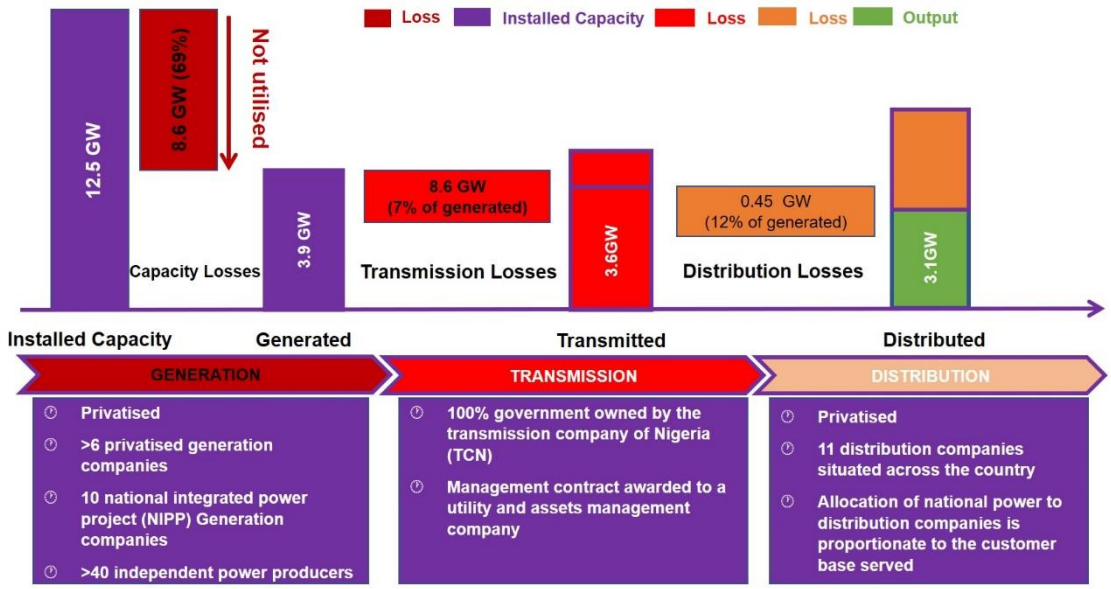

Appendix A - Figure 0.2: Summary of Nigeria's electricity system (Adopted from Wijeratne et al., 2016).

Generation

As of December 2013, Nigeria had a total installed capacity of about 10,396 MW from 23 power generating stations across the country, out of which 8,457.6 MW is from the thermal-based station with an available capacity of 4,996 MW (Bassey-Etuk, and Ifeanyi-Nwaoha, 2017; Ikem et al., 2016; Vincent and Yusuf, 2014). Also, the hydro-based power stations account for about 1,060 MW to 1,938 MW as their available capacity. These 23 power plants are owned and managed by both government (NIPP: National Integrated Power Projects) and

private companies (IPP: Independent Power Producers and privatised Generation Companies), with the government still having the majority of the share (Bassey-Etuk, and Ifeanyi-Nwaoha, 2017; Ikem et al., 2016; Vincent and Yusuf, 2014). Wijeratne et al. (2016) reported that in 2015, the country had an installed capacity of about 12,500 MW with approximately 3,900 MW available capacities, and 3100 MW is supplied. Appendix A Figure 0.2 shows a summary of the power sector in 2015. In 2017, the total installed capacity increased to about 14380 MW from 27 generating plants across the country, out of which only approximately 7,527.5 MW was available and between 3000 to 5000 MW was supplied (Akuru et al., 2017). According to NBS (2017), the peak generation was attained on 24th January 2017, where about 5,846 MW (140,316 MWh) was generated, and about 5,747 MW (137,920 MWh) was supplied. This shows a remarkable improvement in the sector. However, the supply is still inadequate, and more alternative, clean sources must be harnessed.

Transmission

The power transmission is solely managed by the Transmission Company of Nigeria, owned by the government and is characterised by power losses and dilapidated infrastructures. The transmission system has a network of about 12,300 km in length with about 5523.8 km of 330 kV lines and 6801.49 km of 132 kV lines (Vincent and Yusuf, 2014; Ikem et al., 2016; Usman et al., 2015). There are 137 transmission stations across the country consisting of 32 of 330/132 kV substations with an installed capacity to transform 7,688 MVA. The remaining 105 are of 132/33/11 kV substations with an installed capacity of 9,130 MVA (Vincent and Yusuf, 2014).

In recent years, the government has been making efforts in improving the transmission network and its infrastructure. Transmission and distribution (T&D) losses are drastically dropping but are still considered to be high. In 2013, Nigeria recorded losses of about 35% (Ikem et al., 2016), while in 2014, the country recorded losses of about 16.107% through transmission and distribution (WorldBank, 2017a). These losses dropped to about 8% in 2016, the MYTO (Multi-Year Tariff Order) target. Additional projects to expand the transmission

network are ongoing, and it is expected to extend the network to about 986 km of 330 kV and 705 km of 132 kV.

Distribution

Distribution is the third sub-sector of the power system, which interacts with the consumers. The sector comprises 11 distribution companies called the DISCOs with their various load allocations. Their distribution capacity is only around 5,000 MW to 6,000 MW because they inherited old assets, and about 40% of them have been more than 50 years in operation. Poor electricity distribution is a significant contributor to Transmission and Distribution (T&D) losses (Ezeokoli and Ifeanyi-Nwaoha, 2018). The substation transformers at the distribution level receive the voltage at about 115 kV and convert it from 4 kV to 34 kV. In contrast, the line transformer converts the energy to primary voltage, typically about 240 V and 480 V. The distribution sector is facing challenges such as poor infrastructure, weak and inadequate coverage, inadequate working tools, obsolete communication technology, staff that lacks training, insufficient funding and lack of maintenance (Vincent and Yusuf, 2014).

Appendix B - Methodology Flowcharts

Chapter 3 Methodology flow chart

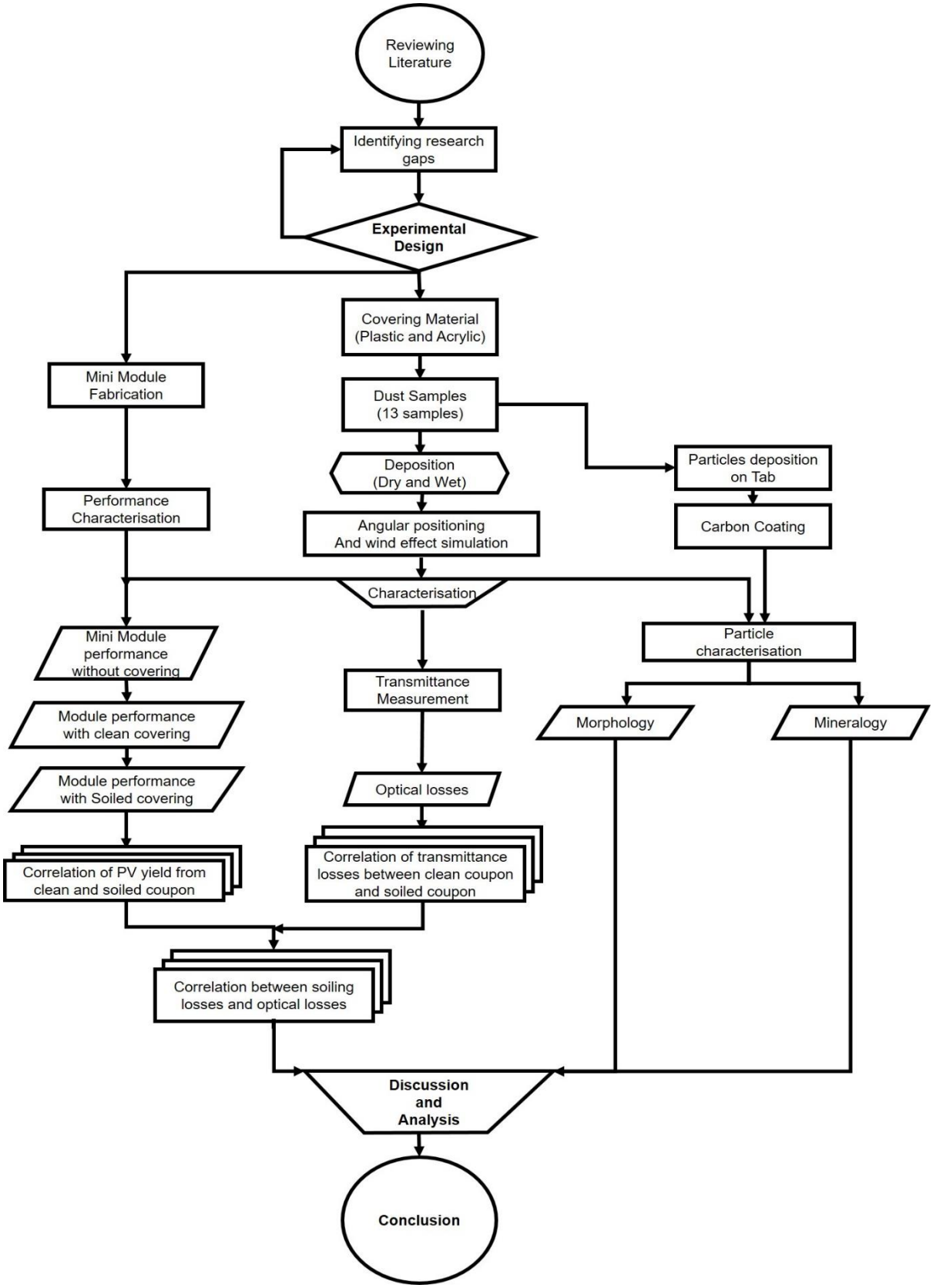

Appendix B - Figure 0.3: Chapter three methodology flow chart.

Chapter 4 Methodology flow chart

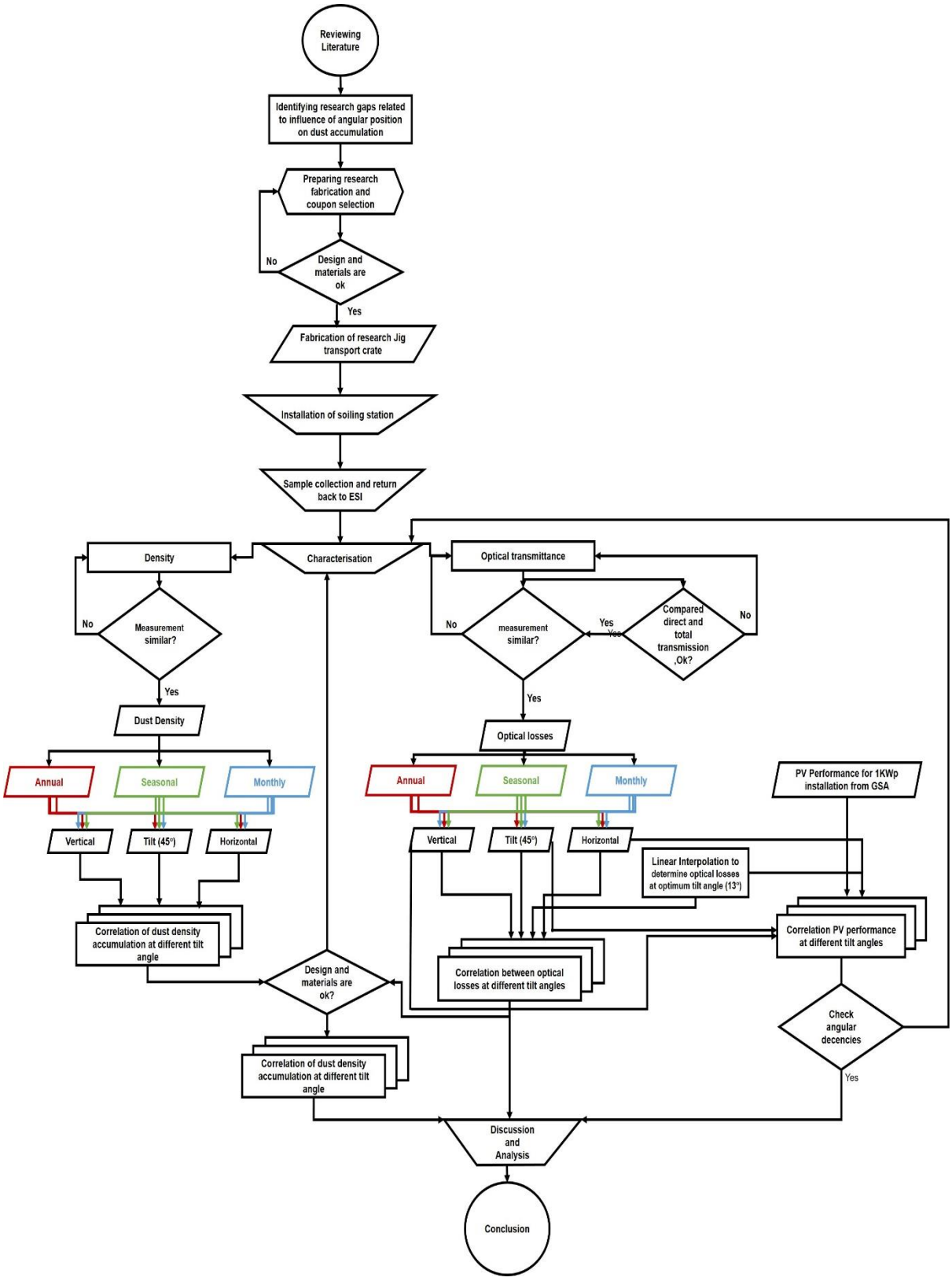

Appendix B - Figure 0.4: Chapter four methodology flow chart.

Chapter 5 Methodology flow chart

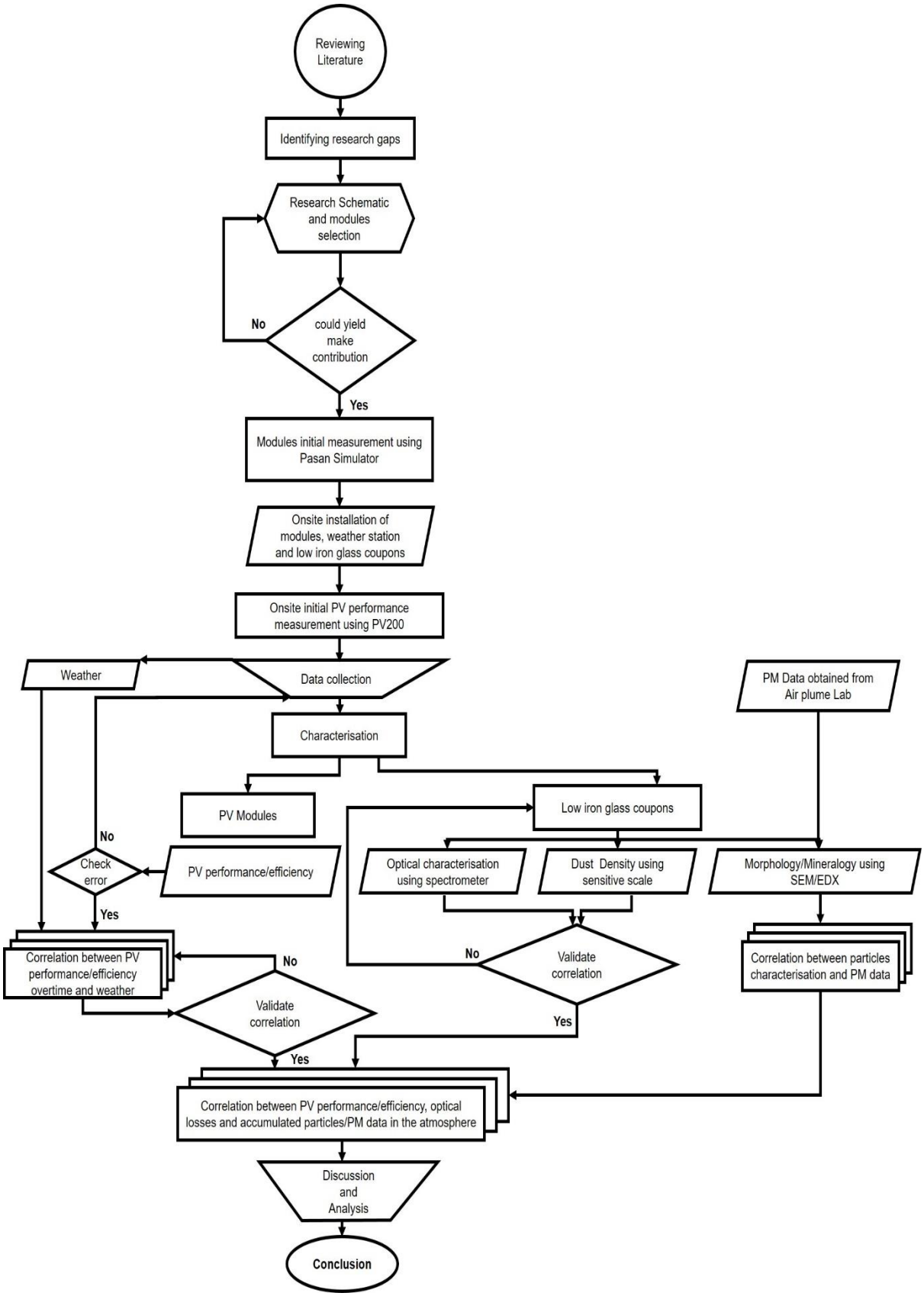

Appendix B - Figure 0.5: Chapter five methodology flow chart.

Chapter 6 Methodology flow chart

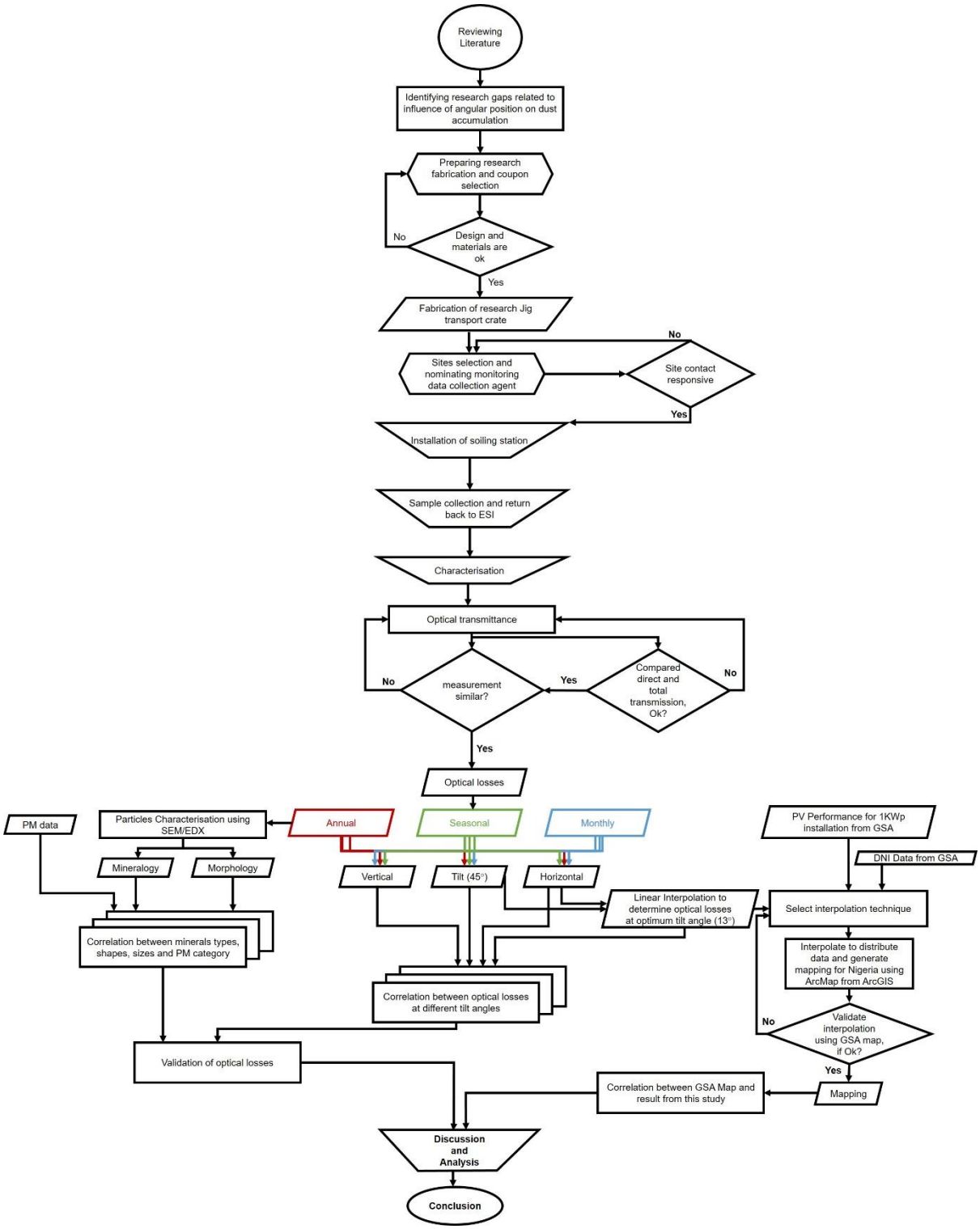

Appendix B - Figure 0.6: Chapter six methodology flow chart.

Chapter 7 Methodology flow chart

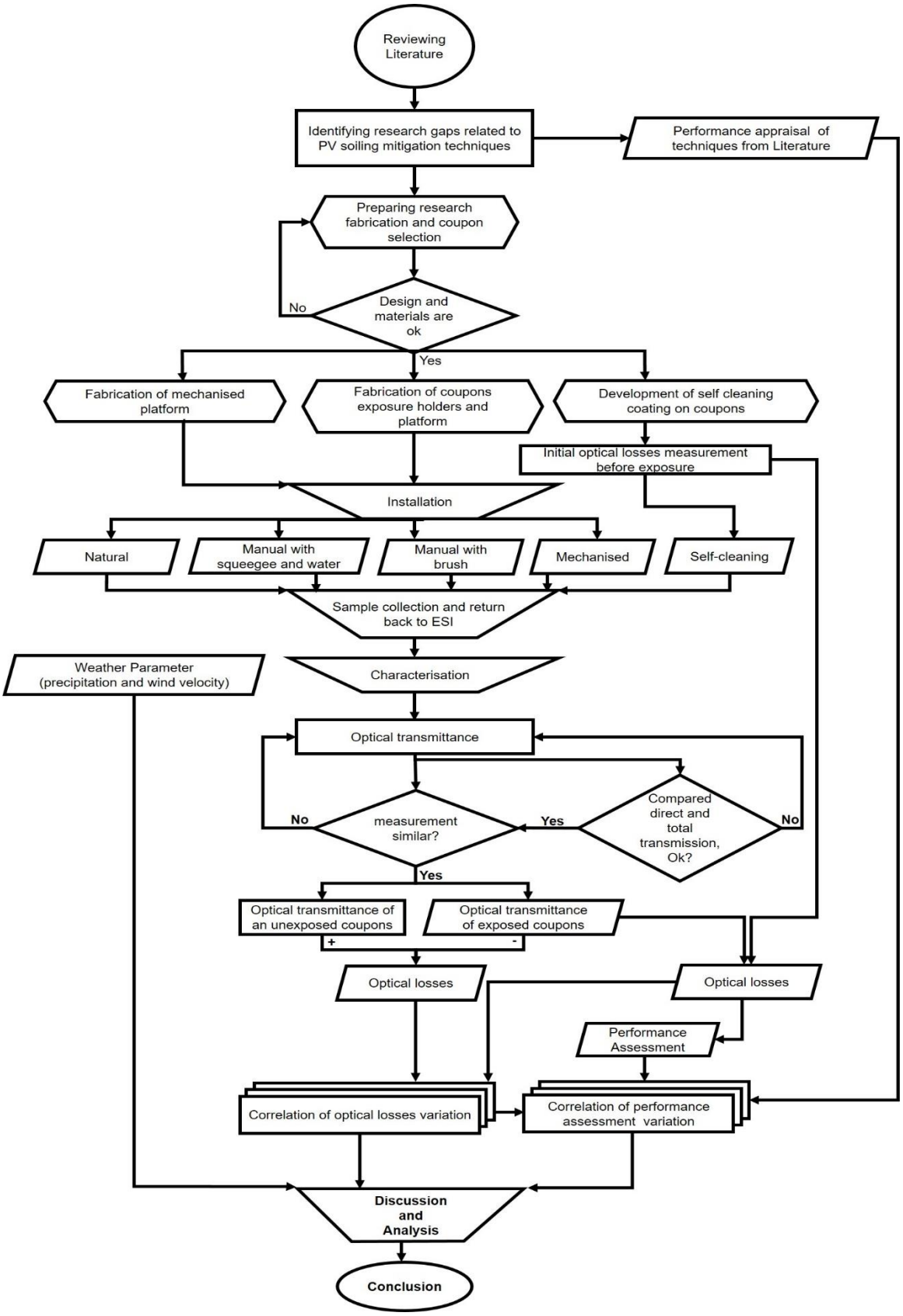

Appendix B - Figure 0.7: Chapter seven methodology flow chart.